

Universidade de Lisboa

Faculdade de Farmácia



Development of new neutrophil elastase inhibitors for topical formulation with improved therapeutic efficacy

Andreia Alexandra Germano Nunes

Dissertation supervised by Professor Francisca Lopes and co-supervised by
Professor Helena Margarida Ribeiro

Master degree in Pharmaceutical and Medicinal Chemistry

2019

Universidade de Lisboa

Faculdade de Farmácia



Development of new neutrophil elastase inhibitors for topical formulation with improved therapeutic efficacy

Andreia Alexandra Germano Nunes

Dissertation supervised by Professor Francisca Lopes and co-supervised by
Professor Helena Margarida Ribeiro

Master degree in Pharmaceutical and Medicinal Chemistry

2019

Agradecimentos

Primeiramente, gostaria de agradecer às minhas orientadoras Professora Doutora Francisca Lopes e Professora Doutora Helena Margarida Ribeiro, por todo o apoio científico, receção nos seus laboratórios, incansável orientação, acompanhamento, opiniões e críticas, oportunidade incrível de aprendizagem e a colaboração no solucionar de dúvidas e problemas que foram surgindo no decorrer do projeto.

À Professora Doutora Joana Marto por toda a dedicação, transmissão de conhecimentos, acompanhamento, preciosa ajuda no trabalho laboratorial e teórico, e disponibilidade do seu tempo no decorrer do projeto.

Gostaria de expressar a minha gratidão também à Doutora Lídia Gonçalves pela sua disponibilidade e bondade em ajudar-me na execução dos ensaios enzimáticos *in vitro*.

À Doutora Sandra Simões pelo empenho, transmissão de conhecimentos e total disponibilidade para a execução dos ensaios *in vivo* de atividade anti psoriática.

À Doutora Tânia Carvalho pela valiosa partilha de conhecimentos e pela disponibilidade na execução dos ensaios de histologia.

À PhD trials pela disponibilidade, execução e tratamento dos resultados dos ensaios de análise sensorial e da pele *in vivo*.

À Mestre Rita Félix por toda a ajuda laboratorial e teórica, enorme dedicação e pela agradável experiência de aprendizagem durante o decorrer do projeto.

Aos meus amigos e colegas de mestrado que no decorrer deste último ano partilharam o laboratório comigo. Por todos os momentos que passamos juntos, todos os almoços, todas as dúvidas solucionadas, risos e sorrisos que contribuíram para o sucesso de cada um de nós.

Quero ainda agradecer aos meus amigos de sempre por me acompanharem, estarem comigo em todos os momentos, pela (enormíssima) paciência e carinho demonstrado, em especial à Andreia Monteiro, Milene Ramos, Pedro Santos, Humberto Nicolau, Ricardo Alves, Filipa Correia e Joana Morgado.

Como não poderia deixar de ser, quero agradecer à minha família, em especial aos meus pais e irmã, por todo o apoio prestado, disponibilidade incondicional e total ajuda na superação dos momentos de maior tensão.

Index

Figures Index	ix
Tables Index	xiii
Schemes Index	xv
Abbreviations.....	xvii
Abstract	xix
Resumo.....	xxi
1. Introduction	1
1.1. Proteases.....	3
1.1.1. Serine Proteases.....	4
1.2. Human Neutrophil Elastase.....	6
1.2.1. Inhibitors of Human Neutrophil Elastase.....	8
1.3. Psoriasis.....	14
1.3.1. Current therapeutics.....	16
1.4. Topical delivery systems.....	17
1.4.1. Emulsions.....	22
1.4.2. Microemulsions	31
2. Aim	35
3. Results and discussion	39
3.1. Synthesis of 4-oxo- β -lactams.	41
3.2. Biological Assays	60
3.2.1. Enzymatic inhibition assays and <i>in vitro</i> cytotoxicity.....	60
3.2.2. Enzymatic inhibition assays, specificity and <i>in vitro</i> cytotoxicity for the compounds with fluorescence.	62
3.3. Pharmaceutical vehicles	64
3.3.1. Emulsion	65
3.3.2. Microemulsion.....	75
3.4. Characterization of final pharmaceutical vehicles: Placebos	81
3.5. Final formulations containing AAN-27	85

3.5.1.	pH	86
3.5.2.	Rheology	86
3.5.3.	Droplet size	88
3.5.4.	Fluorescence microscope	89
3.5.5.	Drug Release	89
3.5.6.	<i>In vivo</i> antipsoriatic activity	94
4.	Conclusion and future work	99
5.	Experimental Section	103
5.1.	Synthesis	105
5.1.1.	Reagents and solvents	105
5.1.2.	Chromatography	105
5.1.3.	Equipment	105
5.1.4.	Synthetic Procedures and Product Characterization	106
5.2.	Biological Assays	114
5.2.1.	Enzymatic Inhibition Assays	114
5.2.2.	<i>In vitro</i> Cytotoxicity – HaCat Cells	115
5.2.3.	Analysis of Inhibitors Specificity	116
5.3.	Pharmaceutical Vehicles	117
5.3.1.	Materials	117
5.3.2.	Methods	118
6.	Bibliography	127
7.	Appendix 1	139
8.	Appendix 2	175

Figures Index

Figure 1 - Proteases active sub-sites. Adapted from (6).	3
Figure 2 - Mechanism of decylation reaction. Adapted from (7).	5
Figure 3 - General structure of the following compounds: 4-oxo- β -lactam [A], benzoxazinones [B], diazo compounds [C] and haloketones [D].	8
Figure 4 - General structure of a peptide aldehyde.	10
Figure 5 - Scheme of the interaction of an irreversible transition state inhibitor. Adapted from (5).	10
Figure 6 - Scheme of the interaction of a reversible transition state inhibitor. Adapted from (22).	10
Figure 7 - Mechanism of inhibition to HNE by Saccharin-like compounds. Adapted from (12).	11
Figure 8 - Chemical structure of β -lactams [A], benzoxazinones [B], azetidine-2,4-diones [C], succinimide-like compounds [D] and coumarinas [E].	12
Figure 9 - Chemical structure of cephalosporins [A] and clavams [B].	12
Figure 10 - Interaction between HNE and compound 1.	13
Figure 11 - Chemical structure of ONO-5046.	13
Figure 12 - Mechanism of inhibition of Sivelestat. Adapted from (26).	14
Figure 13 - Representation of corneocytes and the lipid matrix of stratum corneum (53).	18
Figure 14 - Chemical structure of ethanol.	20
Figure 15 - Chemical structure of isopropyl myristate.	20
Figure 16 - Chemical structure of propylene glycol.	21
Figure 17 - Chemical structure of oleic acid.	21
Figure 18 - Emulsions' process formation.	23
Figure 19 - Representation of the two different emulsions' systems: W/O (left) and O/W (right). Adapted from: (74).	26
Figure 20 - Different structures of emulsions depending on the ratio of water, surfactant and oil used. Adapted from (79).	30
Figure 21 - Representation of a type I, II, III and IV, microemulsion according to Winsor ⁽¹⁰⁵⁾ . Adapted from: (105).	33

Figure 22 - Reaction mechanism of compound 10 with <i>p</i> -toluidine to synthesize compound 11.	42
Figure 23 - ¹ H NMR spectrum for compound 12.	43
Figure 24 - ¹³ C NMR spectrum for compound 12.	43
Figure 25 - ¹ H NMR spectrum for compound 1.	45
Figure 26 - ¹³ C NMR spectrum for compound 1.	45
Figure 27 - ¹ H NMR spectrum for compound 18.	47
Figure 28 - ¹³ C NMR spectrum for compound 18.	47
Figure 29 - COSY NMR spectrum for compound 18.	48
Figure 30 - HSQC NMR spectrum for compound 18.	48
Figure 31 - HMBC NMR spectrum for compound 18.	49
Figure 32 - ¹ H NMR spectrum for compound 21.	51
Figure 33 - ¹³ C NMR spectrum for compound 21.	52
Figure 34 - ¹ H NMR spectrum for compound 22.	53
Figure 35 - ¹³ C NMR spectrum for compound 22.	53
Figure 36 - ¹ H NMR spectrum for compound 26.	55
Figure 37 - ¹ H NMR spectra for compound 27.	57
Figure 38 - ¹³ C NMR spectra for compound 27.	58
Figure 39 - ¹ H NMR spectrum for compound 28.	59
Figure 40 - ¹³ C NMR spectrum for compound 28.	60
Figure 41 - Cytotoxicity assays performed with HaCat cells.	62
Figure 42 - Cell viability in HaCat cells for fluorescent compounds 27 and 28. Compound 1 was used as control.	64
Figure 43 - Emulsions flow curves: Influence of different humectants.	67
Figure 44 - Emulsions oscillatory results obtained from a frequency sweep: Influence of different humectants.	68
Figure 45 - Lamellar phases of an emulsion: gel phase (left) and liquid crystal phase (right). Adapted from (86).	69
Figure 46 - Emulsions flow curves: Influence of different concentration of cetyl alcohol.	70
Figure 47 - Emulsions oscillatory results: Influence of different concentration of cetyl alcohol.	71
Figure 48 - Emulsions flow curves: Influence of different preservatives.	72
Figure 49 - Emulsions oscillatory results: Influence of different preservatives.	74

Figure 50 - Ternary diagram for microemulsions.....	77
Figure 51 - Microemulsions flow curves: Influence of oil carbon chain.	79
Figure 52 - Microemulsions oscillatory results: Influence of oil carbon chain.....	80
Figure 53 - Droplet size distribution by volume (%) of the placebo's emulsion 5.	81
Figure 54 - Droplet size distribution by intensity of the placebo's microemulsion 14... 81	
Figure 55 - <i>In vivo</i> sensory analysis results for O/W emulsion 5 and W/O microemulsion 14 (average; n=10).	82
Figure 56 - Results from the moisturization, hydration (Epidermal Capacitante) and TEWL studies.	84
Figure 57 - AAN-27 E and AAN-27 ME flow curves.....	86
Figure 58 - Oscillatory results of AAN-27 E.	87
Figure 59 - Oscillatory results of AAN-27 ME.....	87
Figure 60 - Droplet size distribution by volume (%) of the AAN-27 E.	88
Figure 61 - Droplet size distribution by intensity of AAN-27 ME.....	88
Figure 62 - Inside structure of (A) AAN-27 E and (B) placebo's emulsion, using an optical fluorescence microscope with video camera (Bresser, Germany) with an enlargement of 100x.....	89
Figure 63 - Drug release studies for AAN-27 ME, AAN-27 E and AAN-27 S.....	90
Figure 64 - Results of the <i>in vivo</i> antipsoriatic activity: erythema, scaling and thickness.	94
Figure 65 - Skin's damage after the application of (A) emulsion placebo's and (B) AAN-27 E in the seventh day of study.	95
Figure 66 - Skin's damage five hours after the application of (A) microemulsions placebo's and (B) AAN-27 ME in the fifth day of study.....	95
Figure 67 - Representative microphotographs of skin (dorsum) of mice exposed to imiquimod. Changes were characterized by epidermal hyperplasia (black arrowhead), and focally extensive inflammation mildly expanding the dermis (white arrowhead). Hematoxylin and eosin stain. Original magnification, 10x (bar, 250µm). Animal 1 was treated with clobetasol propionate, animal 7 was treated with placebo's emulsion and animal 16 was treated with AAN-27 E.	96
Figure 68 - Epidermal and dermal thickness of the skin (dorsum) of mice exposed to imiquimod. Measurements were performed in slides digitally scanned in the Hamamatsu NanoZoomerSQ, with NDP.view2 software (Hamamatsu), and correspond to mean value obtained from 7 to 12 different points, for epidermis (A) and dermis (B), in longitudinal	

skin sections for each individual mice. Animal 1 was treated with clobetasol propionate, animal 7 was treated with placebo's emulsion and animal 16 was treated with AAN-27 E..... 96

Tables Index

Table 1 - Influence of CPP and HLB on emulsion structure. Adapted from (73,99).	28
Table 2 - Correlation between the carbon atoms with the protons already identified. ...	50
Table 3 - Enzymatic inhibition assays.	60
Table 4 – Enzymatic inhibition assays for fluorescent compounds 27 and 28. Compound 1 was used as control.	63
Table 5 - Results of specificity of the compounds 1 (control), 27 and 28.	63
Table 6 - Microemulsions' composition.	76
Table 7 - AAN-27 E O/W emulsion composition.	85
Table 8 - AAN-27 ME Microemulsion composition.	85
Table 9 - Kinetic parameters obtained after fitting the drug release data from AAN-27 E, AAN-27 ME and AAN-27 S, to different release models (mean \pm SD, n = 6). K—release constant; R^2_{adjusted} -adjusted coefficient of determination; AIC-Akaike information criterion; n—release exponent.	93
Table 10 - Emulsion Formulation: aqueous phase.....	118
Table 11 - Emulsion Formulation: oily phase	119
Table 12 - Microemulsion formulation: aqueous phase.....	120
Table 13 - Microemulsion formulation: oily phase	120
Table 14 - Scoring system for histopathologic evaluation of skin lesion	126

Schemes Index

Scheme 1 - Synthesis of compound 12.	41
Scheme 2 - Synthesis of compound 1.	44
Scheme 3 - Synthesis of compound 18.	46
Scheme 4 - Synthesis of compound 21.	51
Scheme 5 - Synthesis of compound 22.	53
Scheme 6 - Synthesis of compound 26.	54
Scheme 7 - Synthesis of compound 27.	56
Scheme 8 - Synthesis of compound 28.	58

Abbreviations

AIC	Akaike minimum information theoretical criterion
Asp	<i>Aspartic acid</i>
CMC	Critical Micellar Concentration
COSY	Correlation spectroscopy
CPP	Critical Packing Parameter
DCM	Dichloromethane
DIPEA	<i>N,N</i> -diisopropylethylamine
DMF	Dimethylformamide
DMSO	Dimethylsulfoxide
EMA	European medicines agency
EWG	Electron withdrawing group
FDA	US Food and Drug Administration
FTIR	Fourier-transform infrared spectroscopy
G'	Elastic component
G''	Viscous component
Gly	Glycine
HaCat	Immortalized human keratinocytes
His	Histidine
HLB	Hydrophilic-Lipophilic Balance
HMBC	Heteronuclear multiple bond correlation
HNE	Human neutrophil Elastase
HPLC	High-performance liquid chromatography
HSQC	Heteronuclear single quantum coherence
IC ₅₀	Concentration of inhibitor that caused 50% inhibition of the enzymatic reaction
INCI	International Nomenclature of Cosmetic Ingredients
Log P	Octanol-water partition coefficient
NBS	<i>N</i> -bromosuccinimide
NMR	Nuclear magnetic resonance
O/A	Oléo-em-água
O/W	Oil-in-water
O/W/O	Oil-water-oil
PEG	Polyethylene glycol
POE	Polyoxyethylene
RPM	Revolutions per minute
SAR	Structure-Activity Relationship
SDS	Sodium dodecyl sulfate
Ser	Serine
SLPI	Secretory leucocyte protease inhibitor
TBTU	<i>O</i> -(Benzotriazol-1-yl)- <i>N,N,N',N'</i> -tetramethyluronium tetrafluoroborate

TEWL	Transepidermal Water Loss
TFA	Trifluoroacetic acid
TLC	Thin layer chromatography
W/O	Water-in-oil
W/O/W	Water-oil-water

Abstract

Human neutrophil elastase (HNE) is a serine protease characterized by a serine residue in the active site. This enzyme is involved in the degradation of matrix proteins playing an important role in inflammation modulation. Hereupon, the excess of HNE may trigger several pathological conditions, such as psoriasis. Active substances may be administered through the skin (topical delivery), allowing the treatment of skin diseases, using suitable vehicles such as emulsions and microemulsions.

In this work different compounds containing a 4-oxo- β -lactams scaffold, that could act against HNE were synthesized, taking into account the preceding studies carried out by our group. The total characterization through NMR, FTIR, melting point, mass spectrometry and elemental analysis, was made for all. To facilitate the localization and quantification of compounds during the drug release studies, a fluorophore was synthesized and coupled to the compounds with highest cell viability (**18** and **22**) originating two new compounds, **27** and **28**. These new compounds were also characterized through NMR, FTIR, melting point, mass spectrometry and elemental analysis. Through the analysis of all characterization performed for the compounds, it could be noted that all compounds were successfully synthesized.

In vitro cytotoxicity and serine proteases assays were performed to determine the activity of each compound regarding cell viability and enzyme selectivity. Compounds **27** and **28** showed similar activities and selectivity against HNE, however compound **27** presented a cell viability of 91.6%, being chosen to be incorporated into the topical delivery systems. Therefore, the results showed that the 4-oxo- β -lactams scaffold is fundamental to the development of HNE inhibitors and some substituents in this scaffold could maintain the activity and improve the cell viability.

Topical delivery systems (oil-in-water (O/W) emulsions and microemulsions) were developed, optimized and characterized. Different humectants, preservatives were studied as well as the influence of different concentration of cetyl alcohol in the final properties of the O/W emulsions. Oils containing different carbon chains were incorporated into microemulsions to mimic the skin lipid layer. All formulations were characterized through organoleptic characteristics, pH and rheology. Droplet size

distribution, *in vivo* biological efficacy (hidration, TEWL and moisture evaluation) and sensorial analysis were performed on final formulations.

All formulations present suitable topical physicochemical properties. There were no significant differences among the formulations and with the control area concerning the *in vivo* biological evaluation. From the sensory data analysis, volunteers preferred the O/W emulsion to microemulsion since this formulation presented an easy application, low oiliness and low shine.

Finally, compound **27** was incorporated in the two formulations: AAN-27 E (emulsion) and AAN-27 ME (microemulsion). Physicochemical characterization (organoleptic characteristics, pH, rheology, droplet size distribution), *in vitro* drug release and *in vivo* antipsoriatic activity studies were performed to evaluate their properties and efficacy.

The *in vitro* drug release studies showed that the amount of AAN-27 released is totally dependent on the type of formulation, where the AAN-27 E releases a higher amount of drug, when compared with AAN-27 ME. The *in vivo* antipsoriatic activity showed that microemulsions are the less indicated for skin application and emulsion can be considered an effective formulation, but it should be noted that there are no significant differences between the placebo and AAN-27 E formulation.

Keywords: 4-oxo- β -lactams, human neutrophil elastase, O/W emulsions and microemulsions, drug release, *in vivo* biological and antipsoriatic activity

Resumo

A elastase neutrófila humana (HNE) é uma protease que se caracteriza pela presença de um resíduo de serina no sítio ativo da enzima. Esta enzima está envolvida na degradação das proteínas da matriz, desempenhando um papel importante na modulação da inflamação. Assim, o excesso de HNE pode desencadear várias condições patológicas, tais como a psoríase. Substâncias ativas podem ser administradas através da pele (administração tópica) utilizando veículos adequados tais como, emulsões e microemulsões.

Tendo em conta estudos anteriores elaborados pelo nosso grupo de investigação, neste trabalho foram sintetizados compostos diferentes, que apresentam na sua estrutura uma 4-oxo- β -lactama, que favorece a atividade contra a HNE. A caracterização total dos compostos foi elaborada através de RMN, IV, ponto de fusão, espectrometria de massa e análise elementar. Para facilitar a localização e quantificação do composto durante os ensaios de libertação de fármacos, um fluoróforo foi sintetizado e acoplado nos compostos que apresentaram a maior viabilidade celular (**18** e **22**) originando dois novos compostos **27** e **28**. Estes dois compostos também foram caracterizados por RMN, IV, ponto de fusão, espectrometria de massa, análise elementar. Através da análise da caracterização realizada para todos os compostos, é possível verificar estes compostos foram obtidos.

Posteriormente, foram realizados ensaios *in vitro* de citotoxicidade, atividade inibitória e seletividade para a HNE, de forma a determinar a viabilidade celular, atividade e a seletividade de cada composto para esta enzima. Os compostos **27** e **28**, demonstram atividades e seletividades semelhantes para a HNE, porém o composto **27** apresentou uma viabilidade celular de 91.6%, sendo o escolhido para ser incorporado nas formulações. Deste modo, os resultados obtidos *in vitro*, demonstraram que é fundamental que os inibidores contêm uma 4-oxo- β -lactama e que através da introdução de alguns substituintes nesta estrutura foi possível manter a atividade e melhorar a viabilidade celular.

Sistemas de administração tópica (emulsões óleo-em-água (O/A) e microemulsões) foram desenvolvidos, otimizados e caracterizados. Foram estudados diferentes humectantes e conservantes bem como a influência de diferentes concentrações de álcool

cetílico nas propriedades finais das emulsões O/A. Óleos contendo diferentes cadeias de carbono foram incorporados nas microemulsões para mimetizar a camada lipídica da pele. Todas as formulações foram caracterizadas (características organoléticas, pH e reologia). Distribuição do tamanho das gotículas, estudos de eficácia biológica *in vivo* (hidratação, TEWL e avaliação da hidratação) e análise sensorial foram realizadas nas formulações finais.

Todas as formulações apresentaram propriedades físico-químicas tópicas adequadas. Em relação à avaliação biológica *in vivo*, não se verificaram diferenças significativas entre as formulações e a área de controlo. A partir da análise dos dados obtidos do estudo sensorial, os voluntários preferiram a emulsão O/A à microemulsão, uma vez que esta formulação apresentava fácil aplicação, baixa oleosidade e brilho.

Por fim, o composto **27** foi incorporado nas duas formulações: AAN-27 E (emulsão) e AAN-27 ME (microemulsão). Foram realizados estudos de caracterização físico-química (características organoléticas, pH, reologia, distribuição do tamanho de gotículas), libertação de fármacos *in vitro* e atividade antipsoriática *in vivo* para avaliar as propriedades e a eficácia de ambas as formulações.

Para concluir, os estudos de libertação de fármacos *in vitro* demonstraram que a quantidade de composto libertada é dependente totalmente do tipo de formulação, onde a AAN-27 E apresenta uma maior quantidade de libertação de fármaco, quando comparado à AAN-27 ME. Através do estudo da atividade antipsoriática *in vivo* verificou-se que as microemulsões são as menos indicadas para aplicação na pele e a emulsão pode ser considerada uma formulação eficaz, porém não existem diferenças significativas entre o placebo e a formulação AAN-27 E.

Palavras-chave: 4-oxo- β -lactamas, elastase neutrófila humana, emulsões e microemulsões O/A, libertação de fármacos, atividade biológica e antipsoriática *in vivo*.

1. Introduction

1.1. Proteases

Proteases are enzymes that hydrolyze peptide bonds of proteins into smaller peptides or amino acids, both in prokaryotic and eukaryotic cells. Proteases can control the cellular reactions, through the cleavage of protein substrates and can be very important in human health. These proteolytic enzymes regulate the proteins' activation, synthesis and turnover, as well as many physiological processes such as digestion, blood coagulation, cell-differentiation and growth, cell-signalling and immune response. ⁽¹⁻⁵⁾

These enzymes must be highly regulated within cellular system. Proteases are not synthesized with an inhibitory prodomain, but are translated as inactive zymogens that require the binding of a cofactor or post-translational modification to become active. After activation, they can be regulated by endogenous inhibitors, changes in subcellular localization and degradation. If not regulated and controlled, the enzymatic activity of the proteases can cause several diseases such as viral infections, inflammation, arthritis and neurodegenerative conditions like Alzheimer's disease. ^(1,6)

The hydrophobicity or hydrophilicity and the size of proteases' active sites define which amino acid side chains of polypeptide substrates can bind to these enzymes. In general, the linkage between the proteases and their substrates takes place in the groove, where hydrolysis of the amide bond occurs. In the groove, the sub-sites of the enzyme, that are occupied by amino acid side chains of substrates, are designated as S₃, S₂, S₁, S₁', S₂', S₃'. Consecutively, the sub-sites bind to the corresponding substrate or inhibitory residues, designated as P₃, P₂, P₁, P₁', P₂', P₃'. The designations are related to the cleavable amide bond, as shown in figure 1. ^(4,6)

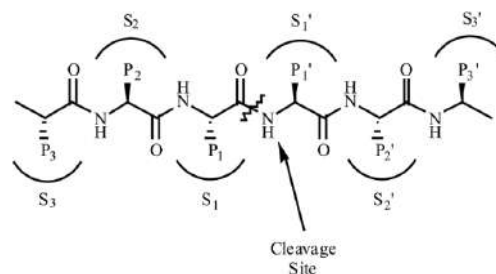


Figure 1 - Proteases active sub-sites. Adapted from (6).

Despite all similarities between the proteases, they present differences in size, location, and quaternary structure. To simplify, proteases are grouped into five different families:

serine proteases, cysteine proteases, threonine proteases, aspartic acid proteases and metalloproteases. The first three proteases use nucleophilic active-site residues to hydrolyze peptide bonds, while the remaining two use active-site residues to activate water molecules for nucleophilic attack. ^(1,6)

1.1.1. Serine Proteases

Serine proteases are the biggest known family of proteases, representing almost one-third of all proteases currently identified and are characterized by a serine residue in the active site of the enzyme. This family of proteases is present in eukaryotes, prokaryotes, bacteria, and archaea and is known for presenting a catalytic triad composed of residues of aspartic acid (Asp), histidine (His) and serine (Ser), more specifically Asp¹⁰², His⁵⁷ and Ser¹⁹⁵. ^(2,7)

The activity of these enzymes is dependent on the catalytic triad where there are many hydrogen bonds established mostly between the OH of Ser¹⁹⁵ and NH of His⁵⁷ and among the NH of His⁵⁷ and O of Asp¹⁰². ^(7,8)

Beyond the catalytic triad, the active site of serine proteases also comprises an oxyanion hole. The reaction between the substrate and the active site of the enzyme consists of an acylation and a subsequent deacylation steps. ^(4,7)

There are some problems that proteases must overcome when they are hydrolyzing a peptide bond, such as: amide bonds are very stable due to electron donation from the amide nitrogen to the carbonyl; amines are poor leaving groups; water is a poor nucleophile. ⁽⁷⁾

The mechanism begins with the nucleophilic attack of Ser¹⁹⁵ to the carbonyl group of the peptide substrate, under base catalysis by the imidazole side chain of His⁵⁷, yielding a tetrahedral intermediate (figure 2). The resulting structure, with the His⁵⁷ protonated, is stabilized by the hydrogen bond of NH to Asp¹⁰², while the oxyanion of the tetrahedral intermediate is stabilized by a hydrogen bond of Ser¹⁹⁵ and Gly¹⁹³ (Glycine), which forms the oxyanion hole. The tetrahedral intermediate break down due to the transferring of a proton from His⁵⁷-H⁺ with expulsion of the fragment amine as a good leaving group, yielding the acyl enzyme intermediate. ^(4,7)

The deacylation reaction occurs with a nucleophilic attack by water, assisted by His⁵⁷, forming a new tetrahedral intermediate. The collapse of this intermediate happens via acid basic catalysis by His⁵⁷, originating a carboxyl acid product and regenerating the amino acid Ser¹⁹⁵. (4,7)

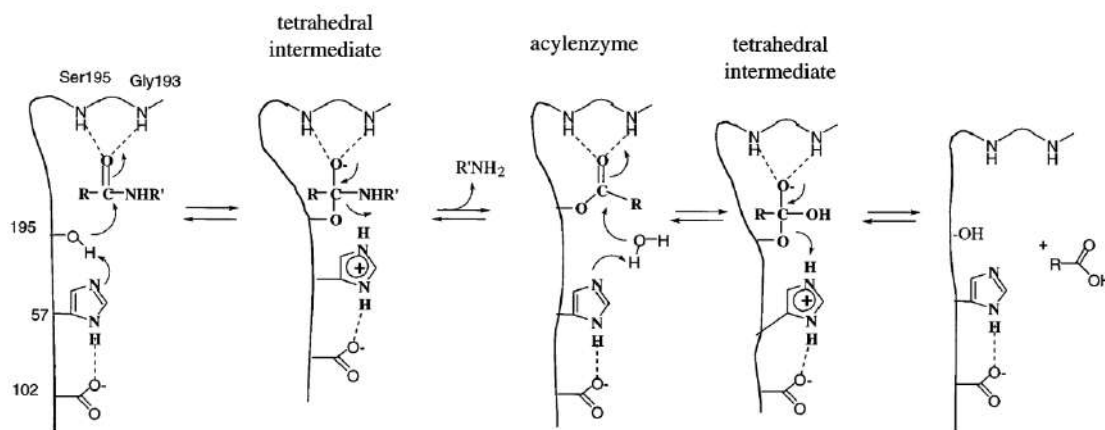


Figure 2 - Mechanism of deacylation reaction. Adapted from (7).

Generally, the kinetic mechanism of the reaction has three main steps: (1) the formation of a complex (E-S, Enzyme-Substrate), (2) the acylation of the active site in the serine protease and (3) the hydrolysis of the acyl enzyme intermediate. (7)

The serine proteases can be divided into clans, due to structural and catalytic similarities, such as PA, SB, SC and SF clans. Each clan presents different types of serine proteases. For example, clans SC and SF contain various types of peptidases, while PA comprises the trypsin-like, chymotrypsin-like and elastase-like serine proteases. (3)

In the PA clan, the serine proteases are classified by their substrate specificity, based on the nature of the P1 residue in their peptide substrates. Thus, the trypsin-like proteases cleave, preferably, the protein substrates positively charged in lysine and arginine residues at P1. The optimal activity for this specific enzyme is between pH 7.5 and 8.5. (4,6,9)

On the other hand, the chymotrypsin-like proteases are the most abundant in nature and are known to cleave substrates after large hydrophobic residues of phenylalanine, tyrosine and leucine amino acids. (4,6,7)

Lastly, the elastase-like proteases cleave substrates after a small hydrophobic residue of alanine and valine at P1. The neutrophil elastase, proteinase 3 and cathepsin G are well

known enzymes that belong to this subfamily. Due to the high level of relevance for this work, the human neutrophil elastase will be further elaborated. ^(3,6)

1.2. Human Neutrophil Elastase

Human neutrophil elastase (HNE) is a serine protease with a single polypeptide chain that belongs to the elastase-like serine proteases subfamily and is stored and secreted from polymorphonuclear neutrophils. In turn, neutrophils are transient cells that can contribute to parenchymal destruction through elastolytic enzymes, such as HNE. ^(3,10-12)

This enzyme is a small soluble glycoprotein that has a molecular weight of 29-33kDa, comprises 218 amino acid residues and is stabilized by four disulphide bridges. Since this is a serine protease, its activity depends on a catalytic triad consisting of Ser¹⁹⁵, His⁵⁷ and Asp¹⁰² which are together at the active site of the enzyme on its tertiary structure. ⁽¹²⁻¹⁴⁾

First, the synthesis of HNE is regulated at the transcriptional level during granulocyte development and then, at the post-translational level. After this, the enzyme is stored in its proteolytically active mature form within neutrophil azurophilic granules. ⁽²⁾

As well as other enzymes, HNE also presents endogenous ligands that act as their inhibitors. Under physiological conditions, and during inflammation, endogenous HNE inhibitors tightly regulate their activity avoiding degradation of connective tissue proteins including elastin, proteoglycans and collagen. The regulation occurs in the extracellular and pericellular space. ^(2,13)

The three main endogenous inhibitors of HNE belong to two different families depending on their tissue location: the serpins and the chelonianins. The α 1-antitrypsin belongs to the serpins' family and elafin and secretory leucocyte protease inhibitor (SLPI) fit into the chelonianins' family. ^(2,15)

The α 1-antitrypsin is a water-soluble glycoprotein with 394 amino acids classified as systemic HNE inhibitor. Mainly, this inhibitor is synthesized by hepatocytes and is particularly abundant in the lungs. The circulating levels of α 1-antitrypsin are between 1.2 and 2 mg/mL in healthy people, but during some phases of inflammation and infection

this value can increase. This inhibitor is considered irreversible and the second-order constant of association with the enzyme is $6.5 \times 10^7 \text{ M}^{-1} \cdot \text{s}^{-1}$.^(2,14)

Elafin and SLPI are nonglycosylated inhibitors with 6kDa and 11.7kDa of weight, respectively. Both inhibitors have almost the same residues in the active site and are considered basic inhibitors with an isoelectric point of 9.7 for elafin and more than 11 for SLPI.⁽²⁾

It is still worth pointing out that elafin was the first to be isolated from the skin of psoriasis patients, however it is also present in lung secretions. *In vivo*, it is usually present under inflammatory conditions, suggesting that this inhibitor is inducible. This inhibitor has a second-order constant of association with the enzyme of $5 \times 10^6 \text{ M}^{-1} \cdot \text{s}^{-1}$, being considered a potent reversible inhibitor to this enzyme.^(2,16)

As for SLPI, it is found in higher concentrations in the upper airways and at low concentrations in the deep lung, however this substrate is present in all body fluids, including tears, salivary glands, bronchial secretions and intestinal mucus. With respect to inhibition, SLPI is a reversible inhibitor of HNE with a second-order constant of association of $6.4 \times 10^6 \text{ M}^{-1} \cdot \text{s}^{-1}$.⁽²⁾

In terms of biological function, HNE has bactericidal properties, since neutrophils are the first line of antibacterial defense of human body, because they can use antimicrobial peptides and proteases to degrade microorganisms. This enzyme is also involved in the preservation of tissue homeostasis and can repair damaged tissue. Moreover, HNE is important in the inflammation process. In a normal inflammatory process, neutrophils (regulated by the endogenous ligands) release a high concentration of HNE to the extracellular medium where this enzyme can modulate the immune response at sites of inflammation through degradation of pro-inflammatory cytokines to reduce the intensity of the inflammation.^(2,14,17)

On the other hand, if an imbalance between HNE and its endogenous inhibitors happens during an inflammatory process, the extracellular HNE, that is now in excess, can degrade some natural substrates, such as structural proteins of the extracellular matrix, like elastin, proteoglycan, collagen and fibronectin. HNE still acts on the cleavage of inflammatory mediators, lung surfactants and receptors, where it, preferentially,

hydrolyses peptide bonds nearby to small aliphatic amino acid residues (alanine and valine).^(2,10,12,18)

Hereupon, the excess of HNE may trigger several pathological conditions, namely tissue injuries inducing chronic inflammatory diseases, such as: chronic obstructive pulmonary disease, acute respiratory distress syndrome, rheumatoid arthritis, psoriasis and cystic fibrosis. In addition to being involved in inflammatory processes, this serine protease is also known to be involved in some processes of skin aging and more recently demonstrated progression of non-small cell lung cancer.^(13,14,17-19)

Therefore, HNE is a valuable therapeutic target and the design of new HNE inhibitors, able to modulate the proteolytic activity of HNE, represents promising therapeutics for all the above mentioned diseases, where there is an excess in the production of this serine protease.⁽¹³⁾

1.2.1. Inhibitors of Human Neutrophil Elastase

Over the years, research and development of HNE inhibitors has experienced a significant increase, to discover new molecular structures. Numerous chemical classes have been developed, including, for example, 4-oxo- β -lactams, benzoxazinones, diazo compounds or haloketones (figure 3).^(5,11,19)

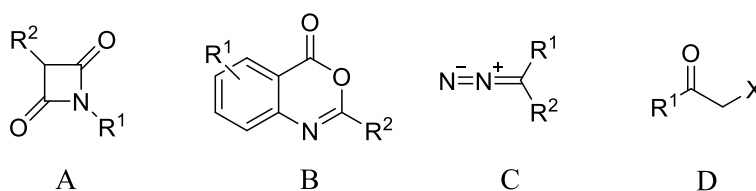


Figure 3 - General structure of the following compounds: 4-oxo- β -lactam [A], benzoxazinones [B], diazo compounds [C] and haloketones [D].

In the development of new inhibitors, it is necessary to consider not only the size and chemical nature of the structure to decide the route of administration (oral, intravenously, topical or aerosol, for example), but also the enzyme selectivity and appropriate pharmacokinetic and pharmacodynamic properties.^(2,4)

Synthetic inhibitors of HNE need to have some peptide character to be effective drugs, since substrates with aliphatic amino acid side chain in the S1 pocket are more favored. The use of peptides as drugs is usually characterized by their instability, poor pharmacological profiles and low bioavailability. Ideally, to use this type of drug in therapy, it must contain low susceptibility to elimination, long lifetimes in the bloodstream and in cells, high selectivity, good bioavailability (for oral delivery), high stability to nonselective proteolytic degradation and good membrane permeability. These properties are usually achieved when low molecular weight drugs are synthesized ($\leq 1000\text{Da}$).^(4,20)

Serine protease inhibitors can be categorized in non-covalent and covalent inhibitors. This last category includes three different types: transition-state analogues, mechanism-based inhibitors and acylating agents. In addition, inhibitors may still be classified as reversible or irreversible. In the case of HNE, reversible inhibitors are preferred since they present less toxic side effects and do not need to have a greater selectivity for this enzyme.^(4,12,21)

1.2.1.1. Transition-state analogues

The transition-state analogues are a type of inhibitors that form a tetrahedral adduct with the active site Ser¹⁹⁵ and, at the active site of the enzyme, explore favorable binding interactions with multiple subsites. Due to their high potency, they usually have an inhibition constant in the nanomolar range.⁽²²⁾

The design of protease inhibitors based on peptide aldehydes (figure 4) was disclosed in 1960 and this approach was used to research new HNE inhibitors, as the peptide structure allows a better recognition by the enzyme. Peptide aldehyde compounds have many metabolism issues due to their intrinsic characteristics. Therefore, the hydrogen atom of these compounds was replaced for an electron withdrawing group (EWG) in order to accomplish higher stability and electrophilicity on the carbonyl carbon atom. Several substituents such as fluoromethyl, bromomethyl, iodomethyl, trifluoromethyl, difluoromethylene ketones, heterocycle, amide and ester groups, were attached to the peptidyl recognition element for a better binding of the inhibitor to the active site.^(5,12,22)

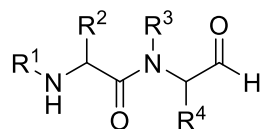


Figure 4 - General structure of a peptide aldehyde.

Peptidyl chloromethyl ketones were one of the first serine protease inhibitors developed, and they are an example of serine protease irreversible inhibitors. In this case, the tetrahedral adduct with the carbonyl group of the inhibitor is formed, but an additional binding between the His⁵⁷ and the inhibitor is established. His⁵⁷ is alkylated by the chloromethyl ketone and forms an irreversible tetrahedral adduct (figure 5).⁽⁵⁾

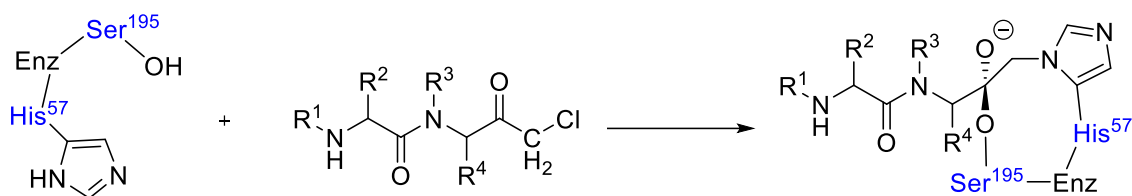


Figure 5 - Scheme of the interaction of an irreversible transition state inhibitor. Adapted from (5).

Since reversible inhibition is preferred relatively to irreversible inhibition, new substituents had to be studied, such as bromomethyl, iodomethyl and fluoromethyl ketones. The first ones showed a higher reactivity, but are less stable in aqueous solutions, while the fluoromethyl ketones revealed a higher reactive and selective irreversible inhibition for cysteine proteases, instead of the serine proteases.⁽⁵⁾

When the EWG trifluoromethyl substituent was tested, it showed a reversible interaction with the HNE active site as intended. The interaction of EWG and serine proteases is present in figure 6.^(5,12,22)

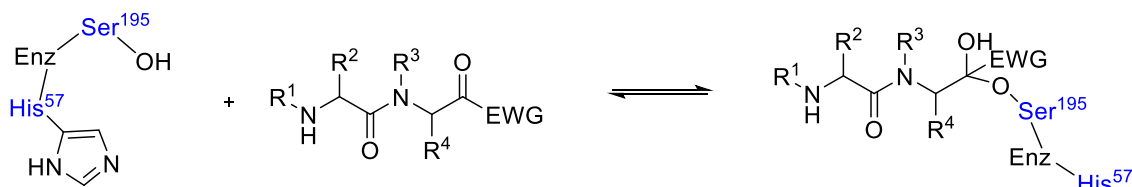


Figure 6 - Scheme of the interaction of a reversible transition state inhibitor. Adapted from (22).

1.2.1.2. Mechanism-based inhibitors

A mechanism-based inhibitor is an inherently unreactive molecule able to inhibit the enzyme after the catalytic process originates a highly reactive electrophilic species. Posteriorly, these species react with an active site nucleophilic residue provoking an irreversible inactivation of the enzyme. ^(12,21)

One example of this type of inhibitors are the saccharin-like compounds. Saccharin is a heterocycle molecule known as an artificial sweetener, but due to its biological activity it has become very popular in the past decades. These compounds are selective for HNE and the inhibition mechanism was proposed to start by the attack of Ser¹⁹⁵ at the carbonyl carbon, following by a Michael addition of the imidazole of His⁵⁷ to the sulfonyl imine conjugated system, leading to the final compound (figure 7). ^(12,22)

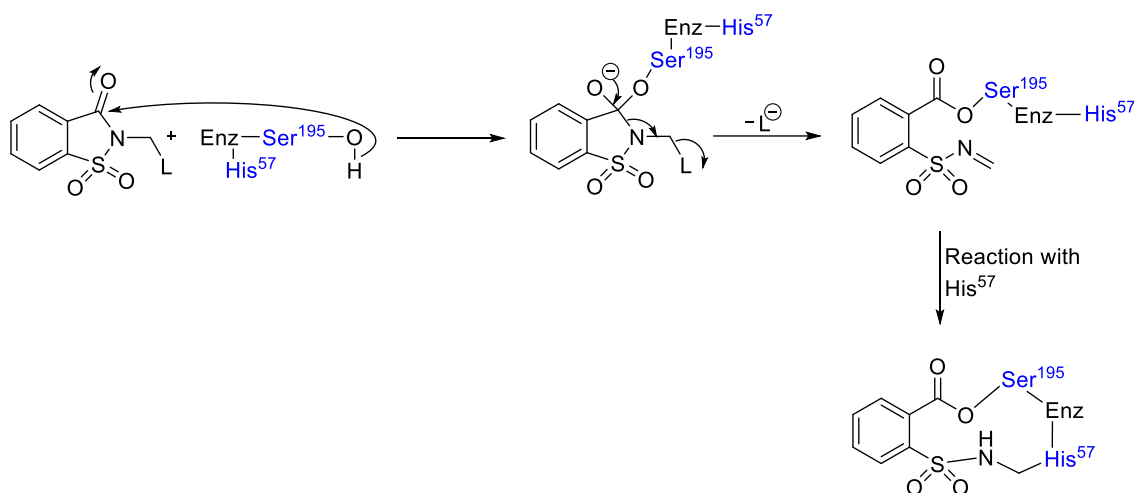


Figure 7 - Mechanism of inhibition to HNE by Saccharin-like compounds. Adapted from (12).

1.2.1.3. Acylating agents

In this last class of inhibitors, the mechanism of action comprises the acylation of HNE, like in some mechanism-based inhibitors. Initially, the hydroxyl group of the Ser¹⁹⁵ attacks the carbon of one carbonyl group of the inhibitor, forming a tetrahedral intermediate. With the expulsion of a leaving group, it is possible to afford a very stable acyl-enzyme complex, stabilized by two hydrogen bonds with the oxyanion hole. This linkage depends on electronic and steric effects. ^(12,21)

For many years, this type of inhibitors was considered irreversible due to the high stability of the complex formed. Therefore, for many years the main aim was the development of reversible acylating agents also capable of forming stable acyl-enzymes.
(12)

Recently, several compounds with HNE inhibitory activity, such as β -lactams, benzoxazinones, azetidine-2,4-diones, succinimide-like compounds and coumarins have been reported (figure 8).

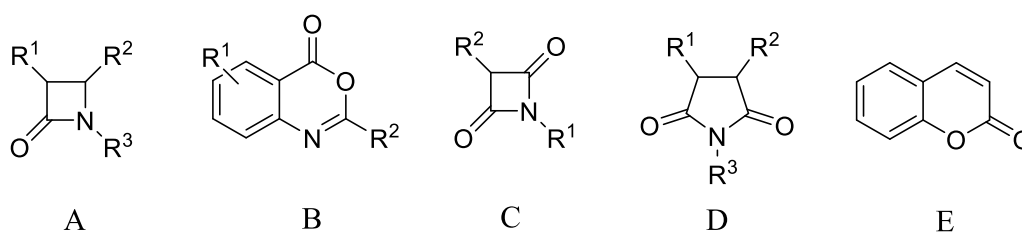


Figure 8 - Chemical structure of β -lactams [A], benzoxazinones [B], azetidine-2,4-diones [C], succinimide-like compounds [D] and coumarinas [E].

The first studies with compounds with a β -lactam structure were performed by the Merck group in 1990, where it is showed that this compound could have activity against some serine proteases, such as human elastase. The first β -lactam compounds which were shown to inhibit this protease were based on natural compounds, such as cephalosporins and clavams (figure 9). Further studies developed by the same group demonstrated, in 1992, that monobactams were stable, potent, specific compounds for this serine protease.
(23–25)

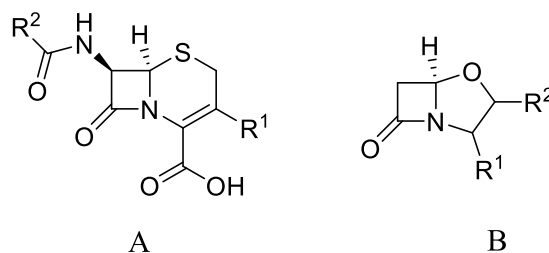


Figure 9 - Chemical structure of cephalosporins [A] and clavams [B].

Recent studies show us that the structure of β -lactams inhibitors allows a great improvement of the rate of serine acylation because they increase the intrinsic chemical reactivity, when compared with other compounds. Therefore, they have been further

studied and investigated as they have become a successful strategy to design more potent elastase inhibitors. ^(12,17,22)

The synthesis of new compounds with a β -lactam structure, such as the azetidine-2,4-diones, has been increasingly studied. These compounds, also known as 4-oxo- β -lactams (figure 8C) demonstrated to be a very potent and selective class of acylating agents for HNE and they follow the mechanism of action described above (figure 7). Thus, due to the high interest in this type of compounds, the azetidine-2,4-diones inhibitors were tested in this study, having used a compound previously synthesized in the group⁽¹⁹⁾, the 3,3-diethyl-1-(4-(((2-oxo-2H-chromen-7-yl)oxy)methyl)phenyl)azetidine-2,4-dione (figure 10 compound **1**) as a control. In figure 10, shown below, it is possible to see the interaction between HNE and this compound. ^(12,17,22)

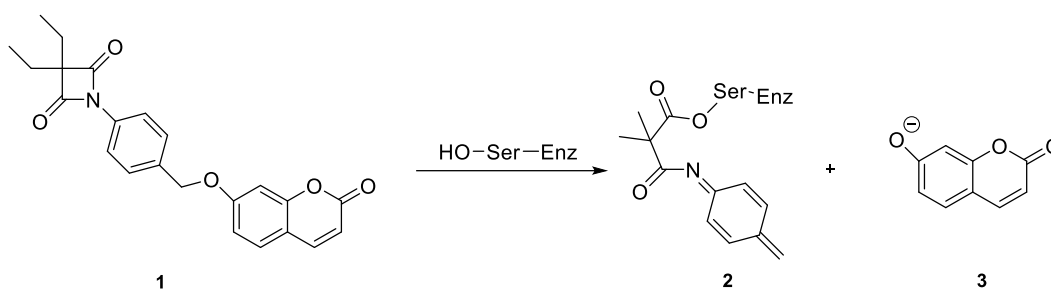


Figure 10 - Interaction between HNE and compound **1**.

Currently, there is one acylating agent used in therapy known as ONO-5046 or Sivelestat (figure 11). This HNE competitive and selective inhibitor is a small molecule only marketed in Japan and Korea for the treatment of acute lung injury associated with systemic inflammatory response syndrome. ^(13,22)

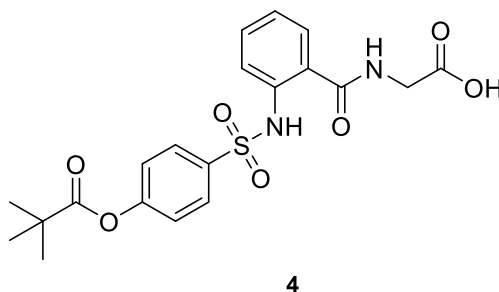


Figure 11 - Chemical structure of ONO-5046.

Sivelestat has an IC_{50} value of $0.044\mu M$ and a K_i value of $0.2\mu M$, is highly specific against HNE, presents a low toxicity and is intravenously effective. This compound has

low oral bioavailability mainly due to the first-pass metabolism. The mechanism of inhibition of this compound is present in figure 12. ^(4,26,27)

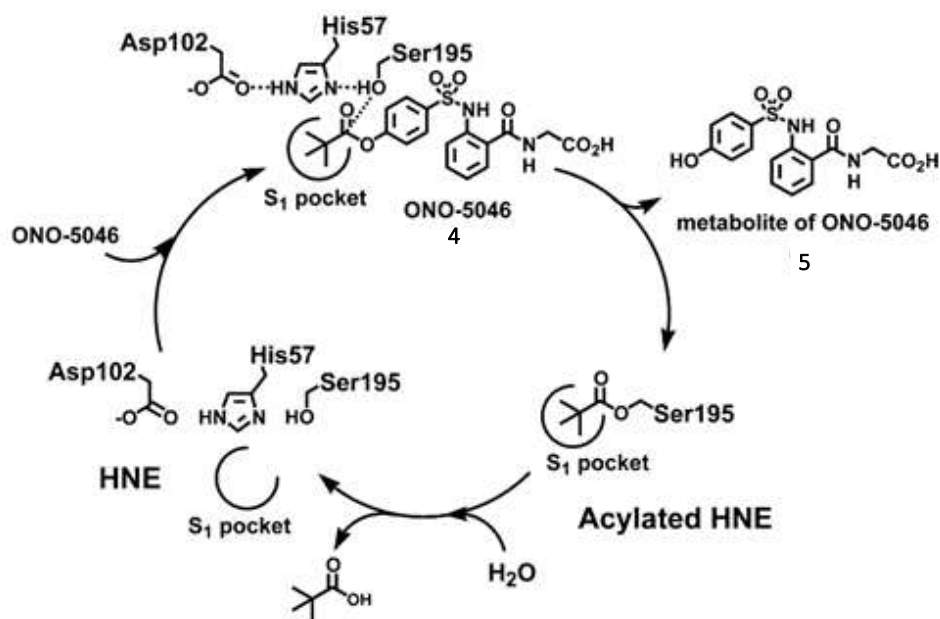


Figure 12 - Mechanism of inhibition of Sivelestat. Adapted from (26).

1.3. Psoriasis

Psoriasis is a chronic inflammatory skin disease that commonly affects people of all ages, and in all countries. This disease is characterized by some red, scaly and erythematous plaques that can be scattered over the entire surface of the body or in a specific area, including the scalp, nails and joints. Psoriasis is considered a non-communicable disease with no cure (medication is only used to reduce the physical symptoms), and it may progressively worsen with age, depending on the degree of severity. ^(28–30)

The diagnosis of psoriasis is focused on the clinical morphologic evaluation of the skin lesion. Since psoriasis may present variable clinical manifestations, the diagnosis can be very difficult. ^(31,32)

This disease affects about 2-5% of the world population, being more prevalent in American, Canadian and European people. Patients report a significant reduction in their quality of life due to the great impact caused on self-image and self-confidence. ^(33–35) Not

only depression and anxiety are commonly seen in these patients but also metabolic diseases, such as diabetes and cardiovascular diseases. ^(34,36)

The causes of psoriasis are not totally understood, but this pathogenesis is associated with genetic and epigenetic modifications that can be triggered by environmental factors, such as smoking, stress, obesity, and alcohol. ^(29,32)

In the same way as mentioned above, neutrophils are the most abundant leukocytes in humans, representing the first line of defense against an immune attack by pathogens. In a psoriatic skin, they are mainly located in the epidermis and neutrophil chemokines, such as CXCL1, CXCL2 and CXCL8/IL-8, are also present. ^(37,38)

The chemokines are considered a subgroup of cytokines and are classified giving the number and arrangement of cysteine residues (structural characteristics). These proteins are involved in the development and recruitment of immune cells in the innate and adaptive immune responses. In inflammatory diseases, like psoriasis, some of the chemokine activity is through the recruitment of cells of innate immunity. ⁽³⁹⁾

Although psoriasis is an inflammatory disease where reactions are driven by endogenous signals, it is also considered an autoimmune skin disease mediated by the cells and molecules of the innate and adaptive immune system, such as T or B cells. These two processes frequently co-exist and one may cause the other. ^(38,40)

Therefore, from the inflammatory point of view, psoriasis consists of an extravascular recruitment of neutrophils that show a central role in the development of tissue injury. When high levels of neutrophils persist in the epidermis, it may cause irreversible destruction of normal skin tissue, leading to thickening of the epidermis, extensive tissue damage, exacerbate inflammation and, in a worst scenario, to organ dysfunction. ⁽⁴¹⁻⁴³⁾

There are a few clinical variants of psoriasis, such as psoriasis vulgaris, guttate, palmoplantar, scalp and pustular psoriasis. The most common type of this disease is psoriasis vulgaris present in, approximately 90% of patients. The lesions are characterized by dry and sharply demarcated plaques. Usually, in the beginning, these lesions start as erythematous papules, extend peripherally, and coalesce to form plaques. Psoriasis plaques can be seen at any part of the body, although they are more commonly seen in elbows, knees and scalp. ^(34,35)

On the other hand, pustular psoriasis can present two different forms localized on hands and feet or generalized, being, the last one, the most uncommon type of psoriasis. The injuries of generalized pustular psoriasis cause debilitation, being considered a life-threatening disease, since neutrophils infiltrate the skin taunting the development of pustules, generalized erythema and desquamation. ^(34,44)

1.3.1. Current therapeutics

The treatment of psoriasis is based on control of symptoms, since there is no cure for this disease. Currently, phototherapy (ultraviolet light), systemic and topical therapies using drug delivery systems, where most drugs include corticosteroids, vitamin D analogous, retinoids and dithranol, are commonly used. ^(30,32,45)

Phototherapy frequently involves exposure to ultraviolet B, short wavelength of ultraviolet light. In cases where the symptoms remain the combination of oral (psoralen) and ultraviolet A, a longer wavelength ultraviolet light, is applied. This method of therapy is avoided and used only in special cases of severe or moderate psoriasis since the side effects of phototherapy include skin damage and an increased risk of developing skin cancer. ⁽⁴⁵⁾

For severe and resistant cases of psoriasis, systemic treatments include orally and intravenously drugs such as methotrexate, ciclosporin and biological agents. These have been released recently into the market and act at the level of immunopathogenesis of the disease. Some examples of these drugs are infliximab, etanercept and efalizumab, but the latter has already been reported by US Food and Drug Administration (FDA) and European Medicines Agency (EMA), because it presents a potential risk for patients to develop progressive multifocal leukoencephalopathy. ⁽⁴⁵⁾

The topical therapies include corticosteroids and vitamin D analogous, which are responsible for the regulation of inflammatory response and the keratinocyte function. They are usually sufficient to treat moderate psoriasis in the face, neck, flexures and genitalia, since they have a mild to moderate potency. More potent corticosteroids only are useful for localized psoriasis on the scalp, palms and soles. The continuous use of corticosteroids is associated with some risk, such as cutaneous atrophy and loss of

efficacy, while vitamin D analogues do not show as severe side effects as corticosteroids. (32,34)

The problems with ultraviolet light and biologic agents, due to their long-term side effects and the toxicity associated with the systemic products, makes these treatments a poor way to treat this disease. Therefore, the use of corticosteroids, dithranol and vitamin D analogues through topical delivery systems is favored. Topical delivery systems reduce side effects and are easier to administer, leading to better acceptance of therapy by the patient. (32,45)

Therefore, there is no cure for this disease and the treatment of psoriasis is based on controlling the symptoms. As cited above, the current therapies have numerous disadvantages and at least 100 million individuals are affected worldwide, by this disease. This disease affects the patient, not only at the skin level, but also at the psychological level. Due to that, it is extremely necessary to keep searching for new alternatives of therapy and discover new active compounds that are able to cure this disease.

1.4. Topical delivery systems

The skin is a continuously self-renewing organ that covers the entire external surface of the body, being the largest human organ, approximately 15% of the total body weight of an adult. (46,47)

The skin multilamellar structure has been of interest to scientists since the 19th century. The developed work by Homalle (1853) and Duriau (1856) allows us to identify the main layers of skin: epidermis and dermis. Epidermis is the first *stratum* and it act as an entirely barrier mainly due to its superficial tier, the *stratum corneum*. Dermis is the second layer of the skin and presents a different degree of permeability and functions, when compared with the epidermis. Finally, the subcutaneous tier is named hypodermis and it is the deepest layer of the skin, which contains the adipose tissue. (48-50)

This organ has several functions such as, preventing the loss of water and electrolytes from the body and provides protection against external agents such as chemical, physical, pathogenic organisms and solar radiation. Beyond this, the skin also accomplishes thermoregulation and mediates inflammatory, immune and sensorial responses. Due to

these functions, mostly attributed to the outermost layer, *stratum corneum*, the skin is a barrier that does not allow the entry of external agents. ⁽⁵⁰⁻⁵²⁾

The *stratum corneum* consists of metabolically inactive corneocytes that, though its highly cross-linking of structural proteins, contribute to the mechanical strength of the skin, once they produce a rigid structure: the cornified envelope. In the cornified envelope, corneocytes are filled with water and microfibrillar keratin. The skin permeability barrier is entirely related and mediated by corneocytes that are embedded in non-polar lipids of the extracellular matrix, which form lamellar membranes with a unique composition of ceramides, cholesterol, and non-esterified fatty acids (figure 13). This membrane allows to prevent the water loss and salts from the skin. ^(47,52-54) It is important to notice that this barrier, which regulates water permeation, is not absolute, meaning that there is a normal movement of water from the *stratum corneum* to the atmosphere, which is known as transepidermal water loss (TEWL). ⁽⁴⁷⁾

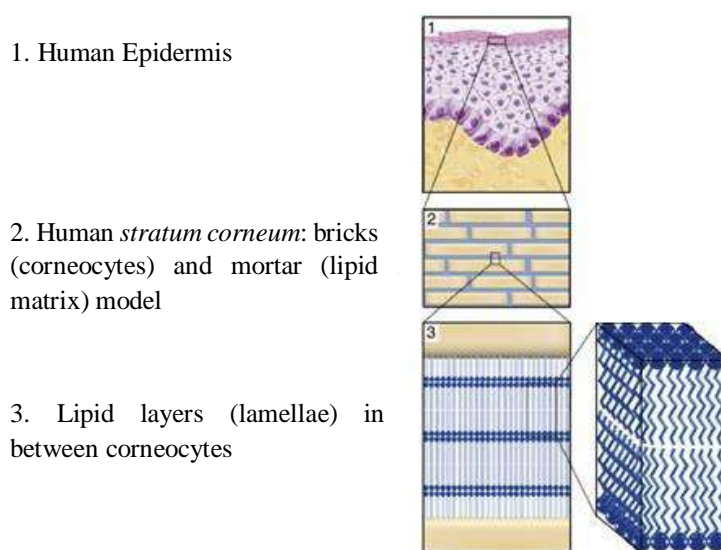


Figure 13 - Representation of corneocytes and the lipid matrix of stratum corneum (53).

The lipids from the *stratum corneum* include approximately 50% of ceramides, 15% of free fatty acids and 25% of cholesterol. The carbon atom chain length of free fatty acids ranges from C12 to C24, and they are mainly saturated, however ceramides consist of a sphingoid base and an acyl chain. ^(50,52,53)

All the mentioned components are crucial to the *stratum corneum* barrier, but they are viewed as challenging to transdermal and topical drug delivery, since it is necessary to interfere with the functional properties of these components. Drugs penetrate either via

the *stratum corneum* (transepidermal) or via the appendages (transappendageal). During penetration through the *stratum corneum*, two possible routes can be distinguished, i) penetration alternating through the corneocytes and the lipid lamellae (transcellular route) and ii) penetration along the tortuous pathway along the lipid lamellae (intercellular route). The appendageal route includes either the duct of the eccrine sweat glands or the follicular duct. ⁽⁵⁵⁻⁵⁸⁾

Due to the innumerable advantages of the topical, transdermal and transappendageal drug delivery, strategies are needed to overcome the skin barrier. However, it is important to notice that the transport through the skin also depends on the physicochemical properties of the drug and the vehicle. Active compounds, which have a higher molecular weight, will have more difficulty passing through *stratum corneum* than those having a lower molecular weight. Other properties, like the octanol-water partition coefficient (log P), the number of hydrogen-bond donors and acceptors that regulate the interactions with the surface of corneocytes and the drug solubility in the pharmaceutical vehicle, are also important properties of active compounds. ^(57,58)

Topical delivery systems are used and play an important role on the transport of active substances across the skin barrier. The vehicle used can affect, not only the potency and action of the active compound, but also the acceptability by the patient, since not all pharmaceutical forms are well accepted by them. Therefore, in addition to being a carrier for the drug, the pharmaceutical vehicle may also have functions of increasing drug permeation/absorption and skin hydration. ⁽⁵⁹⁾

The drug solubility in the vehicle is also important as this parameter is crucial to the efficacy of the final product. Most of the drugs developed in the pharmaceutical industry are practically insoluble in water, which constitutes a major challenge for the pharmaceutical technology. To enhance the solubility of the drug, various techniques can be used, such as physical and chemical modifications, droplet size reduction and formulations strategies. However, it is important to notice that the method to improve the solubility depends, for example, on drug properties and site of absorption. ⁽⁶⁰⁾

Some excipients used in the pharmaceutical formulations exhibit the property of being permeation enhancers, beyond the function already performed in emulsions, such as ethanol, isopropyl myristate, propylene glycol and oleic acid.

Skin permeation enhancers are used in topical and transdermal delivery systems to promote the transport of drugs into and across human skin. The mechanism can occur by increasing the solubility of the permeant in the *stratum corneum* with change in the solubility parameter of the skin. Accordingly, there is an increase in the flux of the drug through the skin. The second possible mechanism is the disturbance of the lipid structure of the *stratum corneum* by changing the skin barrier properties. ^(55,61)

The ideal permeation enhancer should have some properties such as: non-toxic, non-allergenic, non-irritating, compatible with most of excipients (pharmacologically inert) and drugs, and should also have a reversible action on the skin, so that when removed from the skin, the barrier's properties return. ^(56,62)

Ethanol (figure 14) is known as co-solvent for lipophilic drugs among the pharmaceuticals, but since it has a well-established systemic toxicology and local tolerability, it is currently used in commercial transdermal delivery systems as a permeation enhancer. This solvent damages the intercellular material, which results in cutaneous barrier disruption in the *stratum corneum*. Consequently, a drug release increase is observed. ^(55,63,64) The literature describes ethanol as a permeation enhancer, once it delipidates the skin when incorporated in the pharmaceutical vehicle. ^(63,65–67)

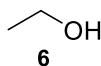


Figure 14 - Chemical structure of ethanol.

Isopropyl myristate (figure 15) is the most common excipient used as permeation enhancer that belongs to the fatty acid esters family. The literature ^(68,69) suggests that the mechanism of action is the integration of this component into the lipid bilayer of the skin with consequent increment in lipid fluidity. Isopropyl myristate interacts with the lipids through the isopropyl group in the polar region of the layer. This excipient may also promote the drug solubility in the skin. ⁽⁵⁶⁾

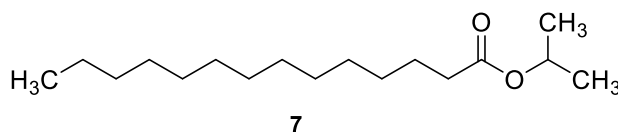


Figure 15 - Chemical structure of isopropyl myristate.

Propylene glycol (figure 16) belongs to the glycol family and has been used in skin formulations since 1932 with the aim of enhancing drug permeation through the skin. However, its mechanism of action is not completely understood. A study made by Bouwstra *et al.* (70) suggests that this component does not incorporate into the lipid bilayers of skin and may be incorporated in the head group regions of the lipids thus not interfering with the lipidic lamellar structure. Besides being able to be used alone, propylene glycol also exhibits synergistic effects with other components used in the formulations such as oleic acid. ^(56,62)

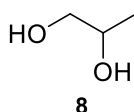


Figure 16 - Chemical structure of propylene glycol.

Oleic acid (figure 17) is the most popular permeation enhancer inside the fatty acid family. The mechanism comprises the destabilization of the lipids' domains of the *stratum corneum*, through the diffusivity of skin permeants, since it has a long carbon side chain. However, Golden *et al.* (71) reports that only the *cis* configuration of the oleic acid molecule is effective as permeation enhancer. The fatty acid compounds have alkyl chains with lengths around C10-C12 and can be saturated or unsaturated, but in unsaturated molecules the *cis* configuration is expected to disturb more the lipid arrangement present in skin than the *trans* configuration. ^(56,62)

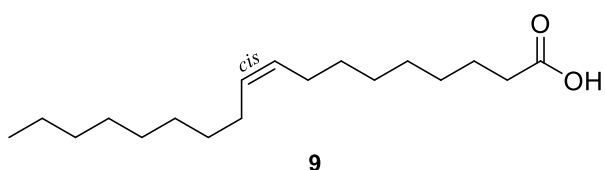


Figure 17 - Chemical structure of oleic acid.

Topical delivery systems comprise some pharmaceutical vehicles such as, ointments, gels, emulsions, microemulsions, suspensions, pastes, solutions, nanoparticles among others. Emulsions and microemulsions are going to be the focus of this chapter since they were the two pharmaceutical forms chosen to develop in this work.

1.4.1. Emulsions

Pharmaceuticals emulsions are heterogeneous systems composed of two immiscible liquids (water and oil). Considered liquid-liquid colloidal systems, they have a dispersed phase (internal phase) and a continuous phase (external phase). ^(57,72,73)

In the microscopic aspect, emulsions contain droplets with a mean diameter of more than 1µm. However, nanoemulsions can be formed with droplet sizes in the 100–50 000nm range, and with proper formulation, highly stable microemulsions can be prepared having droplets as small as a few nanometers. ^(73,74)

From the thermodynamic point of view, these colloidal systems are considered unstable and to understand this behavior it is necessary to take into account the second law of thermodynamics, that allows to state the following equation (1):

$$\Delta G^{form} = \Delta A\gamma_{12} - T\Delta S^{conf} \quad (1)$$

, where the variation of free energy for emulsion formation (ΔG^{form}) comprises two contributions: the surface energy that is represented by $\Delta A\gamma_{12}$ and the entropy of dispersions term which is equal to $T\Delta S^{conf}$, in which the T represents the temperature. ^(75,76)

The increase in surface area, when going from state I to state II (figure 18), is represented by $\Delta A (= A_2 - A_1)$, in which A_1 is, for example, the surface area of the oily phase and A_2 is the total surface area of all emulsion's oil droplets. It is also represented by the interfacial tension between the oily and aqueous phase, which is equal to γ_{12} . ^(77,78)



Figure 18 - Emulsions' process formation.

On another hand, the term $T\Delta S^{\text{conf}}$ corresponds to the increase in entropy when the emulsion is going from state I to state II. It is important to notice that in state II the entropy is higher because there is a larger number of droplets that can arrange themselves in many ways, while state I only has one drop with a much lower entropy. ^(77,78)

In the emulsions' system the term $\Delta A\gamma_{12}$ its higher than the term $T\Delta S^{\text{conf}}$. Therefore, the free energy for the emulsion formation is positive ($\Delta G^{\text{form}} > 0$), making the system non-spontaneous and thermodynamically unstable. ⁽⁷⁷⁾

Since the formation process is nonspontaneous, some energy in the work form must be provided to the system. This energy can be obtained by an emulsification process where it provides mechanical energy to the emulsion, produced by a wide range of agitation techniques. The emulsification process consists in the agitation of the two immiscible liquids with globule formation of various sizes, where the heterogeneity of the sizes is related to the forces involved during the agitation. ^(73,79)

Several methods can be applied to disrupt the droplets by the emulsification process, and it ranges from a simple pipe flow, where the agitation energy is low, to static mixers (low to medium energy), high-speed mixers/homogenizers such as Ultra-Turrax® (medium energy) and high-pressure homogenizers (high energy). In the case of the emulsions, since the droplet size is in the μm range (large droplets), the Ultra-Turrax® is commonly used in the production of emulsions. ^(75,78)

After stirring, the internal phase becomes a spherical shape which gives the minimum surface area for a given volume. However, over time, the droplets, through Brownian movement, tend to collide with each other, to reduce the interfacial area. Consequently, coalescence will happen and continue until full phase separation and the minimum free energy (equilibrium) is reached. For this reason, emulsions are one of the most difficult and complex systems in the pharmaceutical field to develop and stabilize, requiring some knowledge and experience. ^(73,80)

1.4.1.1. *Composition of emulsions*

The use of an emulsifying agent is completely necessary to obtain reasonably stable emulsions. This component can be a surfactant or a solid powder and it is able to stabilize the emulsion and facilitate the emulsification process. ^(74,81)

Surfactants are amphiphilic chemical substances that reduce the interfacial tension between the two immiscible phases in emulsions, facilitating the formation and stability of the emulsion. They show a polar head and a non-polar tail with hydrophilic and lipophilic groups, respectively, and can be classified as non-ionic, anionic, cationic and amphoteric. ^(74,82,83)

Usually, the surfactant concentration is above critical micellar concentration (CMC), in which the surfactant molecules form micelles, where the polar head of the surfactant is oriented to the aqueous phase and non-polar tail is in contact with the oily phase. Regarding the emulsion stabilization mechanism using surfactants, it compromises the adsorption of these molecules to the interface of the oil-water phase, lowering the internal tension, favoring the emulsions' stability and formation. However, the stability of emulsion increases more due to the barrier created around the interface of the droplets. ^(72,75,80,81)

Emulsifiers, fatty alcohols and acids combination interacts with the aqueous continuous phases to form lamellar or crystalline structures. These both stabilize and sometimes control the viscosity of emulsion. Although liquid crystalline phases form in many emulsions at the high temperatures of manufacture, these often convert to gel phases when the emulsion cools so that the properties of this phase dominate the emulsion. ⁽⁸⁴⁻⁸⁶⁾

Thickeners act as structural agents and confer bodying properties to emulsions, improving viscosity. Their choice confers different structures to the emulsions. Different types of thickeners, depending on their source and characteristics, such as fatty alcohols and fatty acids (i.e. cetyl alcohol and stearic acid), natural derived polymers (hydroxyethyl cellulose, xanthan gum and gelatin), mineral derived agents (magnesium aluminium silicate and silica) and synthetic derived polymers (carbomer) can be used. It is important to note that different types of thickeners help to obtain different emulsions' microstructures. ^(75,87,88)

Emollients exhibit smoothing, moisturizing and protective effects and allow to adjust the consistency, spreadability and sensorial feel of formulations. These excipients have properties that allow them to remain on the skin surface or in the *stratum corneum* and act as lubricant, improving the appearance of the skin and reducing flaking. Some characteristics such as low toxicity, skin irritation, good spreadability and stability, are very important properties to consider when choosing an emollient. The most popular emollients used in the topical formulations are lipophilic like waxes, esters, oils, mineral paraffin, and polyethylene glycol (PEG) and can be distinguished into two different categories: non-polar (paraffin, isoparaffin, cera alba and sesame oil) and polar (esters and triglycerides) as a function of their chemical structure. Other examples of emollients are isopropyl myristate (fatty acid ester) and oleic acid (fatty acid).^(80,89-91)

Other group of ingredients used in emulsion formulations are humectants. These are known to be hygroscopic molecules with several hydrophilic groups (mostly hydroxyl groups), able to form hydrogen bonds with molecules of water present in the skin. Its principal function is, therefore, to maintain and increase the amount of water in formulation and skin, acting as moisturizer. Another significant function of some humectants such as propylene glycol, is the ability to increase drug permeation through the skin (permeation enhancers). However, it is important to notice that some of them, such as urea, present a strong osmotic activity and, if not absorbed, may cause TEWL. Other examples of humectants used in pharmaceutical formulations are glycerin and ethoxydiglycol.⁽⁵⁸⁾

Preservatives prevent microbial contamination such as bacterial and fungi, and extend the shelf-life of the formulation. Since water presents an appropriate environment for most microbes, it is important that the preservatives used are water-soluble. The two most commonly used preservatives are parabens and esters of *p*-benzoic acid and phenoxyethanol. Usually, in pharmaceutical vehicles a combination of preservatives can be employed to protect against different bacterial or fungi strains.^(87,89,92,93)

Water is the main component of emulsion formulation and frequently acts as a solvent. Its use is very important to improve transdermal and topical delivery, since the *stratum corneum* is rich in water content (15-20% of the tissue dry weight). Exposing the skin to high humidity or preventing TEWL allows the skin to reach a higher water content in

equilibrium. Thus, by increasing the hydration of the tissue, it is possible to increase the transdermal delivery of hydrophilic and lipophilic permeants. ^(62,87)

Other additives such as colorants and fragrances can also be added to the emulsions, to obtain a higher acceptance by the consumer. The colorants are used to change the color of the emulsion, to change its appearance. Fragrances are added to emulsions, because it constitutes a key factor in a patient/consumer's decision to purchase and/or use a product and can be considered natural and synthetic. ⁽⁸⁷⁾

1.4.1.2. Structure of emulsions

Emulsions can be oil-in-water (O/W) or water-in-oil (W/O) emulsions. Accordingly, if water droplets are dispersed in an oil external phase, the emulsion will be considered W/O. If the external phase is composed by water and presents oil droplets dispersed in it, the emulsion will be O/W (figure 19). ^(73,82,88)

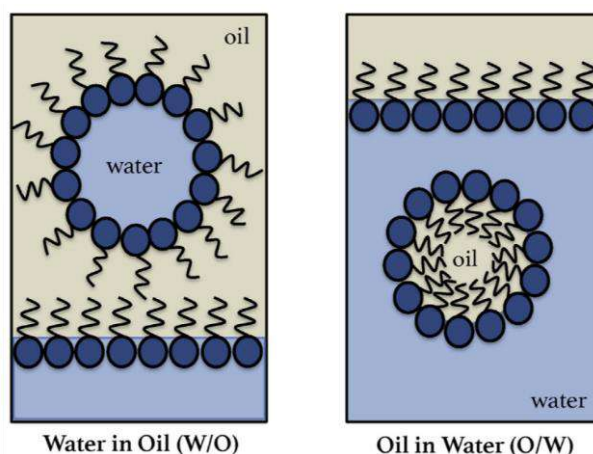


Figure 19 - Representation of the two different emulsions' systems: W/O (left) and O/W (right). Adapted from: ⁽⁷⁴⁾.

The nature of the emulsion is influenced by the water and oil ratio, the type and geometry of the surfactant used in the formulation and the conditions under which the formulations are produced (manufacturing process). There are different emulsification theories. Among these theories there are two different rules regarding the structure presented by the emulsions: Bancroft and Ostwald. The Bancroft rule says that the external phase will preferably be one where the surfactant is most soluble. While, the Ostwald rule states that the concentrations of the oily and aqueous phases determine the

external and internal phases. Thus, if the emulsion presents a high concentration of water the system will present oil droplets dispersed in water, constituting a O/W emulsion, whereas at lower water concentrations, the system will consist of water droplets dispersed in oil (W/O emulsion). ^(72,79,94)

The formation of W/O or O/W emulsions also depends on the type of surfactant used in the formulation, where the choice can be based on various methods, such as: hydrophilic-lipophilic balance (HLB) number and critical packing parameter (CPP). ⁽⁷⁵⁾

The HLB number was first introduced by William C. Griffin in 1949 ⁽⁹⁵⁾ and allows the surfactants to be characterized by the affinity toward a solvent, where a more lipophilic surfactant has a lower HLB, while a more hydrophilic surfactant has a higher HLB. ^(72,75,96)

To calculate HLB number, various recent methods can be used, like Davies' and Kawakami's equations. However, the first equation (equation 2) was proposed by Griffin in 1954 ⁽⁹⁷⁾, based on the quantitative characterization of polyoxyethylene (POE) surfactants, where the HLB number equals the weight fraction of POE moiety in the molecule. ⁽⁷²⁾

$$HLB = \frac{POE \text{ (wt\%)}}{5} \quad (2)$$

This first equation can be expressed by a general equation (equation 3), where M is the molecular weight of a surfactant and M_w is the molecular weight of the hydrophilic group: ⁽⁷²⁾

$$HLB = 20 \times \frac{M}{M_w} \quad (3)$$

According to the Bancroft's rule ⁽⁹⁸⁾ oil-soluble surfactants ($HLB < 10$) preferably form W/O emulsions, while water-soluble surfactants ($HLB > 10$) preferably form O/W emulsions. Knowing the required HLB of an oil or a mixture means that choosing the surfactant with the same HLB will produce an emulsion. Nevertheless, the HLB system does not provide the concentration of surfactant that should be added to the formulation. ^(96,99)

The CPP method was first introduced by Israelachvili, Mitchell and Ninham in 1976⁽¹⁰⁰⁾, and it also relates the type of surfactant used with the emulsion structure. Through some geometrical considerations, the CPP is expressed as:^(78,99)

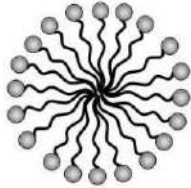
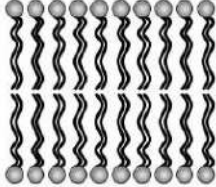
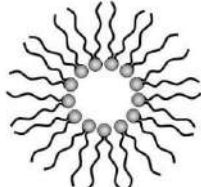
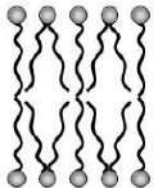
$$CPP = \frac{v}{l \times a_o} \quad (4)$$

, where (v) corresponds to the hydrocarbon chain volume, (l) to the length and (a_o) to the interfacial area occupied by the head group.^(78,99)

Theoretically, surfactants with a CPP < $\frac{1}{3}$ form spherical micelles, being more suitable for O/W emulsions. Surfactants with a CPP > 1 form inverted spherical micelles, being more suitable for W/O emulsions.^(73,75)

It is also important to notice that the HLB and the CPP are closely correlated as shown in table 1.

Table 1 - Influence of CPP and HLB on emulsion structure. Adapted from (73,99).

HLB	CPP	Structures Formed
HLB > 10	CPP ≤ $\frac{1}{3}$	
HLB ≈ 10	CPP ≈ 1	
HLB < 10	CPP ≥ 1	
HLB ≈ 10	CPP ≈ 1	

The bicontinuous or a lamellar structure, which corresponds to a zero curvature, are dependent on the rigidity and on the surfactant layer. In the spherical micellar structures, the interface bends spontaneously towards the aqueous phase, constituting a positive curvature. While, in the inverse micellar structures the curvature is negative, since the interface bends spontaneously towards the oily phase. ⁽⁷³⁾

Some techniques like coloring, electrical conductivity and diluting method, are used to distinguish between the two types of emulsions. The diluting method is the easiest to use, since it is based on the diffusion phenomenon, where the emulsion is placed in a large amount of water or oil. If the formulation mixes readily and spontaneously in water, the emulsion must be O/W type, whereas, if the formulation diffuses spontaneously in oil, the emulsion is considered a W/O type. ^(80,81)

It is important to note that, in practice, emulsions are rarely W/O or O/W systems. In addition, they can be multiple emulsions composed of an internal aqueous phase in an oily phase, both inserted into an external aqueous phase (W/O/W – water-oil-water emulsion) or the reverse (O/W/O – oil-water-oil). ⁽⁷³⁾

As already mentioned, to formulate an emulsion, three components are essential: water, surfactant (emulsifier) and oil (emollient). Depending on the nature and amount used of each of these components, the emulsions' surfactant can create various types of internal structures and in some proportions of water, surfactant and oil, it is not possible to formulate any type of emulsion. To improve the identification of the interactions that may occur accordantly to the percentages of the main components, ternary diagrams are often created, as can be seen in figure 20. ^(73,91)

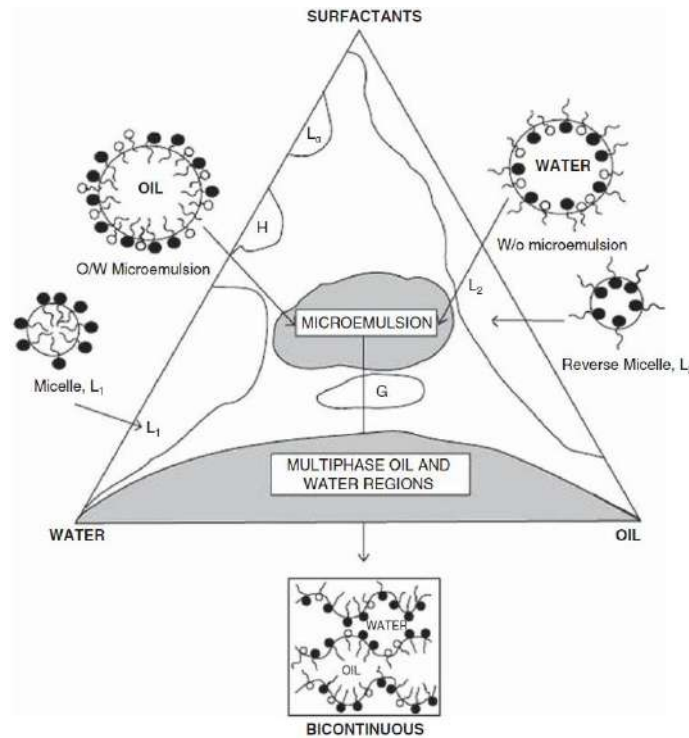


Figure 20 - Different structures of emulsions depending on the ratio of water, surfactant and oil used. Adapted from (79).

In lamellar emulsions, the surfactant molecules are arranged in bilayers separated by water and can be formed by synthetic or natural surfactants. In addition, lamellar emulsions present good skin hydration potential and are analogous to the *stratum corneum* lipidic structure. (73,91)

1.4.1.3. Emulsions' stability

To prepare emulsions with the shelf life stability required for a pharmaceutical product (1-3+ years), the correct choice of emulsifiers must be made. Thickeners, such as polymeric stabilizers must be post-added or both, among other ingredients such as preservatives, humectants, etc. Therefore, the emulsions can be stabilized by using surfactants, co-surfactants, fatty alcohols, polymers (steric stabilization) or solid particles (pickering emulsions). (73,94)

Most pharmaceutical formulations are stabilized by using emulsifying agents, constituting the primary surfactants that are capable of stabilizing emulsions by reducing the interfacial tension. When primary surfactants are used in formulations, they tend to lower interfacial tension through the adsorption of surfactants at the interface, forming a

barrier around the droplet interface. Therefore, they facilitate the production of the emulsions and enhance their stability. In addition, the secondary surfactants modify the external phase allowing to inhibit or delay coalescence, since they create a rheological barrier that prevents droplet movement. The combination of non-ionic surfactants with fatty alcohols, fatty acids or glyceryl esters enhances the stabilization of emulsions, being widely used. These components are part of the co-surfactants or secondary surfactants group, which are defined as amphiphilic, generally lipophilic and soluble substances. When co-surfactants are used in emulsions, they may even inhibit Ostwald rippling, a process of increasing droplet size that results from the diffusion of molecules, from smaller to larger droplets. ^(73,81,94)

The stabilization of an emulsion with solid particles constitutes an alternative to the use of surfactant agents. These emulsions are commonly named Pickering emulsions. The stability of these emulsions only depends of the wettability of solid particles in water or oil, being evaluated through the contact angle between the solid particle and the interface. The type of emulsion produced depends on which phase preferentially wets the solid particles. If the particle is wetted more by the oily phase, such as gas black, is considered a hydrophobic particle and the contact angle is higher than 90° , tending to stabilize W/O emulsions. While if the aqueous phase preferentially wets the solid particle, such as bentonite, the particle is considered hydrophilic with a contact angle is lower than 90° , tending to stabilize O/W emulsions. Therefore, if the particles are wetted by both phases and have sufficient adhesion between them to form a coherent interfacial layer, they can prevent the droplet coalescence, increasing the stability. ^(75,94)

1.4.2. Microemulsions

Microemulsions were first described in 1943 by Hoar and Schulman ^(101,102), through titration of an emulsion with hexanol obtaining a transparent product. Since the microemulsions have been described, they have been increasingly studied as delivery systems, due to their physicochemical properties and multiple advantages. These include its manufacturing process, and being a promising delivery and absorption system, when compared with emulsions. ^(55,77)

Microemulsions are also considered dispersed colloidal systems consisting of two liquid phases. However, they differ from emulsions in many aspects such as: macroscopic appearance, droplet size, stability, formation and composition. ^(103,104)

Therefore, microemulsions present a clear and transparent macroscopic aspect, mainly due to its reduced droplet size, which is characterized by a diameter of less than 150nm. Regarding stability, microemulsions are thermodynamically stable systems allowing a higher shelf-life. However, its stability requires a high content of surfactant, when compared with emulsions, which can decrease their safety (increasing the skin irritation). ^(55,77,104)

In the thermodynamic point of view and considering equation (1) mentioned above, it is possible to state that microemulsions are thermodynamically stable, unlike emulsions. This behavior is mainly due to the ultralow interfacial tension accompanied with microemulsion formation, as the dispersion of droplets in the continuous phase which substantially increase the entropy of the system. Thus, the term $\Delta A\gamma_{12}$ is lower than the term $T\Delta S^{\text{conf}}$ and the free energy for microemulsion formation is negative ($\Delta G^{\text{form}} < 0$). Consequently, the system is produced spontaneously and it is considered thermodynamically stable. ^(73,77)

The formation process for microemulsions is significantly easier than that of emulsions, since microemulsions form spontaneously (almost zero interfacial tension) without the need of high energy input. In practice, only gentle agitation is required. ^(55,73,104)

In addition to the components mentioned above, microemulsions further require a co-surfactant, usually a low molecular weight alcohol. In these formulations, permeation enhancers, such as isopropyl myristate and oleic acid, are also used. ^(55,73,104)

In terms of microemulsions' viscosity, they usually present a Newtonian behavior with low viscosity, regardless of the volume ratio of the phases. In the same way as emulsions, microemulsions can be considered W/O or O/W, depending on the external phase. Multiple microemulsions, such as O/W/O or W/O/W, are also viewed when phase volumes are very different. Furthermore, in 1948 Winsor ⁽¹⁰⁵⁾ describes four different types of microemulsions (figure 21), where the system may have one, two or three phases. The first type (i) is a "two phase system" (biphasic), where the upper phase presents an

excess of oil and the lower phase presents an O/W emulsion. The second type (ii) is also a “two phase system”, where the less dense phase contains W/O emulsion and the denser phase contains excess of water. The third type (iii) presents a single microemulsion phase (monophasic) and, finally, the fourth type (iv) exhibits a three-phase system where the upper phase contains an excess of oil, the middle phase presents a bicontinuous microemulsion and the lower phase shows an excess of water. ^(55,73,74)

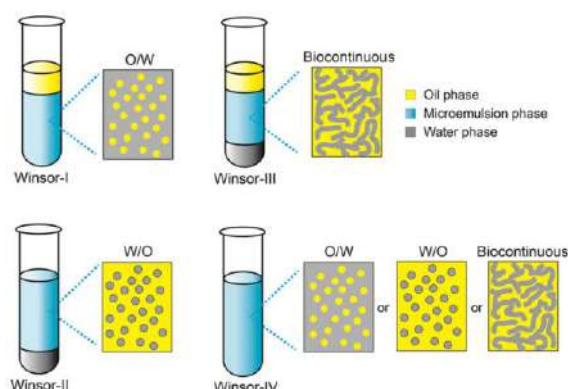


Figure 21 - Representation of a type I, II, III and IV, microemulsion according to Winsor⁽¹⁰⁵⁾. Adapted from: (105).

Microemulsions constitute a new delivery system, which is gaining popularity among pharmaceuticals, due to its numerous advantages such as: ^(55,74)

- i. High solubilizing power, that facilitates and allows the incorporation of hydrophilic and lipophilic drugs, allowing to administer the active substance in a liquid form;
- ii. Easier preparation, when compared with emulsions;
- iii. The capacity to be a permeation enhancer, that is related to small droplet size and the action of each component individually. Consequently, the bioavailability and stability are also improved, due to small droplet sizes;
- iv. The cost involved in the preparation of these formulations, since no special equipment is required, as they form spontaneously with relatively simple raw materials.

Regarding structure, microemulsions can also present different organizations of the surfactant micelles (inside structures) depending, not only on the proportion of water, surfactant and oil, but also on the nature and geometry of the surfactant. Therefore, they

can present different micellar curvatures as can be seen in table 1, and different inside structures (figure 20) previously presented in the emulsions section. ⁽⁷⁴⁾

2. Aim

The structure of this work starts with the synthesis of new HNE inhibitors with 4-oxo- β -lactams scaffold, taking into account the preceding studies made by our group ⁽¹⁹⁾. The compound named ER-143, showed a high potency and selectivity for HNE, however it presented a poor solubility and cell viability when tested in immortalized human keratinocytes (HaCat) cells. Therefore, the first aim of this work is the synthesis and characterization (NMR, FTIR, melting point, mass spectrometry, elemental analysis and *in vitro* cell viability, activity and selectivity against HNE) of new HNE inhibitors with higher solubility and less toxicity.

The development, characterization and optimization of new topical delivery systems comprises another aim of this work: placebos and O/W emulsions and microemulsions with a new human neutrophil elastase inhibitor will be characterized in terms of physicochemical, *in vivo* biological efficacy, sensorial analysis, *in vitro* drug release and *in vivo* antipsoriatic activity.

3. Results and discussion

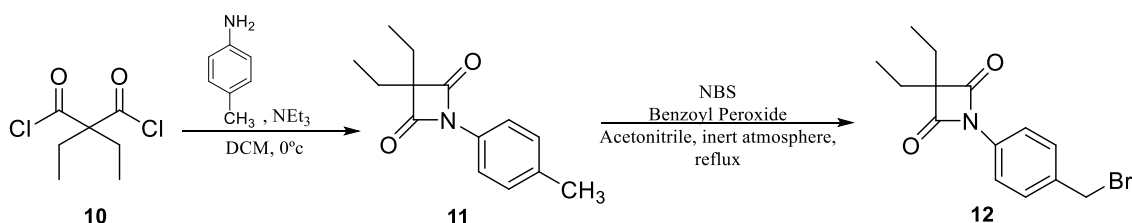
3.1. Synthesis of 4-oxo- β -lactams.

The compounds with 4-oxo- β -lactams scaffold are inhibitors of HNE, through an acylating mechanism, as mentioned in the introduction chapter. Structure-activity relationship (SAR) studies performed by Mulchande, J. *et al.* (107) showed that substituents, at C-3 of the four-membered ring, are very important in the potency of the inhibitor. Furthermore, this study indicates that diethyl substitution in the scaffold of the 4-oxo- β -lactam and an *N*-phenyl derivative of this structure, improves selectively the activity against this enzyme. Thus, previous studies performed by our group⁽¹⁰⁷⁻¹⁰⁹⁾, also showed that this compounds present promising results in the inhibition of serine proteases.

Regarding the preceding studies carried out by our group⁽¹⁹⁾, compound **1** showed a high potency and selectivity for HNE, however it presented a poor cell viability when tested in HaCat cells. Therefore, the synthesis of new HNE inhibitors with improved efficacy and lower cytotoxicity was performed, having the previously synthesized compound as control. In these new inhibitors the 4-oxo- β -lactam scaffold comprises a diethyl substitution and an *N*-phenyl derivative with different substituents directly attached to the phenyl derivate, which modifies the selectivity and the activity against HNE.

The characterization of the synthesized compounds was performed by melting point, NMR, FTIR, mass spectroscopy and elemental analysis (appendix 1).

The first synthesized compound was compound **12** (scheme 1).



Scheme 1 - Synthesis of compound **12**.

Compound **12**, was synthesized reacting diethylmalonyl dichloride (**10**) with *p*-toluidine, to obtain **11**, with a yield of 82.20%. This step comprises a cyclization reaction (figure 22) that occurs in basic media and was initiated by the attack of the aniline nitrogen

to the carbonyl group of **10** with expulsion of the best leaving group (chloride). This step occurs twice to give the compound **11**.

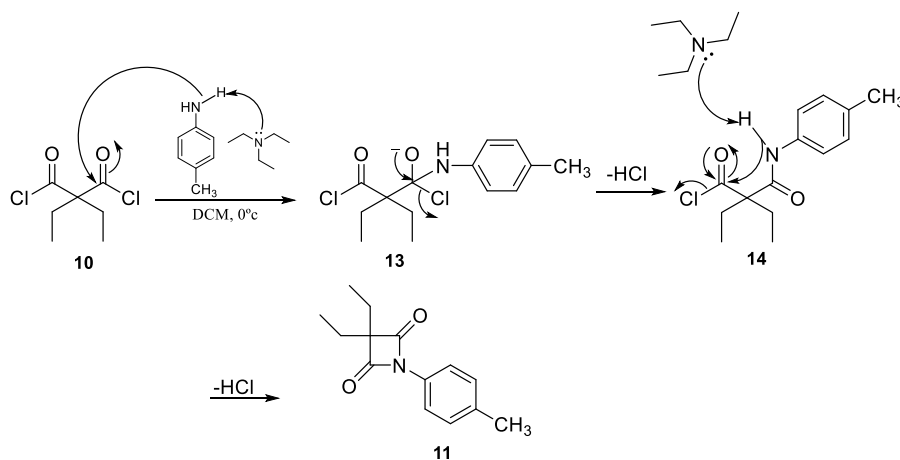


Figure 22 - Reaction mechanism of compound **10** with *p*-toluidine to synthesize compound **11**.

Subsequently, this compound reacted with *N*-bromosuccinimide (NBS) in the presence of benzoyl peroxide to give compound **12**, with a yield of 11.01%. This reaction proceeded under reflux, because it is a radical reaction and it required temperature to begin the reaction. The poor yield of this reaction was probably due to the work up and recrystallization procedures.

Through the ^1H NMR spectrum (figure 23) it is possible to verify that compound **12** was synthesized, demonstrating some characteristic peaks of this structure, such as the four protons of the aromatic ring represented by two doublets at 7.84 ppm and 7.44 ppm (H6 and H7, respectively) and the singlet of the methylene group at 4.48 ppm (H9). The diethyl group also presented two characteristic peaks, like the quartet at 1.84 ppm (H2) of the two methylene groups and the triplet at 1.06 ppm (H1) of the two methyl groups.

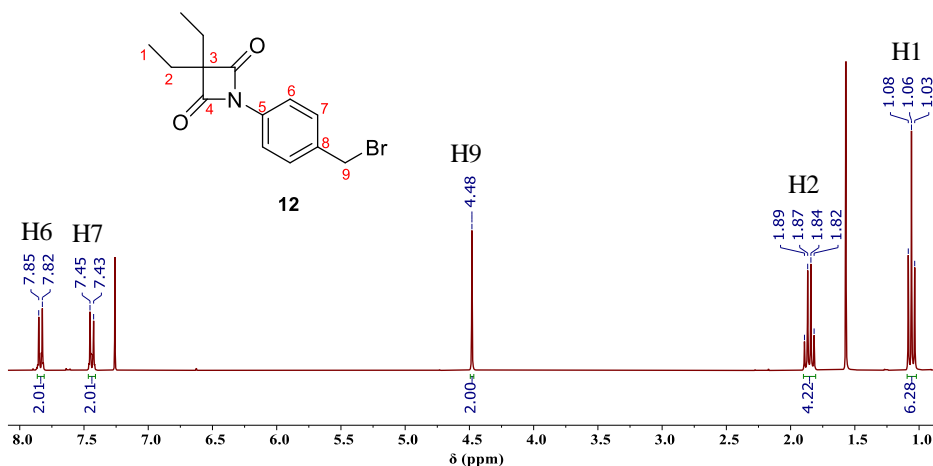


Figure 23 - ^1H NMR spectrum for compound **12**.

Comparing the ^1H NMR spectrum of compounds **11** (see appendix chapter, section 7.1.1) and **12**, the main difference is the singlet at 2.35 ppm corresponding to methyl protons in compound **11**, which, after the bromination, originates a singlet at 4.48 ppm corresponding to the methylene protons in compound **12**. This is due to a deshielding effect of the bromine atom, confirming that compound **12** was synthesized.

Through the COSY (Correlation Spectroscopy), HMBC (Heteronuclear Multiple Bond Correlation) and HSQC (Heteronuclear Single Quantum Coherence) studies performed for this molecule, it is possible to assign the ^{13}C NMR (figure 24) peaks for this molecule.

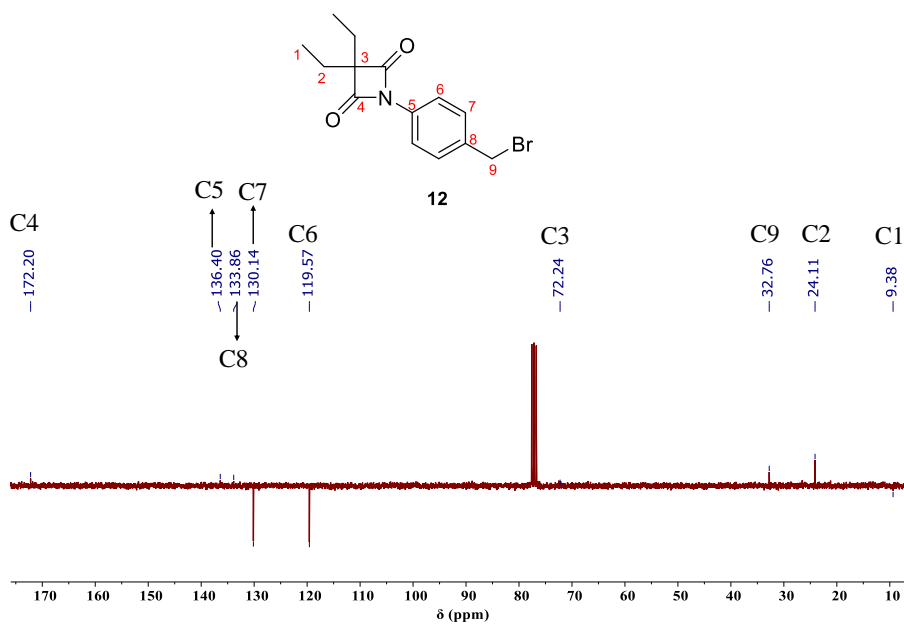
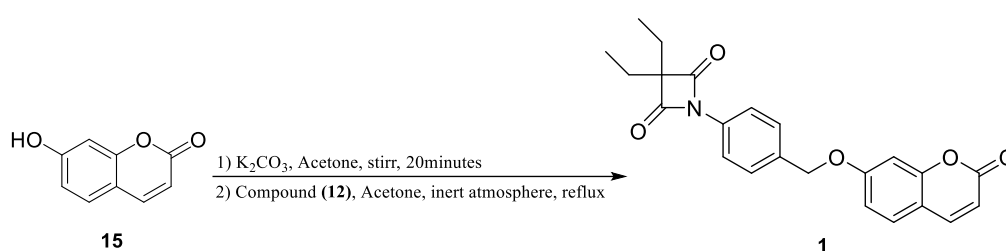


Figure 24 - ^{13}C NMR spectrum for compound **12**.

Therefore, as expected C1 and C2 are in lower fields (9.38 ppm and 24.11 ppm, respectively), while the carbon atoms of the aromatic ring and the carbonyl group are in higher fields. When compared with compound **11** (see appendix chapter, section 7.1.2) the main difference is also C9, which is in higher field in compound **12** than in compound **11** (21.26ppm).

The compound **1** (used as control, since it was already studied by our group⁽¹⁹⁾) was synthesized as shown in scheme 2.



Scheme 2 - Synthesis of compound 1.

This reaction occurs under basic conditions (potassium carbonate) to increase the nucleophilicity of the hydroxyl group through its deprotonation. After that, the substitution reaction occurs with the attack of the electronegative oxygen atom to the methylene group of compound **12** and expulsion of bromide. Compound **1** was obtained with a yield of 29.74%.

Regarding the ¹H NMR and ¹³C NMR spectra (figure 25 and 26, respectively) it is possible to assign the peaks obtained with the protons and carbons of this molecule, taking into account the COSY, HSQC and HMBC spectra for this molecule.

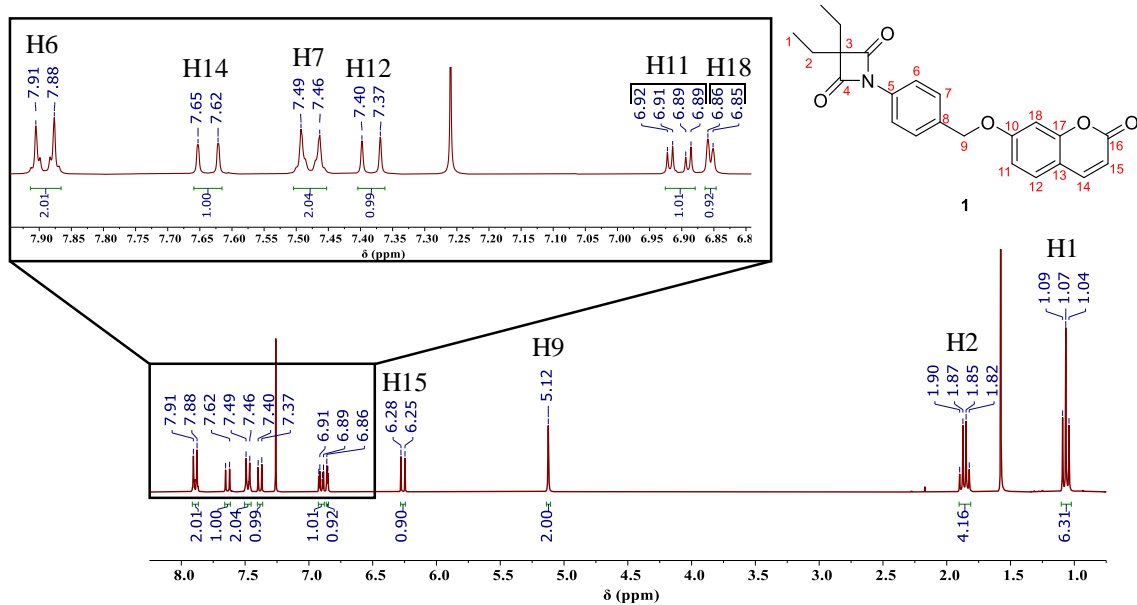


Figure 25 - ^1H NMR spectrum for compound 1.

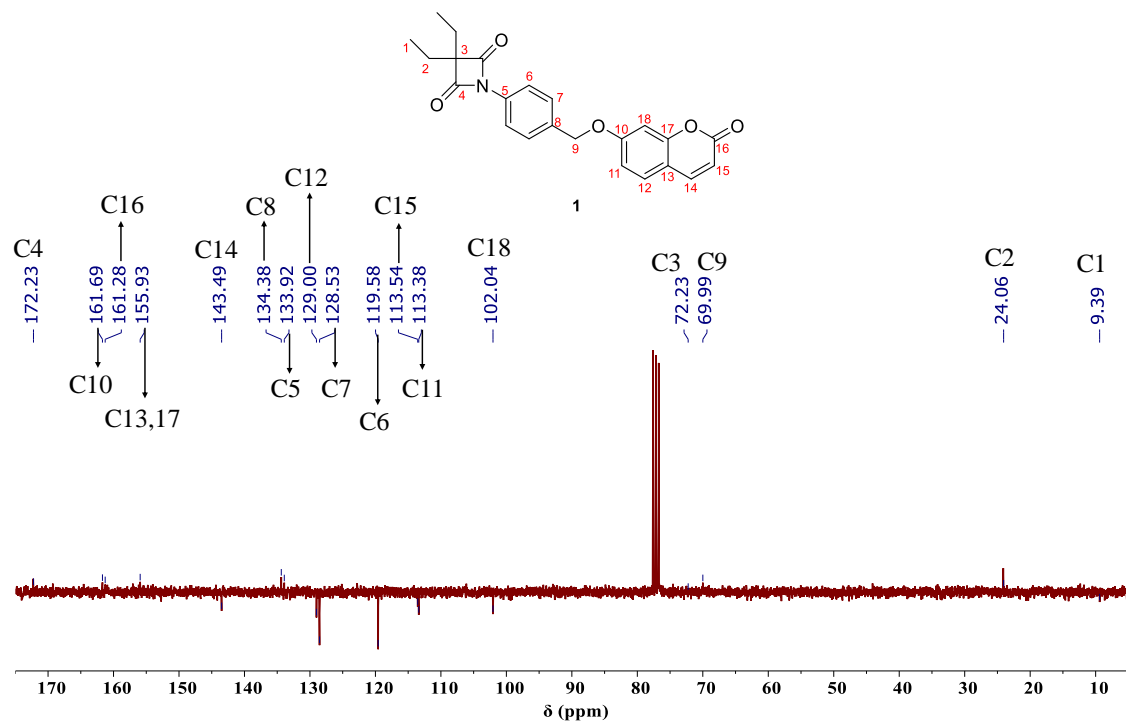


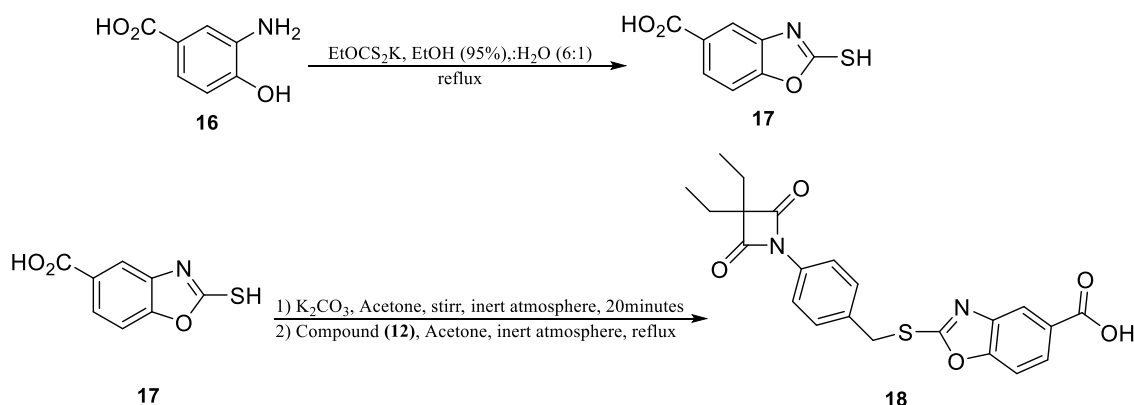
Figure 26 - ^{13}C NMR spectrum for compound 1.

Thus, in ^1H NMR it is possible to confirm the existence of four aromatic protons at 7.89 ppm (H6) and at 7.48 ppm (H7) and two groups of signals corresponding to methylene and methyl protons at 1.86 ppm and 1.07 ppm, respectively, as in compound **12** (see appendix chapter, section 7.2.1). The peak corresponding to the methylene group (H9) becomes more deshielded (5.12 ppm, relatively to compound **12**, due to the presence of the 7-hydroxycoumarin moiety, which is more electron attractor than the bromine

atom. In the aromatic region, the peaks corresponding to 7-hydroxycoumarin (**15**) protons: 7.64 ppm (H14), 7.38 ppm (H12), 6.90 ppm (H11), 6.86 ppm (H18) and 6.26 ppm (H15) can also be highlighted.

In the ^{13}C NMR spectrum, is possible to assign C9 in a lower field (69.99 ppm) when compared with compound **12** (see appendix chapter, section 7.2.2) , and the signals corresponding to the 7-hydroxycoumarin moiety, indicating that compound **1** was obtained. The new carbon peaks are mainly in lower fields between 161.69 ppm and 102.04 ppm, depending if they are more deshielded or shielded by the groups present in this side of the molecule.

Compound **18** was synthesized by reacting intermediate **17** with compound **12**, as present in scheme 3.



Scheme 3 - Synthesis of compound 18.

To obtain intermediate **17**, 3-amino-4-hydroxybenzoic acid (**16**) reacts with potassium ethyl xanthate in a mixture of ethanol:water (6:1). In this reaction a cyclization occurs between these two reagents (yield of 70.16%). In the next step, the thiol group of compound **17** will be deprotonated by potassium carbonate, becoming more nucleophilic, and a substitution reaction in compound **12** will proceed, with the expulsion of bromine, forming compound **18** with a yield of 45.08%.

With the NMR characterization spectra, it is possible to assign the different peaks present in the ^1H and ^{13}C (figure 27 to 31).

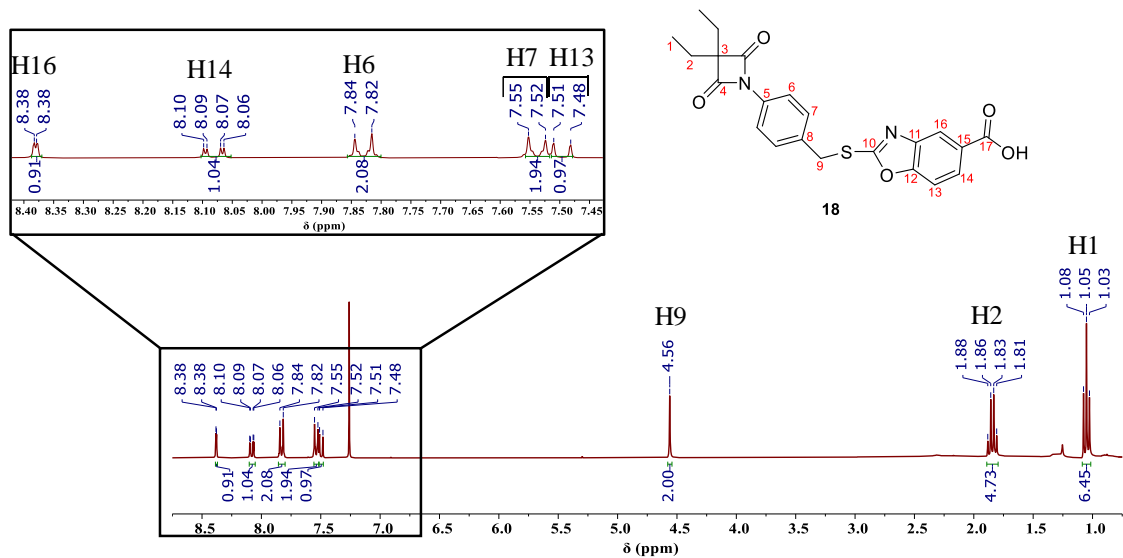


Figure 27 - ¹H NMR spectrum for compound 18.

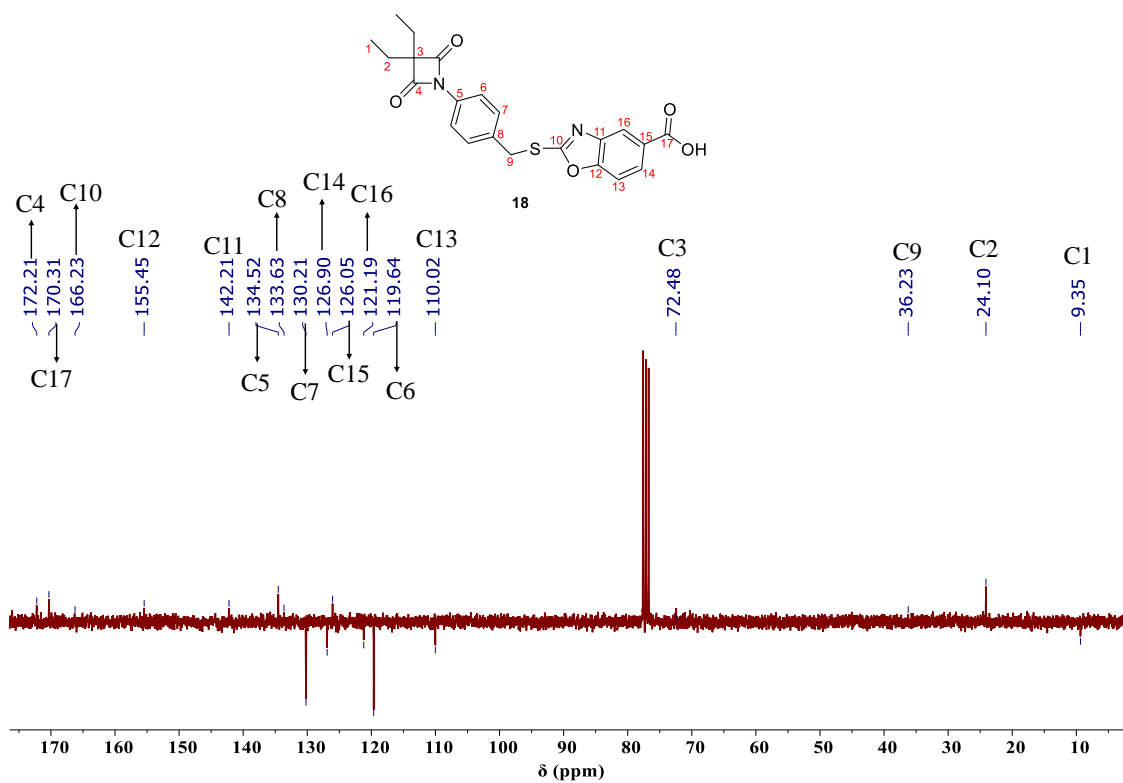


Figure 28 - ¹³C NMR spectrum for compound 18.

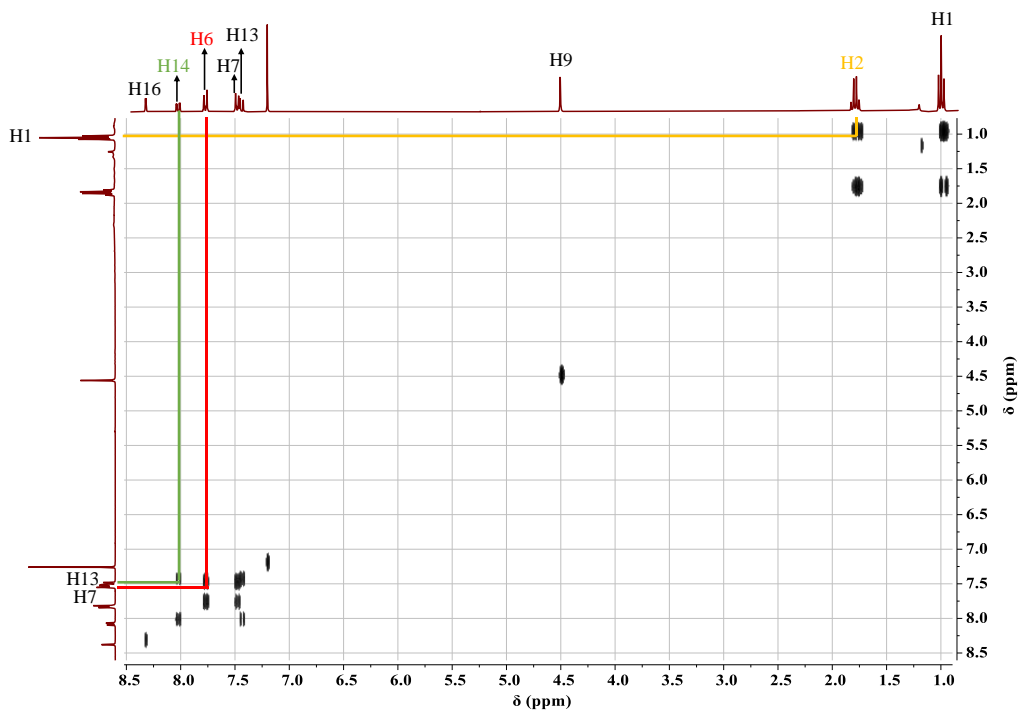


Figure 29 - COSY NMR spectrum for compound 18.

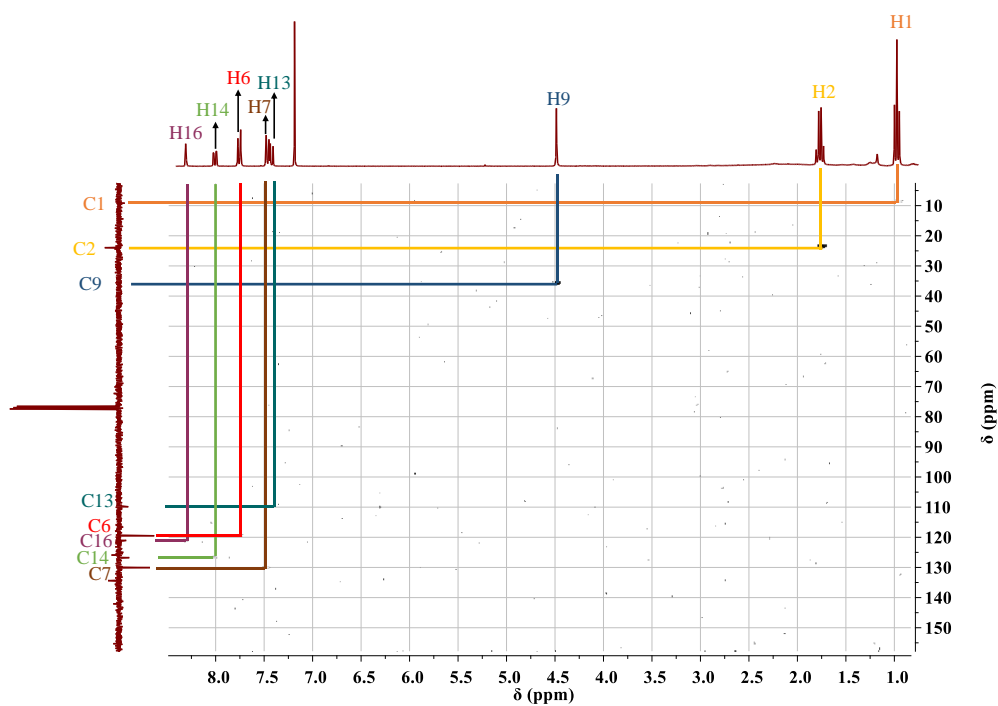


Figure 30 - HSQC NMR spectrum for compound 18.

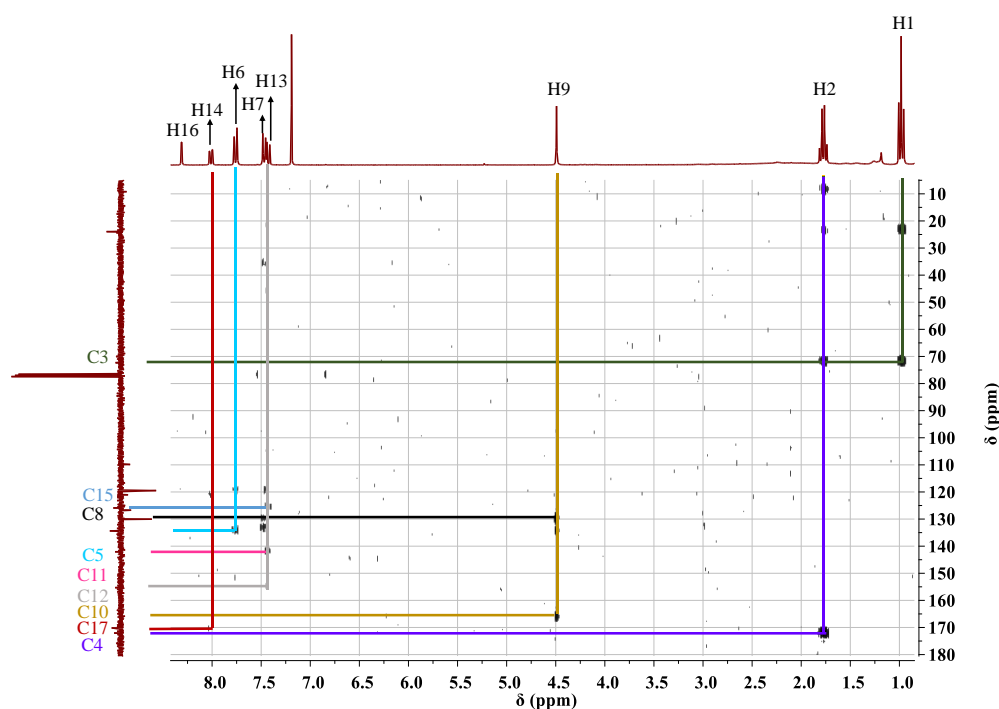


Figure 31 - HMBC NMR spectrum for compound 18.

Regarding the ^1H NMR and COSY spectra (figure 27 and 29) for this molecule, it is possible to identify the peaks that corresponds to the 4-oxo- β -lactam moiety such as the triplet of H1 at 1.05 ppm, the quartet of H2 at 1.84 ppm and protons of the aromatic ring at 7.83 ppm and 7.54 ppm (H6 and H7, respectively). In this case the sulphur atom practically does not influence the chemical shift of protons H9 when compared with molecule **12** (see appendix chapter, section 7.2.1). Through COSY it is possible to verify the correlation between H1-H2 and H7-H6. There are two other peaks that correlate in the COSY spectrum: a double doublet at 8.08 ppm and a doublet at 7.50 ppm, which belong to H14 and H13, respectively, mainly due to the multiplicity, location of peaks in a low field of the spectrum and the correlation between the two protons. The only peak that does not present any correlation is a doublet with chemical shift of 8.38 ppm, which belongs to H16.

Through the analysis of the HSQC spectrum (figure 30) it is possible to understand which protons are directly attached to certain carbons, where C1 corresponds to the carbon directly attached to H1 is at 9.35 ppm (orange). Other carbon atoms possible of identification are: C2 at 24.10 ppm (yellow), C9 at 36.23 ppm (dark blue), C13 at 110.02 ppm (grey), C7 at 130.21 ppm (brown), C14 at 126.90 ppm (green) and C16 at 121.19 ppm (purple).

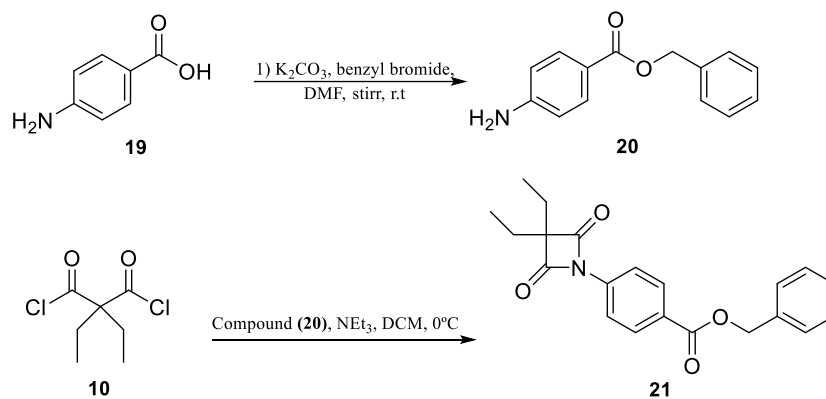
The remaining carbon atoms can be identified with the help of the HMBC spectrum (figure 31) that detects heteronuclear correlations over longer distances (two to four bonds). Therefore, it is possible to build a table to identify the unidentified carbon atoms, taking into account the correlation proton-carbon in the HMBC spectrum.

Table 2 - Correlation between the carbon atoms with the protons already identified.

Carbon atom	C3	C15	C8	C5	C11	C12	C10	C17	C4
Chemical shift (ppm)	72.48	126.05	133.63	134.52	142.21	155.45	166.23	170.31	172.21
Correlation (protons)	H1, H2	H13	H7, H9	H6	H13	H13	H9	H14	H2

Table 2, shows that C11, C12 and C15 were not possible to identify through the correlation with ^1H NMR, because both correlate with the same proton (H13). Therefore, the chemical shift had to be analyzed. C15 presents a chemical shift of 126.05 ppm, since it is directly attached to a carboxyl acid. However, this group shields the carbon atom, since it presents resonance structures with the aromatic ring, donating electrons. C12 is an aromatic carbon directly attached to an oxygen atom, and it will be in a lower field than C11, since this carbon is attached to a nitrogen atom, which is less electronegative than an oxygen. Therefore, C12 is at 155.45 ppm and C11 at 142.21 ppm.

Compound **21** was synthesized as described in scheme 4. The intermediate **20** was obtained by a nucleophilic substitution, after deprotonation of compound **19** with potassium carbonate, which then reacts with benzyl bromide (yield of 59.68%). Compound **21** was obtained through the reaction between intermediate **20** and diethylmalonyl dichloride (**10**) with a yield of 89.00%. This reaction is similar to the first reaction described (figure 22), where a cyclization occurs in the presence of a base. The ^1H and ^{13}C NMR spectra are present in figures 32 and 33.



Scheme 4 - Synthesis of compound 21.

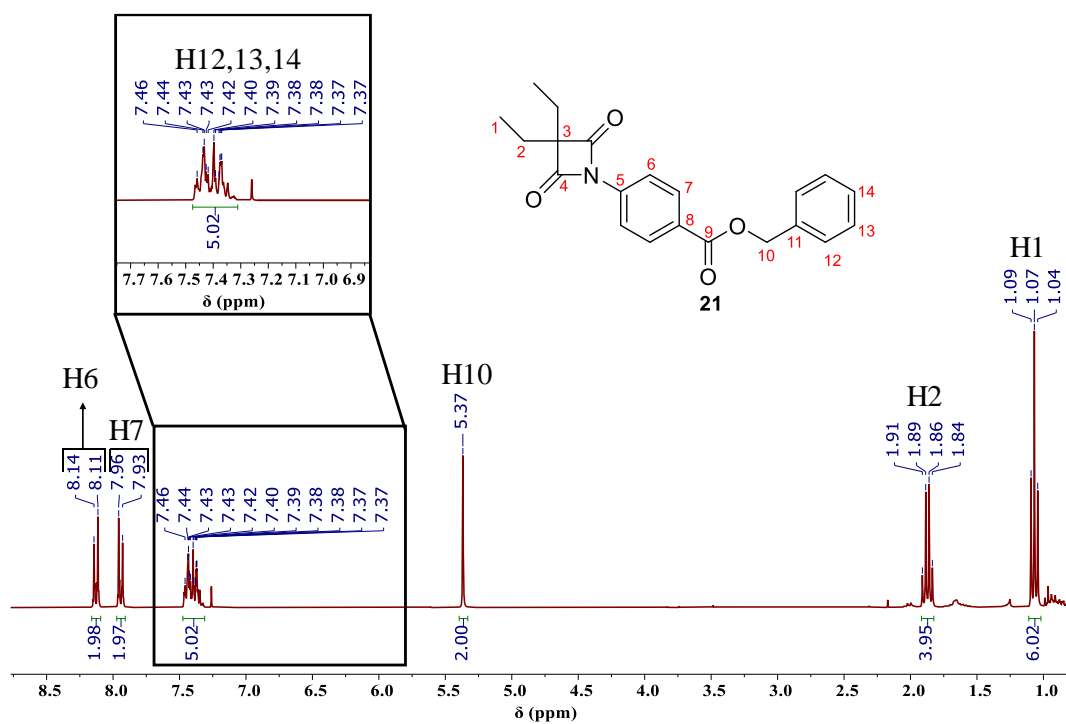


Figure 32 - ^1H NMR spectrum for compound 21.

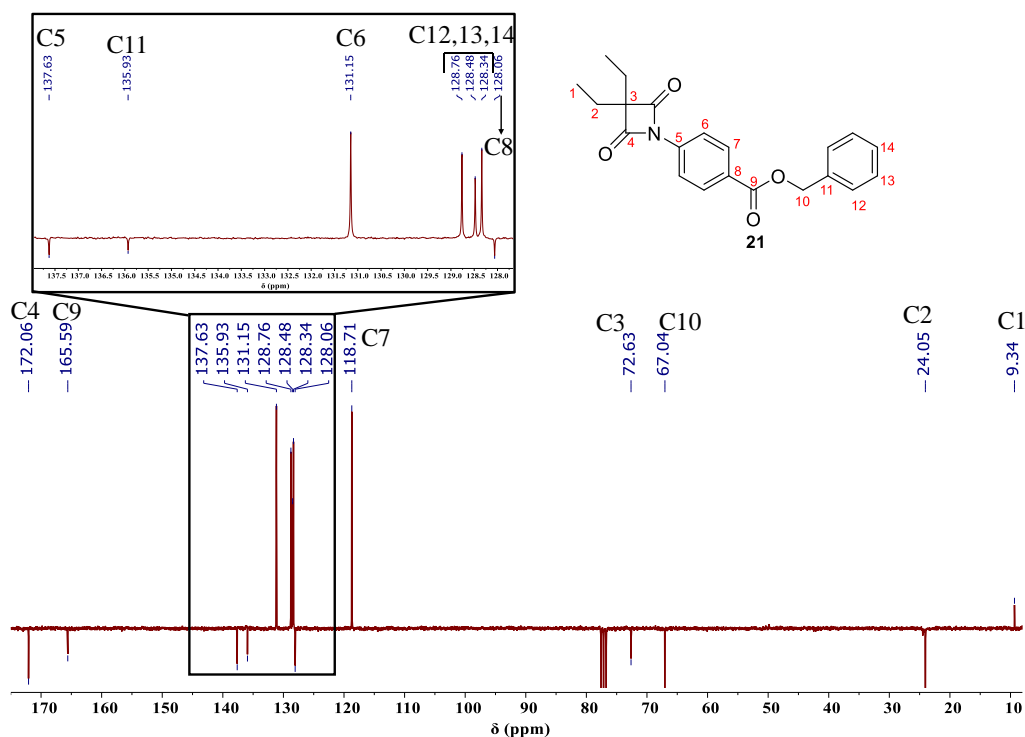
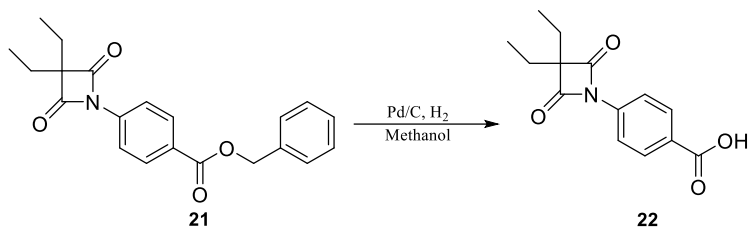


Figure 33 - ^{13}C NMR spectrum for compound 21.

Regarding the ^1H NMR spectrum, it is possible to note a triplet at 1.07 ppm that corresponds to H1 and a quartet at 1.87 ppm for H2. The aromatic protons, H6 and H7, appear at 8.13 ppm and 7.95 ppm, respectively, showing an increase in the chemical shift field, when compared with compound **20** (see appendix chapter, section 7.6.1) (which appears at 7.89 ppm and 6.63 ppm, respectively). Thus, as expected, H6 and H7 appear more deshielded, due to the electroattractive effect of the β -lactam ring, since it constitutes a more electronegative group than the amine.

^{13}C NMR (figure 33) also showed the peaks characteristic of the 4-oxo- β -lactam moiety, namely, 9.34 ppm, 24.05 ppm, 72.63 ppm and 172.06 ppm for C1, C2, C3 and C4, respectively.

Compound **22** was synthesized as outlined in scheme 5 with a yield of 96.42%. This reaction involves a reduction of the ester group to carboxylic acid, which was carried out using palladium and hydrogen atmosphere. The ^1H and ^{13}C NMR spectra are present in figure 34 and 35.



Scheme 5 - Synthesis of compound 22.

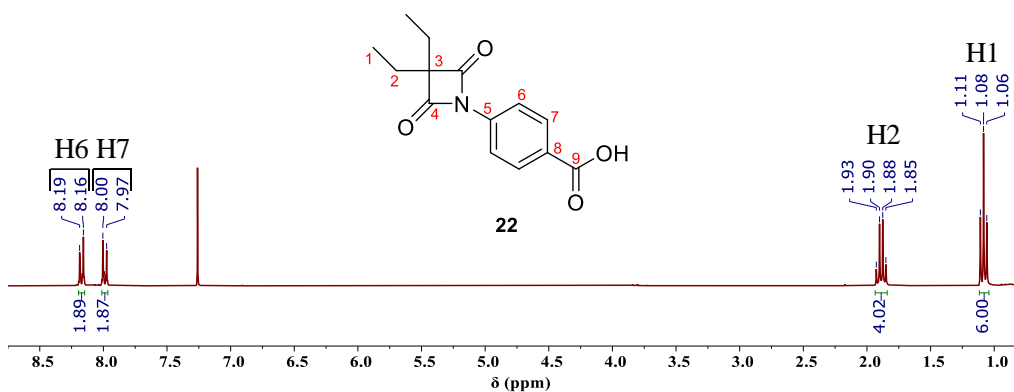


Figure 34 - ^1H NMR spectrum for compound 22.

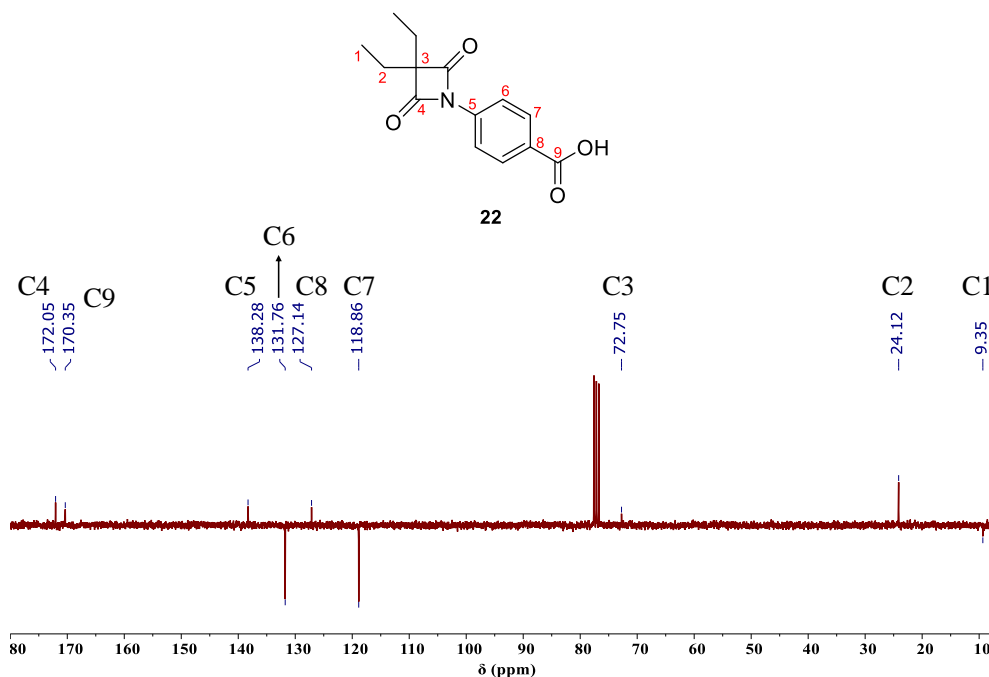


Figure 35 - ^{13}C NMR spectrum for compound 22.

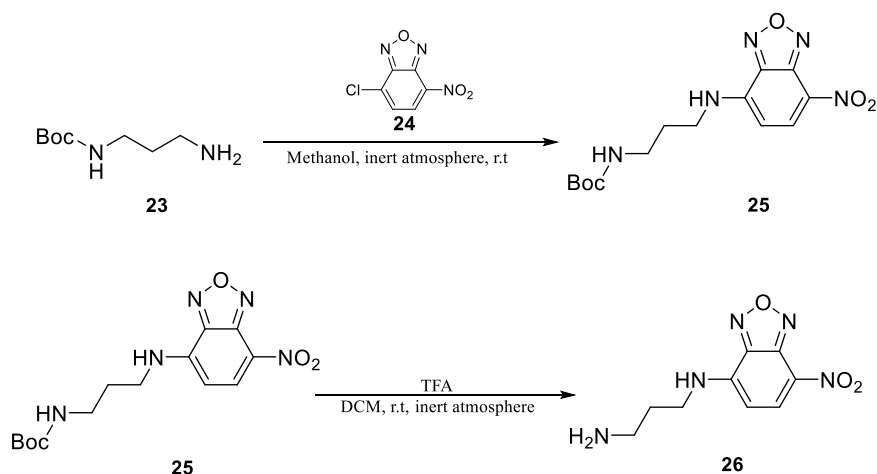
Concerning the ^1H NMR spectrum (figure 34), it is possible to assign the protons of the aromatic ring (two doublets at 8.17 ppm (H6) and 7.99 ppm (H7)) and the protons of the diethyl group (a quartet at 1.89 ppm (H2) and a triplet at 1.08 ppm (H1)). However,

the protons of the ester group disappeared, indicating that the new molecule was formed. Therefore, in this spectrum the chemical shifts of the aromatic ring and the diethyl group do not show significant differences, as expected, when compared with compound **21**.

With respect to the ^{13}C NMR spectrum (figure 35), it only shows the peaks of the diethyl group (C1 and C2 at 9.35ppm and 24.12 ppm), β -lactam ring (C3 and C4 at 72.75 ppm and 172.05 ppm), aromatic ring (C5, C6, C7 and C8 at 138.28 ppm, 131.76ppm, 118.86 ppm and 127.14 ppm) and the carboxylic acid group (C9 at 170.35 ppm), indicating that compound **22** was formed.

After the synthesis of these five compounds, *in vitro* studies were performed in order to know the cell viability and the inhibition against HNE in enzymatic assays. These studies are presented in the next chapter. The best two compounds in these assays were compounds **18** and **22** (chapter 3.2, section 3.2.1 and 3.2.2). Therefore, to facilitate the localization and quantification of the compound during the drug release studies, that will be further developed, a fluorophore was synthesized and coupled with these two molecules.

Fluorophore **25** was synthesized as shown in scheme 6.



Scheme 6 - Synthesis of compound 26.

To obtain intermediate **25**, molecule **23** reacts with 4-chloro-7-nitrobenzo[c][1,2,5]oxadiazole (**24**) by a nucleophilic substitution where the chloride is the leaving group (yield of 40.47%). In the next step, a deprotection reaction with

trifluoroacetic acid (TFA) in dry dichloromethane (DCM), yielded compound **26**. The ^1H NMR spectrum is present in figure 36. Since the all compound was used in the synthesis, the ^{13}C NMR spectrum was not performed.

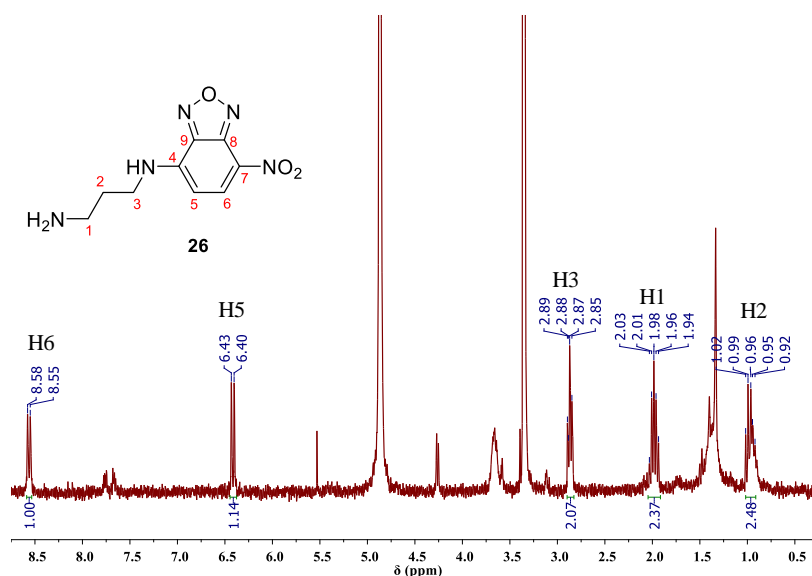
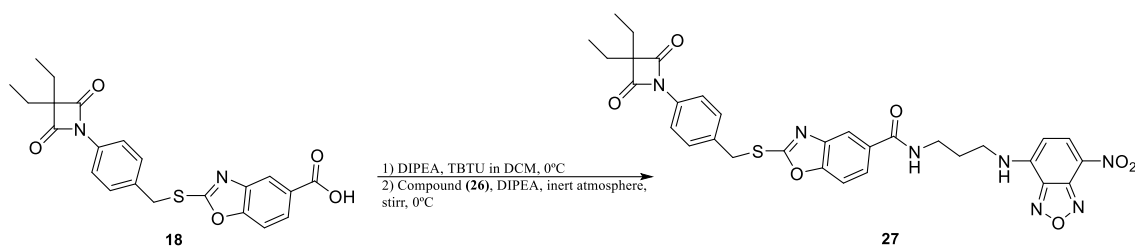


Figure 36 - ^1H NMR spectrum for compound **26**.

From the analysis of the ^1H NMR spectrum for compound **26** (figure 36) it is possible to assign the molecule protons. Therefore, methylene protons, which are directly bound to the amine appear as a multiplet at 2.03-1.94 ppm, H2 as a multiplet at 1.02-0.92 ppm, while H3 constitutes a quartet at 2.87 ppm. Protons H3 and H1 appear more deshielded than H2, mainly due to the electronegative effect of the five-membered ring and the amine. The protons H5 and H6 of the five-membered ring are both a doublet at 6.42 ppm and 8.56 ppm, respectively. The H6 is more deshielded than H5, due to the electronegative effect of the nitro group.

Compound **27** was synthesized as presented in scheme 7. In this reaction two coupling reagents, were used: *N,N*-Diisopropylethylamine (DIPEA) and *O*-(Benzotriazol-1-yl)-*N,N,N',N'*-tetramethyluronium tetrafluoroborate (TBTU).

In the first step, these two reagents promote the coupling between the TBTU and compound **18**, activating the carboxylic acid. After that, intermediate **26** is added to the reaction with more DIPEA, to attack the carbonyl group, with expulsion of the leaving group (TBTU).



Scheme 7 - Synthesis of compound 27.

Through the ^1H NMR spectra (figure 37) obtained for this molecule it is possible to compare this spectrum with that obtained for compound **18** and compound **26**.

With regard to the structure of compound **18**, it is possible to identify the H1 triplet at 1.05 ppm, the H2 quartet at 1.84 ppm, two doublets of the aromatic ring at 7.82 ppm and 7.53 ppm (H6 and H7), and the H9 singlet present at 4.54 ppm, which do not show any substantial differences when compared with compound **18** (chapter 7, section 7.5.1). However, H14 and H16 are at 7.78 ppm and 8.00 ppm, indicating that they are more shielded, due to the exchange between a carboxylic acid group with an amide group.

Comparing with the structure of compound **26** (chapter 7, section 7.10.1), it is possible to identify H19 at 2.10-2.02 ppm, H25 at 8.47 ppm and H26 at 6.19 ppm, which do not show any significant differences in the chemical shifts. However, H18 and H20 in this spectrum are overlapping at 3.72-3.66 ppm and show a decrease in the field, mainly due to the exchange between an amine group to an amide group, which deshielded the protons.

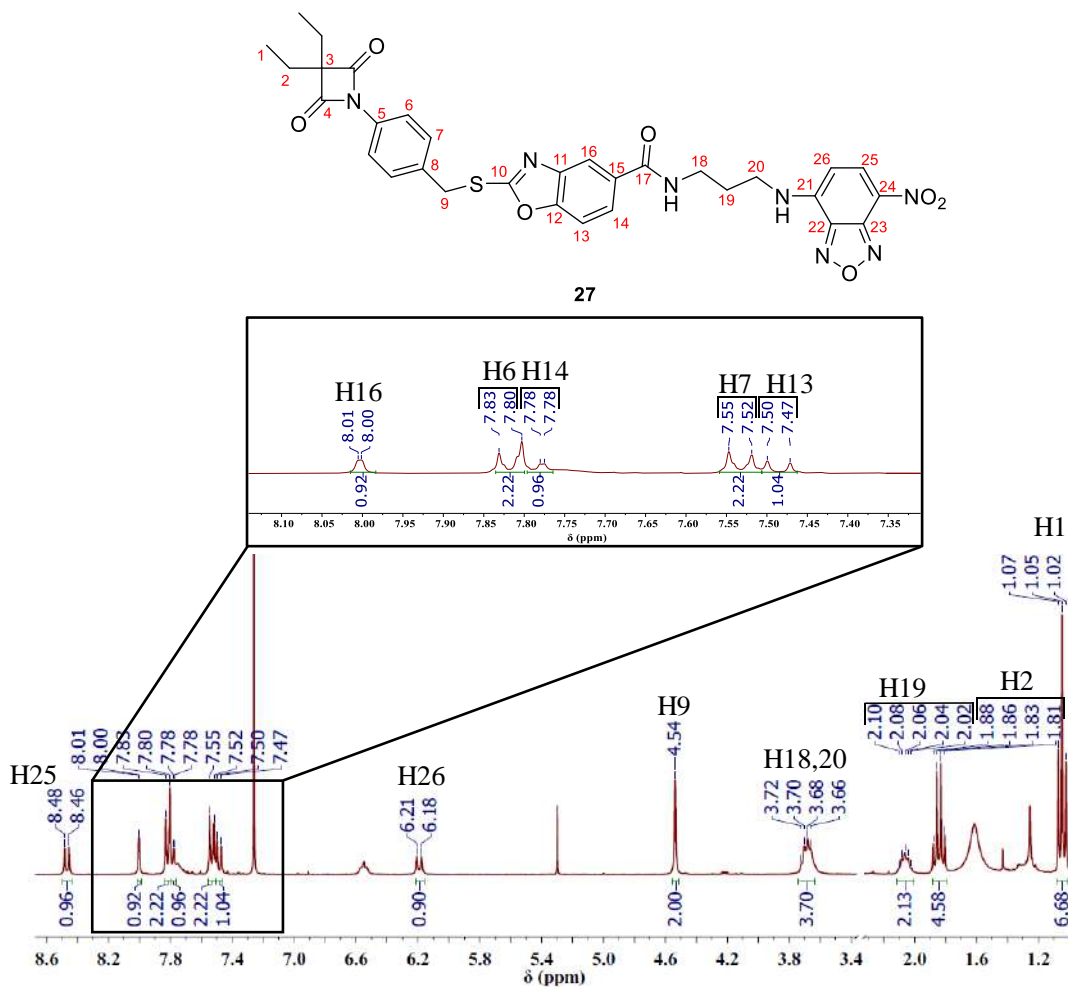


Figure 37 - ^1H NMR spectra for compound **27**.

From ^{13}C NMR (figure 38) for compound **27**, it can be assign the carbon peaks of the 4-oxo- β -lactam moiety, at 9.02 ppm (C1), 24.09 ppm (C2), 72.44 ppm (C3), and 172.23 ppm (C4). In addition, from the two aromatic rings it is possible to assign C5 at 134.60 ppm, C6 at 119.61 ppm, C7 at 130.21 ppm, C8 at 133.60 ppm, C11 at 130.59 ppm, C12 at 154.25 ppm, C13 at 110.32 ppm, C14 at 123.88ppm, C15 at 120.46 ppm and C16 at 117.29 ppm. The methylene group C9 is at 36.24 ppm and C10 is at 166.21 ppm. When compared with molecule **18** (chapter 7, section 7.5.2), these chemical shifts did not show any significant differences, with exception of C17 that present a chemical shift of 162.60 ppm, mainly due to the exchange between a carboxyl acid group to amide group, which is less electronegative.

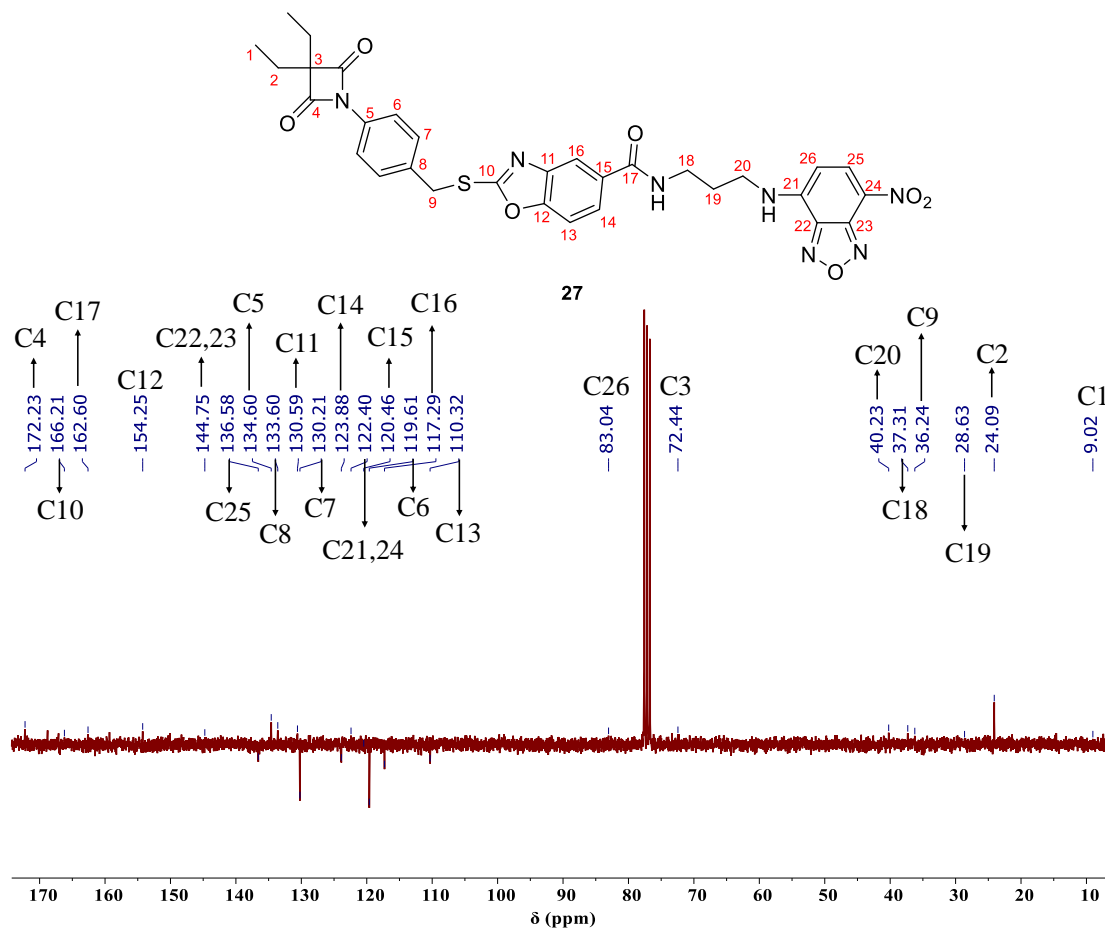
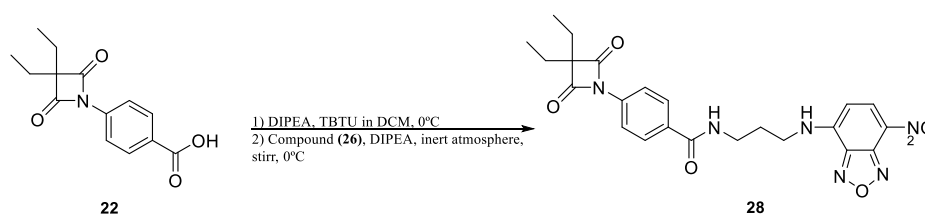


Figure 38 - ^{13}C NMR spectra for compound **27**.

Compound **28** was synthesized using the exact same procedure used for compound **27**, as represented in scheme 8.



Scheme 8 - Synthesis of compound **28**.

The ^1H NMR spectrum (figure 39) of compound **28** shows the proton peaks of the two molecules that gave rise to it: compound **22** and compound **26**.

Comparing with the structure of molecule **22**, it is possible to identify the triplet of H1 at 1.08 ppm, the quartet of H2 at 1.89 ppm and the two doublets of H6 and H7 at 7.97 ppm and 7.88 ppm. When compared with the previous spectrum (chapter 7, section 7.8.1)

the protons do not show any significant differences regarding the chemical shifts or the multiplicity of the peaks.

From the proton peaks that correspond to the structure of molecule **26** it is possible to state that protons H10 and H12 overlap at 3.70-3.64 ppm and H11 is at 2.09-2.01 ppm. When compared with molecule **26** (chapter 7, section 7.10.1), the peaks are in a lower field, mainly due to the exchange from an amide to a group carboxylic acid group. The remaining peaks that are H17 at 8.47 ppm and H18 at 6.19 ppm, do not show any substantial differences.

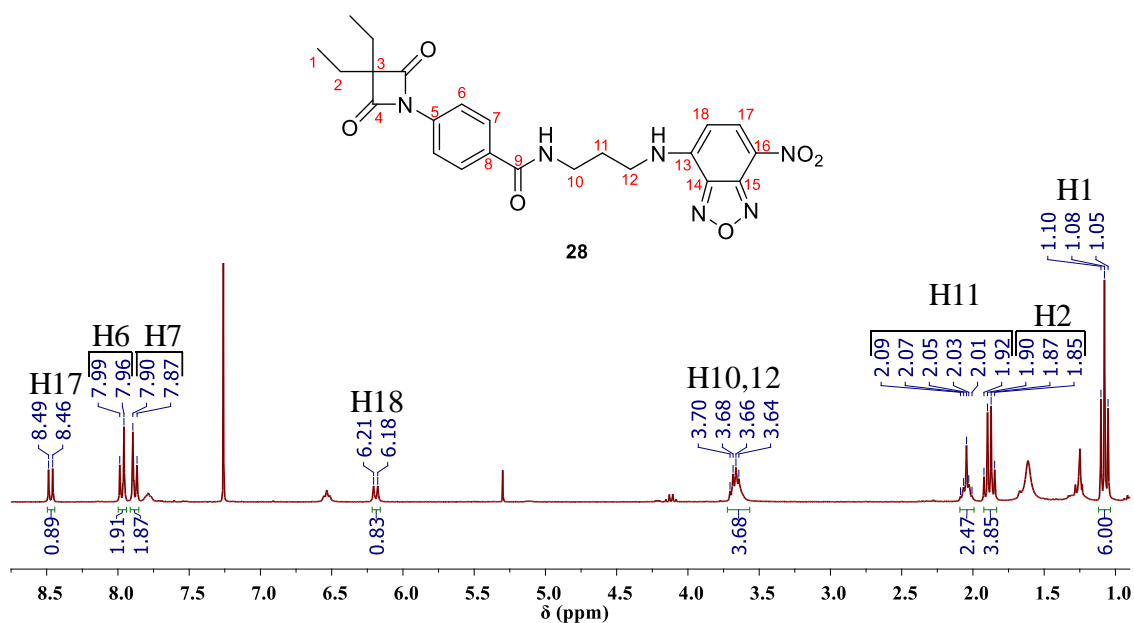


Figure 39 - ^1H NMR spectrum for compound **28**.

^{13}C NMR (figure 40) for compound **28**, showed the characteristic peaks of the 4-oxo- β -lactam moiety at 9.37 ppm (C1), 24.06 ppm (C2), 72.70 ppm (C3), and 172.10 ppm (C4). From the aromatic ring it is possible to assign C5 at 136.87 ppm, C6 at 128.41 ppm, C7 at 119.08 ppm and C8 at 131.41 ppm. All these peaks did not show any significant differences when compared with molecule **22** (chapter 7, section 7.8.2). However, the carbon atom C9 at 168.01 ppm showed a little modification in the chemical shift, mainly due to the exchange between a carboxyl acid group to an amide group.

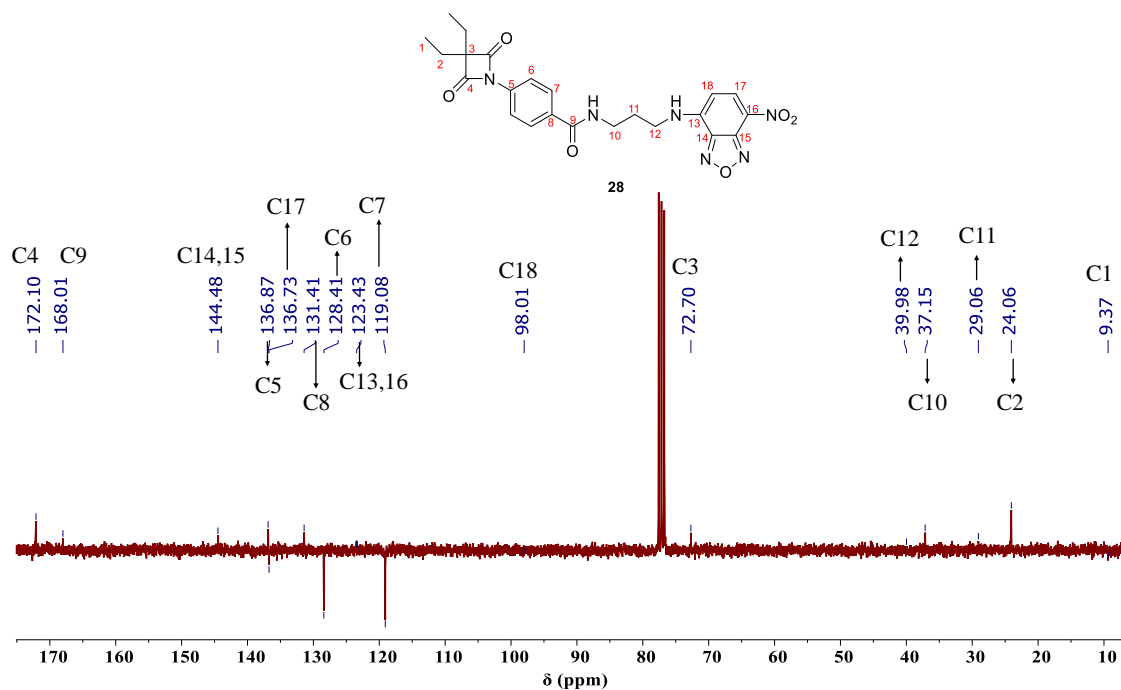


Figure 40 - ^{13}C NMR spectrum for compound 28.

3.2. Biological Assays

3.2.1. Enzymatic inhibition assays and *in vitro* cytotoxicity

In order to understand the activity of compounds against HNE, enzymatic inhibition assays were performed. The results of the inhibition study are shown in table 3.

Table 3 - Enzymatic inhibition assays.

Compounds	Structure	$IC_{50} \pm SD$ (nM)
11		0.85 ± 0.10
12		0.64 ± 0.03
1		0.42 ± 0.09

17		> 1000
18		0.38 ± 0.05
20		20.67 ± 5.31
21		0.96 ± 0.13
22		14.71 ± 5.55

The intermediate compounds used in the synthesis were also tested against HNE (**11**, **17**, **20**) to confirm that the inhibitory activity of the compounds depends on the structure of the compound and the β -lactam ring group.

By analyzing table 3, it is possible to verify that, in general, 4-oxo- β -lactam is essential for activity, with IC_{50} values in a sub-nanomolar range, except for compounds **17**, **20** and **22**. This result is as expected for compound **17** and **20** since they do not present the β -lactam ring. As for compound **22**, although it contains the β -lactam moiety, it also showed a lower activity. The β -lactam ring is extremely important in the structure of the molecule so that it exhibits a better activity against HNE as it allows a great improvement of the rate of serine acylation. ⁽¹⁰⁹⁾

As can be observed, compound **20**, although not having the β -lactam ring, exhibits an activity of 20.67 ± 5.31 nM, still considered an activity in nanomolar range. This result can be explained by the chemical structure of the compound, since it has an extremely reactive carbonyl group, due to its leaving group. Considered an acylating agent, the bond formation to HNE is obtained through the attack of the OH group of Ser¹⁹⁵ to the carbonyl group of compound **20**, with expulsion of the leaving group.

From these results, none of the synthesized compounds with the oxo- β -lactam moiety could be excluded due to the good activity presented. So, cytotoxicity assays were carried

out to choose the compounds with higher cell viability. The *in vitro* assays were performed with skin cells, HaCat cells. Sodium dodecyl sulfate (SDS) was used as positive control and culture medium with the same amount of dimethylsulfoxide (DMSO) used for the compound samples, as negative control. The results obtained are shown in figure 41.

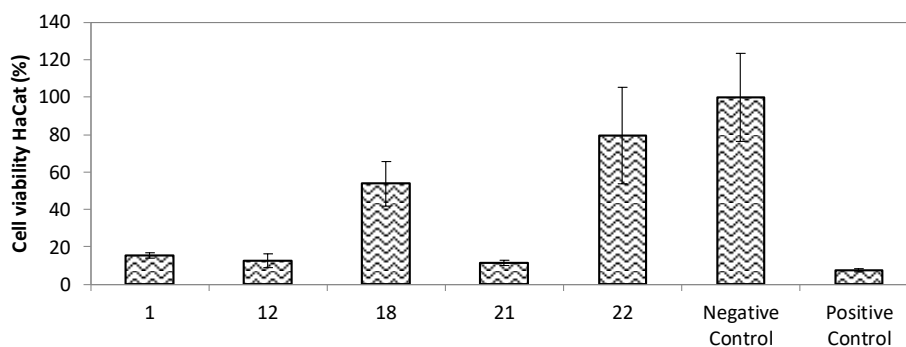


Figure 41 - Cytotoxicity assays performed with HaCat cells.

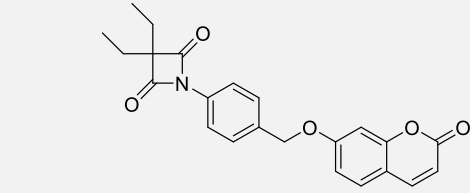
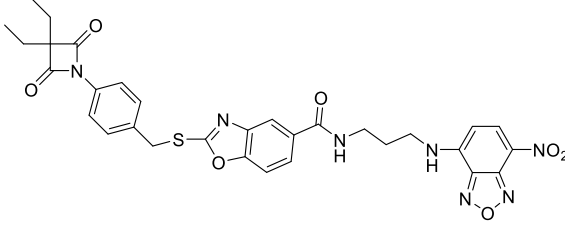
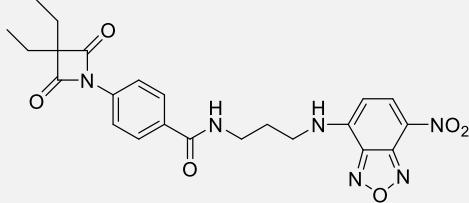
All compounds revealed lower cell viability comparing with the control (compound **1**), where the two best compounds regarding cell viability were compounds **18** and **22**. The lower cell viability of compound **12** might be due to the presence of a bromine atom that is described as potentially cytotoxic causing a decrease in cell viability.⁽¹¹⁰⁾

Compound **21** showed the lowest cell viability of all compounds, including the control. The only difference with compound **22** is the presence of an ester group and this leads to a large increase in toxicity.

3.2.2. Enzymatic inhibition assays, specificity and *in vitro* cytotoxicity for the compounds with fluorescence.

Due to optimal inhibition activity against HNE and good cell viability of compounds **18** and **22**, fluorescent derivatives of the fluorophore NBD, were also synthesized (compounds **27** and **28**, respectively). These two new molecules allow the localization and quantification of the compound during the drug release studies, that will be further developed. The *in vitro* inhibition results against HNE are presented in table 4.

Table 4 – Enzymatic inhibition assays for fluorescent compounds 27 and 28. Compound 1 was used as control.

<i>Compounds</i>	<i>Structure</i>	<i>IC₅₀ ± SD (nM)</i>
1		0.42 ± 0.09
27		0.85 ± 0.10
28		0.64 ± 0.03

These new compounds also showed an enzymatic activity against HNE in the sub-nanomolar range (table 4). Comparing with table 3, it is important to notice that compound **28** shows a higher activity than the parent compound **22**.

Since these new derivatives presented very similar activities, we performed studies of specificity to select the best compound. In this study, different enzymes were used: trypsin, chymotrypsin, urokinas, kalleidrein. The results are present in table 5.

Table 5 - Results of specificity of the compounds 1 (control), 27 and 28.

<i>Compounds</i>	<i>IC₅₀ (μM)</i>			
	Trypsin	Chymotrypsin	Urokinase	Kalleidrein
1	> 1	> 8	> 50	> 8
27	> 1	> 1	> 2	> 5
28	> 1	> 0.5	> 2	> 3

All the enzymes tested belong to the serine protease group, thus allowing to evaluate if the compounds act only in HNE or in other enzymes of the same group as well. The results showed that the tested compounds only inhibit these proteases in a micromolar range, such as the control compound. Once the values used to inhibit these enzymes are

at least 0.5 μM (table 5), it can be considered that all compounds are specific for HNE, since they will be used in a nanomolar range. In other words, due to the high potency of the compounds, only a small amount is required to reveal activity against HNE and it is not sufficient to act on other enzymes of the same class.

Therefore, once again it is not possible to highlight a compound as being the best. Cytotoxicity assays, regarding cell viability, were also carried out. These results are presented in figure 42.

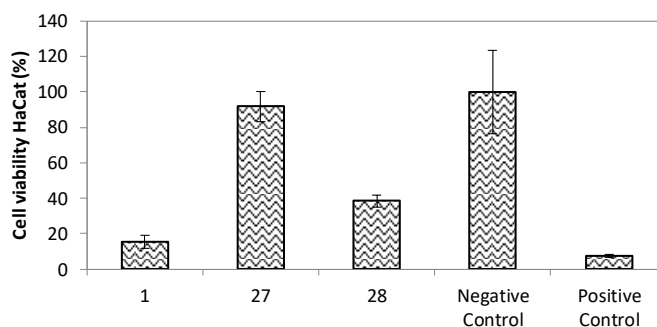


Figure 42 - Cell viability in HaCat cells for fluorescent compounds 27 and 28. Compound 1 was used as control.

From the results obtained, it can be seen that compound **28** is more cytotoxic (38.36% of cell viability) than compound **22** (79.57% of cell viability). It is further noted that this compound demonstrates better cell viability than compound **1**, used as control. However, its cell viability is less than 50%, so cannot be used in therapy.

On the other hand, compound **27** demonstrates to be less toxic than compound **18**, with a change from 53.7% to 91.6% in cell viability. Comparing this result with the obtained for compound **1** (15.50% of cell viability) an increase in cell viability is observed. Thus, it is possible to select a final compound to be incorporated into the formulations that will be further developed: compound **27**.

3.3. Pharmaceutical vehicles

In this chapter, two different pharmaceutical systems will be studied: O/W emulsions and microemulsions, as previously mentioned.

Regarding emulsions, twelve O/W emulsions were developed to study the influence of different humectants, preservatives and the influence of the percentage of cetyl alcohol (thickener). Cetyl alcohol was used as a thickener, due to a previous study, which determined that the formulations containing this thickener had better acceptance and characteristics. Then, all the formulations were characterized regarding their organoleptic characteristics, pH, stability and rheological properties. The chemical structures of all components used are present in appendix 2.

To formulate the microemulsions, a titration method was used, where all the components of the microemulsions were not modified, except for the amount of surfactant. In the end, the final mass changed in every formulation as well as the percentage of each component. According to the definition of microemulsions, it is a liquid with a clear aspect and thermodynamically stable, as previously mentioned. Thus, initially, a macroscopic evaluation was necessary regarding the formation or not of the microemulsion, being possible the accomplishment of a ternary diagram that indicates the region that can obtain microemulsions. Subsequently, the formulations considered microemulsions were characterized by pH and rheology. The chemical structures of all components used are present in appendix 2.

Finally, taking into account the previous studies, two pharmaceutical vehicles were selected for the incorporation of compound **27**. Then, macroscopic aspect, pH, rheology, droplet size and *in vitro* drug release and *in vivo* antipsoriatic activity studies were performed to ensure their quality and efficacy.

3.3.1. Emulsion

The emulsion's macroscopic aspect showed a white and opaque appearance with some consistency, being a semi-solid cream. Thus, the different humectants, thickeners and preservatives used did not influence the macroscopic aspect of the formulations.

To study the influence of pH on formulation characteristics, the pH values of all formulations were measured. To respect the skin's natural pH, it is necessary that all formulations have an acidic - neutral pH. Outside this pH range, from 4.5 to 7, the skin barrier could be damaged as this pH helps to control skin microflora, form an optimal lipid structure and prevent infections. Acidic pH is of great importance in the skin and

can be affected by numerous endogenous factors, such as emulsions. Thus, it is of the utmost importance that these formulations have a pH in this range. ^(47,111)

The results showed that the formulations were in the pH range between 5.3 and 6.7, being appropriated for the skin and in agreement with the described in the datasheets of the components used, since the pH of each component changes the pH of the final formulation.

From a stability point of view, physical stability studies were performed with the aim of characterize which formulations would be unstable in the long term. The results showed that only formulation 8 is unstable, presenting phase separation. Formulation 8 differs from the others due to the application of an alternative preservative: gluconolactone (and) sodium benzoate. In the formulation of this natural preservative, sodium benzoate is a known preservative, whereas gluconolactone acts as a preservative only when it is changed to gluconic acid structure. This change in structure occurs slowly over time. ⁽¹¹²⁾

The stability difficulties arising from this preservative may be related to the chemical changes of this last component. Thus, when physical stability tests of the formulation are performed, the gluconolactone structure can be rapidly changed to gluconic acid. As a result, the emulsion may undergo structural changes between its various components making it difficult to bond as previously. As the test is performed at room temperature it may also make it difficult to harmonize the components, as was initially obtained.

3.3.1.1. Rheology

The rheological characterization was performed by continuous shear and oscillation experiments. From the obtained data, it can be evaluated the influence of shear rate on viscosity and the study of the elastic and viscous modulus of the formulation, when different frequency values are applied to it. As previously mentioned, three different studies were carried out on the formulations: the influence of humectants, thickeners and preservatives. The emulsions will be labeled in the results using the abbreviation “E” followed by the corresponding numbers.

The influence of humectants

In this study, the influence of the three different humectants was studied: formulations 3, 5 and 7 containing ethoxydiglycol, propylene glycol and glycerin, respectively. The results are shown in figures 43 and 44.

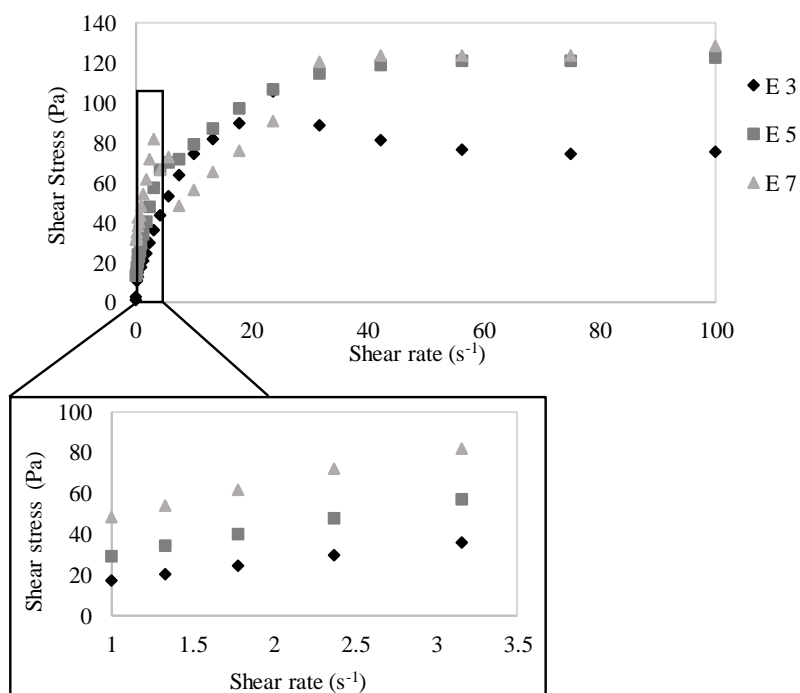


Figure 43 - Emulsions flow curves: Influence of different humectants.

In figure 43 it is possible to identify the formulation with a higher viscosity value, formulation 7, while formulation 3 is the one with the lowest viscosity. The only difference between the three emulsions is the humectant.

The viscosity presented by formulation 3 is the lowest with an apparent viscosity of 39.0Pa.s at 0.1s⁻¹ shear rate, since the humectant of this formulation is ethoxydiglycol. This humectant is commonly used in pharmaceutical formulations because of its properties of decreasing viscosity. This compound has a lower viscosity than other formulations, as it has a lower ability to make hydrogen bonds with water, the main component of emulsions. The weak water connections can be justified by the component structure and the log P value (-0.15).⁽¹¹³⁾ It is further noted that when a molecule has lower water bonds, the breakdown of molecules when a shear rate is applied becomes easier, decreasing the viscosity.

Concerning viscosity, emulsion 5 presents an apparent viscosity of 131.3Pa.s at $0.1s^{-1}$ shear rate, while emulsion 7 presents an apparent viscosity of 313.9Pa.s at $0.1s^{-1}$ shear rate. Thus, the viscosity presented by propylene glycol (emulsion 5) is lower than that presented by glycerin (emulsion 7). This, is the expected result, since the log P value for glycerin is -1.76 and -0.92 for propylene glycol. Therefore, glycerin has a higher viscosity than propylene glycol, mainly due to its higher affinity to water (more hydrophilic) than propylene glycol (more lipophilic).

Through figure 43, it is still possible to notice that all formulations are considered non-Newtonian fluids, being in accordance with the literature ^(84,114–116). They present a shear-thinning behavior, as viscosity decreases with increasing shear rate, due to the orientation of the molecules in the structure. ^(117–119)

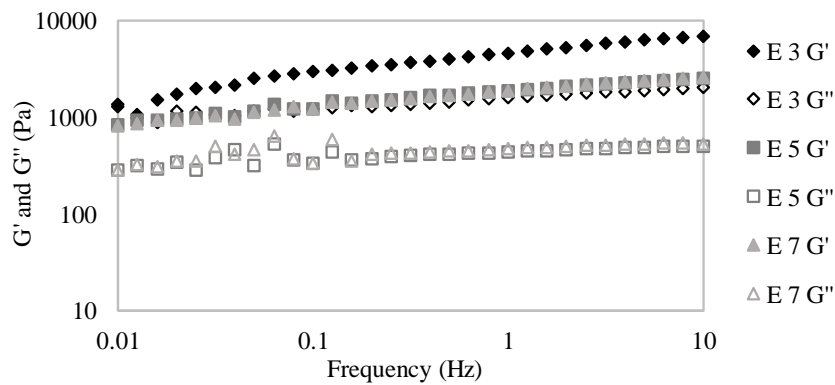


Figure 44 - Emulsions oscillatory results obtained from a frequency sweep: Influence of different humectants.

Figure 44 represents the oscillatory frequency results, which measures the system response as a function of frequency with constant shear strain. The results of this test made it possible to obtain the storage modulus (G') (elastic component) and the loss modulus (G'') (viscous component) in which the energy lost is reflected. ⁽¹²⁰⁾

Through the results it is possible to verify that in all cases $G' > G''$, where the values of elastic modulus overcome the values of viscosity modulus. These emulsions have a strong network structure, with a suitable spreadability of the product on the skin. In addition, due to the fact that viscosity values decrease with increasing shear rate, they also can easily be rubbed into the skin.

The value of the loss tangent for each of the formulations is 0.29, 0.34 and 0.35 for formulation 3, 5 and 7, respectively, at a frequency of 0.01Hz. This value is the expected

since the $G' > G''$ and loss tangent values must be smaller than 1⁽¹²⁰⁾, indicating that the formulations can be considered a gel-like solution. The loss tangent values also suggest that the droplets are highly associated due to the Van der Waals interactions involved in emulsion formation.

The influence of percentage of cetyl alcohol (thickener)

Cetyl alcohol provides a lamellar structure to most personal care products, giving a superior consistency and added stability to emulsions. This component is capable of thickening formulations containing ionic or non-ionic surfactants. Understanding the thickening mechanism of cetyl alcohol and its interactions with primary emulsifiers is crucial to imparting the desired aesthetics and stability.^(84,121)

As mentioned in the introduction chapter, emulsions can present a lamellar structure, in which the surfactant molecules are arranged in bilayers separated by layers of water. The lamellar phases can also be considered a gel phase (ordered) or liquid crystal phase (disordered), as can be seen in figure 45.⁽⁸⁶⁾

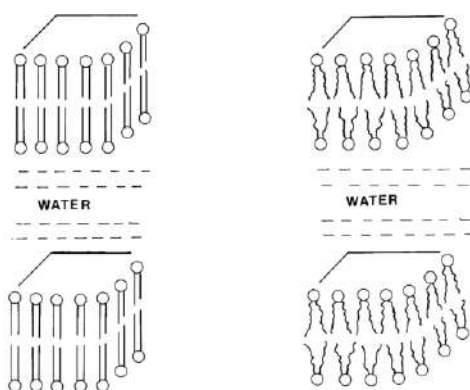


Figure 45 - Lamellar phases of an emulsion: gel phase (left) and liquid crystal phase (right). Adapted from (86).

Fatty amphiphiles, like cetyl alcohol, are considered too lipophilic to form bilayers phases in water, although they exhibit marked crystalline polymorphism. At high temperatures, such as those of the manufacturing process, the L_{α} -liquid crystalline form of this fatty alcohol predominates (liquid-like). Thus, the hydrocarbon chains of the compound are fully extended and there is rotational motion of the molecule, decreasing the viscosity. On other hand, after the formulation cools, the temperature is lower and the Gel β -form and γ -form co-exist, where the hydrocarbon chains are non-rotating or tilted,

respectively. Usually the β -form is in excess. It is important to notice that, in the presence of water, the crystals of this fatty alcohol often show limited swelling, thus not being considered as gel phase. ⁽⁸⁶⁾

Hydrogenated lecithin (and) C12-16 alcohols (and) palmitic acid, are also capable of forming lamellar phases in the emulsion structures. When this non-ionic surfactant and cetyl alcohol are mixed a limited swelling can happen to create gel phases increasing the emulsions viscosity and structure. ⁽⁸⁶⁾

To study the influence of percentage of thickener, formulations 1, 2 and 3 were elaborated. In formulation 1 was not used any thickener, while in formulations 2 and 3 was used 1% and 2.5%, respectively, of cetyl alcohol as thickener. The rheological results of these formulations are presented in figure 46 and 47.

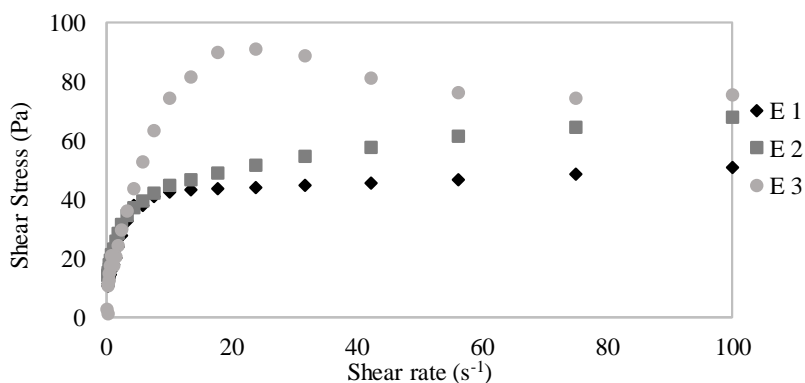


Figure 46 - Emulsions flow curves: Influence of different concentration of cetyl alcohol.

Figure 46 allows us to understand more about the viscosity behavior of formulations 1 to 3. The lowest viscosity formulation is emulsion 1 with an apparent viscosity of 6.8Pa.s at 5.6s⁻¹ shear rate. This was expected, as it has no percentage of cetyl alcohol in its structure or any other thickener. The formulation with the highest viscosity is emulsion 3 with an apparent viscosity of 9.37Pa.s at 5.6s⁻¹ shear rate, which is also an expected result, since this formulation has 2.5% cetyl alcohol. The viscosity behavior may be justified by the fact that when emulsions have cetyl alcohol and non-ionic surfactants as components of the formulations, the increase in viscosity occurs through the swelling of the crystals of cetyl alcohol during the cooling of the system. Since, below the transition temperature, the solubility of these chains increases and their subsequent hydration occurs, because both gel and crystalline phases formed can swell to incorporate

significant quantities of water in the interlamellar space. Consequently, the viscosity of the formulation increase. ^(86,121)

Comparing formulation 2 and 3, the first one presents an apparent viscosity of 7.0Pa.s at $5.6s^{-1}$ shear rate. Thus, emulsion 3 presents a higher viscosity value, since it has a higher percentage of cetyl alcohol (2.5%). This is justified by the fact that formulation 3 has a higher amount of cetyl alcohol and will present a higher swelling of the crystals of cetyl alcohol during the cooling of the system, in the same process that was described before. Therefore, the viscosity of the formulation increases for higher amounts/percentages of cetyl alcohol. ^(86,121)

Regarding the behavior presented by these formulations, they can also be considered as non-Newtonian fluids, more specifically shear-thinning materials, which are in accordance with the literature ^(79,116,121,122). In this behavior, the viscosity decreases under a shear rate, mainly due to its molecular semi-flexible structure.

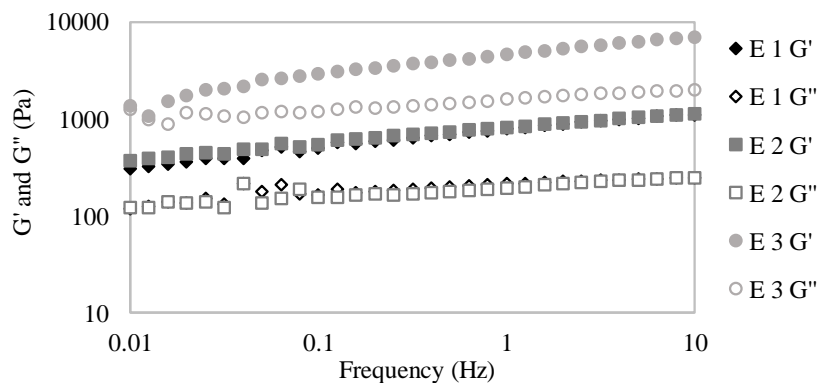


Figure 47 - Emulsions oscillatory results: Influence of different concentration of cetyl alcohol.

Through figure 47 we can determine the nature of the material under study. Thus, it should be noted that the value presented by the storage modulus is always dominant throughout the measurement, in relation to the loss modulus. In other words, it is found, once again, that the $G' > G''$ and the system can be considered a gel-like structure, with few changes in viscoelastic characteristics. Despite having some frequency dependence, typical of viscoelastic solids, the network of the system can be considered strong, being its disturbance difficult. Thus, adhesion and tackiness for topical application to the skin should be appropriate. The sensorial analysis will confirm it.

In relation to the loss tangent values, these are again less than 1 with 0.38, 0.32 and 0.29 for formulations 1, 2 and 3 respectively, at a frequency of 0.01Hz. These values confirm, once again, the gel-like structure of the emulsion, where the structure becomes more rigid approaching the structure of a solid. In this structure, the molecules of the components are more bound and organized than in liquids, but less than in solids.

In this case, it is still possible to point out that formulation 3 can be considered the most structured formulation since the values of the viscous and elastic modulus are the highest, compared to the other formulations. This result can be related to the percentage of the cetyl alcohol used in the formulation, as mentioned before.

The influence of preservatives

To understand the behavior of the formulations when different preservatives are used, formulations 7 to 12 were developed. Formulation 7 has the traditional methyl and propyl paraben as preservative, while other formulations (8, 9, 10, 11 and 12) have gluconolactone (and) sodium benzoate, chlorphenesin, 1,2-hexanediol, caprylyl glycol (and) glyceryl caprylate (and) glycerin (and) phenylpropanol (and) aqua and *o*-cymen-5-ol, respectively. The results are shown in figures 48 and 49.

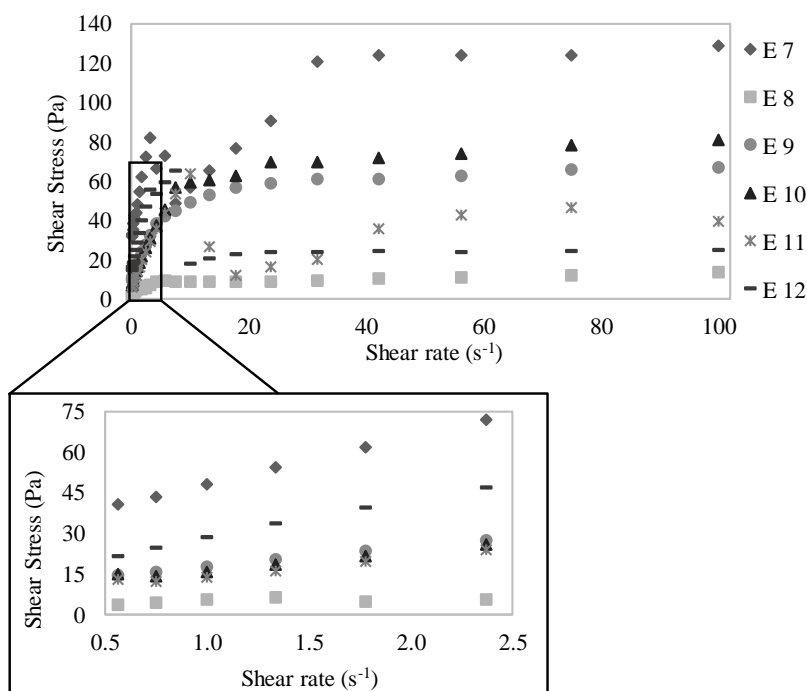


Figure 48 - Emulsions flow curves: Influence of different preservatives.

A preservative should prevent microbial proliferation or limit the contamination in normal storage and use. In addition, they should exhibit broad-spectrum activity against all kinds of microorganisms, such as fungi and gram-positive and gram-negative bacteria. It is not usual to have a chemical substance that acts as a preservative against all kinds of microorganisms, since those that act against fungi do not act against bacteria, and the opposite is also valid. Thus, the preservatives used are generally combined or already include in their final composition various types of preservatives. Another essential property of preservatives is that they act with as little concentration as possible. Nevertheless, the preservatives should not interfere with the structure and stability of the preparations. ^(92,93)

Parabens are esters of *p*-hydroxybenzoic acid, an antimicrobial that exhibits maximum activity at pH 3-8, since at higher pH it hydrolyses. Parabens have been used for several years, but have been the target of controversy over time, as they have suffered with claims of toxicity. Their use is limited, as manufacturers attempt to remove all controversial ingredients as much as possible. Therefore, the industry is trying to replace these chemical substances with alternative preservatives. In this category, excipients which contain a different function than preservative are used. These compounds only acquire a preservative function, as the ones used in this study from a certain percentage in the formulation. ^(92,123)

Regarding viscosity values, it can be increased by the number of hydrogen bonds between the preservative and the water molecules, as well as by the rigidity of the molecule. Preservatives containing in their structure cyclic groups or long carbon chains, automatically increase the viscosity of the formulations. Cyclic groups such as benzene are highly rigid and, when substituted with a long carbon chain, tend to further increase the viscosity of the formulation.

Figure 48 allows us to recognize that the formulation with the highest viscosity is emulsion 7 with an apparent viscosity of 313.9Pa.s at 0.1s⁻¹ shear rate, while the lower viscosity is emulsion 8 with an apparent viscosity of 14.1Pa.s at 0.1s⁻¹ shear rate. Parabens are the most viscous preservatives because they contain a highly rigid structure with two substituents: a methyl ester or a propyl ester and a hydroxyl group. On one hand, the ester groups make the molecule not only stiffer but also more hydrophilic and the hydroxyl

group adds more hydrophilic characteristics to the molecule, as it is able of binding to water molecules, through hydrogen bridges.

On the other hand, the lower viscosity formulation has a preservative with a composition based on gluconolactone (70-80%) and sodium benzoate (22-28%). This latter compound is a highly rigid cyclic aromatic system, whereas gluconolactone is a tetrahydropyran, composed by five carbon atoms and one oxygen, substituted by several OH groups. However, the first chemical structure gives the formulation more viscosity than the second, but it is in a smaller percentage in the preservative composition. In addition, it is still necessary to remember that this formulation proved to be unstable when physical stability tests were performed. Thus, for all these reasons, this is the preservative that causes the lowest viscosity.

Preservatives present in formulations 9 and 12, contains a six-membered aromatic ring substituted by carbon side chains and OH groups. These structures make the molecule acquire rigidity and make more hydrogen bonds with water. Finally, formulations 10 and 11 are mostly C4-8 carbon chains and hydroxyl groups. Thus, although they do not have cyclic aromatic groups, they have long carbon chains (stiffness) and OH groups.

Regarding the behavior of the formulations, as excepted given the literature ^(79,84,114), they present a shear thinning behavior, which means that they can be easily rubbed into the skin.

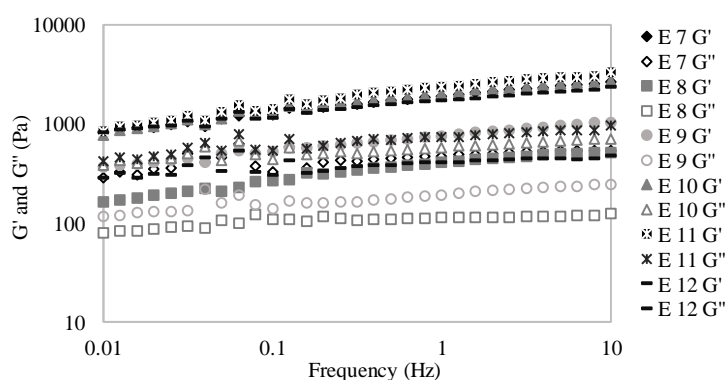


Figure 49 - Emulsions oscillatory results: Influence of different preservatives.

Figure 49 shows the results obtained from the oscillatory study. Once again it can be seen that the elastic component is far superior to the viscous component, showing that the system is more elastic than viscous, and the formulations can be considered structure fluid

emulsions. Both the elastic and viscous components prove to be nearly constant with frequency, but still show some dependence. Thus, the interaction formed between droplets causes a strong network.

Once again, the loss tangent values are less than 1, with values of 0.35, 0.48, 0.32, 0.50, 0.49 and 0.35 for formulation 7, 8, 9, 10, 11, and 12, respectively, at a frequency of 0.01Hz. Thus, the structured fluid emulsions' nature is confirmed and it is found that system disturbance is not easy.

After all the previous studies, the formulation chosen as the best for incorporation of compound **27** and other placebo studies was emulsion 5. This emulsion has glycerin as a humectant, 2.5% cetyl alcohol as thickener and parabens as preservative. Glycerin was chosen as a humectant not only because it has an intermediate viscosity among all humectants, but also because it is the most water-soluble humectant, allowing a homogenization of the formulation. To obtain a more consistent viscosity of the formulation, the incorporation of 2.5% cetyl alcohol was chosen. Finally, parabens have been used as preservatives, since they are already widely used in the pharmaceutical industry, well-known in terms of the formulation and their cytotoxic effects, being less likely to cause any kind of allergic reactions.

3.3.2. Microemulsion

The organoleptic characteristics and pH were evaluated for all microemulsions formulations. The macroscopic aspect showed that all formulations presented a liquid aspect, however, most of them had an opaque and heterogeneous appearance. Only formulations 5, 8, 13 and 14 presented clear, homogenous and liquid appearance, which corresponds to microemulsion systems. The composition of these formulations is shown in table 6. In formulation 5, 13 and 14 a percentage of 40.30% of surfactant was used, while 20.00% was incorporated in formulation 8.

Table 6 - Microemulsions' composition.

<i>Ingredients (INCI)</i>	<i>Formulations (%)</i>			
	5	8	13	14
<i>Water</i>	5.97	8.00	5.97	5.97
<i>PEG-20 Glyceryl Triisostearate</i>	40.30	20.00	40.30	40.30
<i>Propylene Glycol</i>	5.97	8.00	5.97	5.97
<i>Methylparaben</i>	0.11	0.15	0.11	0.11
<i>Propylparaben</i>	0.01	0.02	0.01	0.01
<i>Caprylic/Capric Triglycerides</i>	47.60	-	-	15.90
<i>C15-19 Alkane</i>	-	63.80	-	15.90
<i>C21-C28 Alkane</i>	-	-	47.60	15.90

The pH values of the formulations are in the pH range between 7.5 and 8.2, respecting the skin's natural pH. ⁽⁴⁷⁾ Therefore, only formulation 8 showed a higher pH (8.2). This result may be related to the use of C15-19 alkane oil or/and a higher percentage of propylene glycol.

3.3.2.1. Ternary diagram

A ternary diagram (figure 50) was created for formulations 5, 8, 13 and 14. Only formulation 8, where the C15-19 alkane was used as the oil, allows to obtain a microemulsion with less surfactant, as mentioned before. It is important to notice that the mix of surfactants comprises the emulsifier PEG-20 glyceryl triisostearate and the co-surfactant present in all formulations, propylene glycol.

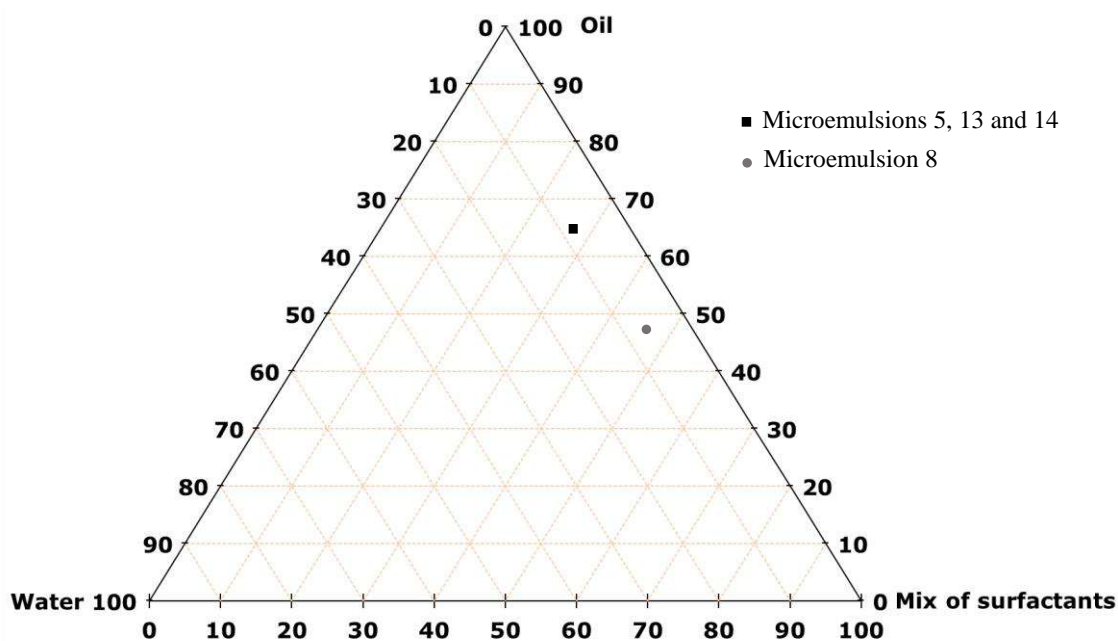


Figure 50 - Ternary diagram for microemulsions.

Ternary diagrams are commonly used, because they are useful to identify the complex interactions that may occur with different percentages of ingredients, and help to understand the structure of the water-surfactant-oil systems. ⁽⁷³⁾

According to the ternary diagram present in the literature ⁽⁷⁹⁾, these systems correspond to an W/O microemulsions, which is in accordance with the Bancroft and Ostwald rules. The Ostwald rule states that the concentrations of the oily and aqueous phases determine the external and internal phases, where at lower water concentrations, the system will consist of water droplets dispersed in oil (W/O emulsion). Whereas the Bancroft rule says that the external phase will preferably be the one where the surfactant is most soluble. ^(72,79,94)

Therefore, the microemulsions present in this study constitute an W/O system, which compromises water droplets dispersed in an oily phase, since it presents a low water concentration (Ostwald rule), and a surfactant (PEG-20 glyceryl triisostearate) that is considered oil-soluble, leading to the formation of an W/O emulsion (Bancroft rule).

Besides the surfactant, this formulation also compromises propylene glycol, which was used as humectant and co-surfactant, mainly due to its important properties, since it contributes to low interfacial tension and to reach an microemulsion. The molecules of propylene glycol are capable of intersperses between the molecules of surfactant,

attenuating the interactions between them, thus making the layer more flexible so that it easily deforms. Making the interfacial film sufficiently flexible, allows different curvatures required to form microemulsion. Usually, short to medium chain length alcohols are used as co-surfactants, once they reduce the interfacial tension and increase the fluidity of the interface, leading to the spontaneous formation of a thermodynamically stable microemulsion. ^(73,124,125)

The result obtained for formulation 8 may be related to the molecular weight of the oil, since oils with higher molecular weight interfere in the formation of microemulsions, requiring a higher amount of surfactant. ⁽¹²⁶⁾ The oil present in microemulsion 8 is a linear alkane composed of 15 to 19 carbon atoms. This structure is the smallest in terms of carbon atoms and the system may acquire lower free energy, further causing a higher difference between the free energy separating the oily phase from the aqueous phase. Thus, less surfactant is required to stabilize the system.

3.3.2.2. *Rheology*

The rheological characterization was performed by continuous shear and oscillation experiments. In these experiments, where three types of oils were used, the oil carbon chain was evaluated. Microemulsion 8 has the lowest carbon chain, while microemulsion 13 has the higher carbon chain. Microemulsion 14 is a blend of the three oils used in the previous formulations to better mimic the lipid structure of the skin. The results for the viscosity and oscillatory experiments are show in figure 51 and 52. The microemulsions will be labeled in the results using the abbreviation “ME” followed by the corresponding numbers.

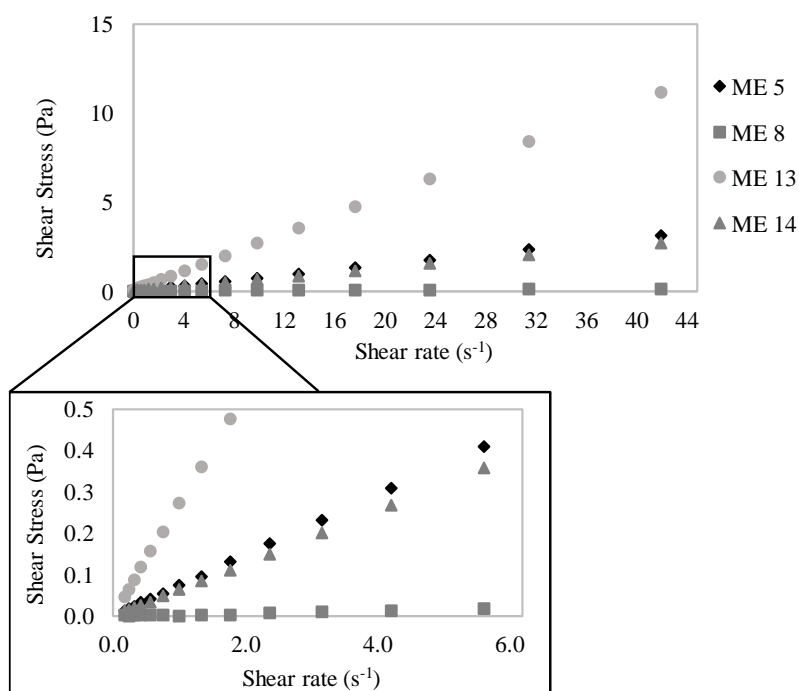


Figure 51 - Microemulsions flow curves: Influence of oil carbon chain.

Regarding the viscosity presented by the different oils, it is found that once again it depends on the carbon chain present in each molecule. With the help of figure 51, it is possible to determine that the formulation with the highest viscosity is emulsion 13, which presents an apparent viscosity of 0.140Pa.s at 0.2s⁻¹ shear rate, while the formulation with the lowest viscosity is emulsion 8, that presents an apparent viscosity of 0.013Pa.s at 0.2s⁻¹ shear rate. This is an expected result, since it is related to the carbon chain length.

Formulation 5 has a viscosity between the above two formulations with an apparent viscosity of 0.028Pa.s at 0.2s⁻¹ shear rate, because despite having twenty-nine carbon atoms in its structure, the main chain of the molecule has only twenty-one carbon atoms. The large viscosity difference between this formulation and formulation 13, is due to the structure of the caprylic/capric triglyceride used in the first formulation. On the one hand, the chemical structure of formulation 13 is a linear alkane chain of C21 to C28, while formulation 5 has C7 to C9 linear alkane chains separated by ester groups. Thus, caprylic/capric triglyceride oil has a less rigid structure than C21-28, despite having the same number of carbons in the molecule.

Formulation 14 has an initial viscosity slightly above that of formulation 5 (0.034Pa.s of apparent viscosity at 0.2s⁻¹ shear rate), since this formulation has all 3 types of oils in

the same proportion. Not only is its viscosity influenced by the lower carbon chain oil, but also by the C21-28 oil. Thus, its viscosity acquires an intermediate value.

With respect to the variation of viscosity with the application of a shear rate, all formulations can be considered Newtonian fluids, where the viscosity does not change when a shear rate is applied. The microemulsions present a very low viscosity, since the initial viscosity is 0.03Pa.s, 0.01Pa.s, 0.14Pa.s and 0.03Pa.s at $0.2s^{-1}$ shear rate for microemulsion 5, 8, 13 and 14, respectively, which is in accordance with the literature (55,73,74).

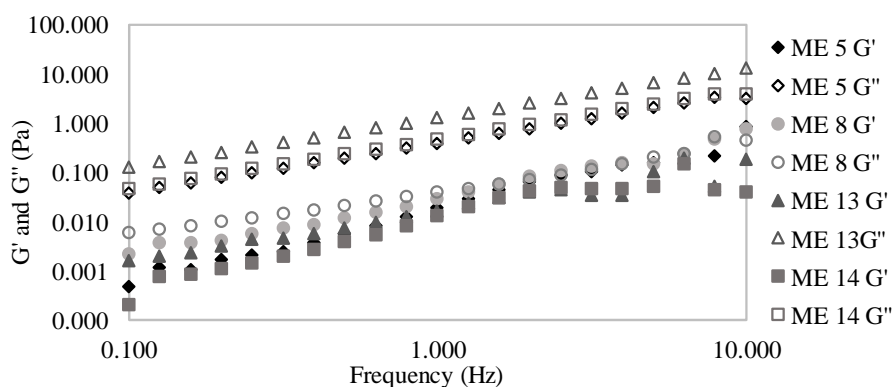


Figure 52 - Microemulsions oscillatory results: Influence of oil carbon chain.

Figure 52 provide us with the results from the oscillatory test, where it is possible to identify that in all cases the viscous module is quite superior to the elastic module. Therefore, the system presents a weak network, easily disturbed. Since $G'' > G'$ the system presents a liquid-like structure with good spreadability of the microemulsion.

In the case of microemulsions the expected loss tangent is higher than one. Formulations 5, 8, 13 and 14 have the value of loss tangent of 9.95, 2.11, 10.95 and 8.28, respectively, at a 0.01Hz frequency. These values confirm the liquid nature of microemulsion and the molecules of the colloid system are not tightly bound, as in the case of emulsions. Thus, all structures are disordered being closer to the structure of liquids.

After all previous studies, the formulation chosen as the best for incorporation of compound **27** was microemulsion 14. This formulation was chosen because it has in its composition all the different oils studied in order to mimic the lipid layer of the skin.

3.4. Characterization of final pharmaceutical vehicles: Placebos

The final two formulations chosen were emulsion 5 and microemulsion 14. These two formulations without any drug (placebo) were characterized considering droplet size, *in vivo* sensorial and skin analysis.

3.4.1.1. Droplet Size

Droplet size of the placebo's emulsion and microemulsion was measured to characterize and compare the values. The results are shown in figures 53 and 54. Since the microemulsion was very concentrated and could not be diluted, so as not to modify the system, some errors occurred in the measurement.

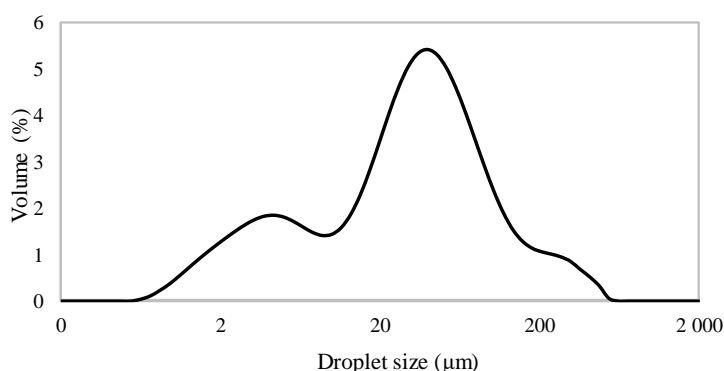


Figure 53 - Droplet size distribution by volume (%) of the placebo's emulsion 5.

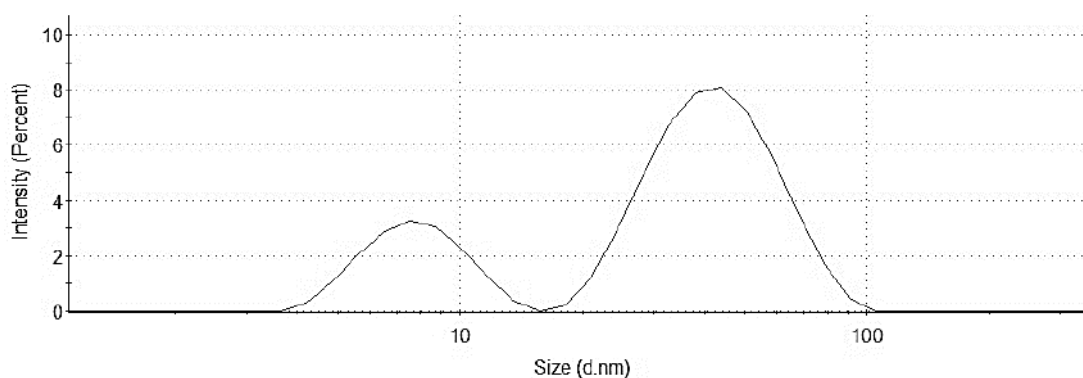


Figure 54 - Droplet size distribution by intensity of the placebo's microemulsion 14.

The d(50) for the emulsion 5 was 34.50µm with a span of 3.731, while microemulsion 14 presented a d(50) of 39.25nm with a PdI of 0.549.

With the result obtained for the droplet size of the emulsion, it is possible to confirm that it is in accordance with the droplet sizes described in the literature for these formulations. ^(73,74) On another hand, the literature indicates that microemulsions should have a droplet size diameter less than 150nm, which is in accordance with the results obtained. ⁽⁵⁵⁾

It should also be noted that droplet size may influence the viscosity of the formulations, since larger droplet sizes present higher viscosity values, because it hinders the movement of droplets within the formulation, making it more rigid, and therefore, with a higher viscosity. Thus, the O/W emulsion not only has, as expected, a larger droplet size than microemulsions, but also a higher viscosity than microemulsions. The initial viscosity of emulsion 5 is 131.3Pa.s at 0.1s⁻¹ shear rate, while the initial viscosity of microemulsion 14 is 0.03Pa.s at 0.2s⁻¹ shear rate.

3.4.1.2. Sensory analysis

Sensory analysis tests were performed to evaluate some parameters such as: appearance, fragrance, application, spreading, sticky, feeling after application, oiliness, brightness, whitish stain, softness, hydration and acceptance by the consumer. The results obtained are shown in figure 55.

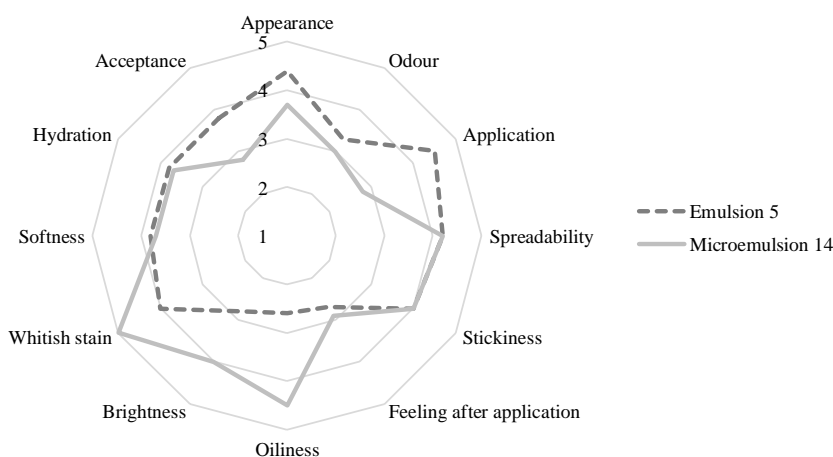


Figure 55 - *In vivo* sensory analysis results for O/W emulsion 5 and W/O microemulsion 14 (average; n=10).

From the figure shown above, it is clear, with a perceptible difference, that volunteers preferred the O/W emulsion to the microemulsion. Regarding the organoleptic aspects (appearance and odor) spreadability, texture (stickiness and softness) feeling after

application, and hydration, the evaluation does not show significant differences between the two formulations.

On the other hand, there are significant differences regarding application, oiliness, shine and whitish stain. In the case of application, volunteers indicated that application of the emulsion was better than application of microemulsion. This result had already been expected since the microemulsion is a very liquid product which makes its application more difficult, due to the fact that this product oozes when applied to the skin.

Regarding oiliness, it is found that the oiliness presented by the microemulsion is higher than the oiliness presented by the emulsion. This result is related to the fact that the microemulsion has about 48% oil in the formulation, whereas the emulsion contains only about 13% oil in its formulation. Thus, the result obtained is as expected, since the oiliness of the microemulsion is significantly higher than the emulsions'.

The brightness displayed by the formulations relates to the amount of oil present as well as the macroscopic aspect of the formulations. The emulsion has a more solid appearance than the microemulsion and a lower amount of oil. Thus, the emulsion tends to look more matte than microemulsion. On the other hand, having a more solid appearance than microemulsions also made them differ in the whitish stain parameter. Thus, when applying the emulsion, the volunteers found that it produced a slight whitish stain, whereas the microemulsion did not produced a whitish stain.

3.4.1.3. *In vivo skin analysis.*

The *in vivo* skin analysis studies were performed to understand the behavior of each formulation when in contact with the skin, regarding the moisturizing, hydration and TEWL parameters. The results for both placebos' formulations are presented in figure 56, where D0 corresponds to day 0 (where there is no application of this formulations) and D28 corresponds to the twenty-eighth day of application of both formulations. It is important to highlight that both formulations were applied in different locations, but always in the same anatomical region, so that there is no influence of one formulation on another.

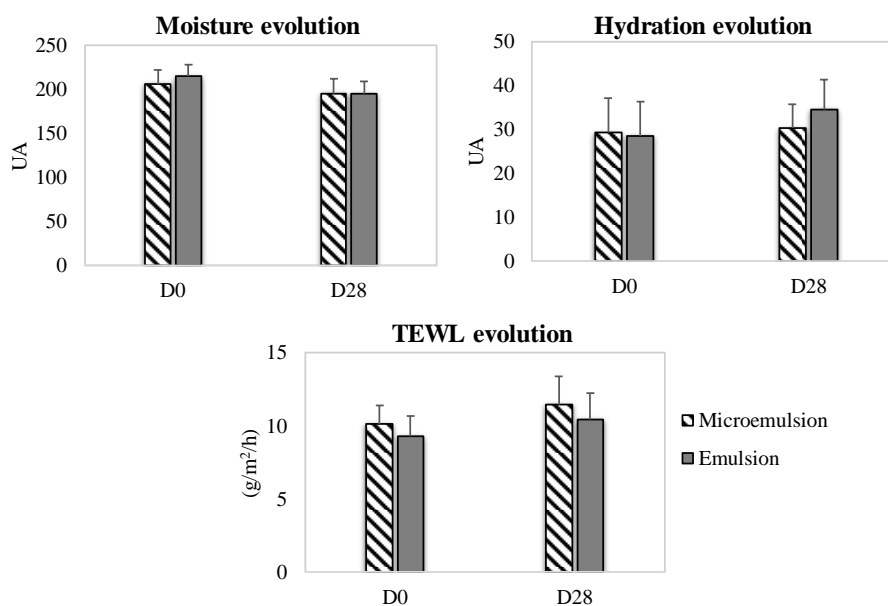


Figure 56 - Results from the moisturization, hydration (Epidermal Caparicante) and TEWL studies.

Regarding hydration, the two formulations do not show any significant differences when compared with each other or with the control over the twenty-eight days. Although, in regards to this parameter, the O/W emulsion shows a higher tendency of hydration, as it has a higher percentage of water and is considered an O/W structure with lamellar phases, due to the use of surfactant and fatty alcohols, that promote this structure in the formulation, as previously discussed. These lamellar phases provide a greater affinity to the skin, as it also has a lamellar structure (figure 13). Thus, the internal structure of the emulsion allows for a higher similarity to the structure of the skin, enhancing the permeation of this formulation into the skin. Therefore, the hydration capacity of this formulation is higher because of its structure and its higher amount of water.

The moisturization parameter allows to understand how the formulation helps to prevent the TEWL, through the moisture retention, since it helps build the skin's protective barrier. The two formulations showed a decrease in this parameter, but with no significant differences, when compared with the measurement performed in the first day. Thus, TEWL would be expected to increase when comparing to the two measurements. This result is shown in the TEWL graphic, where this parameter is higher for the microemulsion than the emulsion, which is related to the oils used in both formulations. Microemulsions' oils are mainly hydrophobic, which theoretically allows to reduce the TEWL. However, this formulation also presents high amounts of surfactant which destroys the lipidic layer of the skin inducing a higher TEWL.

3.5. Final formulations containing AAN-27

The AAN-27 (compound 27) was incorporated into O/W emulsion 5 and microemulsion 14, “AAN-27 E” and “AAN-27 ME”, respectively, at the same concentration (0.1mg of compound 27 per gram of formulation). In this section the pH, rheology and droplet size will be compared between these two final formulations where the compound was incorporated. The drug release and the *in vivo* antipsoriatic activity of each formulation were performed, to understand which of the formulations would be most appropriate for the therapy of inflammatory diseases, such as psoriasis. The composition of the formulations is present in tables 7 and 8.

Table 7 - AAN-27 E O/W emulsion composition.

<i>Ingredients (INCI)</i>	<i>Formulation (%)</i>
	AAN-27 E
<i>Water</i>	72.79
<i>Glycerin</i>	5.00
<i>Methylparaben</i>	0.18
<i>Propylparaben</i>	0.02
<i>Hydrogenated lecithin (and) C12-16 alcohols (and) palmitic acid</i>	6.00
<i>Caprylic/capric triglycerides</i>	2.50
<i>C10-18 Triglycerides</i>	4.00
<i>Isopropyl myristate</i>	5.00
<i>Oleic acid</i>	1.00
<i>Alpha bisabolol</i>	1.00
<i>Cetyl alcohol</i>	2.50
<i>Compound 27</i>	0.01

Table 8 - AAN-27 ME Microemulsion composition.

<i>Ingredients (INCI)</i>	<i>Formulations (%)</i>
	AAN-27 ME
<i>Water</i>	5.97
<i>PEG-20 Glyceryl triisostearate</i>	40.27
<i>Propylene glycol</i>	5.97
<i>Methylparaben</i>	0.11
<i>Propylparaben</i>	0.01
<i>Caprylic/capric triglycerides</i>	15.90
<i>C15-19 Alkane</i>	15.90
<i>C21-C28 Alkane</i>	15.90
<i>Compound 27</i>	0.01

3.5.1. pH

The AAN-27 E present a pH of 6.7, while the AAN-27 ME shows a pH of 7.5. The pH value obtained for both formulations is appropriate for the skin according to the literature ^(47,111). Comparing with the pH obtained in relation to placebos, it is verified that there are no significant changes.

3.5.2. Rheology

The rheological characterization was performed by continuous shear and oscillation experiments, in the same as what has previously been done. The results for the viscosity and oscillatory experiments are shown in figures 57 to 59.

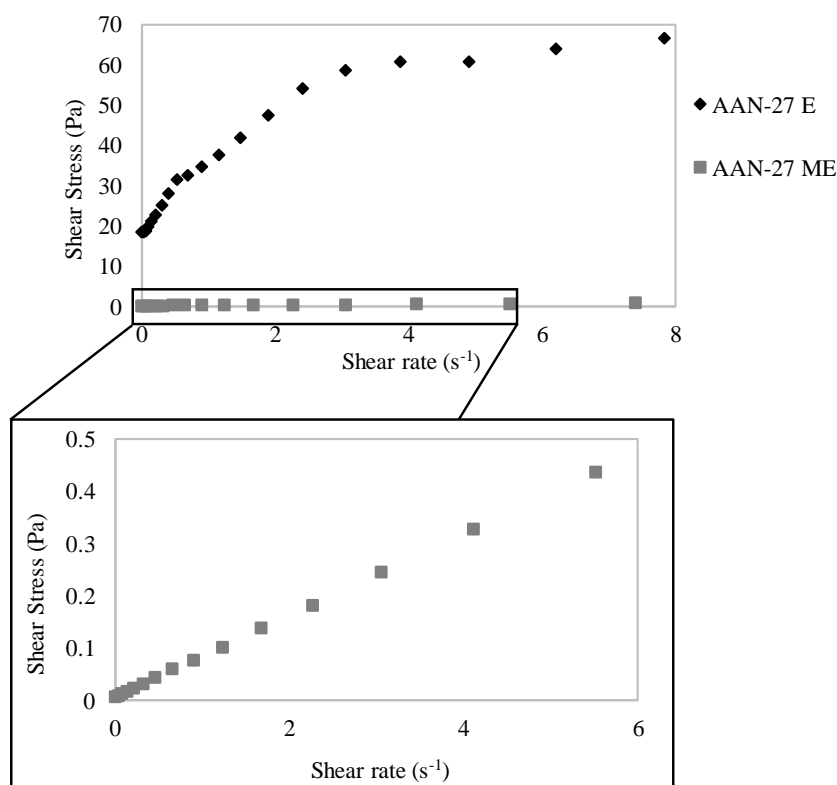


Figure 57 - AAN-27 E and AAN-27 ME flow curves.

Concerning viscosity, it can be seen in figure 57 that the emulsion once again has a much higher viscosity than the microemulsion. The AAN-27 E has an apparent viscosity of 182.5Pa.s at 0.1 s⁻¹, while the AAN-27 ME has an apparent viscosity of 0.05Pa.s at the same shear rate. These values remained constant without any significant differences

when compared with placebos for both formulations, as those previously observed were 131.3Pa.s and 0.03Pa.s at $0.1s^{-1}$, for emulsion and microemulsion, respectively.

The AAN-27 ME remains with a Newtonian behavior, similar to placebo microemulsion and the AAN-27 E maintained its shear-thinning behavior, which is in agreement with other studies performed. ^(55,73,74,79,84,116)

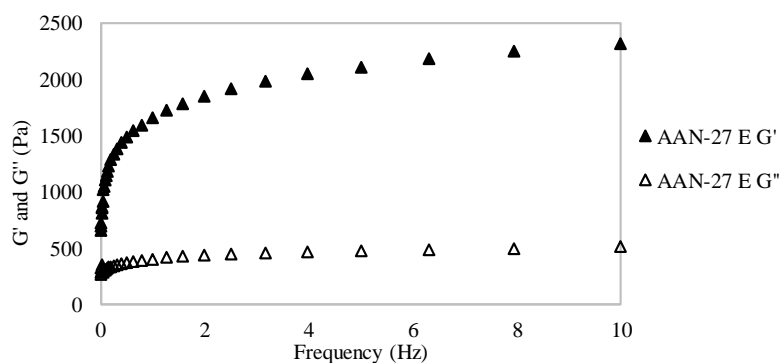


Figure 58 - Oscillatory results of AAN-27 E.

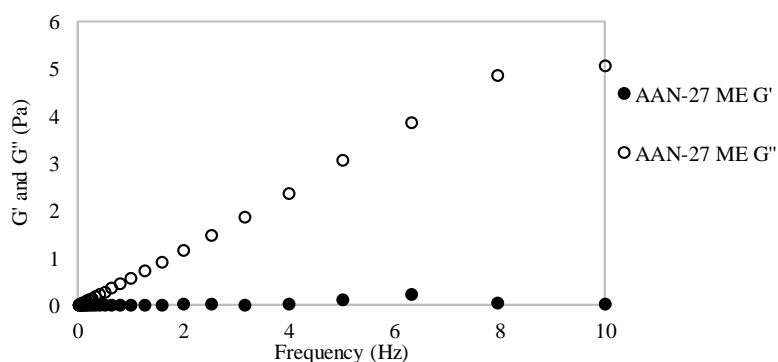


Figure 59 - Oscillatory results of AAN-27 ME.

With respect to the oscillatory results (figure 58), by comparing the emulsion with the placebo, it is once again found that the elastic component has a higher value than the viscous component, having a strong network. The loss tangent remains practically the same with a value of 0.36 and 0.34 for the AAN-27 E and the placebo's emulsion, respectively, at a frequency of 0.01Hz. This is the expected value, since the $G' > G''$ and loss tangent values must be less than 1 ⁽¹²⁰⁾, indicating that the system can be considered as a solid-like solution.

The oscillatory study shown in figure 59 corresponds to AAN-27 ME, where again the elastic modulus is lower than the viscous modulus, presenting a weak network.

Concerning the loss tangent, the values are 12.9 and 8.28 for AAN-27 ME and placebo's microemulsion, respectively, at a frequency of 0.01Hz. Thus, the microemulsion structure can once again be considered liquid-like structure, despite presenting slight differences in loss tangent.

3.5.3. Droplet size

The droplet size results are shown in figure 60 and 61. As mentioned before, some errors occurred in the measurement of the microemulsions' droplet size.

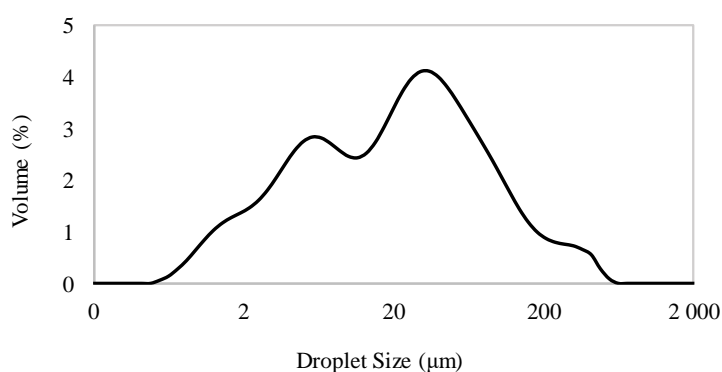


Figure 60 - Droplet size distribution by volume (%) of the AAN-27 E.

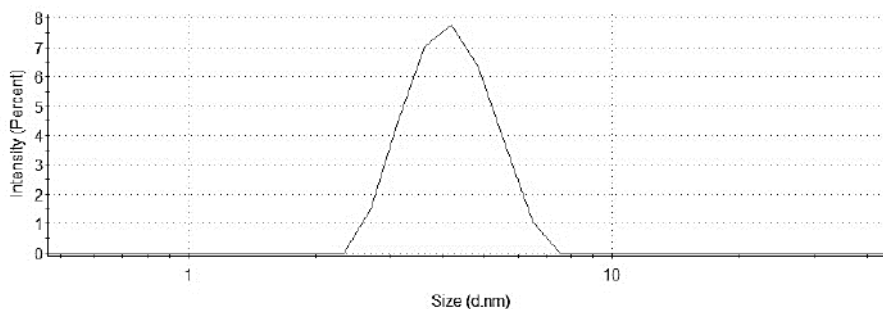


Figure 61 - Droplet size distribution by intensity of AAN-27 ME.

The d(50) for AAN-27 E was 23.52µm with a span of 5.028, while AAN-27 ME presented a d(50) of 9.92nm with a PdI of 0.834.

Comparing these results with the placebo's emulsion and placebo's microemulsion, the droplet size values decreased, being different from those obtained with the placebo's of both formulations (the d(50) for the emulsion 5 was 34.50µm with a span of 3.731, while the microemulsion 14 presented a d(50) of 39.25nm with a PdI of 0.549).

3.5.4. Fluorescence microscope

To understand the internal structure of the AAN-27 E and AAN-27 ME with and without compound **27**, were used a fluorescence microscope and the results are presented in figure 62.

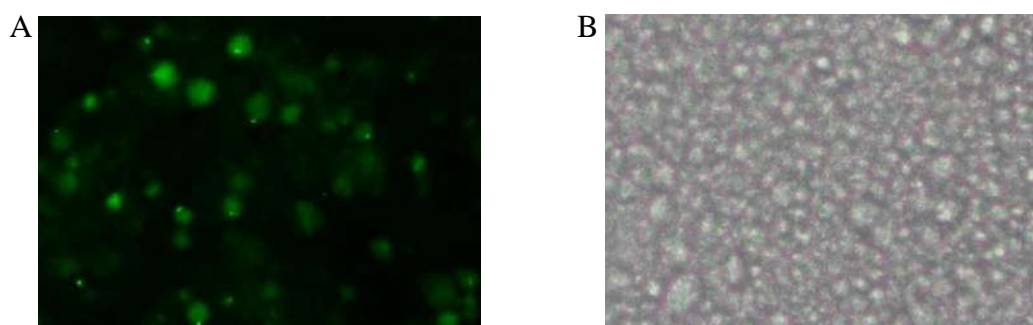


Figure 62 - Inside structure of (A) AAN-27 E and (B) placebo's emulsion, using an optical fluorescence microscope with video camera (Bresser, Germany) with an enlargement of 100x.

Figure 62 shows the two photographs corresponding to the emulsion with and without compound **27**. It is possible to observe the emulsions droplets. It is further noted that the compound is dissolved, as expected, in the oily phase. Thus, as presented in figure 62A, the formulation droplets are fluorescent due to the compound.

Regarding to the microemulsion the results are not shown in a figure, because unlike the emulsion it is not possible to identify the droplets (probably due to the reduced droplet size) or see any difference between the placebo and the AAN-27 ME, except for the fluorescence presented by the compound. The microemulsion' placebo presented a black aspect while the AAN-27 ME present a green fluorescent aspect, as expected.

3.5.5. Drug Release

In vitro drug release studies were performed in Franz Cells. The results are shown in figure 63: the solution used in this study (AAN-27 S), as a control, compromises the same concentration of compound **27** (0.1mg/mL) in water:ethanol (50:50 w/w) with 2.5% of

PEG-40 Hydrogenated Castor Oil. The composition of the receptor phase is the same as the solution.

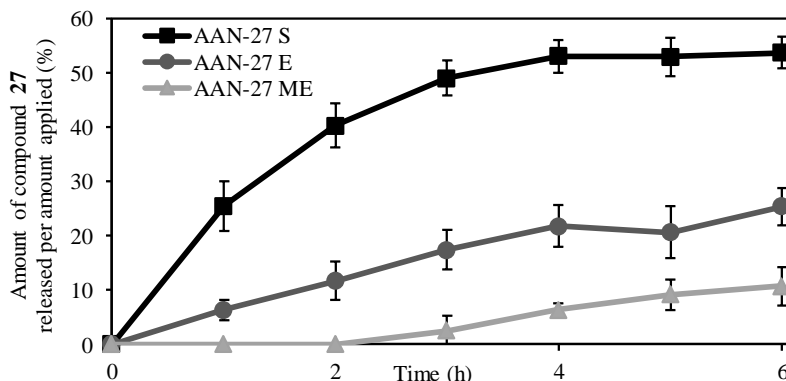


Figure 63 - Drug release studies for AAN-27 ME, AAN-27 E and AAN-27 S.

After 6 hours, the amount of the active compound released was $2.90 \pm 1.2 \mu\text{g}/\text{cm}^2$ ($10.0 \pm 3.5\%$), $7.94 \pm 2.1 \mu\text{g}/\text{cm}^2$ ($24.4 \pm 7.4\%$) and $17.93 \pm 1.6 \mu\text{g}/\text{cm}^2$ ($55.1 \pm 5.7\%$) for AAN-27 ME, AAN-27 E and AAN-27 S, respectively.

The results of the drug release are related with the vehicle, as it plays a key role in dermal drug delivery. Formulating includes the optimization of drug delivery and bioavailability as well as chemical and physical stability, non-toxicity of the vehicle and aesthetic acceptance. ⁽¹²⁷⁾

The process of diffusion of a drug into the membrane or into the skin may be influenced by the vehicle itself, and the interactions that may occur between it and the drug and/or skin. Thus, drug permeation into the skin is constantly influenced by interactions between skin, drug and vehicle. ⁽¹²⁷⁾

Regarding the permeation of the drug into the skin, it is necessary to consider some important factors such as drug molecular weight, log P and charge (anionic or cationic) as well as skin condition, namely, hydration. ⁽¹²⁸⁾

Topical formulations can reversibly swell corneocytes and change the structure of the *stratum corneum* and increase permeation. ⁽¹²⁸⁾ However, the results obtained in the biological studies (*in vivo*) do not show any significant changes in skin hydration (figure 56). Therefore, this parameter did not interfere in drug release.

Compound **27** has a log P of 4.68, indicating that the compound is mainly lipophilic, and it is not charged. However, its molecular weight ($M = 643.68\text{g}\cdot\text{mol}^{-1}$) can be responsible for the low drug release in all formulations, making it difficult to diffuse through the membrane.

Since the drug release is not influenced by the factors discussed above (since they are present in all formulations) some other vehicle characteristics need to be studied, such as its composition, internal structure, its viscosity and the solubility of the drug in the formulation.

The AAN-27 S was the formulation that showed the highest percentage of drug release over time. It is a liquid disperse system where the drug is completely soluble. The diffusion through the membrane was possible because de donor and the receptor phases were the same. Although, despite being the formulation with the highest percentage of drug released, the AAN-27 S can only be used in hair zone and not *in vivo* because it is not suitable for skin application, since it does not contain other essential components for topical application, such as emollients, oils and humectants, which help maintain the properties of the skin.

On the other hand, AAN-27 E presents an oil in water gel-like structure while AAN-27 ME presents a liquid-like structure with a high content of surfactants and occlusive lipids. In these systems, it is not possible to ensure a complete solubility of the active substance.

AAN-27 E is an O/W emulsion, where the drug is incorporated in the internal phase of the formulation (oily phase). To reach the membrane and the receptor phase, the compound needs to pass through all the external phase (aqueous phase) that constitutes a barrier between the compound and the membrane, making drug diffusion more difficult. However, this formulation presents permeation enhancers (isopropyl myristate, propylene glycol and oleic acid) which can affect skin solubility and/or disturb the lipid structure of the *stratum corneum*.^(55,61) On the other hand, this formulation has 6% of emulsifier (Hydrogenated Lecithin (and) C12-16 Alcohols (and) Palmitic Acid), that can disrupt the *stratum corneum* barrier allowing the diffusion of the drug⁽¹²⁷⁾. This emulsifier is considered a phospholipid-based O/W lamellar emulsifier and should present high affinity to the skin leading to higher drug release values (figure 13). Through these two

components the AAN-27 E exhibits higher drug release over time when compared to AAN-27 ME.

It would be expected that the microemulsion exhibit a higher drug release, like presented by other authors^(55,73,104). Nevertheless, as noted, the interactions between the membrane, the drug and the vehicle influenced the release of the active compound. As far as AAN-27 ME is concerned, this is a W/O microemulsion where the compound is dissolved in the oily phase of the formulation. The presence of 40% of a non-ionic surfactant (PEG-20 Glyceryl Triisostearate) and 6% of permeation enhancer (propylene glycol) could also promote a higher drug diffusion. For these reasons, a higher drug diffusion when compared with O/W emulsions was expected, but the results obtained show the opposite. Several studies^(129–131) indicate that drug flow is inversely proportional to the amount of surfactant, since when it is above its CMC, the drug is solubilized within the surfactant micelles, leaving a smaller amount of free drug (no solubility in micelles) in the vehicle. Thus, when the surfactant concentration is very high, the availability of the drug is diminished decreasing its diffusion through membranes.⁽¹²⁷⁾ When the active compound is too compatible to the formulation, there is no driving force causing a decrease in drug flux.⁽¹²⁷⁾ Thus, although AAN-27 ME is a W/O formulation and the study compound is lipophilic, the high amount of surfactant makes it difficult to diffuse the drug into the membrane, due to the interactions of the surfactant with permeation enhancers and the active compound.

For the characterization of the drug release mechanism four different kinetic models were applied (zero order, first order, Higuchi and Korsmeyer–Peppas) and the results are shown in table 9. Besides R^2_{adjusted} , AIC was also used as a fit measure.

For the AAN-27 E and AAN-27 S, the best fitting kinetic model was the Korsmeyer–Peppas ($R^2_{\text{adjusted}} = 0.949 \pm 0.014$ and $R^2_{\text{adjusted}} = 0.939 \pm 0.062$, respectively), but the Higuchi can be also applied, since the value of the R^2_{adjusted} does not demonstrate a significant difference. ($R^2_{\text{adjusted}} = 0.934 \pm 0.029$ and $R^2_{\text{adjusted}} = 0.924 \pm 0.052$, for AAN-27 E and AAN-27 S, respectively). Regarding the AIC values, in both models the difference was not significant for these two formulations. Therefore, both AAN-27 E and AAN-27 S follow the Higuchi and Korsmeyer–Peppas kinetics which are models that describe the diffusion kinetic mechanism of the vehicle through the skin.

Table 9 - Kinetic parameters obtained after fitting the drug release data from AAN-27 E, AAN-27 ME and AAN-27 S, to different release models (mean \pm SD, n = 6). K—release constant; R^2_{adjusted} -adjusted coefficient of determination; AIC-Akaike information criterion; n—release exponent.

Formulation	Model	K	R^2_{adjusted}	AIC
AAN-27 E	Zero order	4.60 \pm 0.80	0.875 \pm 0.061	27.43 \pm 4.13
	First order	0.05 \pm 0.01	0.907 \pm 0.048	25.39 \pm 3.50
	Higuchi	9.56 \pm 1.85	0.934 \pm 0.029	23.45 \pm 6.27
	Korsmeyer-Peppas	$\frac{7.84 \pm 2.15}{n = 0.65 \pm 0.11}$	0.949 \pm 0.014	22.83 \pm 4.35
AAN-27 ME	Zero order	1.57 \pm 0.45	0.793 \pm 0.068	24.45 \pm 4.66
	First order	0.016 \pm 0.005	0.784 \pm 0.069	24.75 \pm 4.77
	Higuchi	3.04 \pm 0.87	0.568 \pm 0.084	29.84 \pm 4.50
	Korsmeyer-Peppas	$\frac{0.44 \pm 0.31}{n = 1.969 \pm 0.44}$	0.896 \pm 0.047	19.94 \pm 2.93
AAN-27 S	Zero order	11.86 \pm 1.34	0.633 \pm 0.133	47.23 \pm 3.71
	First order	0.18 \pm 0.03	0.836 \pm 0.070	41.78 \pm 4.43
	Higuchi	25.08 \pm 2.07	0.924 \pm 0.052	36.02 \pm 6.20
	Korsmeyer-Peppas	$\frac{28.25 \pm 5.57}{n = 0.42 \pm 0.13}$	0.939 \pm 0.062	33.82 \pm 8.18

Although, through the Korsmeyer–Peppas kinetics model it is possible to identify the type of diffusion by the value of the diffusional exponent. For the case of AAN-27 E the diffusional exponent was 0.65 ± 0.11 , being higher than 0.5. Consequently, according to the literature, ^(132–134) the release is considered non-Fickian (anomalous) which means that the drug release follows both a diffusion and an erosion controlled mechanism. On another hand, the AAN-27 S showed a diffusion exponent lower than 0.5 ($n = 0.42 \pm 0.13$) which, and according to the literature ^(132–134), indicates that this formulation follows the Fickian diffusion.

The best fitting kinetic model for the AAN-27 ME was the Korsmeyer–Peppas, where the R^2_{adjusted} is 0.896 ± 0.047 and the AIC shows a minimum value of 19.94 ± 2.93 . Since the diffusion exponent is much higher than 0.5 ($n = 1.969 \pm 0.44$) the release is considered non-Fickian, according to the literature ^(132–134). These results are in accordance with the drug release study, since the AAN-27 ME was the one with lower drug release over the time and as a higher diffusion exponent, followed by the AAN-27 E and AAN-27 S.

The results obtained from the *in vitro* permeation study using in silicone membranes did not show any drug in the receptor phase or in the silicone membrane. Thus, the *in vitro* drug release using a porcine membrane was not performed.

3.5.6. *In vivo* antipsoriatic activity

The *in vivo* antipsoriatic activity studies were performed to evaluate the therapeutic efficacy of these new topical platforms containing compound **27**. The results of this study regarding scaling, erythema and skin thickness are presented in figure 64.

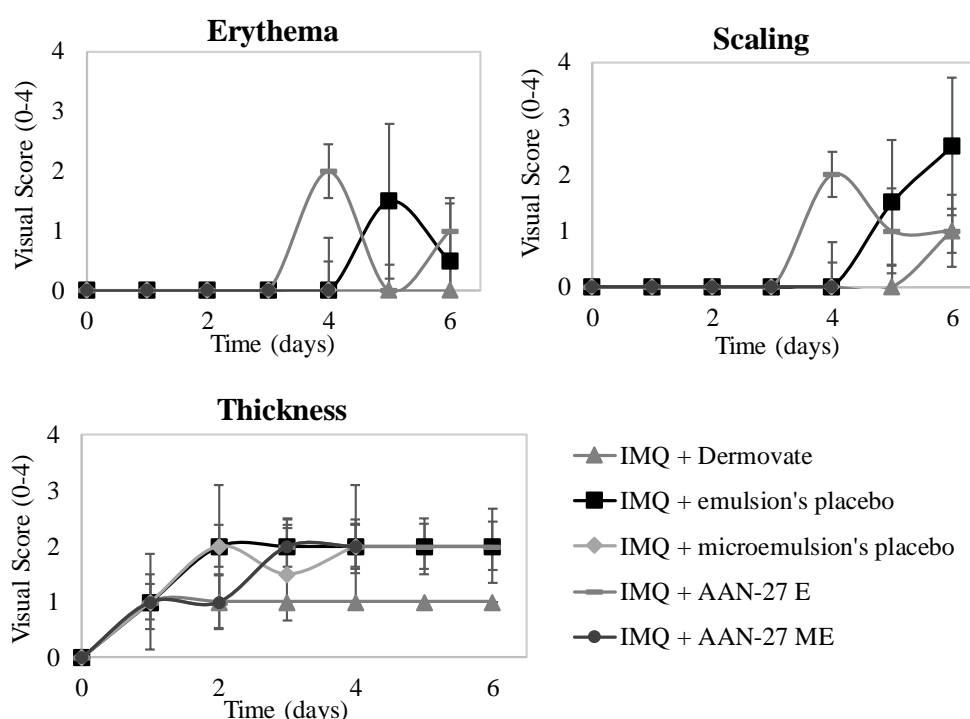


Figure 64 - Results of the *in vivo* antipsoriatic activity: erythema, scaling and thickness.

Mice skin challenged with imiquimod and treated with clobetasol propionate (Dermovate®) presented the smallest scores for all the parameters observed. The AAN-27 E and the placebo are the formulations with the highest score. *Stratum corneum* disturbance by imiquimod dramatically promotes cutaneous drug absorption.⁽¹³⁵⁾ However, there are no significant differences between AAN-27 E and the placebo's emulsion, figure 65. Thus, it is noted that the therapeutic effect observed in the animals is not due to compound **27** alone, but due to the formulation used instead.

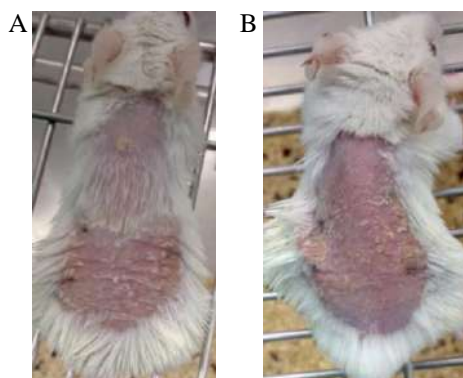


Figure 65 - Skin's damage after the application of (A) emulsion placebo's and (B) AAN-27 E in the seventh day of study.

Regarding AAN-27 ME and the placebo's microemulsion, it should be noted that the animals treated with these formulations, had to be sacrificed within 4 days of application due to their condition, as can be observed in figure 64. AAN-27 ME and its respective placebo were not able to treat skin lesions. Moreover, the impairment of the skin's barrier might have increased in the microemulsion due to the surfactant absorption.

The surfactant itself (appendix 2, section 8.20) was not expected to present skin irritation in intact skin. However, in the presence of skin barrier damage its toxic potential is not perfectly clear.

In figure 66, it is possible to observe the damage in the skin's mice after five hours of the application of AAN-27 ME and the microemulsions placebo's.

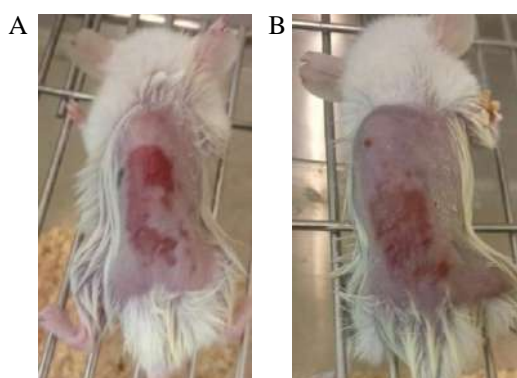


Figure 66 - Skin's damage five hours after the application of (A) microemulsions placebo's and (B) AAN-27 ME in the fifth day of study.

The two microemulsions (AAN-27 ME and placebo) were composed of 40% surfactant that probably does not allow a fast skin barrier recovery. Therefore, in this animal model, where imiquimod was used to induce psoriasis in animals and damaged the skin barrier, AAN-27 ME and the placebo's microemulsion, did not treat the skin lesion. It is still necessary to emphasize that there is no significant difference between the use of the compound alone or the AAN-27 ME.

Figures 67 and 68 show the histopathology results of mice skin exposed to imiquimod.

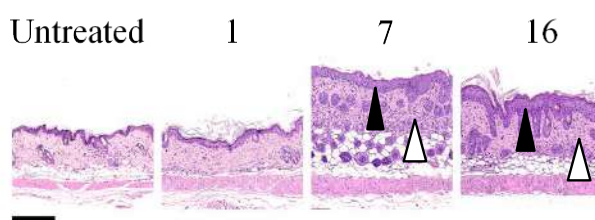


Figure 67 - Representative microphotographs of skin (dorsum) of mice exposed to imiquimod. Changes were characterized by epidermal hyperplasia (black arrowhead), and focally extensive inflammation mildly expanding the dermis (white arrowhead). Hematoxylin and eosin stain. Original magnification, 10x (bar, 250 μ m). Animal 1 was treated with clobetasol propionate, animal 7 was treated with placebo's emulsion and animal 16 was treated with AAN-27 E.

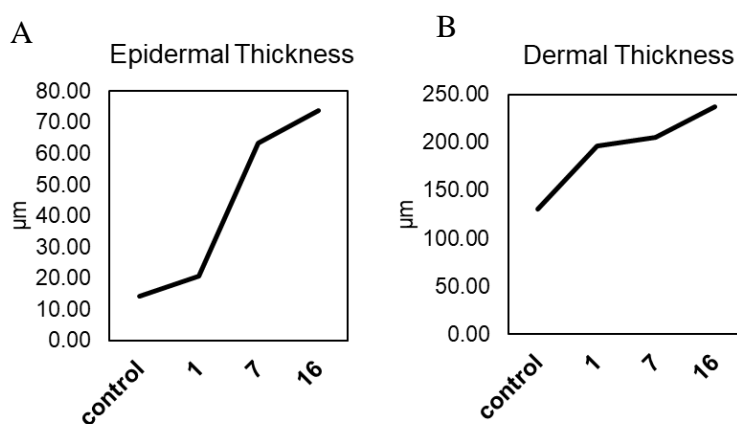


Figure 68 - Epidermal and dermal thickness of the skin (dorsum) of mice exposed to imiquimod. Measurements were performed in slides digitally scanned in the Hamamatsu NanoZoomerSQ, with NDP.view2 software (Hamamatsu), and correspond to mean value obtained from 7 to 12 different points, for epidermis (A) and dermis (B), in longitudinal skin sections for each individual mice. Animal 1 was treated with clobetasol propionate, animal 7 was treated with placebo's emulsion and animal 16 was treated with AAN-27 E.

Through the present study, it is possible to identify that the lesions were characterized by diffuse epidermal hyperplasia, which causes an increased thickness of the Malpighian layer (highlighted with a black arrow), which is composed by *stratum basale* and *stratum spinosum* (figures 67 and 68A).

A focally extensive minimal to mild inflammation expanding to the dermis was also observed as can be seen in figure 67 (highlighted with a white arrow), resulting in diffuse thickening (figure 68B). In this inflammation's case, the infiltrates corresponded to a mixed cell population with marked mononuclear-cell component.

It is also important to notice that the edema present in the mice was minimal and the untreated animal was used as control and no changes were found.

Therefore, considering all the results above it is noteworthy that the microemulsions are the least indicated for skin application, mainly due to the high amount of surfactant. The emulsion can be considered an effective formulation, but it should be noted that there are no significant differences between the placebo and AAN-27 E formulations. Thus, it indicates that the therapeutic effect may be related to the formulation itself and not with the use of compound **27**. This result does not mean that the formulations cannot have therapeutic action in other models of acute or chronic cutaneous inflammatory disease.

4. Conclusion and future work

From the results presented in this work, we can conclude that these new inhibitors, showed high activities (nanomolar range) against HNE, constituting promising scaffolds. Initially, the two best synthesized compounds were **18** and **22**, showing high activity and high cell viability. Subsequently, two new compounds **27** and **28** were synthesized with fluorescence which, in addition to their high activity and cell viability, also showed selectivity for HNE, constituting promising compounds. Comparing with the control (compound **1**), the two compounds showed an increase in cell viability.

Compounds **27** and **28**, showed similar activities and selectivity against HNE. However, compound **27** presented a cell viability of 91.6%, being chosen to be incorporated into the topical delivery systems.

Regarding O/W emulsions we can conclude that different components such as humectants, thickeners and preservatives, influence the internal structure of the formulation, causing variations in rheology or even stability of the formulation. Accordingly, after all studies, emulsion 5 was chosen as the best for incorporation of compound **27**.

A three dimensional representation of the three component (ternary) system was used to determine the composition of all phases present in microemulsions: formulations 5, 8, 13 and 14 presented microemulsions macroscopic characteristics. Nevertheless, microemulsions 5, 13 and 14 has a higher amount of surfactant when compared to formulation 8.

It was possible to verify the influence of the carbon chain oils on microemulsions' structures. Different oils cause a variation in formulation rheology properties: higher carbon chain oils increase viscosity and G' .

From the *in vivo* evaluation (biological and sensory analysis) there were no significant differences among the formulations and with the control area and volunteers preferred the O/W emulsion to microemulsion, since this formulation presented an easy application, low oiliness and low shine.

From the results obtained, emulsion 5 and microemulsion 14 were chosen to allow the incorporation of compound **27**.

The *in vitro* drug release studies showed the amount of compound **27** released is totally dependent on the type of formulation. After 6 h, the amount of compound **27** released was $2.90 \pm 1.2 \mu\text{g}/\text{cm}^2$ ($10.0 \pm 3.5\%$), $7.94 \pm 2.1 \mu\text{g}/\text{cm}^2$ ($24.4 \pm 7.4\%$) and $17.93 \pm 1.6 \mu\text{g}/\text{cm}^2$ ($55.1 \pm 5.7\%$) for AAN-27 ME, AAN-27 E and AAN-27 S, respectively.

Regarding the *in vivo* antipsoriatic activity and considering all the results obtained it is noteworthy that the microemulsions are the least indicated for skin application, mainly due to the high amount of surfactant. The emulsion can be considered an effective formulation, but it should be noted that there are no significant differences between the placebo and AAN-27 E formulation. Thus, it indicates that the therapeutic effect may be related to the formulation itself and not with the use of the compound **27**. This does not mean that the formulations cannot have therapeutic action in other models of acute or chronic cutaneous inflammatory disease.

Considering the results obtained in this work, it would be interesting to continue to study compounds within this scaffold, since their *in vitro* activity and cell viability proved to be effective. In future work, it would be interesting to study similar compounds but with a lower molecular weight and higher solubility to be incorporated in pharmaceutical formulations with higher drug releases, dermal permeation in order to administer a medicine with *in vivo* antipsoriatic activity.

5. Experimental Section

5.1. Synthesis

5.1.1. Reagents and solvents

All the reagents and solvents used in the synthesis were from Sigma-Aldrich, Alfa Aesar and TCI, and were used without purification. DCM and acetone were dried by distillation from calcium hydride and potassium carbonate, respectively.

5.1.2. Chromatography

The flash chromatography was performed using silica gel (0.040-0.063mm) from Merck. The thin layer chromatography (TLC) was accomplished using Merck aluminium backed sheets (20x20cm) coated with 60 F254 silica gel and revealed under UV light or iodine, potassium permanganate and vanillin.

5.1.3. Equipment

NMR spectra were accomplished on a Bruker 300 ultra-Shield (^1H 300MHz; ^{13}C 75 MHz) in chloroform-d or acetone-d₆. All chemical shifts (δ) are quoted in a ppm scale, coupling constants (J) are described in Hz and multiplicity is described with the following abbreviations: s = singlet, d = doublet, t = triplet, m = multiplet. Melting points were determined using a Bock-Monoscop.

The FTIR spectra were made using a IRAffinity-1, SHIMADZU. Each compound was blended with potassium bromide (KBr), pressed with a hydraulic press until it formed a pellet. Then, each pellet was read in the FTIR equipment with the support of cells.

The elemental analysis was performed at Structural Analysis Lab in Faculdade de Farmácia da Universidade de Lisboa, using an elemental analyzer Flash2000 Series CHNS/O Analyzers (ThermoScientific™) equipped with a thermal conductivity detector. Eager Xperience software was used for data acquisition and processing.

UV-Vis and high-performance liquid chromatography (HPLC) were used to measure the purity of an oil compound. The UV-Vis spectrum was accomplished on a

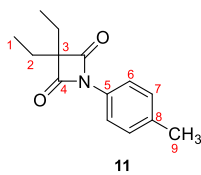
spectrophotometer (Shimadzu UV-1280), while the HPLC was performed using VWR HITACHI equipped with pump L-2130, column oven L-2300 and UV detector L-2400.

5.1.4. Synthetic Procedures and Product Characterization

Synthesis of 3,3-diethyl-1-(*p*-tolyl)azetidine-2,4-dione (**11**)

To the solution of diethylmalonyl dichloride (**10**) (10.15mmol, 1.75mL, 1eq) in dry DCM (20mL) was added, dropwise, a solution of *p*-toluidine (7.79mmol, 834.5mg, 0.77eq) and triethylamine (30.52mmol, 4.25mL, 3eq) in dry DCM (40mL). The reaction proceeded in an ice bath until it was completed (verified by TLC). The solvent was evaporated with formation of a white solid.

Cyclohexane (47mL) was added to the mixture obtained and was stirred for 15 minutes. Then, the solution was filtered, the solvent was evaporated and the product was purified by flash chromatography on silica gel (hexane:ethyl acetate with increasing polarity between 9:1 to 5:1) yielding a colorless oil (1.48g, 82.2%).

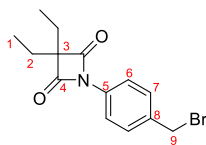


11 $^1\text{H NMR}$ (300 MHz, CDCl_3) δ 7.71 (d, $J = 8.4\text{Hz}$, 2H, H6), 7.21 (d, $J = 8.1\text{Hz}$, 2H, H7), 2.35 (s, 3H, H9), 1.84 (q, $J = 7.5\text{Hz}$, 4H, H2), 1.06 (t, $J = 7.5\text{Hz}$, 6H, H1); $^{13}\text{C NMR}$ (75 MHz, CDCl_3) δ 172.34 (C4), 136.75 (C5), 131.41 (C8), 129.79 (C7), 119.23 (C6), 72.11 (C3), 24.03 (C2), 21.26 (C9), 9.34 (C1); ν_{max} (KBr, cm^{-1}) 2360.87, 2343.51, 1739.79, 1384.89, 1516.05.

Synthesis of 1-(4-(bromomethyl)phenyl)-3,3-diethylazetidine-2,4-dione (**12**)

To a solution of (**11**) (5.14mmol, 1.19g, 1eq) in dry acetonitrile (45.5mL), NBS (7.78mmol, 1.38g, 1.5eq) and benzoyl peroxide (0.53mmol, 127.7mg, 0.1eq) were added. The reaction was refluxed (82°C) under an inert atmosphere for 3.5 hours (verified by TLC). Then, the solvent was evaporated and the product obtained was purified by flash chromatography on silica gel (hexane:ethyl acetate with increasing polarity between 9:1

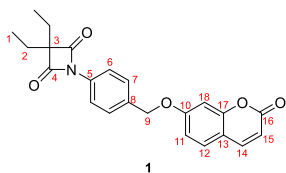
to 5:1) yielding a white solid (1.05g, 65.8%). The obtained compound was further purified by treatment with hexane yielding a white solid. (175.6mg, 11.0%). m.p. 63-65 °C.



12 $^1\text{H NMR}$ (300 MHz, CDCl_3) δ 7.84 (d, $J = 8.5\text{Hz}$, 2H, H6), 7.44 (d, $J = 8.5\text{Hz}$, 2H, H7), 4.48 (s, 2H, H9), 1.85 (q, $J = 7.5\text{Hz}$, 4H, H2), 1.06 (t, $J = 7.5\text{Hz}$, 6H, H1); $^{13}\text{C NMR}$ (75 MHz, CDCl_3) δ 172.20 (C4), 136.40 (C5), 133.86 (C8), 130.14 (C7), 119.57 (C6), 72.24 (C3), 32.76 (C9), 24.11 (C2), 9.38 (C1); ESI-MS (+) m/z : 392.1 $[\text{M}+\text{H}]^+$; ν_{max} (KBr, cm^{-1}) 2360.87, 2343.58, 1743.65, 1516.05, 1379.10, 592.15; Anal. Calcd. ($\text{C}_{14}\text{H}_{16}\text{BrNO}_2$): C, 54.21; H, 5.20; N, 4.52. Found: C, 53.95; H, 5.12; N, 3.88%.

Synthesis of 3,3-diethyl-1-(4-(((2-oxo-2H-chromen-7-yl)oxy)methyl)phenyl)azetidine-2,4-dione (**1**)

To a solution of 7-hydroxycoumarin (**15**) (0.39mmol, 63.2mg, 1eq) in dry acetone (1mL), potassium carbonate (0.69mmol, 95.4mg, 1.77eq) was added. The reaction mixture was stirred for 20 minutes. Then, a solution of (**12**) (1.16mmol, 360.5mg, 2.98eq) in dry acetone (1mL) was added to the first solution. The mixture was stirred for 43.5 under inert atmosphere at room temperature. The reaction was not completed after this time (by TLC) and the mixture was refluxed (60°C) for 4 more hours. After that, the solvent was evaporated, the crude was diluted with water (5mL) and the product was extracted with ethyl acetate (3x5mL). The organic layers were combined and the resultant solution was washed with brine, dried with anhydrous Na_2SO_4 , filtered and the solvent was evaporated. The obtained product was purified by flash chromatography on silica gel (hexane:ethyl acetate with increasing polarity between 9:1 to 3:1) yielding a white solid (94.1mg, 61.6%). The obtained solid was further purified by washing with hexane yielding a white solid. (45.4mg, 29.7%). m.p. 115-117 °C.

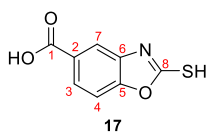


1 $^1\text{H NMR}$ (300 MHz, CDCl_3) δ 7.89 (d, $J = 8.6\text{Hz}$, 2H, H6), 7.64 (d, $J = 9.4\text{Hz}$, 1H, H14), 7.48 (d, $J = 8.7\text{Hz}$, 2H, H7), 7.38 (d, $J = 8.6\text{Hz}$, 1H, H12), 6.90

(dd, $J = 2.4, 8.6\text{Hz}$, 1H, H11), 6.86 (d, $J = 2.4\text{Hz}$, 1H, H18), 6.26 (d, $J = 9.5\text{Hz}$, 1H, H15), 5.12 (s, 2H, H9), 1.86 (q, $J = 7.5\text{Hz}$, 4H, H2), 1.07 (t, $J = 7.5\text{Hz}$, 6H, H1); ^{13}C NMR (75 MHz, CDCl_3) δ 172.23 (C4), 161.69 (C10), 161.28 (C16), 155.93 (C13,17), 143.49 (C14), 134.38 (C8), 133.92 (C5), 129.00 (C12), 128.53 (C7), 119.58 (C6), 113.54 (C15), 113.38 (C11), 102.04 (C18), 72.23 (C3), 69.99 (C9), 24.06 (C2), 9.39 (C1); ESI-MS (+) m/z : 392.0 $[\text{M}+\text{H}]^+$; ν_{max} (KBr, cm^{-1}) 2362.8, 1732.08, 1705.07, 1616.35, 1386.82; Anal. Calcd. ($\text{C}_{23}\text{H}_{21}\text{NO}_5$): C, 70.58; H, 5.41; N, 3.58; O, 20.44. Found: C, 70.71; H, 5.43; N, 2.92; O, 20.94%.

Synthesis of 2-mercaptobenzo[*d*]oxazole-5-carboxylic acid (17)

A solution of 3-amino-4-hydroxybenzoic acid (**16**) (4.99mmol, 763.6mg, 1eq) and potassium ethyl xanthate (7.64mmol, 1.22g, 1.5eq) in a mixture of ethanol:water (6:1) was refluxed (80°C) for 5 hours. The reaction mixture was concentrated, under vacuum, and acidified with HCl (1M) until pH 2 with stirring in an ice bath. The product obtained was filtered under vacuum and dried, yielding grey crystals (679.9mg, 70.2%). This product was used without further purification. m.p. 302-304°C.

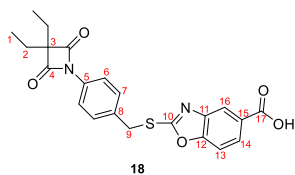


^1H NMR (300 MHz, Acetone- d_6) δ 8.01 (dd, $J = 8.5, 1.7\text{Hz}$, 1H, H3), 7.88 (d, $J = 1.1\text{Hz}$, 1H, H7), 7.54 (d, $J = 8.5\text{Hz}$, 1H, H4); ^{13}C NMR (75 MHz, Acetone- d_6) δ 126.93, 112.24, 110.06 (It is not possible to assign carbon peaks as not all peaks appear); ν_{max} (KBr, cm^{-1}) 2360.87, 2343.51, 2330.01, 1695.43, 1516.05.

Synthesis of 2-((4-(3,3-diethyl-2,4-dioxoazetidin-1-yl)benzyl)thio)benzo[*d*]oxazole-5-carboxylic acid (18)

To a solution of (**17**) (2.36mmol, 460.7mg, 1.43eq) in dry acetone (6mL), potassium carbonate (2.14mmol, 295.4mg, 1.3eq) was added, and the resultant solution was stirred for 20 minutes. Then, a solution of precursor (**12**) (1.65mmol, 513.13mg, 1eq) in dry acetone (11mL) was added to the first solution. The reaction was refluxed (70°C) under inert atmosphere and was followed by TLC.

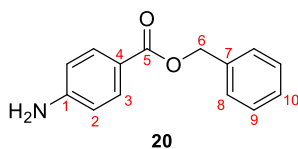
The reaction mixture was concentrated, diluted in water and acidified with HCl (1M) until pH 2 with stirring. The resultant solution was extracted with ethyl acetate and the organic layer was washed with brine, dried with anhydrous Na₂SO₄, filtered and the solvent was evaporated. The obtained product was purified by flash chromatography on silica gel (hexane:ethyl acetate, with increasing polarity between 9:1 to 6:1 and hexane:acetone with increasing polarity between 9:1 to 1:6) yielding a white solid. (321.1mg, 45.9%). In order to have a more purified compound, the solid was crystallized with diethyl ether and hexane yielding a white solid. (315.7mg, 45.1%). m.p. 181-183°C.



¹H NMR (300 MHz, CDCl₃) δ 8.38 (d, J = 1.1Hz, 1H, H16), 8.08 (dd, J = 8.5, 1.7Hz, 1H, H14), 7.83 (d, J = 8.5Hz, 2H, H6), 7.54 (d, J = 8.6Hz, 2H, H7), 7.50 (d, J = 8.6Hz, 1H, H13), 4.56 (s, 2H, H9), 1.84 (q, J = 7.5Hz, 4H, H2), 1.05 (t, J = 7.5Hz, 6H, H1); ¹³C NMR (75 MHz, CDCl₃) δ 172.21 (C4), 170.31 (C17), 166.23 (C10), 155.45 (C12), 142.21 (C11), 134.52 (C5), 130.21 (C7), 126.90 (C14), 126.05 (C15), 121.19 (C16), 119.64 (C6), 110.02 (C13), 72.48 (C3), 36.23 (C9), 24.10 (C2), 9.35 (C1); ESI-MS (+) m/z: 425.0 [M+H]⁺; ν_{max} (KBr, cm⁻¹) 2360.87, 2341.58, 1734.01, 1683.86, 1516.05, 1500.62, 1386.82, 678.94; Anal. Calcd. (C₂₂H₂₀N₂O₅S): C, 62.25; H, 4.75; N, 6.60; S, 7.55; O, 18.85%. Found: C, 62.17; H, 4.81; N, 5.93; S, 7.72; O, 19.37%.

Synthesis of benzyl 4-aminobenzoate (20)

To a solution of 4-aminobenzoic acid (**19**) (7.32mmol, 1.00g, 1eq) in DMF (40mL), potassium carbonate (36.41mmol, 5.03g, 4.97eq) and benzyl bromide (8.02mmol, 954μL, 1.10eq) were added. The solution was stirred at room temperature in an inert atmosphere for 2 hours. Then, the reaction mixture was diluted in ethyl acetate (30mL) and the product was washed with water (4x80mL). The organic layer was washed with brine, dried with anhydrous Na₂SO₄, filtered and the solvent was evaporated. The obtained product was purified by flash chromatography on silica gel (only hexane, hexane:acetone with increasing polarity between 5:1 to 1:1 and finally only acetone) yielding a yellow solid. (992.8mg, 59.7%). m.p. 78-79°C.

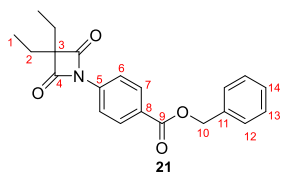


20 $^1\text{H NMR}$ (300 MHz, CDCl_3) δ 7.89 (d, $J = 8.7\text{Hz}$, 2H, H2), 7.47 – 7.28 (m, 5H, H8,9,10), 6.63 (d, $J = 8.8\text{Hz}$, 2H, H3), 5.32 (s, 2H, H6); $^{13}\text{C NMR}$ (75 MHz, CDCl_3) δ 151.05 (C5), 136.75 (C1,4), 131.93 (C2), 128.66, 128.18, 128.16, 119.86 (C7), 113.95 (C3), 66.22 (C6); ν_{max} (KBr, cm^{-1}) 3360.00, 2364.73, 2331.94, 1683.86, 1633.71, 1600.92, 1570.06.

Synthesis of benzyl 4-(3,3-diethyl-2,4-dioxoazetidin-1-yl)benzoate (**21**)

To a solution of diethylmalonyl dichloride (**10**) (5.58mmol, 960 μL , 1.5eq) in dry DCM (24mL), dropwise, a solution of (**20**) (3.62 mmol, 822mg, 1eq) and triethylamine (2.33mL) in dry DCM (48mL) was added. The reaction proceeded in an ice bath until it was completed (by TLC). The solvent was evaporated with formation of a brown oil.

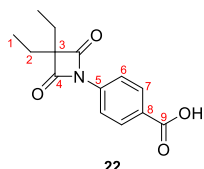
Cyclohexane (30mL) was added to the product obtained and the mixture was stirred for 15 minutes. Then, the solution was filtered, the solvent was evaporated and the product purified by flash chromatography on silica gel (hexane:ethyl acetate with increasing polarity between 9:1 to 3:1) yielding a white oil (1.13g, 89.1%).



21 $^1\text{H NMR}$ (300 MHz, CDCl_3) δ 8.13 (d, $J = 8.9\text{Hz}$, 2H, H6), 7.94 (d, $J = 8.9\text{Hz}$, 2H, H7), 7.48 – 7.29 (m, 5H, H12,13,14), 5.37 (s, 2H, H10), 1.87 (q, $J = 7.5\text{Hz}$, 4H, H2), 1.07 (t, $J = 7.5\text{Hz}$, 6H, H1); $^{13}\text{C NMR}$ (75 MHz, CDCl_3) δ 172.06 (C4), 165.59 (C9), 137.63 (C5), 135.93 (C11), 131.15 (C6), 128.76, 128.48, 128.34, 128.06 (C8), 118.71 (C7), 72.63 (C3), 67.04 (C10), 24.05 (C2), 9.34 (C1); ESI-MS (+) m/z : 352.0 $[\text{M}+\text{H}]^+$; ν_{max} (KBr, cm^{-1}) 2360.87, 2343.51, 1743.65, 1716.65. The purity was measured by HPLC with a retention time of 5.45minutes and the results indicate that the compound is 100% pure.

Synthesis of benzyl 4-(3,3-diethyl-2,4-dioxoazetidin-1-yl)benzoate (**22**)

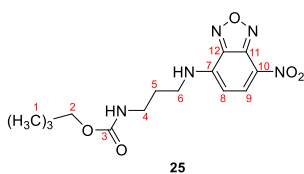
To a solution of (**21**) (0.88mmol, 309.4mg, 1eq) in dry methanol (8.5mL), palladium on carbon (10%) (0.29mmol, 30.9mg, 0.33eq) was added, and the mixture was purged with N₂. The reaction was hydrogenated and proceeded under a hydrogen atmosphere until completed (verify by TLC). The palladium was filtered in celite and the solvent was evaporated yielding a white solid. (221.7mg, 96.4%). m.p. 119-121°C.



¹H NMR (300 MHz, CDCl₃) δ 8.17 (d, J = 8.9 Hz, 2H, H₆), 7.99 (d, J = 8.9 Hz, 2H, H₇), 1.89 (q, J = 7.5 Hz, 4H, H₂), 1.08 (t, J = 7.5 Hz, 6H, H₁); ¹³C NMR (75 MHz, CDCl₃) δ 172.05 (C₄), 170.35 (C₉), 138.28 (C₅), 131.7 (C₆), 127.14 (C₈), 118.86 (C₇), 72.75 (C₃), 24.12 (C₂), 9.35 (C₁); ESI-MS (+) m/z: 260.1 [M+H]⁺; ν_{max} (KBr, cm⁻¹) 2362.8, 2345.44, 1743.65, 1683.86, 1606.70; Anal. Calcd. (C₁₄H₁₅NO₄): C, 64.36; H, 5.79; N, 5.36; O, 24.49%. Found: C, 63.77; H, 5.74; N, 5.31; O, 25.18%

Synthesis of *tert*-butyl (3-((7-nitrobenzo[*c*][1,2,5]oxadiazol-4-yl)amino)propyl) carbamate (**25**)

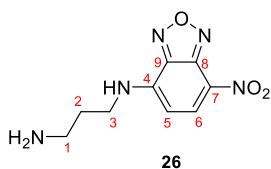
To a solution of *tert*-butyl (3-aminopropyl) carbamate (**23**) (2.24mmol, 358.1mg, 1eq) in dry methanol (10mL), 4-chloro-7-nitrobenzo[*c*][1,2,5]oxadiazole (**24**) (2.08mmol, 415.7mg, 0.9eq) in inert atmosphere, was added. The reaction proceeded for 2 hours, at room temperature until completed (by TLC). The product was purified by flash chromatography on silica gel (hexane:ethyl acetate with increasing polarity between 9:1 to 1:6) yielding an orange gum. (272.6mg, 38.8%).



¹H NMR (300 MHz, CDCl₃) δ 8.47 (d, J = 8.6 Hz, 1H, H₉), 6.17 (d, J = 8.7 Hz, 1H, H₈), 3.60 (q, J = 6.1 Hz, 2H, H₄), 3.31 (q, J = 6.3Hz, 2H, H₆), 1.95 – 1.87 (m, 2H, H₅), (s, 9H, H₁). Only the proton spectrum was performed, once the compound was all used in the synthesis.

Synthesis of *N*¹-(7-nitrobenzo[*c*][1,2,5]oxadiazol-4-yl)propane-1,3-diamine (**26**)

To a solution of (**25**) (0.808mmol, 272.6mg, 1eq) in dry DCM (6.2mL), TFA (80.8mmol, 6.2mL, 100eq) was added. The resultant solution was stirred at room temperature, in an inert atmosphere, until completed (30min., by TLC). A solution of sodium carbonate (1M) was added, to the reaction mixture, until pH 8 with stirring. The resultant solution was extracted with DCM and the organic layer was washed with brine, dried with anhydrous Na₂SO₄, filtered and the solvent was evaporated yielding an orange solid. (57mg, 29.7%).



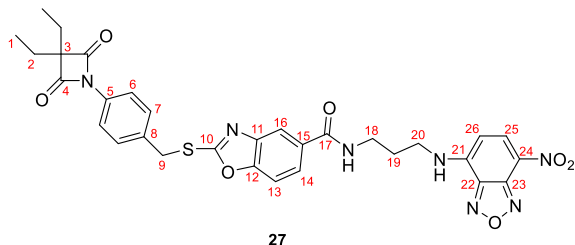
¹H NMR (300 MHz, CD₃OD) δ 8.56 (d, J = 8.5 Hz, 1H, H6), 6.42 (d, J = 8.8 Hz, 1H, H5), 2.87 (q, J 4.7 = Hz, 2H, H3), 2.03-1.94 (m, 2H, H1), 1.02 – 0.92 (m, 2H, H2). Only the proton spectrum was performed, since the compound was all used in the synthesis.

Synthesis of 2-((4-(3,3-diethyl-2,4-dioxoazetid-1-yl)benzyl)thio)-*N*-(3-((7-nitrobenzo[*c*][1,2,5]oxadiazol-4-yl)amino)propyl)benzo[*d*]oxazole-5-carboxamide (**27**)

A solution of (**18**) (0.247mmol, 105.0mg, 1eq) in dry DCM (4mL) was maintained in an inert atmosphere and cool bath until it reached 0°C. Then, DIPEA (0.259mmol, 45μL, 1.1eq) and TBTU (0.357mmol, 114.7mg, 1.4eq) were added. The reaction proceeded for 2h with stirring, in cool bath and inert atmosphere. Since the reaction was not completed (by TLC), more TBTU (0.118mmol, 37.9mg, 0.5eq) was added. The reaction proceeded for one more hour, under the same conditions.

When the reaction was completed (by TLC) compound (**26**) (0.216mmol, 51.4mg, 0.87eq) and DIPEA (0.259mmol, 45μl, 1.1eq) were added. The reaction proceeded with stirring, in a cool bath and inert atmosphere until completed (by TLC). The solvent was evaporated and the product was extracted with ethyl acetate and water (3x30mL). The organic layer was washed with brine, dried with anhydrous Na₂SO₄, filtered and the

solvent was evaporated. The product was purified by flash chromatography on silica gel (hexane:ethyl acetate with increasing polarity between 1:1 to 1:5 and only ethyl acetate) yielding an orange solid. (74mg, 53.1%). m.p. 109-111°C.

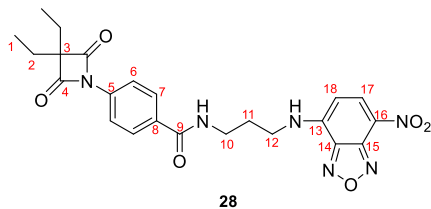


^1H NMR (300 MHz, CDCl_3) δ 8.47 (d, $J = 8.6\text{Hz}$, 1H, H25), 8.00 (d, $J = 1.2\text{Hz}$, 1H, H16), 7.82 (d, $J = 8.5\text{Hz}$, 2H, H6), 7.78 (dd, $J = 8.5, 1.7\text{ Hz}$, 1H, H14), 7.53 (d, $J = 8.5\text{Hz}$, 2H, H7), 7.49 (d, $J = 8.5\text{Hz}$, 1H, H13), 6.19 (d, $J = 8.6\text{Hz}$, 1H, H26), 4.54 (s, 2H, H9), 3.72-3.66 (m, 4H, H18,20), 2.10 – 2.02 (m, 2H, H19), 1.84 (q, $J = 7.5\text{Hz}$, 4H, H2), 1.05 (t, $J = 7.5\text{Hz}$, 6H, H1); ^{13}C NMR (75 MHz, CDCl_3) δ 172.23 (C4), 166.21 (C10), 162.60 (C17), 154.25 (C12), 144.75 (C22,23), 136.58 (C25), 134.60 (C5), 133.60 (C8), 130.59 (C11), 130.21 (C7), 123.88 (C14), 122.40 (C21,24), 120.46 (C15), 119.61 (C6), 117.29 (C16), 110.32 (C13), 83.04 (C26), 72.44 (C3), 40.23 (C20), 37.31 (C18), 36.24 (C9), 28.63 (C19), 24.09 (C2), 9.02 (C1); ESI-MS (+) m/z : 642.3 $[\text{M}+\text{H}]^+$; ν_{max} (KBr, cm^{-1}) 3325.28, 2303.01, 1735.93, 1581.63, 1496.76, 1296.16, 1261.45, 1132.21; Anal. Calcd. ($\text{C}_{31}\text{H}_{29}\text{N}_7\text{O}_7\text{S}$): C, 57.85; H, 4.54; N, 15.23; S, 4.98; O, 17.84%. Found: C, 58.55; H, 5.35; N, 12.69; S, 5.01; O, 18.4%

Synthesis of 4-(3,3-diethyl-2,4-dioxoazetidin-1-yl)-N-(3-((7-nitrobenzo[*c*][1,2,5]oxadiazol-4-yl)amino)propyl)benzamide (28)

A solution of (**22**) (0.294mmol, 76.9mg, 1eq) in dry DCM (4mL) was maintained in an inert atmosphere and cool bath until it reached 0°C. Then, DIPEA (0.324mmol, 56.4 μ L, 1.1eq) and TBTU (0.425mmol, 161.7mg, 1.4eq) were added. The reaction proceeded with stirring for 30minutes. Since the reaction was not completed (by TLC) after this time, a new addition of TBTU (0.147mmol, 55.9mg, 0.5eq) was done and the reaction proceeded until completed. Compound (**26**) (0.279mmol, 66.3mg, 0.95eq) and DIPEA (0.32 mmol, 56.4 μ l, 1.1eq) were added to the mixture and the reaction proceeded under the same conditions until completed (by TLC). The solvent was evaporated and the product was extracted with ethyl acetate and water (3x30mL). The organic layer was washed with brine, dried with anhydrous Na_2SO_4 , filtered and the solvent was evaporated.

The product was purified by flash chromatography on silica gel (hexane:ethyl acetate with increasing polarity between 9:1 to 1:9, acetone and methanol:acetone 1:9) yielding an orange solid. (85mg, 63.3%). m.p. 83-84°C.



¹H NMR (300 MHz, CDCl₃) δ 8.47 (d, J = 8.7Hz, 1H, H17), 7.97 (d, J = 8.9Hz, 2H, H6), 7.88 (d, J = 8.9Hz, 2H, H7), 6.19 (d, J = 8.7Hz, 1H, H18), 3.70-3.64 (m, 4H, H10,12), 2.09 – 2.00 (m, 2H, H11), 1.89 (q, J = 7.5Hz, 4H, H2), 1.08 (t, J = 7.5Hz, 6H, H1); ¹³C NMR (75 MHz, CDCl₃) δ 172.10 (C4), 168.01 (C9), 144.48 (C14,15), 136.87 (C5), 136.73 (C17), 131.41 (C8), 128.41 (C6), 123.43 (C13,16), 119.08 (C7), 98.01 (C18), 72.70 (C3), 39.98 (C12), 37.15 (C10), 29.06 (C11), 24.06 (C2), 9.37 (C1); ESI-MS (+) m/z: 479.2 [M+H]⁺; ν_{max} (KBr, cm⁻¹) 2366.66, 2345.44, 1737.86, 1568.13, 1504.48, 1307.74, 1296.16, 1269.16, 1124.50; Anal. Calcd. (C₂₃H₂₄N₆O₆): C, 57.50; H, 5.03; N, 17.49%. Found: C, 57.01; H, 5.75; N, 14.23%

5.2. Biological Assays

5.2.1. Enzymatic Inhibition Assays

Fluorometric assays for HNE (Merck, Germany) inhibition activity were conducted as previously described.⁽¹³⁶⁾ Briefly, the assays were carried out in 200μL assay buffer (0.1 M HEPES pH 7.5 at 25°C) containing 20μL of 0.17μM HNE in assay buffer (stock solution 1.7μM in 0.05M acetate buffer, pH 5.5), 155μL of assay buffer and 5μL of each concentration of the tested inhibitors. The reaction was initiated by adding 20μL of fluorogenic substrate to the final concentration 200μM (MeO-Suc-Ala-Ala-Pro-Val-AMC, Merck, Germany) and the activity was monitored (excitation 380nm; emission 460nm) for 30min, at 25°C on a Fluorescence Microplate Reader FLUOstar Omega (BMG Labtech GmbH, Germany). The K_m of this substrate of HNE was previously determined to be 185μM (data not shown). For all assays, saturated substrate concentration was used, throughout, in order to obtain linear fluorescence curves. Inhibitors stock solutions were prepared in DMSO, and serial dilutions were made in DMSO. Controls were performed using enzyme alone, substrate alone, enzyme with

DMSO and a positive control (Sivelestat sodium salt hydrate, Sigma Aldrich, UK). By computing the log of inhibitors concentrations versus the percentage of activity and using the GrafPad program, the IC₅₀ values were determined by non-linear regression analysis. Assays were performed in triplicate and data presented as the mean and the standard deviation.

5.2.2. *In vitro* Cytotoxicity – HaCat Cells

In order to predict the irritant potential of the compounds, an *in vitro* cytotoxicity, the assay method was used with a human cell line, HaCat, wherein cell viability was evaluated by reduction of formazan blue – MTT. ⁽¹³⁷⁾ The biocompatibility of starch polymers was quantitatively evaluated *in vitro* using a general cell viability endpoint MTT reduction (3-(4,5-dimethyl-2-thiazolyl)-2,5-diphenyl- 2H-tetrazolium bromide) assay. MTT is a yellow and water-soluble tetrazolium dye that is converted by viable cells to a water-insoluble, purple formazan.

Cell viability was assessed after 24h of incubation of both cell lines with 50mg/mL concentration of each sample. The day before experiment, the cells were seeded in sterile flat bottom 96 well tissue culture plates (Griner, Germany) in DMEM/F12 culture medium, supplemented with 10% FBS, 100 units of penicillin G (sodium salt), 100µg of streptomycin sulfate and 2mM L-glutamine, at a cell density of 2x10⁵ cells/mL. Cells were incubating at 37°C and 5% CO₂. On the next day, medium was replaced by fresh medium containing the different samples to be analyzed and each concentration was tested in five wells per plate. The negative control was the culture medium and DMSO and the positive control was SDS at 0.1mg/mL. After the time of exposure (15 min.), the culture medium was replaced by medium containing 0.5mg/mL MTT. The cells were further incubated for 3h. In the plates containing reduced MTT, the media was removed and the intracellular formazan crystals were solubilized and extracted with DMSO. After fifteen minutes at room temperature, the absorbance was measured at 570nm in the same microplate reader.

The relative cell viability (%) compared to control cells was calculated by the following equation (5):

$$\text{Cell viability (\%)} \text{ for the MTT assay} = \frac{[\text{Absorbance}_{570 \text{ nm}}]_{\text{sample}}}{[\text{Absorbance}_{570 \text{ nm}}]_{\text{control}}} \times 100 \quad (5)$$

One-way analysis of variance (ANOVA) and Tukey–Kramer post-hoc multiple comparison test were used to identify the significant differences between the groups and were performed using GraphPad PRISM[®] 5 software. An alpha error of 5% was chosen to set the significance level.

5.2.3. Analysis of Inhibitors Specificity

The three selected compounds (**1**, **27**, **28**) were evaluated for their ability to inhibit other human serine proteases, namely trypsin, chymotrypsin, urokinase and kallikrein in 200µL reaction volumes at 25°C. Trypsin's analysis of (Calbiochem) inhibition was performed in reaction mixtures containing 0.05M Tris-HCl, 0.138M NaCl, pH 8.0, 30nM human pancreas Trypsin, test compounds, and 50µM substrate (Z-Gly-Gly-Arg-AMC.HCl) (Bachem). Chymotrypsin's analysis of (Calbiochem) inhibition was performed in reaction mixtures containing 0.05M Tris-HCl, 0.138M NaCl, pH 8.0, 30nM human pancreas chymotrypsin, test compounds, and 100µM substrate (Suc-Ala-Ala-Pro-Phe-7-amino-4-methylcoumarin) (Bachem). Urokinase's analysis of (Calbiochem) inhibition assay was performed in reaction mixtures containing 0.05M Tris-HCl, 0.138M NaCl, pH 8.0, 30U/mL human urine urokinase, test compounds, and 50µM substrate (Z-Gly-Gly-Arg-AMC.HCl). Finally, the analysis of kallikrein (Calbiochem) inhibition was performed in reaction mixtures containing 0.05M Tris-HCl, 0.138M NaCl, pH 8.0, 2nM human plasma kallikrein, test compounds, and 50µM substrate (H-Pro-Phe-Arg-AMC acetate salt) (Bachem).

For all serine proteases the activity was measured at excitation and emission wavelengths of 360nm and 460nm, respectively in a microplate reader (FLUOstar Omega, BMG Labtech, Germany). For all compounds tested, the concentration of inhibitor that caused 50% inhibition of the enzymatic reaction (IC₅₀) was determined by non-linear regression using GraphPad PRISM software as previously published.⁽¹³⁶⁾

5.3. Pharmaceutical Vehicles

5.3.1. Materials

5.3.1.1. Emulsion Formulation

To perform this work, different humectants: ethoxydiglycol (Transcutol CG from Gattefossé), glycerin (from Quimidroga (Portugal)) and propylene glycol (Propylene Glycol EP from Mosselman), were used. Also, seven different preservatives: sodium methylparaben and sodium propylparaben (Nipagin M Sodium™ and Nipazol M Sodium™ from Clariant, respectively), gluconolactone (and) sodium benzoate (Geogard Ultra™ from Lonza), chlorphenesin (Saliphenesin from Salicylates and chemicals), 1,2-hexanediol (Dermosoft® Hexiol from drstratmans), caprylyl glycol (and) glyceryl caprylate (and) glycerin (and) phenylpropanol (and) aqua (Dermosoft® LP from drstratmans) and *o*-cymen-5-ol (SymOcide® C from Symrise), were added. To all formulations, hydrogenated lecithin (and) C12-16 alcohols (and) palmitic acid (Biophilic™ H MB from IFF | Lucas Meyer cosmetics), caprylic/capric triglycerides (TEGOSOFT® CT from Evonik), C10-18 triglycerides (Lipocire™ A SG from Gattefossé), isopropyl myristate (TEGOSOFT® M from Evonik), oleic acid from Sigma-Aldrich, alpha bisabolol (Alpha Bisabolol Natural from Esperis), cetyl alcohol (from the galenic and technology pharmaceutical department of Faculdade de Farmacia – Universidade de Lisboa) and water were added. Formulation 1 is the only that does not contain alpha bisabolol and cetyl alcohol.

5.3.1.2. Microemulsion Formulation

In order to develop the microemulsions, three different carbon chain oils were used: C21-C28 alkane (Emosmart™ C28, Seppic™), a plant-based and renewable C15-19 alkane oil (Emogreen™ L15, Seppic™) and a triglyceride-based oil, more specifically caprylic/capric triglycerides (Tegosoft® CT, Evonik). PEG-20 glyceryl triisostearate (Cithrol™ 10GTIS from Croda Inc.) was used as surfactant, propylene glycol (Propylene Glycol EP from Mosselman) was used as humectant and co-surfactant and sodium methylparaben and sodium propylparaben (Nipagin M Sodium™ and Nipazol M Sodium™ from Clariant, respectively) were used as preservatives. Water was added to all formulations.

5.3.2. Methods

5.3.2.1. Emulsion preparation

In this work, twelve emulsion formulations where the percentage of thickener, humectants and preservatives varied were performed. The percentages and components used, identified by INCI (International Ingredient Nomenclature of Cosmetics), are shown in tables 10 and 11.

For the production of the emulsions a hot method was used, where the oily phase was melted separately from the aqueous phase. After the addition of the oily phase to the aqueous phase, the formulations were mixed through a vertical stirrer (IKA® T25 Digital – ULTRA TORRAX®) and stirred with a glass rod until they reached room temperature. All formulations were carried out using a digital scale (VWR).

Table 10 - Emulsion Formulation: aqueous phase.

<i>Ingredients (INCI)</i>	<i>Formulations (%) – Aqueous phase</i>											
	1	2	3	4	5	6	7	8	9	10	11	12
<i>Water</i>	76.30	74.30	72.80	74.30	72.80	74.30	72.80	71.00	72.70	70.00	71.50	72.90
<i>Hydrogenated lecithin (and) C12-16 alcohols (and) palmitic acid</i>	6.00	6.00	6.00	6.00	6.00	6.00	6.00	6.00	6.00	6.00	6.00	6.00
<i>Ethoxydiglycol</i>	5.00	5.00	5.00	-	-	-	-	-	-	-	-	-
<i>Glycerin</i>	-	-	-	5.00	5.00	-	-	5.00	5.00	5.00	5.00	5.00
<i>Propylene glycol</i>	-	-	-	-	-	5.00	5.00	-	-	-	-	-
<i>Sodium methylparaben</i>	0.18	0.18	0.18	0.18	0.18	0.18	0.18	-	-	-	-	-
<i>Sodium propylparaben</i>	0.02	0.02	0.02	0.02	0.02	0.02	0.02	-	-	-	-	-
<i>Gluconolactone (and) sodium benzoate</i>	-	-	-	-	-	-	-	2.00	-	-	-	-
<i>Chlorphenesin</i>	-	-	-	-	-	-	-	-	0.30	-	-	-

<i>1,2-Hexanediol</i>	-	-	-	-	-	-	-	-	-	3.00	-	-
<i>Caprylyl glycol (and) glyceryl caprylate (and) glycerin (and) phenylpropanol (and) Aqua o-cymen-5-ol</i>	-	-	-	-	-	-	-	-	-	-	1.50	-
	-	-	-	-	-	-	-	-	-	-	-	0.10

Table 11 - Emulsion Formulation: oily phase

<i>Ingredients (INCI)</i>	<i>Formulations (%) – Oily phase</i>											
	1	2	3	4	5	6	7	8	9	10	11	12
<i>Caprylic/capric triglycerides</i>	2.50	2.50	2.50	2.50	2.50	2.50	2.50	2.50	2.50	2.50	2.50	2.50
<i>C10-18 Triglycerides</i>	4.00	4.00	4.00	4.00	4.00	4.00	4.00	4.00	4.00	4.00	4.00	4.00
<i>Isopropyl myristate</i>	5.00	5.00	5.00	5.00	5.00	5.00	5.00	5.00	5.00	5.00	5.00	5.00
<i>Oleic acid</i>	1.00	1.00	1.00	1.00	1.00	1.00	1.00	1.00	1.00	1.00	1.00	1.00
<i>Alpha bisabolol</i>	-	1.00	1.00	1.00	1.00	1.00	1.00	1.00	1.00	1.00	1.00	1.00
<i>Cetyl alcohol</i>	-	1.00	2.50	1.00	2.50	1.00	2.50	2.50	2.50	2.50	2.50	2.50

5.3.2.2. Microemulsion preparation

In this work, fourteen microemulsions where a titration method was used, and all components were fixed, apart from the surfactant wherein their amount, in grams, was varied between formulations in order to obtain a microemulsion, were performed. The percentage and components used, identified by INCI, are shown in tables 12 and 13.

For the production of the microemulsions a cold method was used. After the addition of all components, the formulations were stirred with a glass rod. All formulations were carried out using a digital scale (VWR).

Table 12 - Microemulsion formulation: aqueous phase

<i>Ingredients (INCI)</i>	<i>Formulations (%) – Aqueous phase</i>													
	1	2	3	4	5	6	7	8	9	10	11	12	13	14
<i>Water</i>	9.76	8.99	8.00	6.96	5.97	9.76	8.99	8.00	9.76	8.99	8.00	6.96	5.97	5.97
<i>PEG-20 Glyceryl triisostearate</i>	2.44	10.1	20.0	30.4	40.3	2.44	10.1	20.0	2.44	10.1	20.0	30.4	40.3	40.3
<i>Propylene glycol</i>	9.76	8.99	8.00	6.96	5.97	9.76	8.99	8.00	9.76	8.99	8.00	6.96	5.97	5.97
<i>Sodium methylparaben</i>	0.18	0.17	0.15	0.13	0.11	0.18	0.17	0.15	0.18	0.17	0.15	0.13	0.11	0.11
<i>Sodium propylparaben</i>	0.02	0.02	0.02	0.01	0.01	0.02	0.02	0.02	0.02	0.02	0.02	0.01	0.01	0.01

Table 13 - Microemulsion formulation: oily phase

<i>Ingredients (INCI)</i>	<i>Formulations (%) – Oily phase</i>													
	1	2	3	4	5	6	7	8	9	10	11	12	13	14
<i>Caprylic/capric triglycerides</i>	77.9	71.7	63.8	55.5	47.6	-	-	-	-	-	-	-	-	15.9
<i>C15-19 Alkane</i>	-	-	-	-	-	77.9	71.7	63.8	-	-	-	-	-	15.9
<i>C21-C28 Alkane</i>	-	-	-	-	-	-	-	-	77.9	71.7	63.8	55.5	47.6	15.9

5.3.2.3. pH determinations

In this study, the pH values were determined using a potentiometer (METTLER TOLEDO). The pH measurement was performed 24 hours after the production of the formulations and at room temperature.

5.3.2.4. Characterization of physical stability

In order to verify the physical stability of each emulsion formulation one gram of emulsion was placed into a test tube and centrifuged (Heraeus Sepatech) for 10minutes at 3000RPM. This test allows to predict the stability of each formulation because it exposes each of the formulations to an accelerated stability test.

For microemulsions, only the macroscopic appearance of each formulation as physical stability characterization was used, since the stability of the system is determined when these formulations are carried out. After mixing all the ingredients, the microemulsion may be stable (translucent and clean) or unstable (opaque and/or two or more phases).

5.3.2.5. *Rheology*

The rheological characteristics of the formulations were examined at high shear rates using continuous shear techniques and in the viscoelastic region using oscillation techniques. These experiments were performed with a controlled stress Kinexus Rheometer (Malvern) using cone geometry (truncated cone angle 4° and radius 40mm). All the studies were performed at room temperature.

Viscosity

The table of shear rate method was carried out using a destructive measurement, where the shear stress of each formulation was obtained by increasing the shear rate from 0.1s⁻¹ to 100s⁻¹ and 8 samples per decade.

Oscillatory

First, in the oscillatory method, an amplitude sweep test where the shear strain was between 0.01Hz and 100Hz, the frequency was 1Hz and 10 samples per decade was carried out. Then, a frequency sweep test was performed with a shear strain of 0.1% for emulsions and 5% for the microemulsions; frequency between 0.01Hz and 10Hz and 10 samples per decade.

5.3.2.6. *Characterization of droplet size*

The droplet size in the emulsion was determined using a Malvern Mastersizer 2000 with a Hydro 2000S module. The emulsion was applied directly in the equipment, and the results were treated using the Excel software.

Regarding microemulsions, the characterization of the droplet size was performed in Zetasizer Nano from Malvern. To characterize this type of formulations it was only necessary to place the microemulsion in a cuvette.

5.3.2.7. *In vivo* studies

For *in vivo* studies with sensorial evaluation and skin analysis, the ethics protocols were by the protection of the Ethical Committee of PhD Trials, known to be an International Contract Research Organization engaged into the clinical assessment of safety and efficacy of products for topical application (cosmetics and raw materials). After the Ethical Committee's approval, the good clinical practices were approved by the Helsinki Declaration and the *Agence Francaise de Sécurité Sanitaire des Produits de Santé*. These regulations are intended to guarantee that all the technical questions are evaluated meticulously during the application of the products in humans.

5.3.2.8. *In vivo* sensory analysis

The *in vivo* sensory analysis study were performed in collaboration with PhD Trials where the placebo of emulsion 5 and microemulsion 14 were applied for twenty-seven consecutive days. Ten volunteers were chosen, where all were healthy, Caucasian and female with ages between 22 and 27. In order to avoid the formulations influence one under another, each formulation was applied in a delineated and specific area of the ventral side of the forearm. All applications of the formulations except the first were carried out by the volunteers. After completing the study, the volunteers answered an anonymous questionnaire using a scale on 1 to 5 (1-bad, 5-very good). The questionnaire was based on the organoleptic characteristics (appearance and odor), practicality of application, spreadability, texture (stickiness and softness), feeling after application, oiliness, brightness, whitish stain, hydration, acceptance by the consumer.

5.3.2.9. *In vivo skin analysis*

An efficacious evaluation study was performed, in a group of ten female healthy volunteers (aged between 22 and 27), using three complementary 2D skin capacitance instruments. A capacitance imaging method, was performed using a MoistureMap MM 100 device. The sensor gives graphical information through the images on close surface distribution of hydration and micro-topography of skin tissue. The capacitance values are ranged in 255 gray levels (0=black and 255=white), and the skin hydration was characterized by a gray level histogram on specific software. For this specific study only the mean grey level parameter was analyzed. The Corneometer CM 825, was also used with the intention of complementing the characterization of skin hydration, attending to the hydration level of the *stratum corneum*. This device determines the hydration level of the *stratum corneum* by measuring the change in dielectric constant due to skin hydration surface. In addition, Tewameter® TM 300 was used for the assessment of the TEWL in order to evaluate the water barrier function of the skin as well as any damage present in this barrier. Measurements were performed on three areas (two formulation and control) on the ventral side of the forearm of each volunteer, at T0 and T28 days, in order to understand and compare the moisturizing cream effects. Two moisturizing products were then applied during 28 days on the forearms according to the previously defined schedule, maintaining one of the areas free of any product (control area).

5.3.2.10. *Solubility studies*

To perform the solubility studies, 1 mg of compound **27** was used, where the oily phase of the formulations was added until obtain the total solubilization of the compound. The maximal solubility for compound **27** was 0.1mg/g of formulation.

5.3.2.11. *Finals emulsion and microemulsion formulation with compound 27*

The emulsion and microemulsion with compound **27** were prepared according to the previously described procedure (in the present chapter, sections 5.3.2.1 and 5.3.2.2.) and according to the solubility studies presented in section 5.3.2.10. Thus, for the two

formulations the active compound was dissolved first on the oily phase and then added to the aqueous phase. The concentration of compound **27** in both formulations is 0.1 mg/g.

5.3.2.12. Drug Release Studies

In vitro drug release studies were performed using vertical Franz diffusion cells with synthetic membranes, Tuffryn®, 0.45µm and silicone membranes. Water:ethanol (50:50 w/w) with 2.5% of PEG-40 Hydrogenated Castor Oil were used as receptor phase. The study was performed for 6 hours at 36°C and each sample was collected with an interval of one hour. The amount of released drug was analysed by a fluorescence method (excitation 380nm; emission 460nm) at 25°C on a Fluorescence Microplate Reader FLUOstar Omega (BMG Labtech GmbH, Germany) and data was expressed in drug cumulative amount of permeated as function of time.

The data obtained from the drug release studies was computed using DDSolver⁽¹³⁸⁾ which is an Excel-plugin module, and the resultant data were fitted to different kinetic models, such as: zero order, first order, Higuchi model and Korsmeyer-Peppas model. (139,140)

The zero order model comprises the following equation (6), in which K_0 is the zero order release constant. (139,140)

$$F = K_0 \times t \quad (6)$$

The first order model comprises equation 7, in which K_1 is the first order release constant. (139,140)

$$F = 100 \times (1 - e^{-k_1 \times t}) \quad (7)$$

The Higuchi model follows equation 8, where K_H is the Higuchi release constant. (139,140)

$$F = K_H \times t^{1/2} \quad (8)$$

The Korsmeyer-Peppas model used equation 9, in which K_{KP} is the release constant incorporating the structural and geometric characteristics of the drug-dosage form, and n is the diffusional exponent indicating the drug-release mechanism. ^(139,140)

$$F = K_{KP} \times t^n \quad (9)$$

For all models, F is the fraction (%) of released drug in time, t . The adjusted coefficient of determination (R^2_{adjusted}) was estimated for each model and used to describe and to interpret the results. The R^2_{adjusted} values and the Akaike minimum information theoretical criterion (AIC) were used as a measure of fit to compare the different models. ^(139,140)

5.3.2.13. *In vivo antipsoriatic activity*

The *in vivo* studies were performed according to Pivetta *et al.* (141). The study lasted six days, where the signs of inflammation (erythema and skin thickness) were evaluated. In the first day, all mice were shaved in the dorsum and kept in individual cages throughout the experiment. Animals were randomly selected and five groups of animals were tested:

- Group 1 ($n = 5$) was treated with 60mg of Dermovate® (containing 0.05% clobetasol propionate) as a positive control of inflammation inhibition;
- Group 2 ($n = 4$) was treated with 60mg of classic emulsion placebo's.
- Group 3 ($n = 4$) was treated with 60mg of microemulsion placebo's.
- Group 4 ($n = 5$) was treated with 60mg of classical emulsion containing 0.01% of compound **27**.
- Group 5 ($n = 5$) was treated with 60mg of microemulsion containing 0.01% of compound **27**.

All tested compounds were spread over the mice's back skin with a spatula. Five hours after the treatment, 60 mg of Aldara® cream containing 5% of imiquimod was applied on the back skin. Treatment with the samples followed by Aldara® cream lasted for five consecutive days. Except for the first day, the animals were always subjected to daily visual inspection and measurement of skin thickness and weight. On the sixth day the mice were sacrificed and their skin was preserved in a 10% formalin solution and sent to histopathological analysis. The psoriasis-inflammation evaluation criteria was assessed

according to the clinical Psoriasis Area and Severity Index. Erythema, scaling and thickening were scored from 0 to 4 (0: none; 1: minimal; 2: mild; 3: moderate; 4: marked), as described in table 14.

Table 14 - Scoring system for histopathologic evaluation of skin lesion

<i>Points</i>	Inflammation	Epidermal hyperplasia
<i>0</i>	none	none
<i>1</i>	minimal	minimal
<i>2</i>	mild	mild
<i>3</i>	moderate	moderate
<i>4</i>	marked	marked

5.3.2.14. Histopathology

Animals were euthanized and dorsal skin from control mice exposed to the test compound was excised, formalin-fixed and trimmed into longitudinal sections. Samples were then paraffin-embedded, sectioned at 4µm and stained with heamtoxylin and eosin. Lesions were scored by a pathologist blinded to experimental groups, based on modifiers and severity grades depicted in table 14. Measurements were performed in in slides digitally scanned in the Hamamatsu NanoZoomerSQ with NDP.view2 software (Hamamatsu), and correspond to mean value obtained from 7 to 12 different points, for epidermis and dermis.

6. Bibliography

1. Sanman LE, Bogyo M. Activity-Based Profiling of Proteases. *Annu Rev Biochem.* 2014;83:249–73.
2. Korkmaz B, Horwitz MS, Jenne DE, Gauthier F. Neutrophil Elastase, Proteinase 3, and Cathepsin G as Therapeutic Targets in Human Diseases. *Pharmacol Rev.* 2010;62:726–59.
3. Heutinck KM, ten Berge IJM, Hack CE, Hamann J, Rowshani AT. Serine proteases of the human immune system in health and disease. *Mol Immunol.* 2010;47:1943–55.
4. Leung D, Abbenante G, Fairlie DP. Protease inhibitors: Current status and future prospects. *J Med Chem.* 2000;43:305–41.
5. Powers JC, Asgian JL, Ekici OD, James KE. Irreversible inhibitors of serine, cysteine, and threonine proteases. *Chem Rev.* 2002;102:4639–750.
6. Abbenante G, Fairlie D. Protease Inhibitors in the Clinic. *Med Chem (Los Angeles).* 2005;1:71–104.
7. Hedstrom L. Serine Protease Mechanism and Specificity. *Chem Rev.* 2002;102:4501–23.
8. Hunkapiller MW, Forgac MD, Richard JH. Mechanism of Action of Serine Proteases: Tetrahedral Intermediate and Concerted Proton Transfer. *Biochemistry.* 1976;15:5581–8.
9. Chen JM, Radisky ES, Férec C. Human Trypsins. In: *Handbook of Proteolytic Enzymes.* 3rd ed. 2013. p. 2600–9.
10. Hansen G, Gielen-haertwig H, Reinemer P, Schomburg D, Harrenga A, Niefind K. Unexpected Active-Site Flexibility in the Structure of Human Neutrophil Elastase in Complex with a New Dihydropyrimidone Inhibitor. *J Mol Biol.* 2011;409:681–91.
11. Shreder KR, Cajica J, Du L, Fraser A, Hu Y, Kohno Y, et al. Synthesis and optimization of 2-pyridin-3-yl-benzo[d][1,3]oxazin-4-one based inhibitors of human neutrophil elastase. *Bioorganic Med Chem Lett.* 2009;19:4743–6.
12. Lucas SD, Costa E, Guedes RC, Moreira R. Targeting COPD: Advances on Low-Molecular-Weight Inhibitors of Human Neutrophil Elastase. *Med Res Rev.* 2013;33(S1):E73–101.
13. Crocetti L, Giovannoni MP, Schepetkin IA, Quinn MT, Khlebnikov AI, Cilibrizzi A, et al. Design, synthesis and evaluation of N-benzoylindazole derivatives and analogues as inhibitors of human neutrophil elastase. *Bioorganic Med Chem.* 2011;19:4460–72.
14. Giovannoni MP, Schepetkin IA, Quinn MT, Cantini N, Crocetti L, Guerrini G, et al. Synthesis, biological evaluation, and molecular modelling studies of potent human neutrophil elastase (HNE) inhibitors. *J Enzyme Inhib Med Chem.* 2018;33(1):1108–24.
15. Yang X, Yan H, Zhai Z, Hao F, Ye Q, Zhong B. Neutrophil elastase promotes

- proliferation of HaCaT cell line and transwell psoriasis organ culture model. *Int J Dermatol.* 2010;49:1068–74.
16. Guyot N, Butler MW, McNally P, Weldon S, Greene CM, Levine RL, et al. Elafin, an elastase-specific inhibitor, is cleaved by its cognate enzyme neutrophil elastase in sputum from individuals with cystic fibrosis. *J Biol Chem.* 2008;283(47):32377–85.
 17. Santana AB, Lucas SD, Gonçalves LM, Correia HF, Cardote TAF, Guedes RC, et al. N-Acyl and N-sulfonyloxazolidine-2,4-diones are pseudo-irreversible inhibitors of serine proteases. *Bioorganic Med Chem Lett.* 2012;22:3993–7.
 18. Syntia F, Nehmé R, Claude B, Morin P. Human neutrophil elastase inhibition studied by capillary electrophoresis with laser induced fluorescence detection and microscale thermophoresis. *J Chromatogr A.* 2016;1431:215–23.
 19. Marto J, Ruivo E, Lucas SD, Gonçalves LM, Simões S, Gouveia LF, et al. Starch nanocapsules containing a novel neutrophil elastase inhibitor with improved pharmaceutical performance. *Eur J Pharm Biopharm.* 2018;127:1–11.
 20. Maryanoff BE, Costanzo MJ. Inhibitors of proteases and amide hydrolases that employ an α -keto heterocycle as a key enabling functionality. *Bioorganic Med Chem.* 2008;16:1562–95.
 21. Zhong J, Groutas W. Recent Developments in the Design of Mechanism-based and Alternate Substrate Inhibitors of Serine Proteases. *Curr Top Med Chem.* 2005;4:1203–16.
 22. Groutas WC, Dou D, Alliston KR. Neutrophil Elastase Inhibitors. *Expert Opin Ther Pat.* 2012;21(3):339–54.
 23. Wilmouth RC, Kassamally S, Westwood NJ, Sheppard RJ, Claridge TDW, Aplin RT, et al. Mechanistic insights into the inhibition of serine proteases by monocyclic lactams. *Biochemistry.* 1999;38(25):7989–98.
 24. Knight WB, Green BG, Chabin RM, Gale P, Weston H, Kuo DW, et al. Specificity, Stability, and Potency of Monocyclic β -Lactam Inhibitors of Human Leucocyte Elastase. *Biochemistry.* 1992;31(35):8160–70.
 25. Firestone RA, Barker PL, Judith MP, Ashe BM, Dahlgren ME. Monocyclic β -Lactam inhibitors of human leukocyte elastase. *Tetrahedron.* 1990;46(7):2255–62.
 26. Nakayama Y, Odagaki Y, Fujita S, Matsuoka S, Hamanaka N, Nakai H, et al. Clarification of mechanism of human sputum elastase inhibition by a new inhibitor, ONO-5046, using electrospray ionization mass spectrometry. *Bioorganic Med Chem Lett.* 2002;12(17):2349–53.
 27. Watanabe F, Sato M, Kato A, Higashi Y, Yata N. First-pass metabolism of ONO-5046 (N-[2-[4-(2,2-dimethylpropionyloxy)phenylsulfonylamino]benzoyl]aminoacetic acid), a novel elastase inhibitor, in rats. *Biol Pharm Bull.* 1997;20(4):392–6.
 28. Hawkes JE, Chan TC, Krueger JG. Psoriasis pathogenesis and the development of novel targeted immune therapies. *J Allergy Clin Immunol.* 2017;140(3):645–53.

29. Parisi R, Symmons DPM, Griffiths CEM, Ashcroft DM. Global epidemiology of psoriasis: A systematic review of incidence and prevalence. *J Invest Dermatol*. 2013;133:377–85.
30. World Health Organization. Noncommunicable diseases and their risk factors [Internet]. Psoriasis. 2016 [cited 2019 Apr 22]. p. 3. Available from: <https://www.who.int/ncds/management/psoriasis/en/>
31. Jiang S, Hinchliffe TE, Wu T. Biomarkers of An Autoimmune Skin Disease — Psoriasis. *Genomics Proteomics Bioinforma*. 2015;13:224–33.
32. Deng Y, Chang C, Lu Q. The Inflammatory Response in Psoriasis: a Comprehensive Review. *Clin Rev Allergy Immunol*. 2016;50(3):377–89.
33. Harden JL, Krueger JG, Bowcock AM. The immunogenetics of Psoriasis: A comprehensive review. *J Autoimmun*. 2015;64:66–73.
34. Higgins E. Psoriasis. *Medicine (Baltimore)*. 2017;45(6):368–78.
35. Raychaudhuri SK, Maverakis E, Raychaudhuri SP. Diagnosis and classification of psoriasis. *Autoimmun Rev*. 2014;13:490–5.
36. Reich K. The concept of psoriasis as a systemic inflammation: implications for disease management. *J Eur Acad Dermatology Venereol*. 2012;26(SUPPL. 2):3–11.
37. Kim J, Krueger JG. The Immunopathogenesis of Psoriasis. *Dermatol Clin*. 2015;33:13–23.
38. Liang Y, Sarkar MK, Tsoi LC, Gudjonsson JE. Psoriasis: a mixed autoimmune and autoinflammatory disease. *Curr Opin Immunol*. 2017;49:1–8.
39. Yung SC, Farber JM. Chemokines. In: *Handbook of Biologically Active Peptides*. 2nd ed. Elsevier Inc.; 2013. p. 656–63.
40. Sevimoglu T, Turanli B, Bereketoglu C, Arga K, Karadag A. Systems biomarkers in psoriasis : Integrative evaluation of computational and experimental data at transcript and protein levels. *Gene*. 2018;647:157–63.
41. Dallegri F, Ottonello L. Tissue injury in neutrophilic inflammation. *Inflamm Res*. 1997;46:382–91.
42. Baliwag J, Barnes DH, Johnston A. Cytokines in psoriasis. *Cytokine*. 2015;73:342–50.
43. Henry CM, Sullivan GP, Clancy DM, Afonina IS, Kulms D, Martin SJ. Neutrophil-Derived Proteases Escalate Inflammation through Activation of IL-36 Family Cytokines. *Cell Rep*. 2016;14:708–22.
44. Johnston A, Xing X, Wolterink L, Barnes DH, Yin ZQ, Reingold L, et al. IL-1 and IL-36 are dominant cytokines in generalized pustular psoriasis. *J Allergy Clin Immunol*. 2017;140(1):109–20.
45. Todd A, Anderson R, Groundwater P, George S. Current and potential new therapies for the treatment of psoriasis [Internet]. 2010 [cited 2019 Jul 19].

Available from: <https://www.pharmaceutical-journal.com/news-and-analysis/news/current-and-potential-new-therapies-for-the-treatment-of-psoriasis/11013061.article?firstPass=false>

46. Lai-Cheong JE, McGrath JA. Structure and function of skin, hair and nails. *Medicine (Baltimore)*. 2013;41(6):317–20.
47. Baroni A, Buommino E, De Gregorio V, Ruocco E, Ruocco V, Wolf R. Structure and function of the epidermis related to barrier properties. *Clin Dermatol*. 2012;30:257–62.
48. Arda O, Göksügür N, Tüzün Y. Basic histological structure and functions of facial skin. *Clin Dermatol*. 2014;32:3–13.
49. Menon GK, Cleary GW, Lane ME. The structure and function of the stratum corneum. *Int J Pharm*. 2012;435:3–9.
50. Darlenski R, Sassning S, Tsankov N, Fluhr JW. Non-invasive in vivo methods for investigation of the skin barrier physical properties. *Eur J Pharm Biopharm*. 2009;72:295–303.
51. Kendall AC, Kiezel-Tsugunova M, Brownbridge LC, Harwood JL, Nicolaou A. Lipid functions in skin: Differential effects of n-3 polyunsaturated fatty acids on cutaneous ceramides, in a human skin organ culture model. *Biochim Biophys Acta - Biomembr*. 2017;1859:1679–89.
52. Proksch E, Brandner JM, Jensen JM. The skin: An indispensable barrier. *Exp Dermatol*. 2008;17:1063–72.
53. Van Smeden J, Janssens M, Gooris GS, Bouwstra JA. The important role of stratum corneum lipids for the cutaneous barrier function. *Biochim Biophys Acta - Mol Cell Biol Lipids*. 2014;1841:295–313.
54. Radner FPW, Fischer J. The important role of epidermal triacylglycerol metabolism for maintenance of the skin permeability barrier function. *Biochim Biophys Acta - Mol Cell Biol Lipids*. 2014;1841:409–15.
55. Lopes LB. Overcoming the cutaneous barrier with microemulsions. *Pharmaceutics*. 2014;6:52–77.
56. Lane ME. Skin penetration enhancers. *Int J Pharm*. 2013;447:12–21.
57. Raposo SC, Simões SD, Almeida AJ, Ribeiro HM. Advanced systems for glucocorticoids' dermal delivery. *Expert Opin Drug Deliv*. 2013;10(6):857–77.
58. Dominguez S, Mackert GA, Dobke MK. Nanotechnology to enhance transdermal delivery of hydrophilic humectants for improved skin care: a model for therapeutic applications. In: Andronescu E, Grumezescu AM, editors. *Nanostructures for Drug Delivery*. Elsevier Inc.; 2017. p. 919–39.
59. Carneiro R, Salgado A, Raposo S, Marto J, Simões S, Urbano M, et al. Topical emulsions containing ceramides: Effects on the skin barrier function and anti-inflammatory properties. *Eur J Lipid Sci Technol*. 2011;113:961–6.

60. Savjani KT, Gajjar AK, Savjani JK. Drug Solubility: Importance and Enhancement Techniques. *ISRN Pharm.* 2012;(2012):1–10.
61. Mohammed D, Hirata K, Hadgraft J, Lane ME. Influence of skin penetration enhancers on skin barrier function and skin protease activity. *Eur J Pharm Sci.* 2014;51:118–22.
62. Williams AC, Barry BW. Penetration enhancers. *Adv Drug Deliv Rev.* 2012;64:128–37.
63. Levang AK, Zhao K, Singh J. Effect of ethanol/propylene glycol on the in vitro percutaneous absorption of aspirin, biophysical changes and macroscopic barrier properties of the skin. *Int J Pharm.* 1999;181:255–63.
64. Ng KW. Penetration enhancement of topical formulations. *Pharmaceutics.* 2018;10(51).
65. Martin C, Alcock N, Hiom S, Birchall J. Development and evaluation of topical gabapentin formulations. *Pharmaceutics.* 2017;9(3):31.
66. Haq A, Michniak-Kohn B. Effects of solvents and penetration enhancers on transdermal delivery of thymoquinone: permeability and skin deposition study. *Drug Deliv.* 2018;25:1943–9.
67. Kouchak M, Handali S. Effects of Various Penetration Enhancers on Penetration of Aminophylline Through Shed Snake Skin. *Jundishapur J Nat Pharm Prod.* 2014;9(1):24–9.
68. Hirvonen J, Rajala R, Vihervaara P, Laine E, Paronen P, Urtti A. Mechanism and reversibility of penetration enhancer action in the skin. *Eur J Pharm Biopharm.* 1995;40:81–5.
69. Leopold CS, Lippold BC. An attempt to clarify the mechanism of the penetration enhancing effects of lipophilic vehicles with differential scanning calorimetry (DSC). *J Pharm Pharmacol.* 1995;47:276–81.
70. Bouwstra JA, de Vries MA, Gooris GS, Bras W, Brussee J, Ponc M. Thermodynamic and structural aspects of the skin barrier. *J Control Release.* 1991;15:209–20.
71. Golden GM, McKie JE, Potts RO. Role of stratum corneum lipid fluidity in transdermal drug flux. *J Pharm Sci.* 1987;76:25–8.
72. Yamashita Y, Miyahara R, Sakamoto K. Emulsion and emulsification technology. In: Kazutami Sakamoto, Robert Y. Lochhead, Howard I. Maibach YY, editor. *Cosmetic Science and Technology: Theoretical Principles and Applications.* Elsevier Inc.; 2017. p. 489–506.
73. Simões S, Ribeiro HM, Almeida AJ. Microemulsões e nanoemulsões. In: *Novas Formas Farmacêuticas para Administração de Fármacos.* Porto: Edições Universidade Fernando Pessoa; 2011. p. 271–96.
74. Callender SP, Mathews JA, Kobernyk K, Wettig SD. Microemulsion utility in pharmaceuticals: Implications for multi-drug delivery. *Int J Pharm.* 2017;526:425–

- 42.
75. Tadros TF. *Emulsions: Formation, Stability, Industrial Applications*. Germany: Gruyter Graduate; 2016. 225 p.
 76. Tadros TF. *Applications of Surfactants in Emulsion Formation and Stabilisation*. In: *Applied Surfactants: Principles and Applications*. Wiley-VCH Verlag GmbH & Co. KGaA; 2005. p. 115–85.
 77. Tadros TF. *Microemulsions*. In: *Applied Surfactants: Principles and Applications*. Wiley-VCH Verlag GmbH & Co. KGaA; 2005. p. 309–34.
 78. Tadros TF. *Emulsion Formation, Stability, and Rheology*. In: *Emulsion Formation and Stability*. 2013. p. 1–75.
 79. Eccleston GM. *Emulsions and microemulsions*. In: *Encyclopedia of Biomedical Polymers and Polymeric Biomaterials*. 2015. p. 3259–76.
 80. Sakamoto K, Lochhead RY, Maibach HI, Yamashita Y. *Cosmetic Science and Technology: Theoretical Principles and Applications*. 1st ed. *Cosmetic Science and Technology: Theoretical Principles and Applications*. Elsevier; 2017.
 81. Chang Q. *Emulsion, Foam, and Gel*. In: *Colloid and Interface Chemistry for Water Quality Control*. Academic Press; 2016. p. 227–45.
 82. Bajpai P. *Colloid and Surface Chemistry*. In: *Biermann's Handbook of Pulp and Paper*. 3rd ed. Elsevier Inc.; 2018. p. 381–400.
 83. Tadros TF. *Surfactants in Pharmaceutical Formulations*. In: *Applied Surfactants: Principles and Applications*. Wiley-VCH Verlag GmbH & Co. KGaA; 2005. p. 433–501.
 84. Ribeiro HM, Morais JA, Eccleston GM. *Structure and rheology of semisolid o/w creams containing cetyl alcohol/non-ionic surfactant mixed emulsifier and different polymers*. *Int J Cosmet Sci*. 2004;26:47–59.
 85. Eccleston GM. *Functions of mixed emulsifiers and emulsifying waxes in dermatological lotions and creams*. *Colloids Surfaces A Physicochem Eng Asp*. 1997;123–124:169–82.
 86. Eccleston GM. *Multiple-phase oil-in-water emulsions*. *J Soc Cosmet Chem*. 1990;41:1–22.
 87. There are thousands of different cosmetic products on the market, all with differing combinations of ingredients. [Internet]. [cited 2019 Jul 13]. Available from: <https://www.science.org.au/curious/people-medicine/chemistry-cosmetics>
 88. Hiroshi I, Shimada K. *Formulas, Ingredients and Production of Cosmetics. Technology of Skin- and Hair-Care Products in Japan*. Japan: Springer; 2013. 157–163 p.
 89. Castro J. *Cosmetic Chemistry* [Internet]. [cited 2019 Jul 13]. Available from: <http://www.chemistryexplained.com/Co-Di/Cosmetic-Chemistry.html>
 90. Grisel M, Loubat-bouleuc N, Picard C, Douguet M, Savary G, Merlaud F.

- Spreading properties of cosmetic emollients: Use of synthetic skin surface to elucidate structural effect. *Colloids Surfaces B Biointerfaces*. 2017;154:307–14.
91. Terescenco D, Picard C, Clemenceau F, Grisel M, Savary G. Influence of the emollient structure on the properties of cosmetic emulsion containing lamellar liquid crystals. *Colloids Surfaces A*. 2018;536:10–9.
 92. Johnson A, Roden K. The selection and use of preservatives in skin and sun care products. *Household and Personal Care Today*. 2018;13(September/October):16–20.
 93. Rahali Y, Pensé-Lhéritier AM, Mielcarek C, Bensouda Y. Optimization of preservatives in a topical formulation using experimental design. *Int J Cosmet Sci*. 2009;31(6):451–60.
 94. Ascenso A, Simões S, Marto J, Ribeiro HM, Almeida AJ. Sistemas dispersos. Formas farmacêuticas e sistemas de libertação de fármacos. 2007. 413–470 p.
 95. Griffin WC. Classification of Surface-Active Agents by “HLB.” *J Soc Cosmet Chem*. 1949;1:311–26.
 96. Cassiday L. Emulsions: making oil and water mix [Internet]. 2014 [cited 2019 Sep 10]. Available from: <https://www.aocs.org/stay-informed/inform-magazine/featured-articles/emulsions-making-oil-and-water-mix-april-2014>
 97. Griffin WC. Calculation of HLB values of non-ionic surfactants. *J Soc Cosmet Chem*. 1954;5:249–56.
 98. Bancroft WD. The theory of emulsification, V. *J Phys Chem*. 1913;17(6):501–19.
 99. Mehta SK, Kaur G. Microemulsions: Thermodynamic and Dynamic Properties. In: Prof. Mizutani Tadashi, editor. *Thermodynamics*. 2011. p. 382–406.
 100. Israelachvili JN, Mitchell DJ, Ninham BW. Theory of self-assembly of hydrocarbon amphiphiles into micelles and bilayers. *72*:1525–68.
 101. Hoar T, Schulman J. Transparent water-in-oil dispersions: the oleopathic hydro-micelle. *Nature*. 1943;152:102–3.
 102. Prince LM. *Microemulsion Theory and Practice*. New York: Academic Press; 1977.
 103. Anton N, Vandamme TF. Nano-emulsions and micro-emulsions: Clarifications of the critical differences. *Pharm Res*. 2011;28:978–85.
 104. Kogan A as transdermal drug delivery vehicles, Garti N. Microemulsions as transdermal drug delivery vehicles. *Adv Colloid Interface Sci*. 2006;123–126:369–85.
 105. Winsor PA. Hydrotrophy, solubilization and related emulsification processes. *Trans Faraday Soc*. 1948;44:376–98.
 106. Du X, Lucia LA, Ghiladi RA. A Novel Approach for Rapid Preparation of Monophasic Microemulsions That Facilitates Penetration of Woody Biomass. *ACS Sustain Chem Eng*. 2016;4(3):1665–72.

107. Mulchande J, Oliveira R, Carrasco M, Gouveia L, Guedes RC, Iley J, et al. 4-Oxo- β -lactams (Azetidine-2 , 4-diones) Are Potent and Selective Inhibitors of Human Leukocyte Elastase. *J Med Chem*. 2010;53:241–53.
108. Mulchande J, Simões SI, Gaspar MM, Eleutério C V., Oliveira R, Cruz MEM, et al. Synthesis, stability, biochemical and pharmacokinetic properties of a new potent and selective 4-oxo- β -lactam inhibitor of human leukocyte elastase. *J Enzyme Inhib Med Chem*. 2011;26(2):169–75.
109. Mulchande J, Guedes RC, Tsang W, Page MI, Moreira R, Iley J. Azetidine-2,4-diones (4-Oxo- β -lactams) as Scaffolds for Designing Elastase Inhibitors. *J Med Chem*. 2008;51(6):1783–90.
110. (CDC) C for DC and P. Facts about Bromine [Internet]. [cited 2019 Jul 26]. Available from: <https://emergency.cdc.gov/agent/bromine/basics/facts.asp>
111. Lambers H, Piessens S, Bloem A, Pronk H, Finkel P. Natural skin surface pH is on average below 5, which is beneficial for its resident flora. *Int J Cosmet Sci*. 2006;28:359–70.
112. Lonza PC-. Geogard™ Ultra™ - Next-Generation Preservation. 2013;
113. PubChem [Internet]. [cited 2019 Jul 24]. Available from: <https://pubchem.ncbi.nlm.nih.gov/>
114. Logaraj T V., Bhattacharya S, Udaya Sankar K, Venkateswaran G. Rheological behaviour of emulsions of avocado and watermelon oils during storage. *Food Chem*. 2008;106:937–43.
115. Gore E, Picard C, Savary G. Spreading behavior of cosmetic emulsions: Impact of the oil phase. *Biotribology*. 2018;16:17–24.
116. Gilbert L, Picard C, Savary G, Grisel M. Rheological and textural characterization of cosmetic emulsions containing natural and synthetic polymers: Relationships between both data. *Colloids Surfaces A Physicochem Eng Asp*. 2013;421:150–63.
117. Barnes HA, Hutton JE, S. KWFR. *An Introduction to Rheology*. Rheology Series. 1st ed. Elsevier Science; 1989.
118. Schramm G. *A Practical Approach to Rheology and Rheometry*. 2nd ed. Gebrueder HAAKE GmbH; 2000.
119. Corporation UIRAD o. SC. *An Introductory Guide to Rheology*. Corporation UIRAD o. SC, editor. US Ink; 1995.
120. Lippacher A, Müller RH, Mäder K. Liquid and semisolid SLN™ dispersions for topical application: Rheological characterization. *Eur J Pharm Biopharm*. 2004;58:561–7.
121. Bahadur P, Narasimhan S, Johnson & Johnson, Skillman NU. Cetyl Alcohol: A Multifunctional Addition to Formulators ' Toolboxes. *Cosmetic Science and Technology: Theoretical Principles and Applications*. 2018;1–6.
122. Kulawik-Pióro A, Potykanowicz A. Determining the quality of hydrophobic

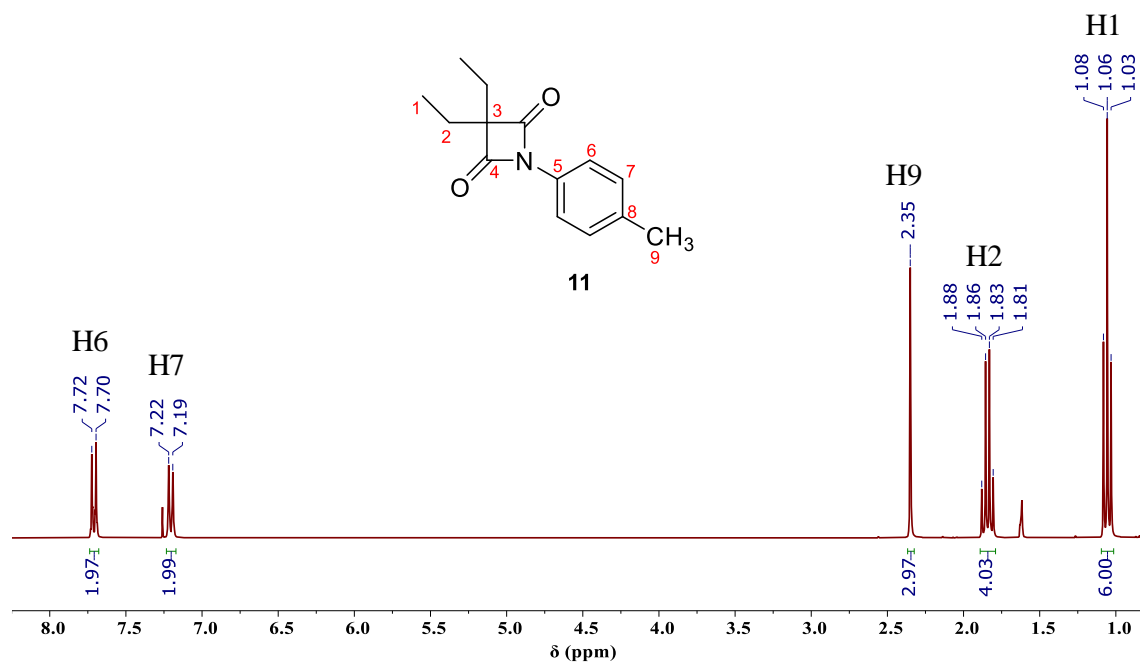
- barrier creams by rheological measurements, sensory analysis, pH determination and permeation time measurements. *Chemom Intell Lab Syst.* 2016;156:14–20.
123. The preservative challenge. *Cosmetics&Toiletries.* 2018;2–44.
 124. Vispute M, Nazim S, Khan T, Shaikh S. An overview on exploring nasal microemulsion for treatment of CNS disorders. *Int J Pharm Sci Res.* 2013;4(4):1294–311.
 125. Chudasama A, Patel V, Nivsarkar M, Vasu K, Shishoo C. Investigation of microemulsion system for transdermal delivery of itraconazole. *J Adv Pharm Technol Res.* 2011;2(1):30–8.
 126. Syed HK, Peh KK. Identification of phases of various oil, surfactant/ co-surfactants and water system by ternary phase diagram. *Acta Pol Pharm - Drug Res.* 2014;71(2):301–9.
 127. Otto A, Du Plessis J, Wiechers JW. Formulation effects of topical emulsions on transdermal and dermal delivery. *Int J Cosmet Sci.* 2009;31:1–19.
 128. Tan G, Xu P, Lawson LB, He J, Freytag LC, Clements JD, et al. Hydration Effects on Skin Microstructure as Probed by High- Resolution Cryo-Scanning Electron Microscopy and Mechanistic Implications to Enhanced Transcutaneous Delivery of Biomacromolecules. *J Pharm Sci.* 2010;99(2):730–40.
 129. Dalvi UG, Zatz JL. Effect of nonionic surfactants on penetration of dissolved benzocaine through hairless mouse skin. *J Soc Cosmet Chem.* 1981;32:87–94.
 130. Florence AT, Gillan JMN. Biological implications of the use of surfactants in medicines and the biphasic effects of surfactants in biological systems. *Pestic Sci.* 1975;6:429–39.
 131. Sarpotdar PP, Zatz JL. Evaluation of penetration enhancement of lidocaine by nonionic surfactants through hairless mouse skin in vitro. *J Pharm Sci.* 1986;75:176–81.
 132. Chime SA, Onunkwo GC, Onyishi II. Kinetics and mechanisms of drug release from swellable and non swellable matrices: A review. *Res J Pharm Biol Chem Sci.* 2013;4(2):97–103.
 133. Siepmann J, Peppas NA. Higuchi equation: Derivation, applications, use and misuse. *Int J Pharm.* 2011;418:6–12.
 134. Mircioiu C, Voicu V, Anuta V, Tudose A, Celia C, Paolino D, et al. Mathematical modeling of release kinetics from supramolecular drug delivery systems. *Pharmaceutics.* 2019;11(140):1–45.
 135. Lin YK, Yang SH, Chen CC, Kao HC, Fang JY. Using imiquimod-induced psoriasis-like skin as a model to measure the skin penetration of anti-psoriatic drugs. *PLoS One.* 2015;10(9):1–19.
 136. Lucas SD, Gonçalves LM, Cardote TAF, Correia HF, Moreira R, Guedes RC. Structure Based Virtual Screening for Discovery of Novel Human Neutrophil Elastase Inhibitors. *Med Chem Commun.* 2012;3:1299–304.

137. Strober W. Trypan Blue Exclusion Test of Cell Viability. *Curr Protoc Immunol*. 2015;111:A3.B.1.
138. Zhang Y, Huo M, Zhou J, Zou A, Li W, Yao C, et al. DDSolver: An add-in program for modeling and comparison of drug dissolution profiles. *AAPS J*. 2010;12(3):263–71.
139. Mateus D, Marto J, Trindade P, Gonçalves H, Salgado A, Machado P, et al. Improved morphine-loaded hydrogels for wound-related pain relief. *Pharmaceutics*. 2019;11(76):1–16.
140. Costa P, Lobo JMS. Modeling and comparison of dissolution profiles. *Eur J Pharm Sci*. 2001;13:123–33.
141. Pivetta TP, Simões S, Araújo MM, Carvalho T, Arruda C, Marcato PD. Development of nanoparticles from natural lipids for topical delivery of thymol: Investigation of its anti-inflammatory properties. *Colloids Surfaces B Biointerfaces*. 2018;164:281–90.

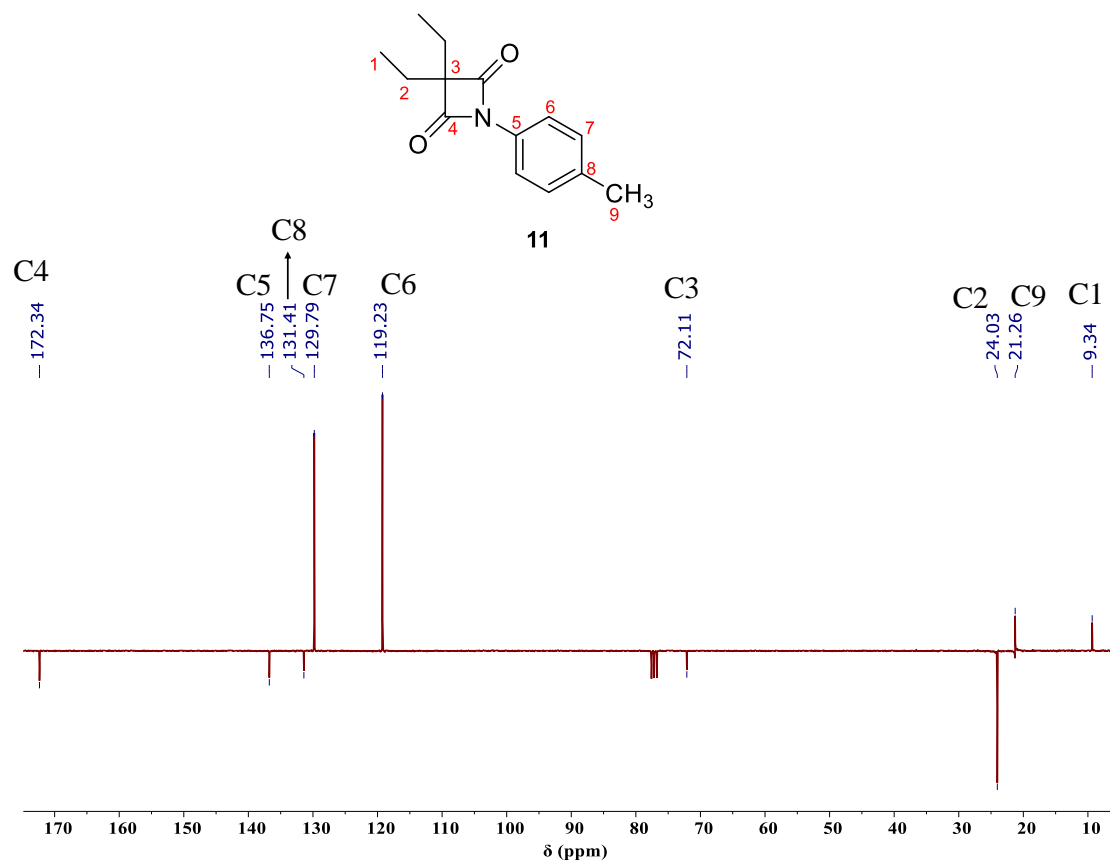
7. Appendix 1

7.1. Characterization of compound (11)

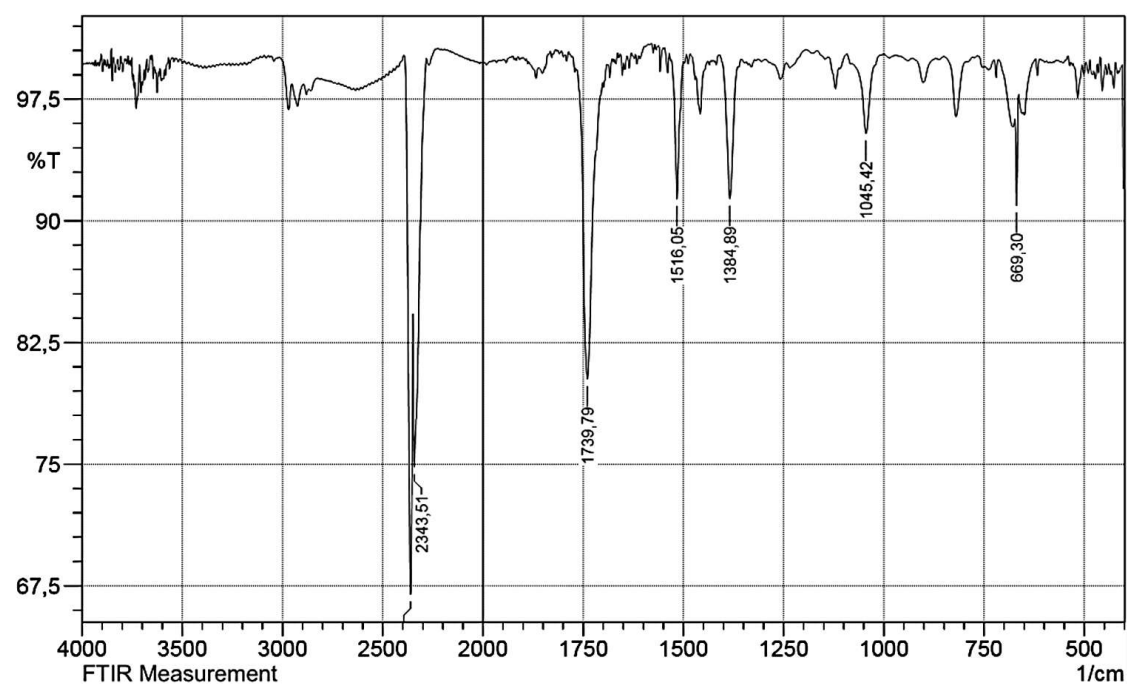
7.1.1. ^1H NMR spectra



7.1.2. ^{13}C NMR spectra

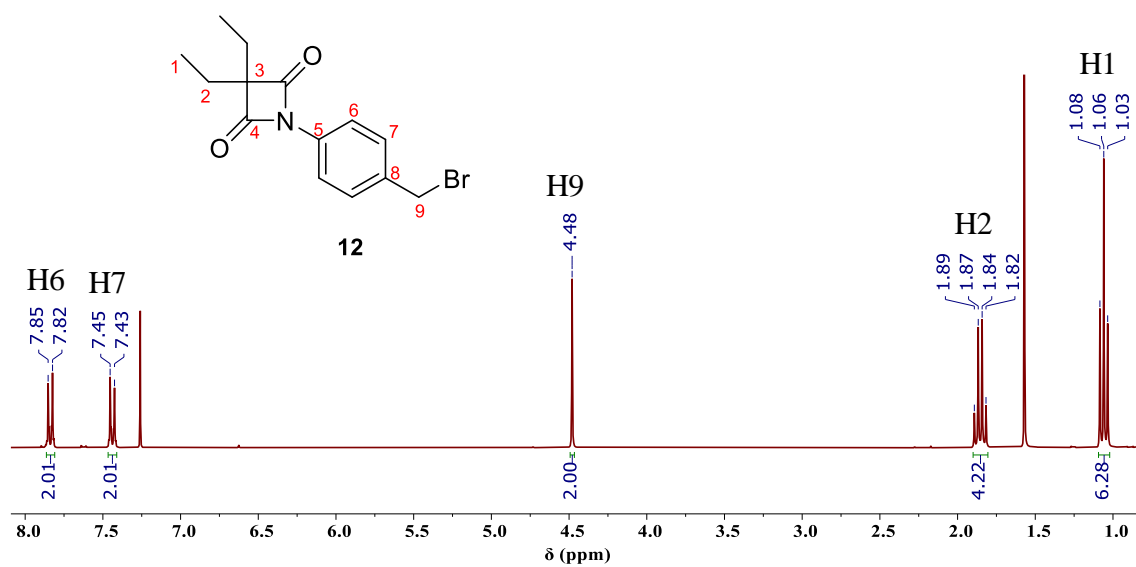


7.1.3. FTIR spectra

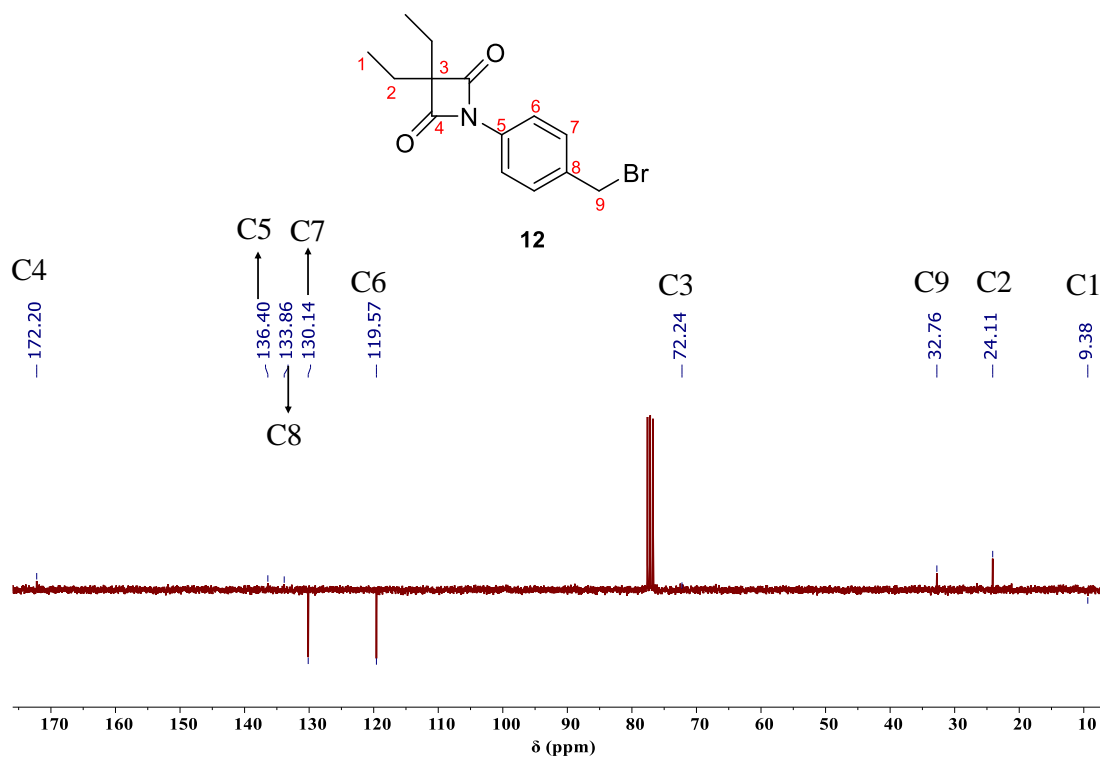


7.2. Characterization of compound (12)

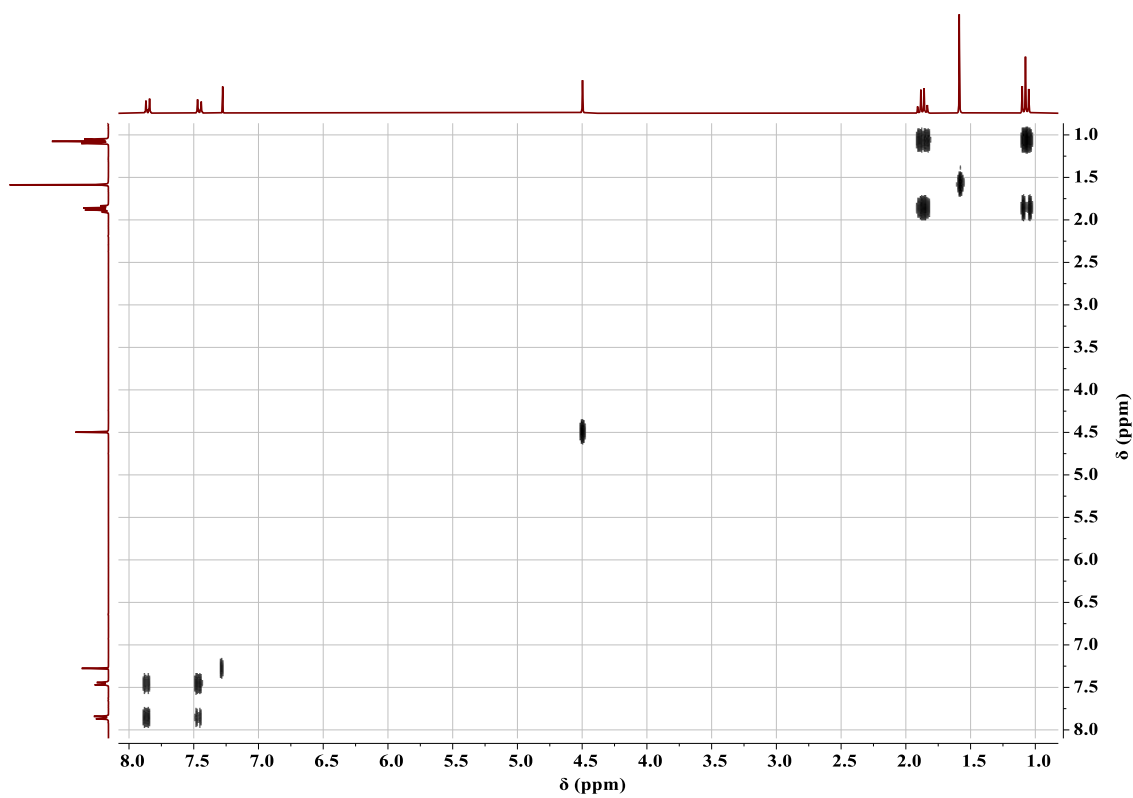
7.2.1. ¹H NMR spectra



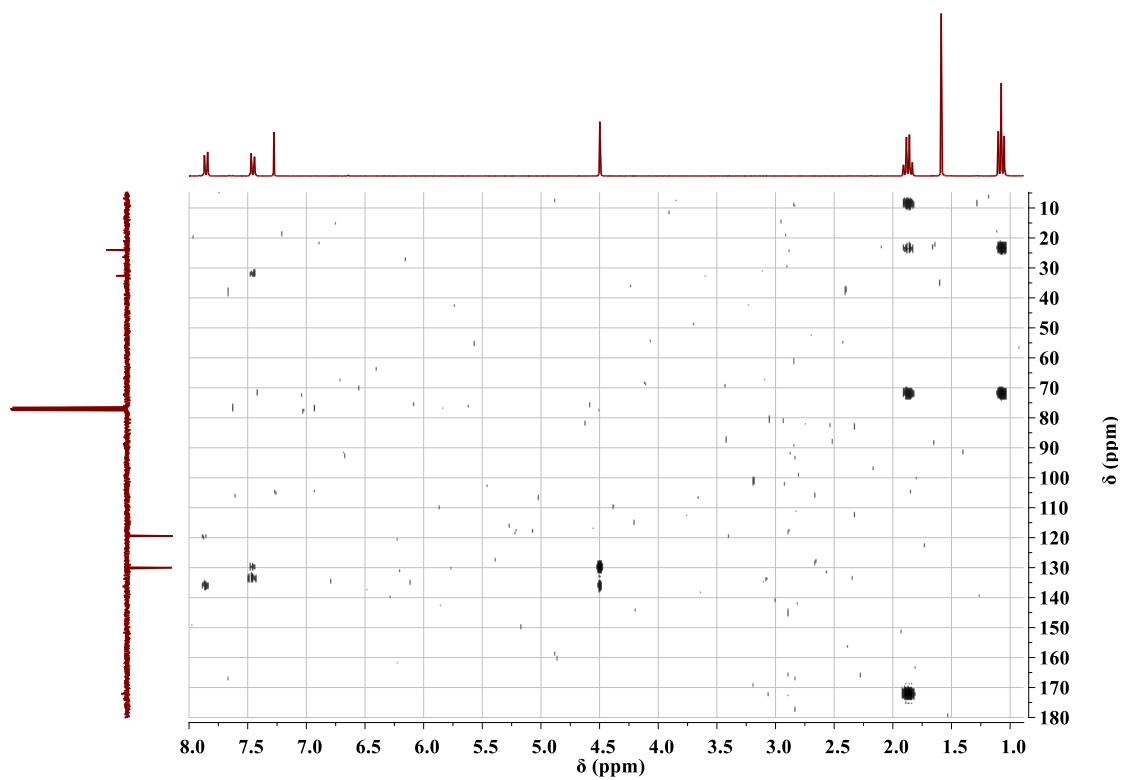
7.2.2. ^{13}C NMR spectra



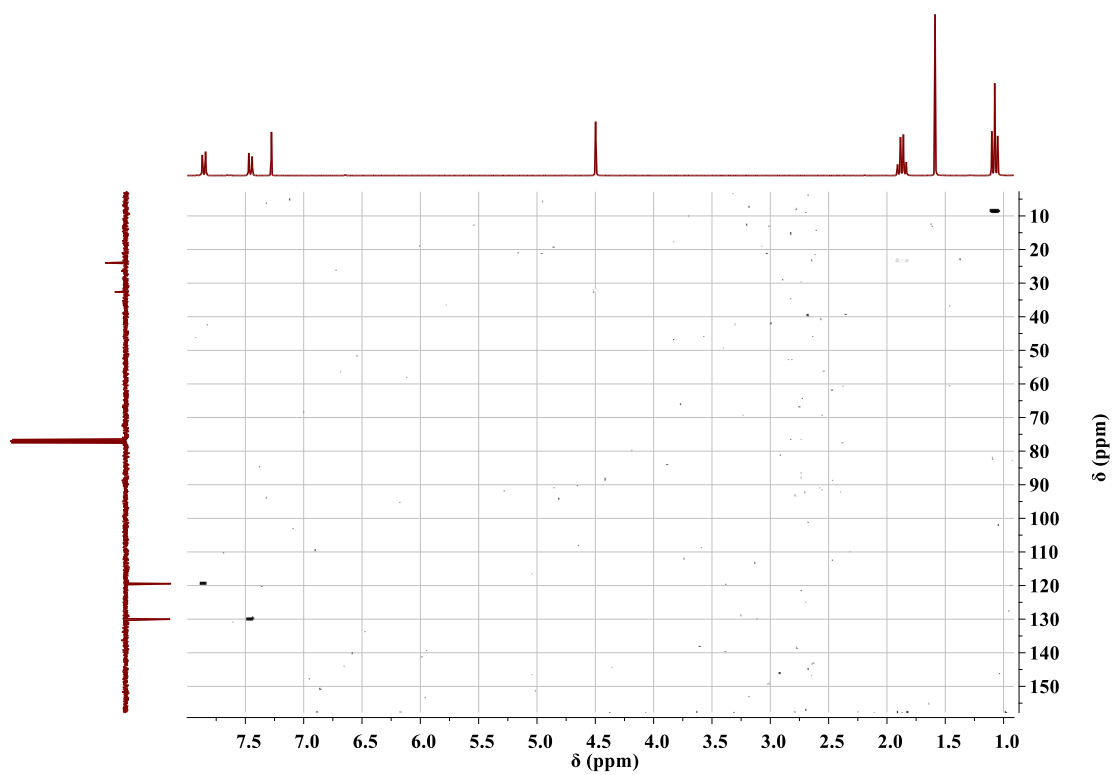
7.2.3. COSY NMR spectra



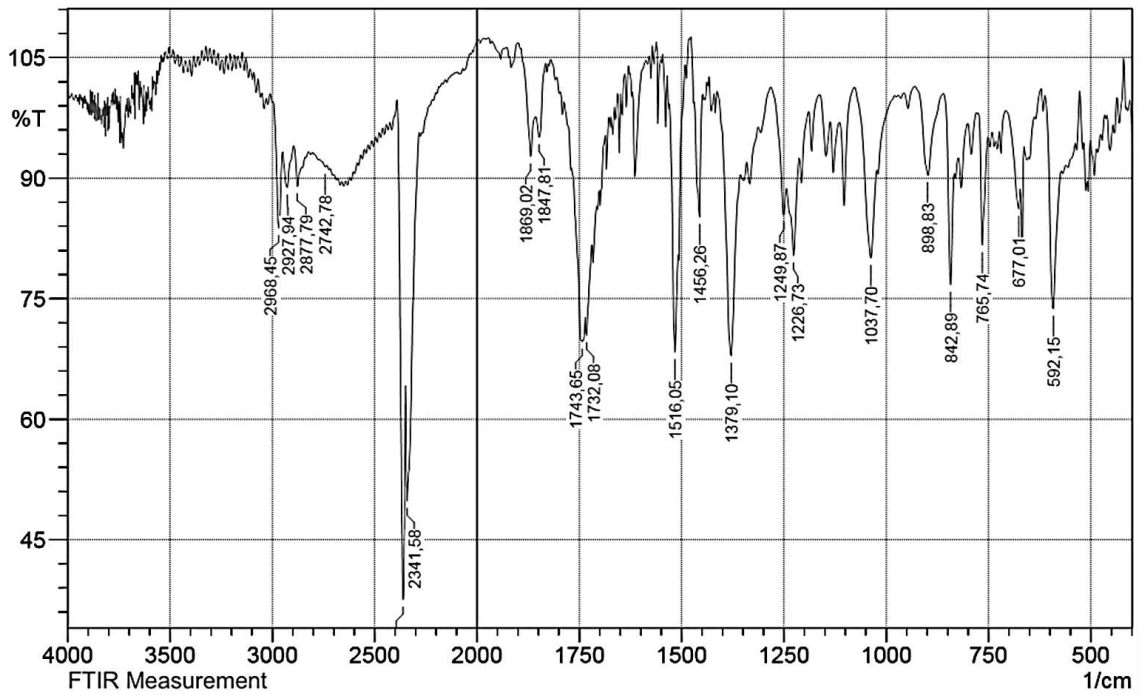
7.2.4. HMBC NMR spectra



7.2.5. HSQC NMR spectra



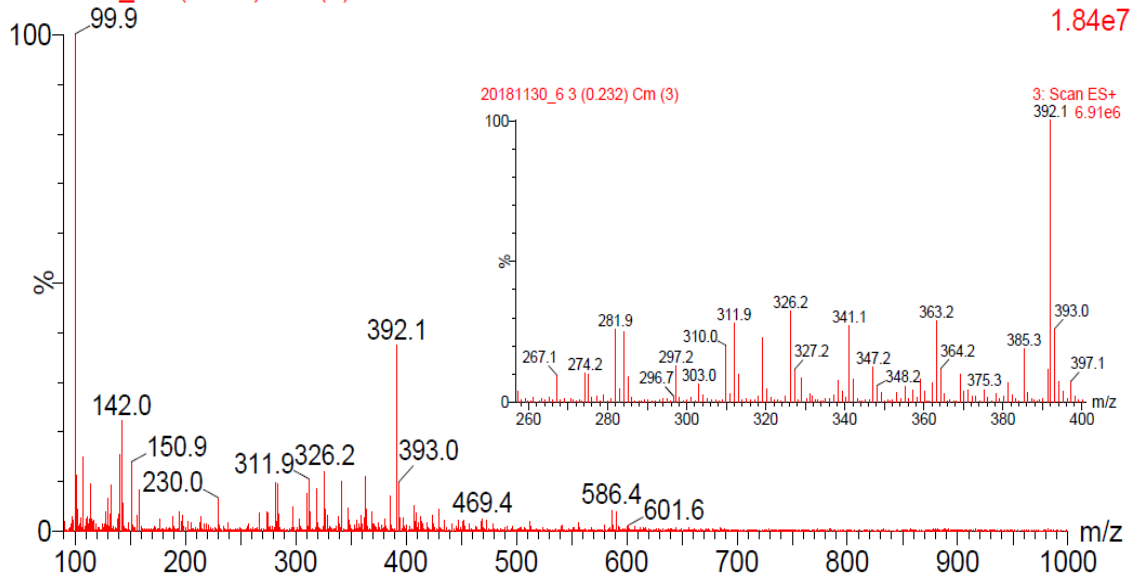
7.2.6. FTIR spectra



7.2.7. Mass spectra

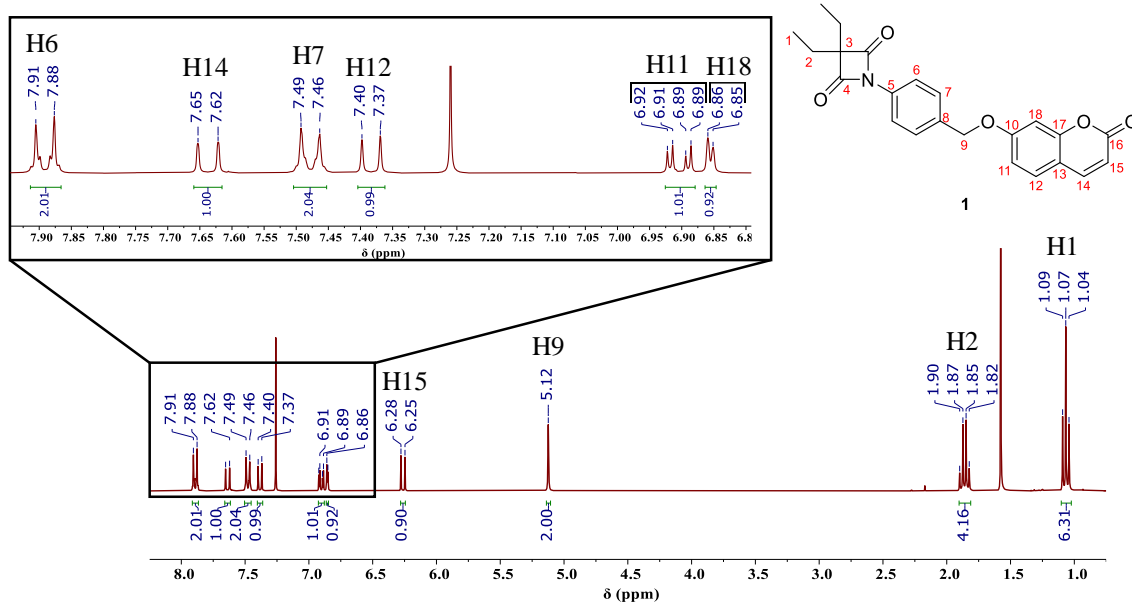
20181130_6 3 (0.232) Cm (3)

3: Scan ES+
1.84e7

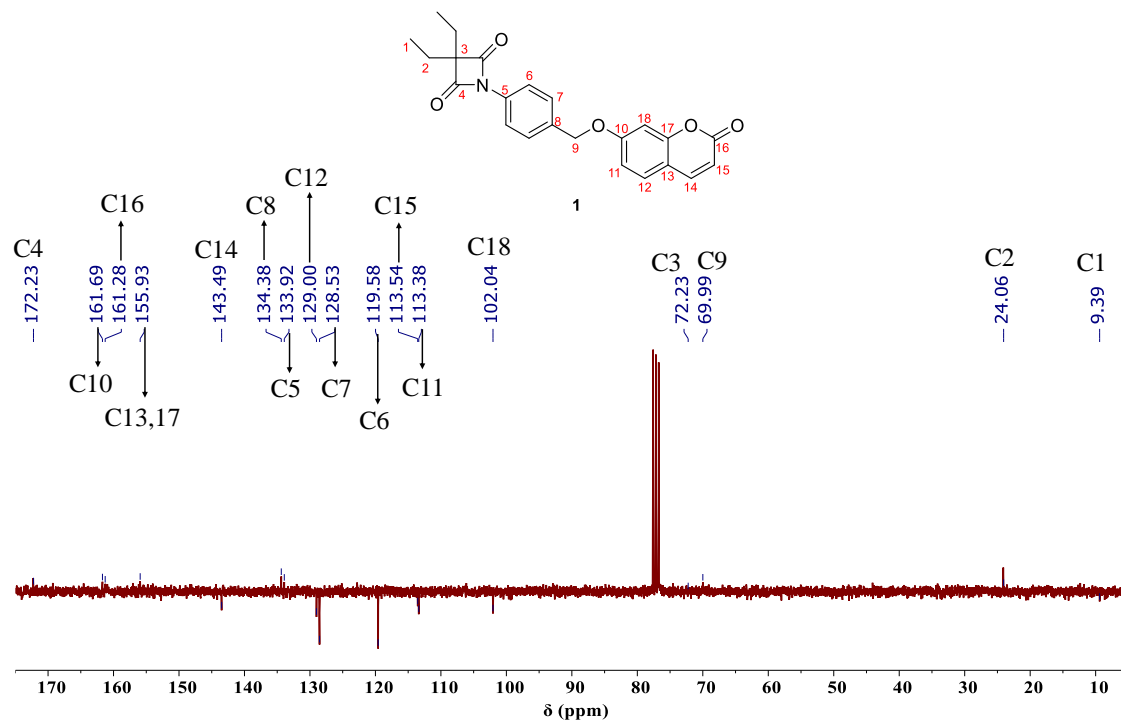


7.3. Characterization of compound (1)

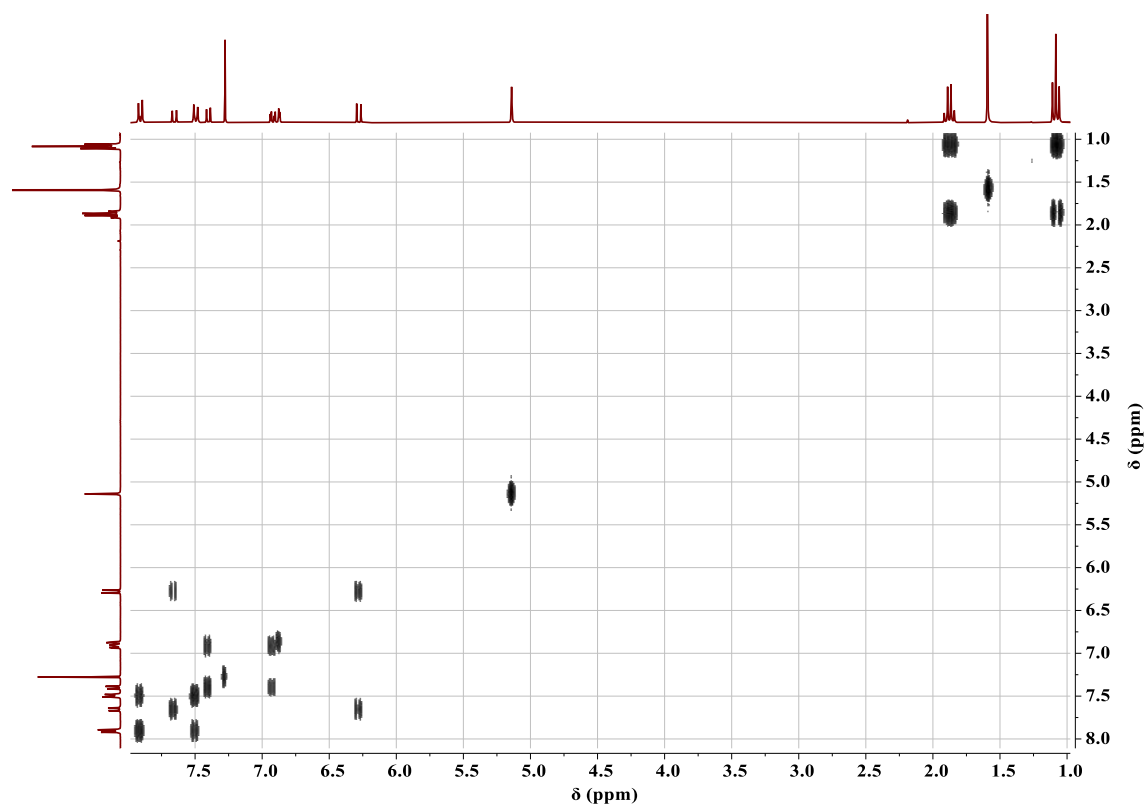
7.3.1. ¹H NMR spectra



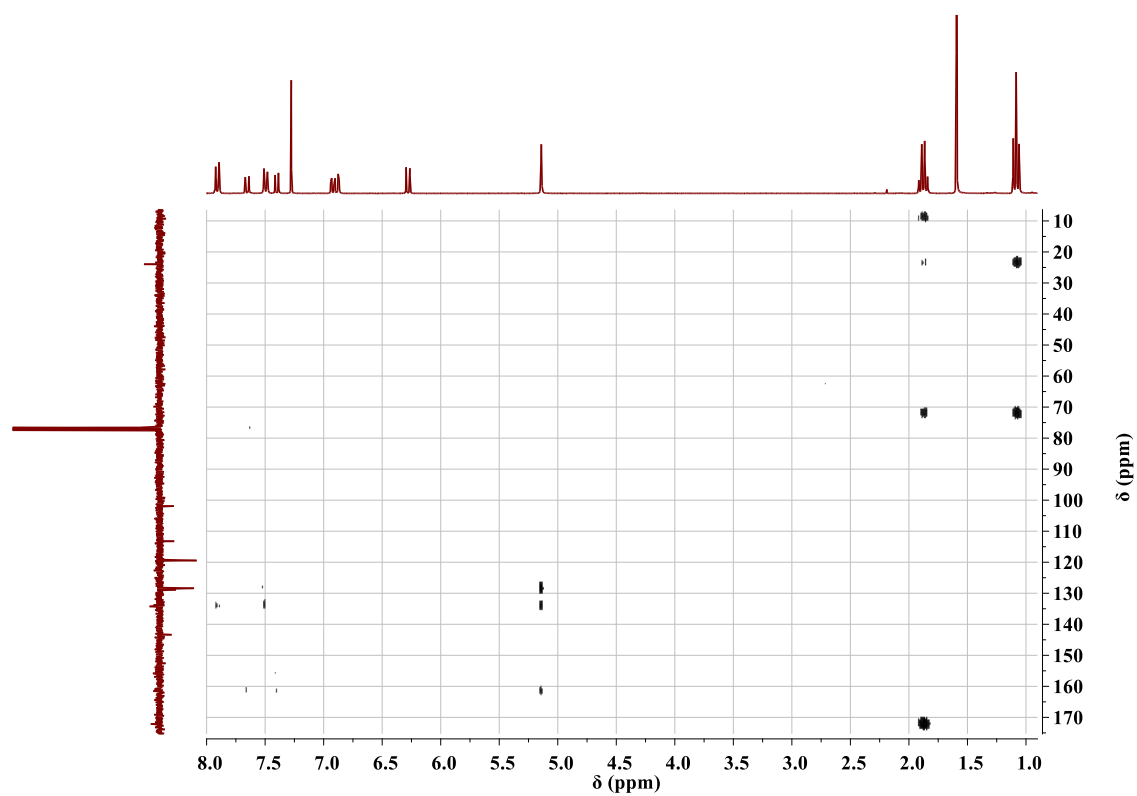
7.3.2. ¹³C NMR spectra



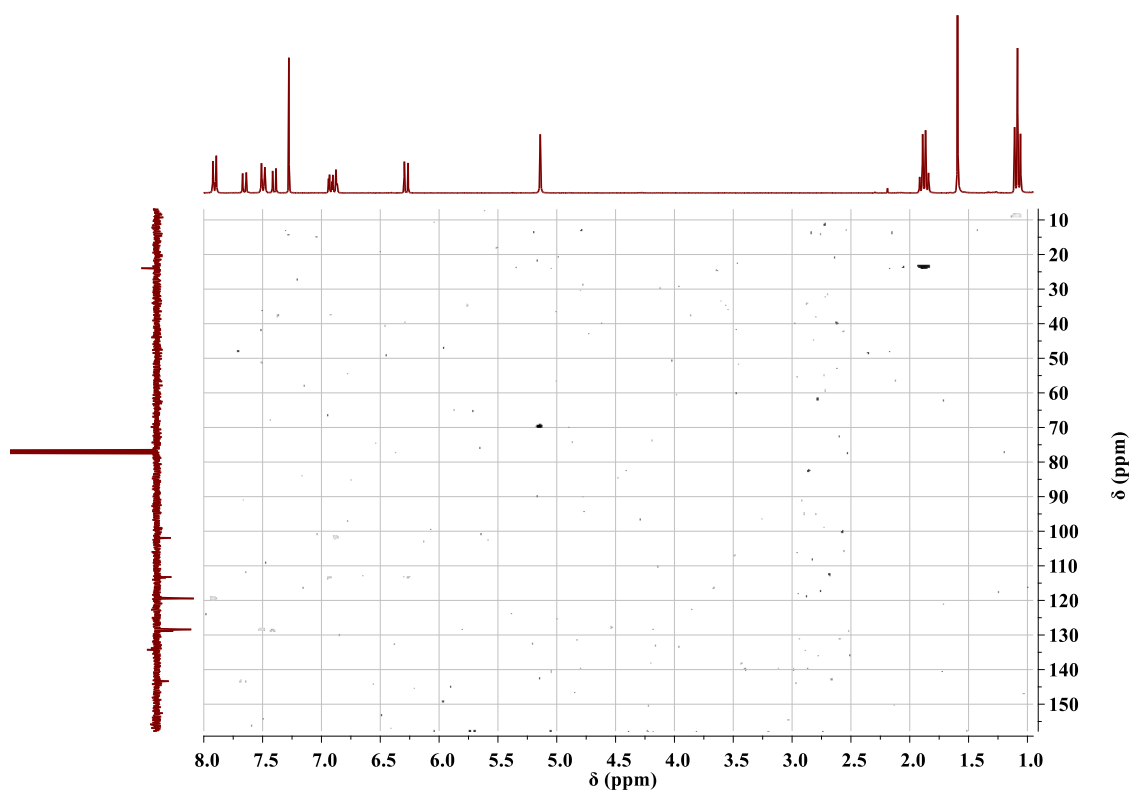
7.3.3. COSY NMR spectra



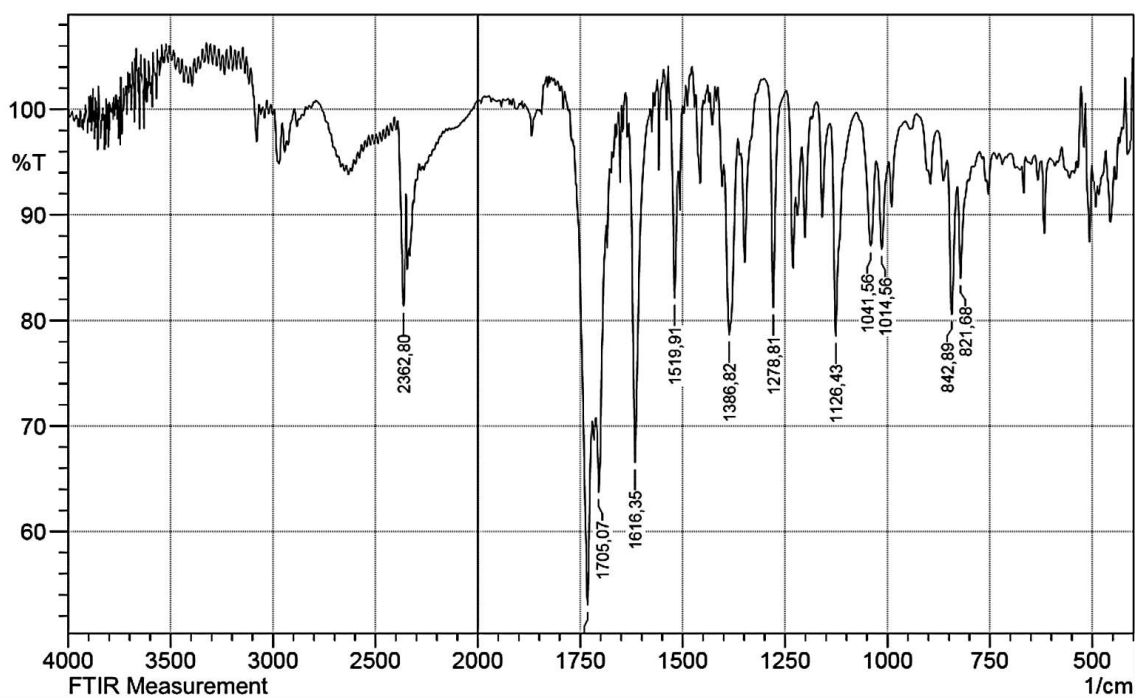
7.3.4. HMBC NMR spectra



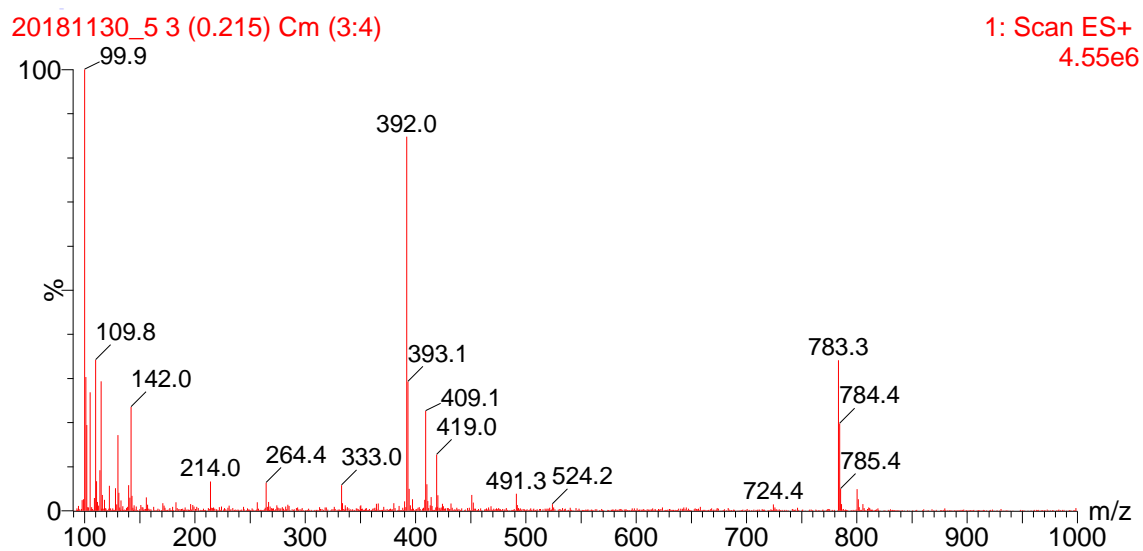
7.3.5. HSQC NMR spectra



7.3.6. FTIR spectra

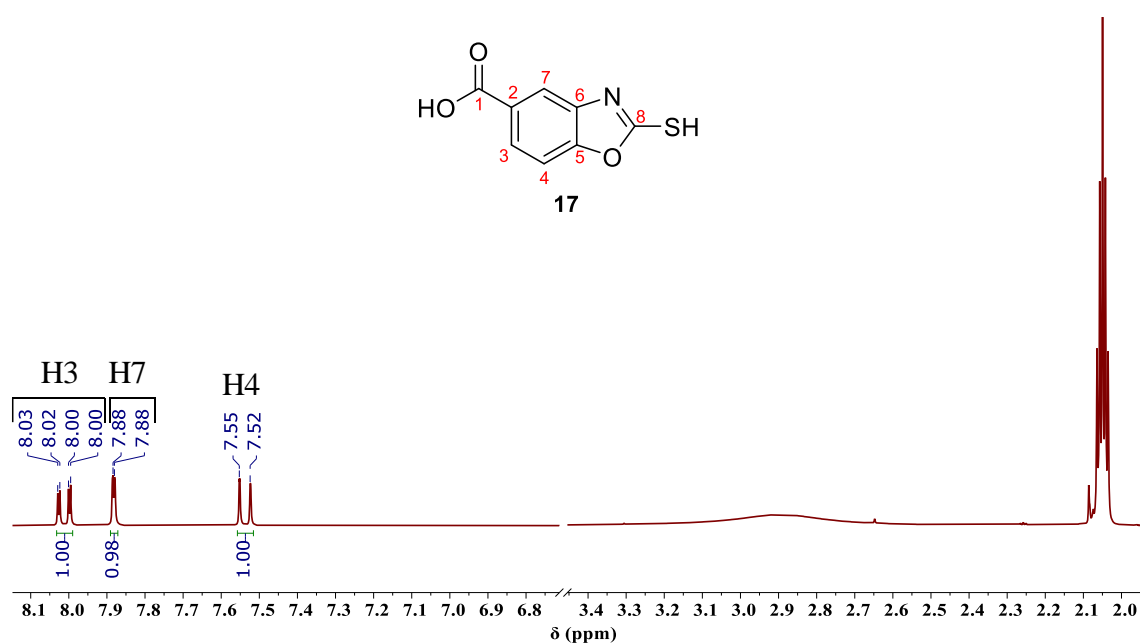


7.3.7. Mass spectra

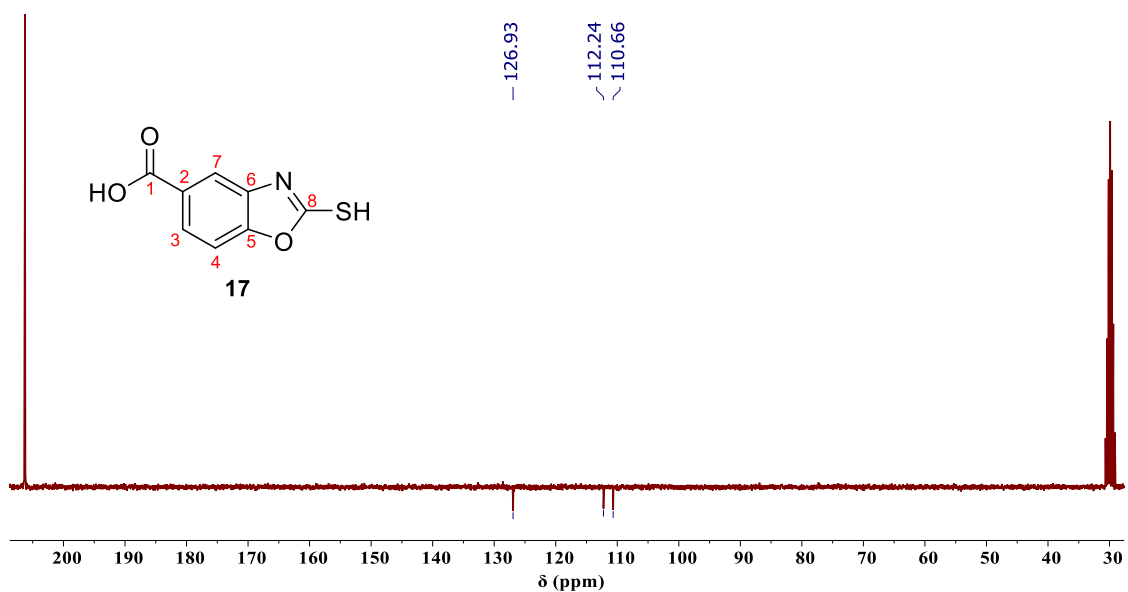


7.4. Characterization of compound (17)

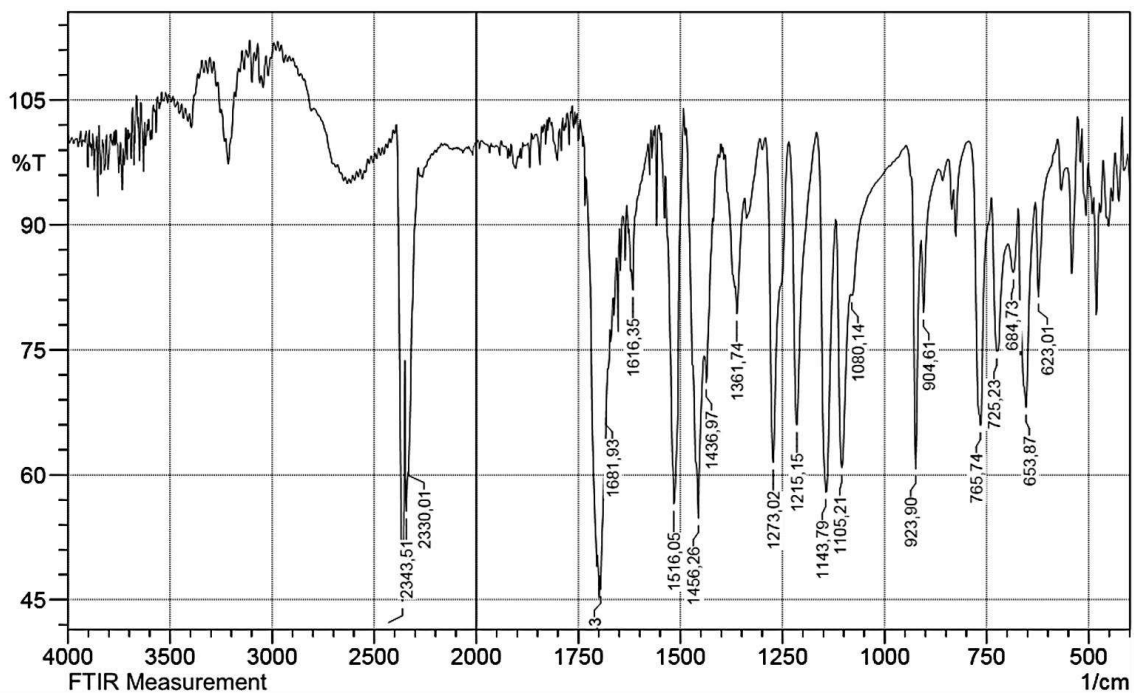
7.4.1. ¹H NMR spectra



7.4.2. ¹³C NMR spectra

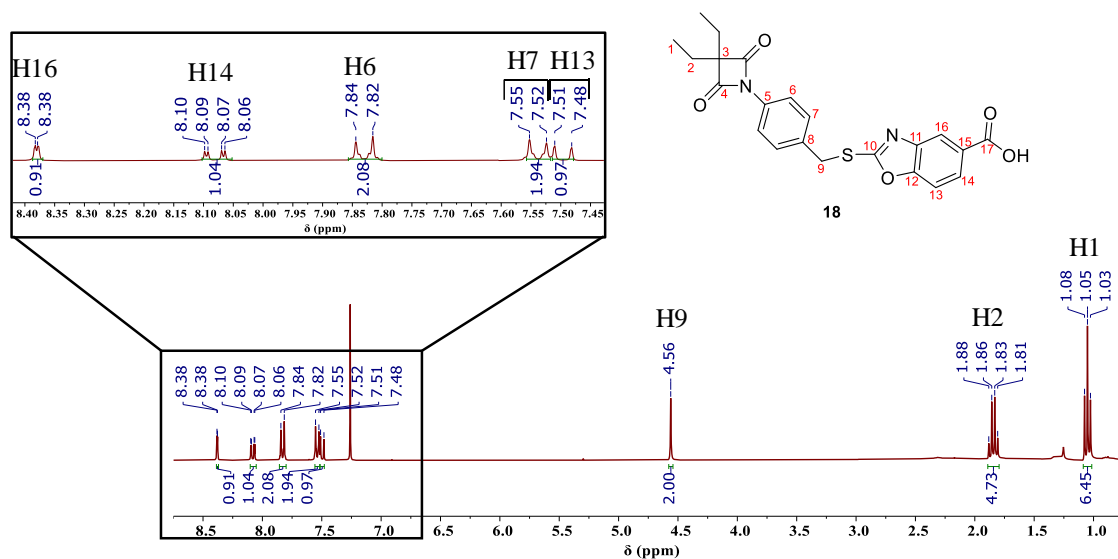


7.4.3. FTIR spectra

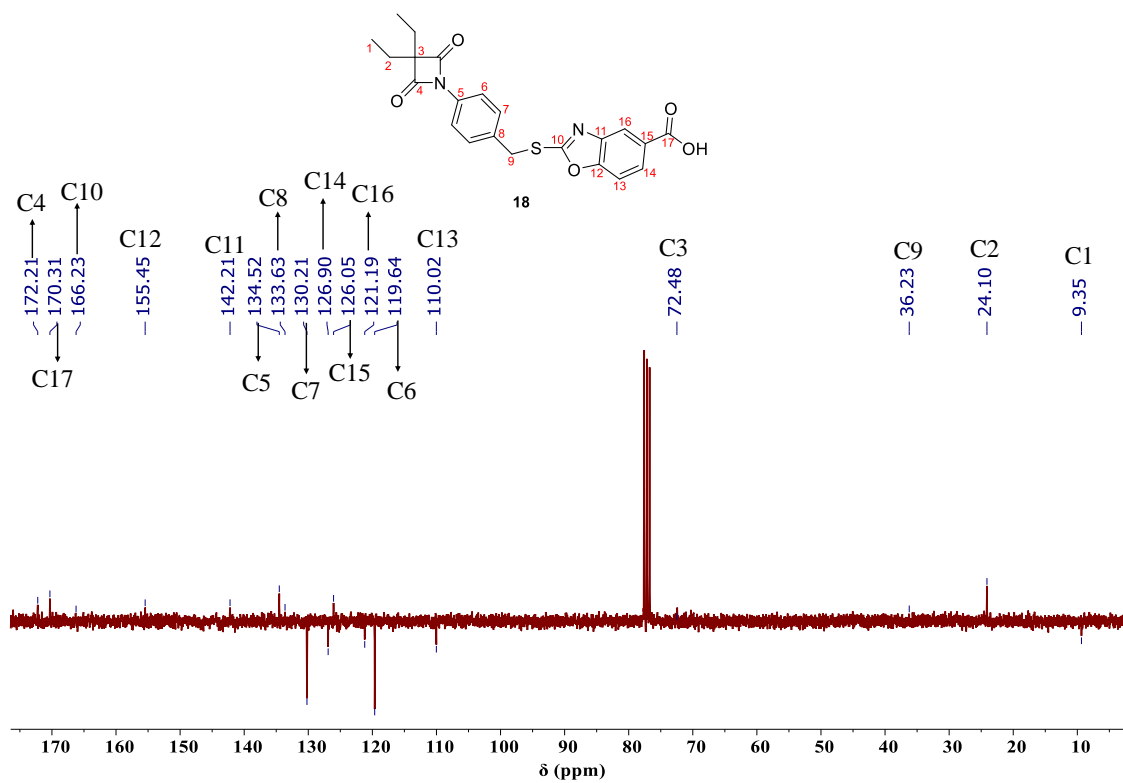


7.5. Characterization of compound (18)

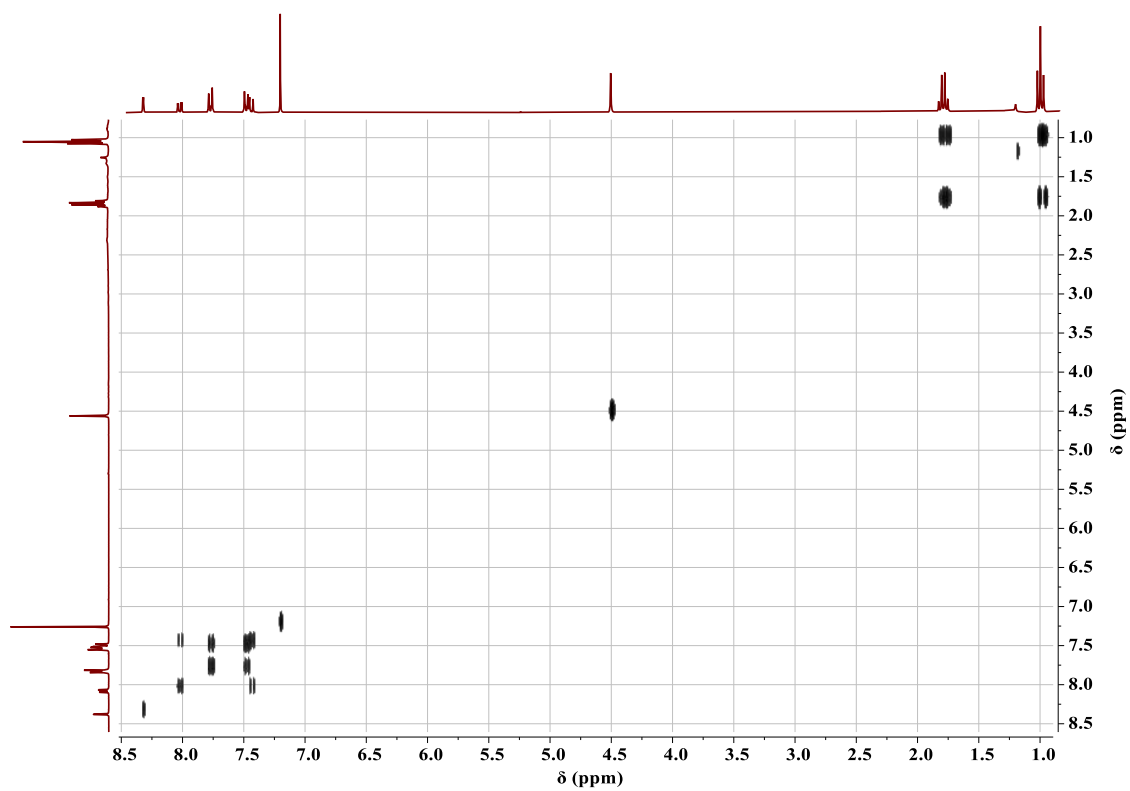
7.5.1. ¹H NMR spectra



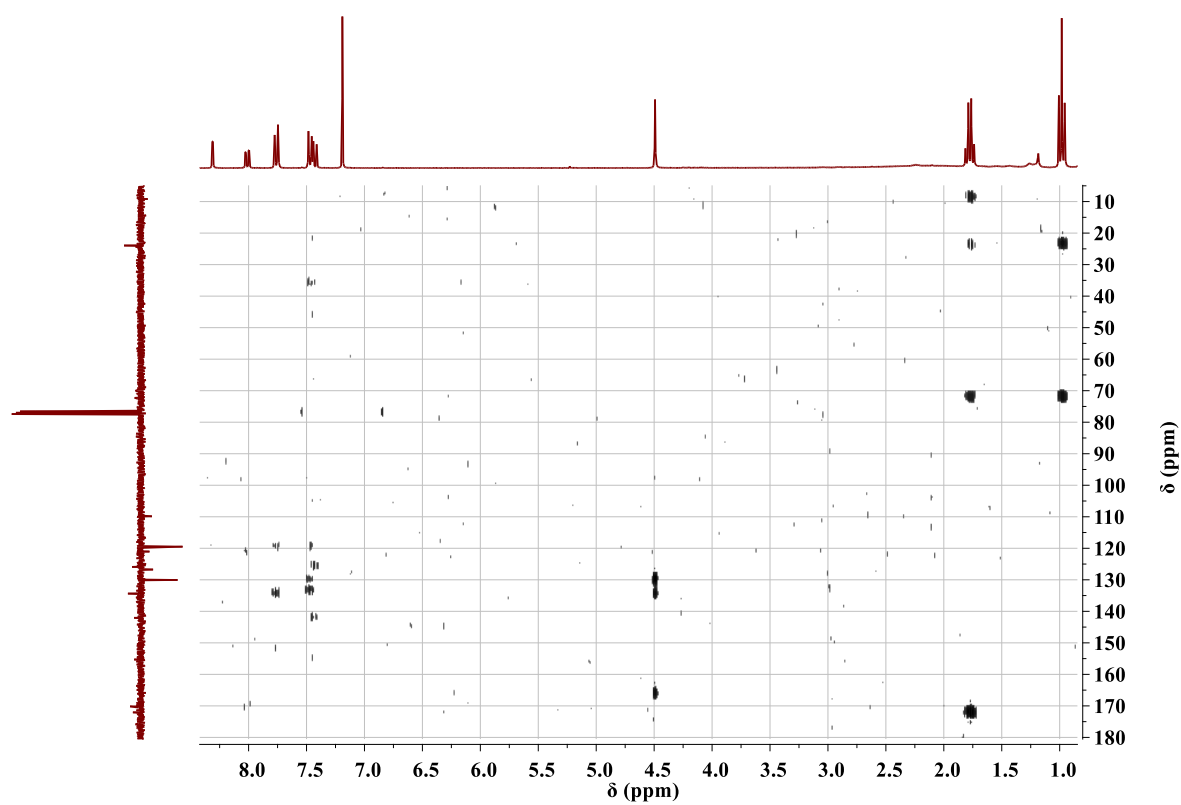
7.5.2. ¹³C NMR spectra



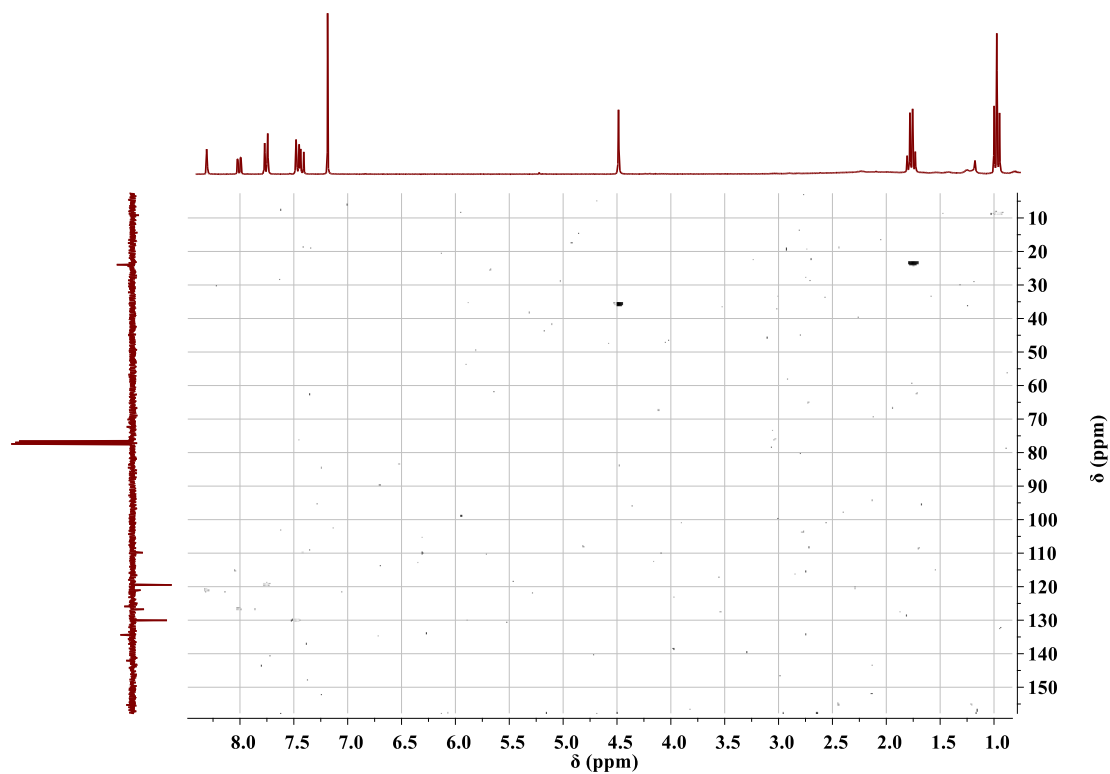
7.5.3. COSY NMR spectra



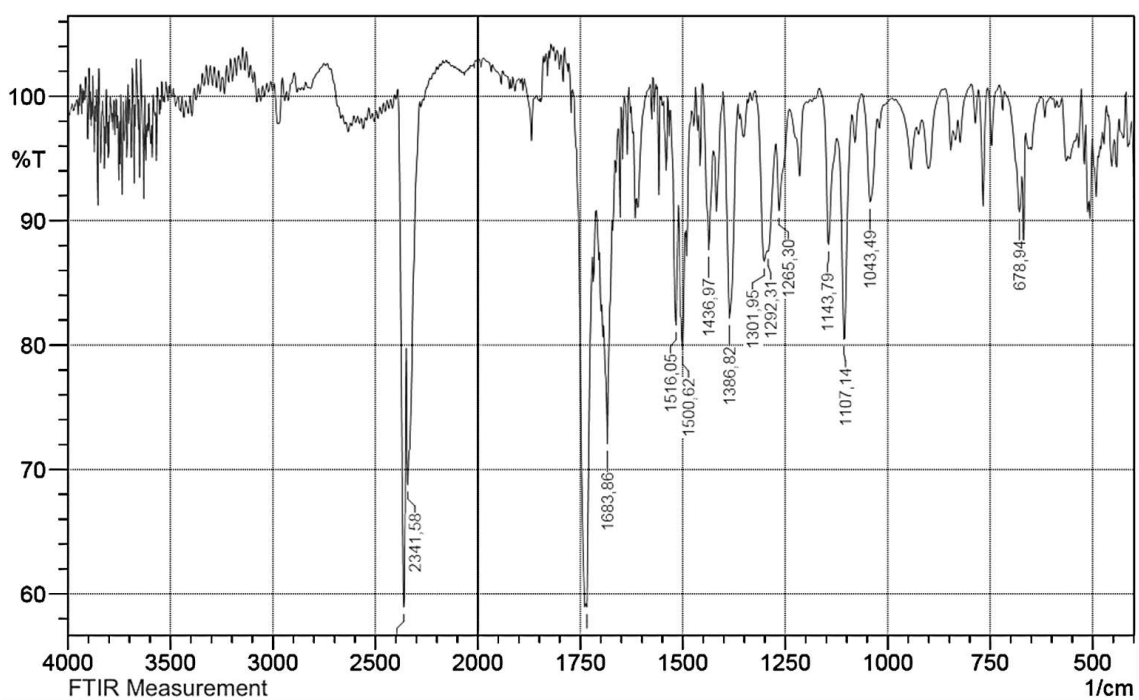
7.5.4. HMBC NMR spectra



7.5.5. HSQC NMR spectra



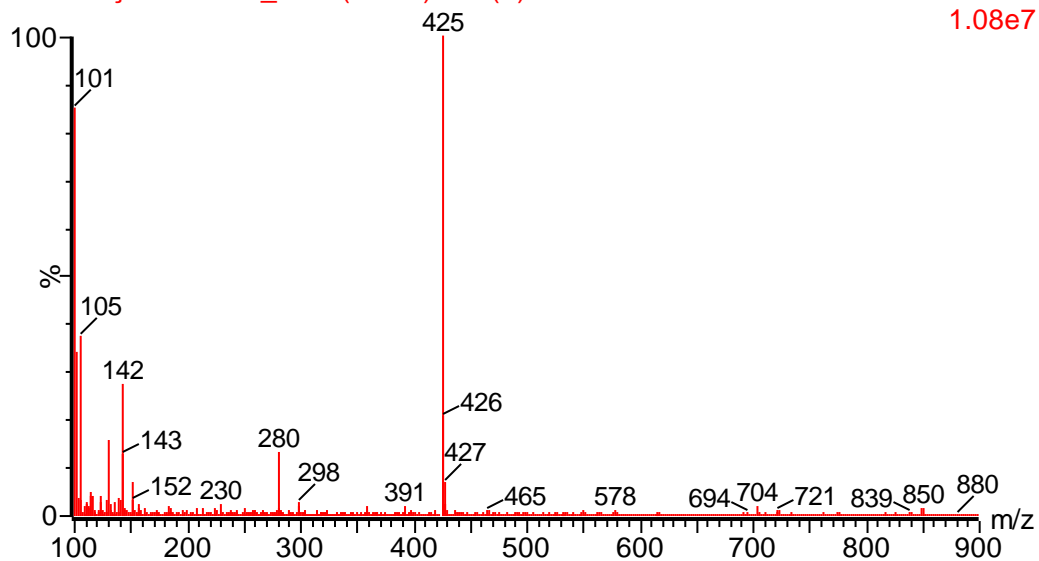
7.5.6. FTIR spectra



7.5.7. Mass spectra

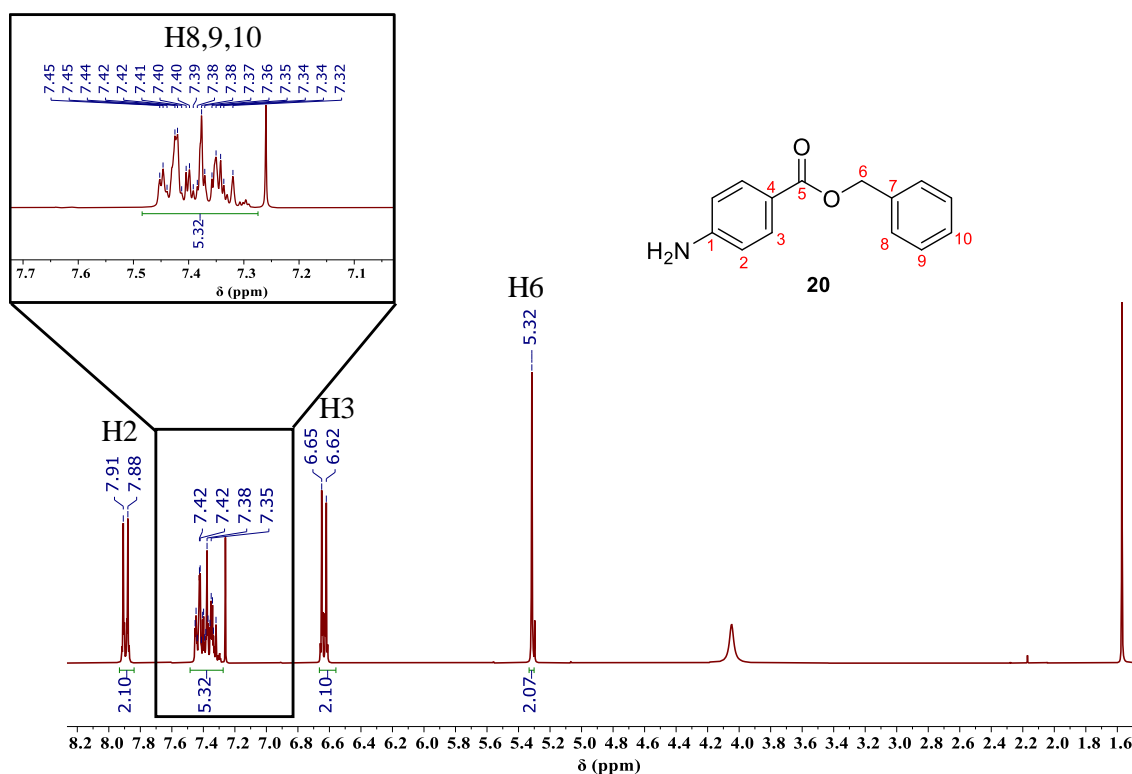
MS serviço 11Dez18_05 6 (0.589) Cm (6)

1: Scan ES+
1.08e7

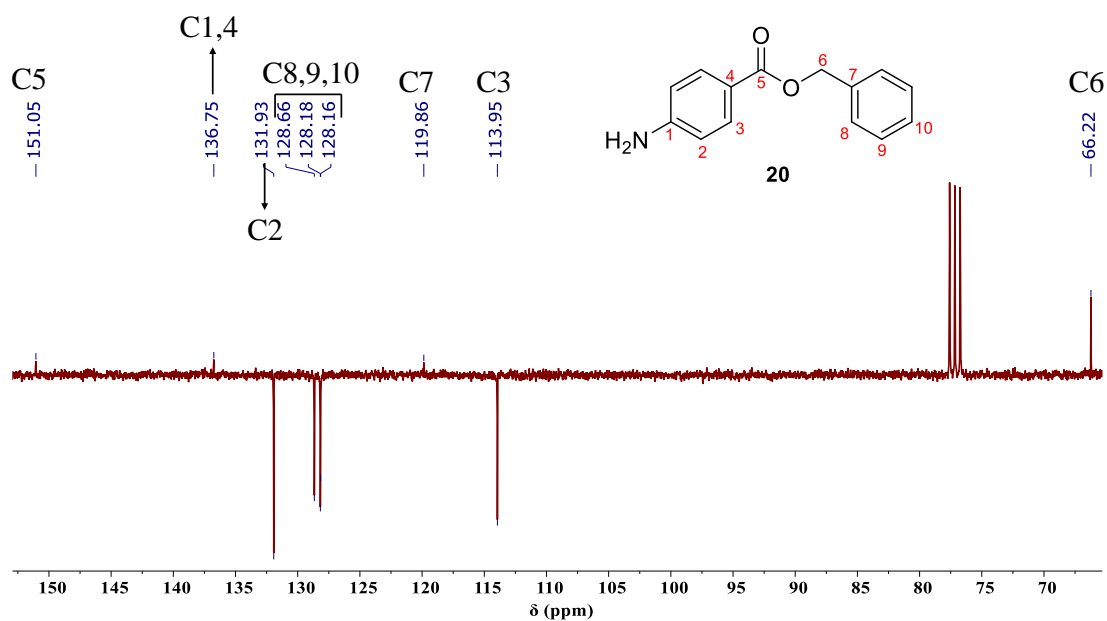


7.6. Characterization of compound (20)

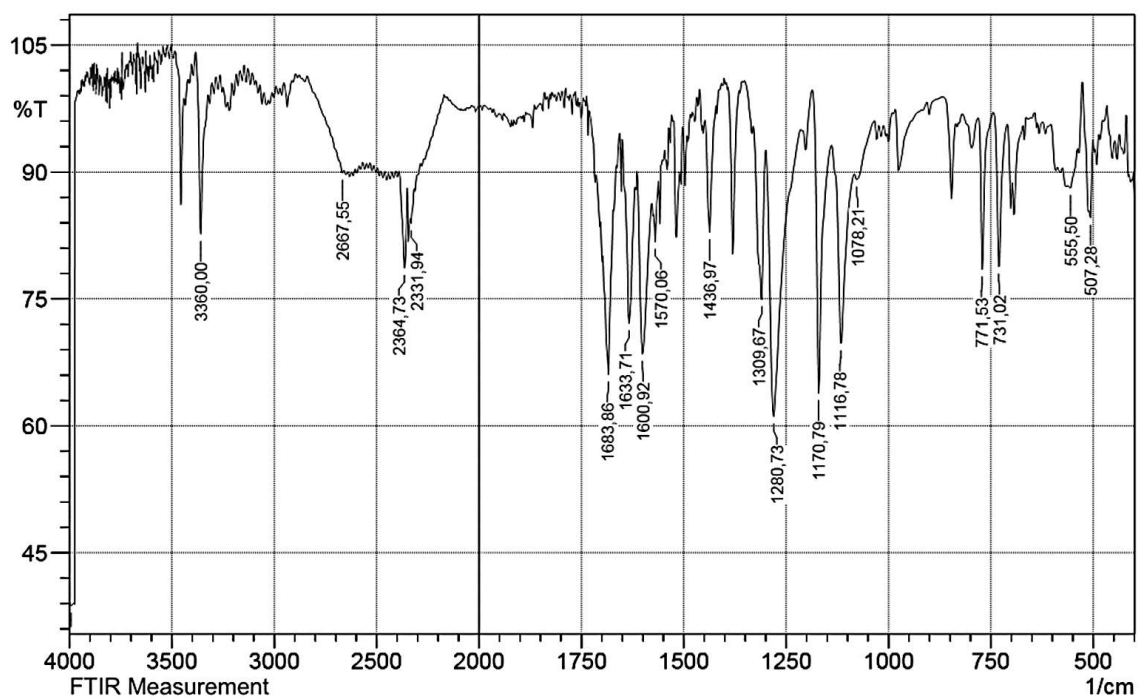
7.6.1. ¹H NMR spectra



7.6.2. ^{13}C NMR spectra

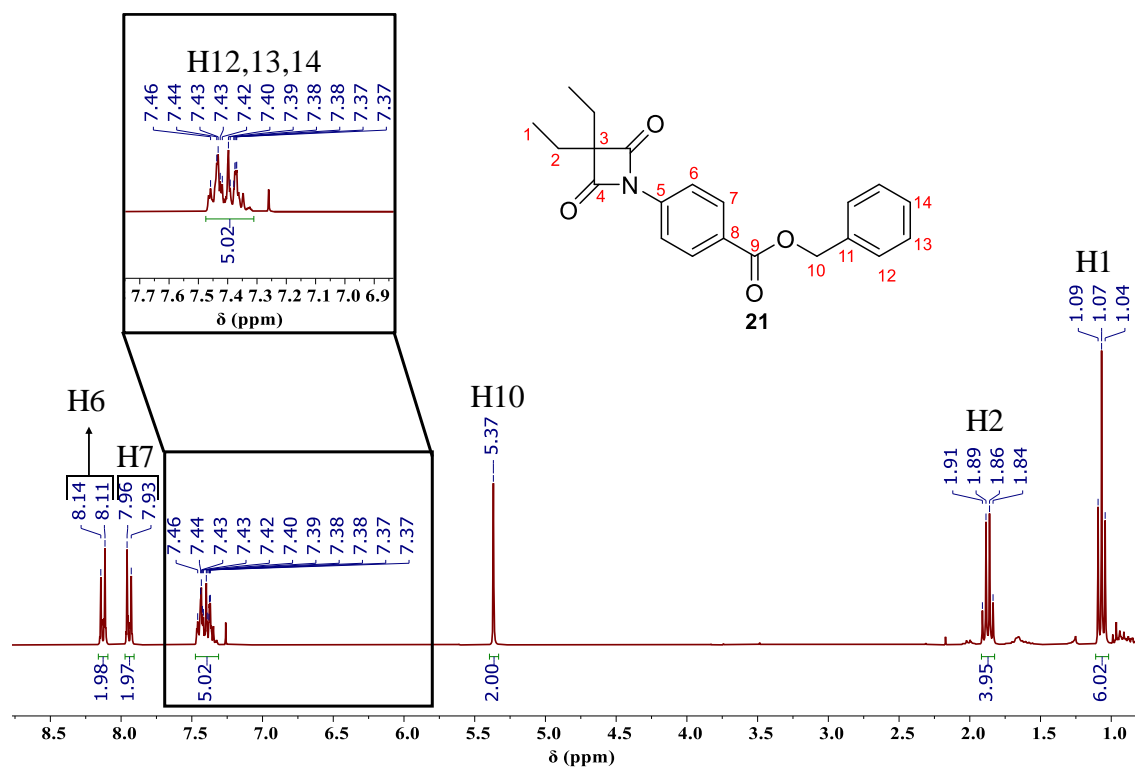


7.6.3. FTIR spectra

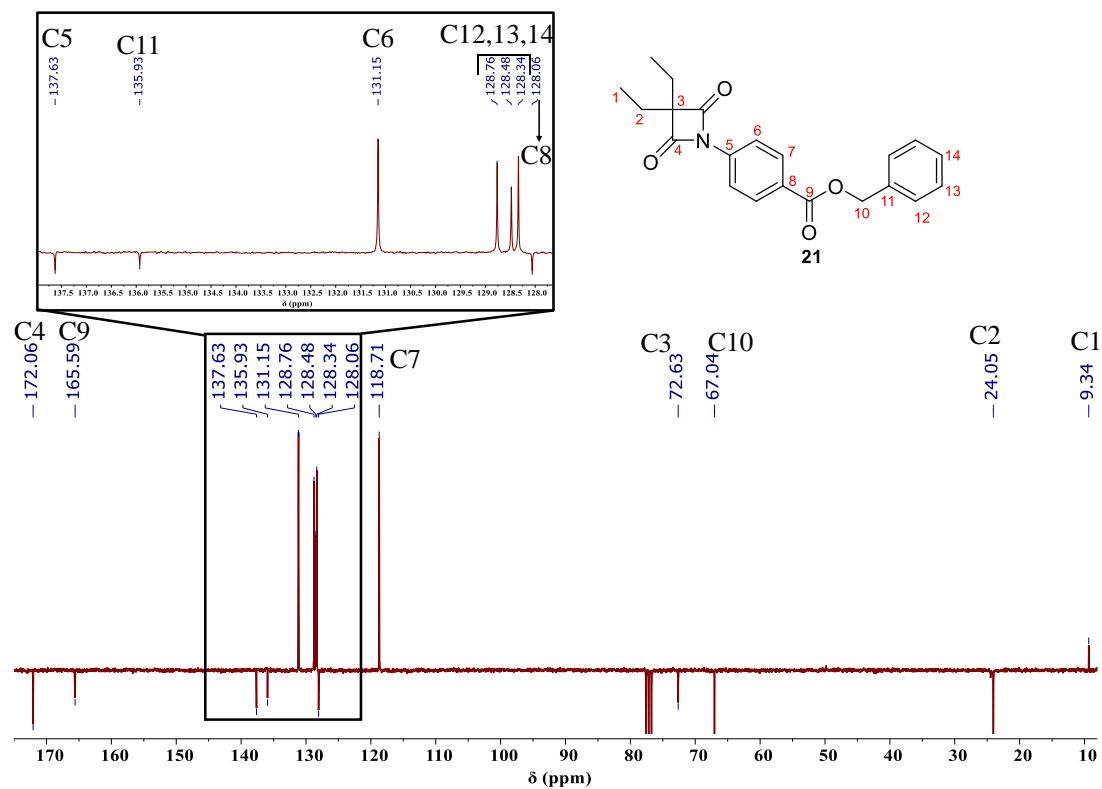


7.7. Characterization of compound (21)

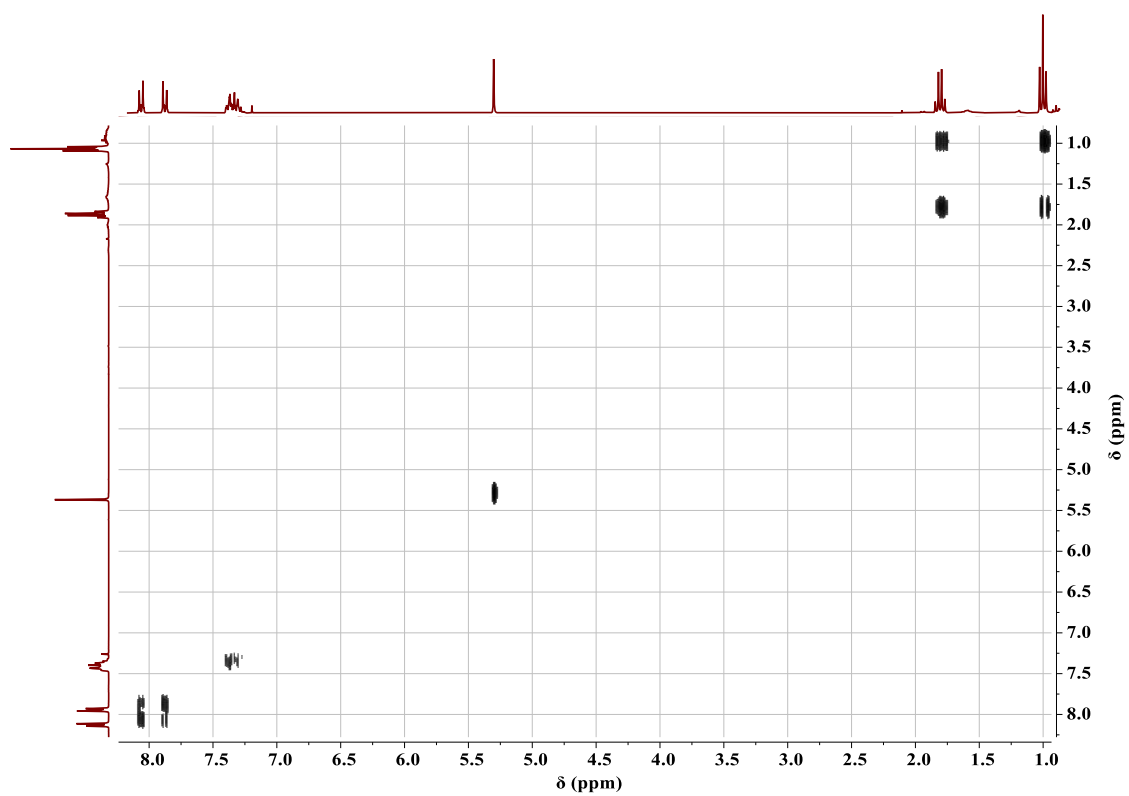
7.7.1. ^1H NMR spectra



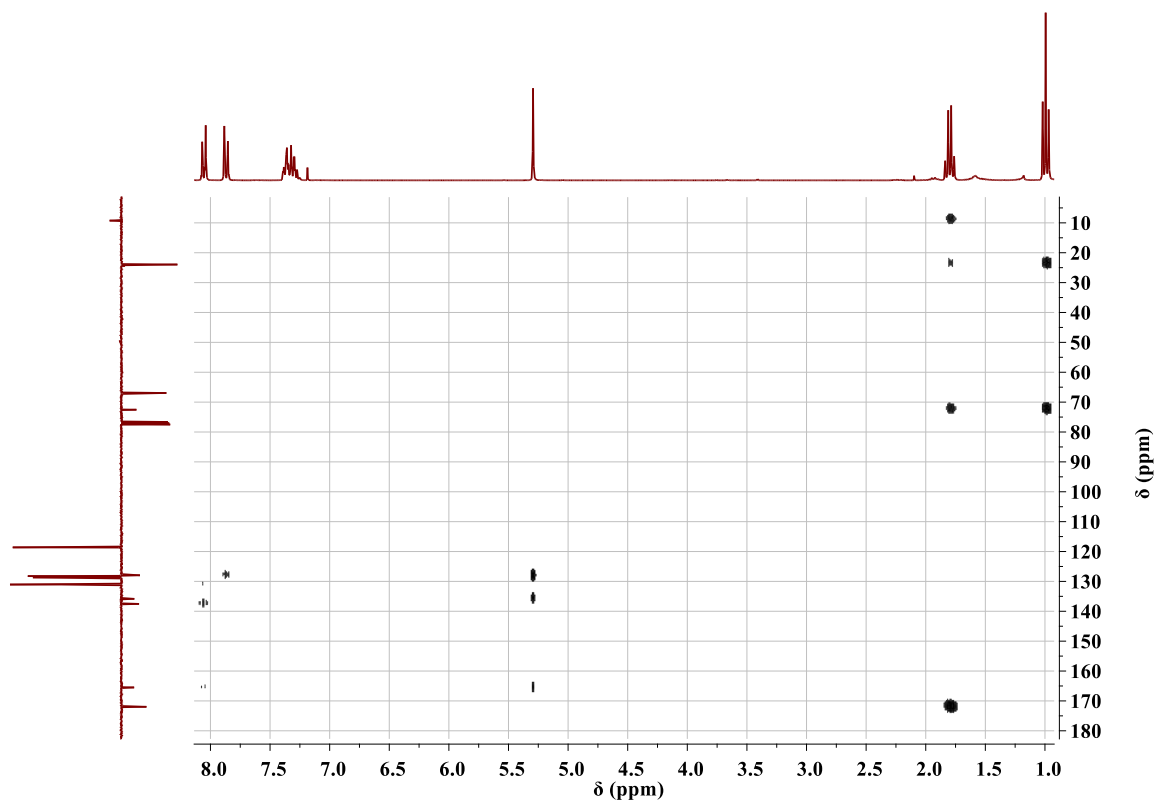
7.7.2. ^{13}C NMR spectra



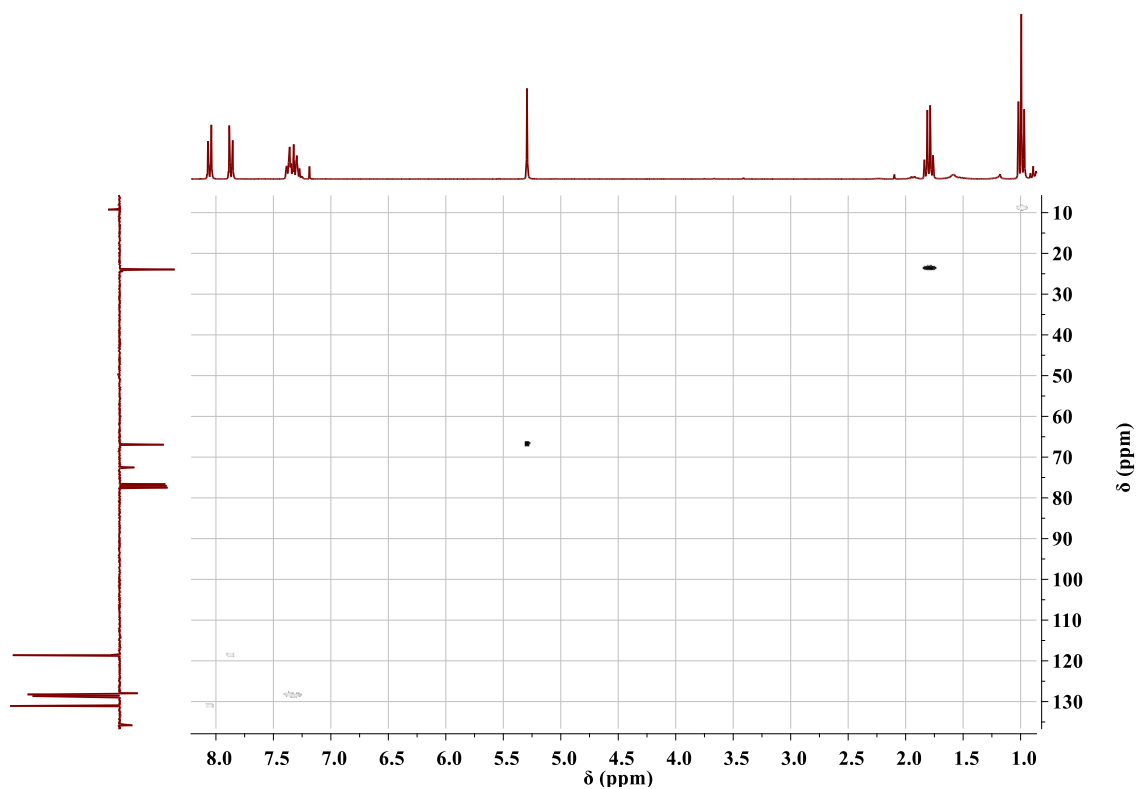
7.7.3. COSY NMR spectra



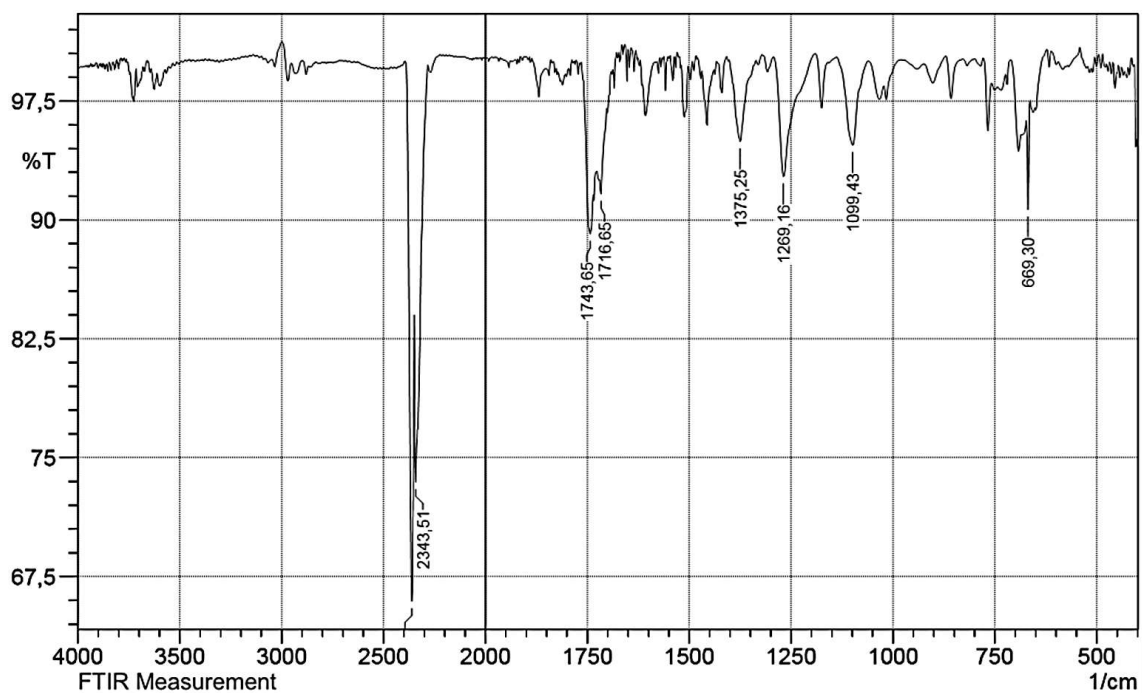
7.7.4. HMBC NMR spectra



7.7.5. HSQC NMR spectra



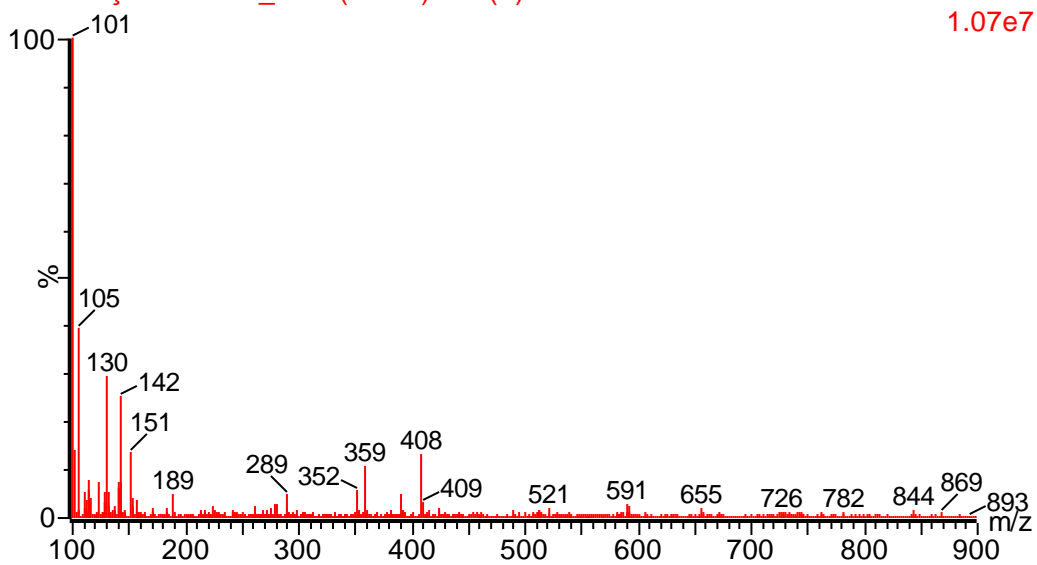
7.7.6. FTIR spectra



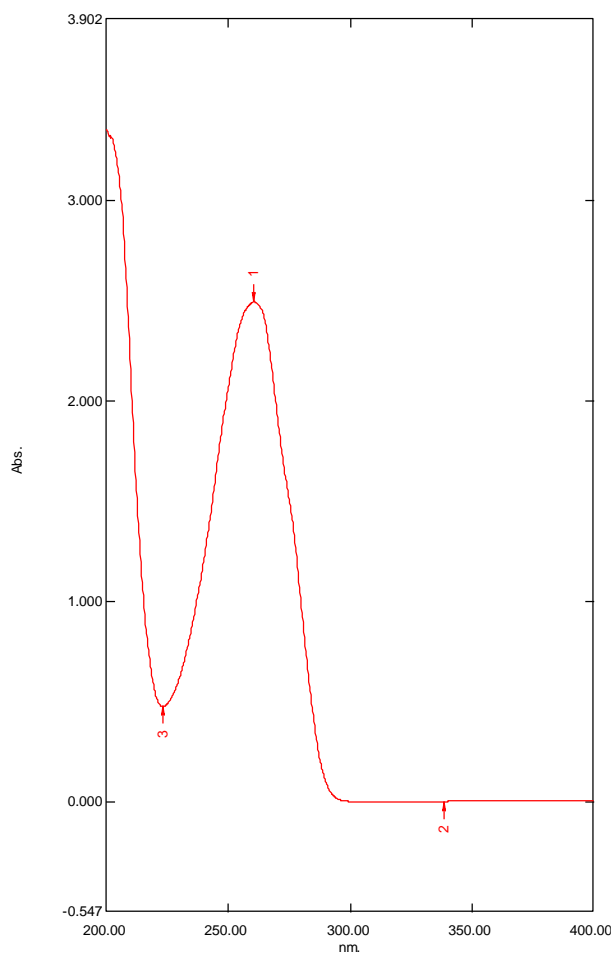
7.7.7. Mass spectra

MS serviço 11Dez18_13 6 (0.589) Cm (6)

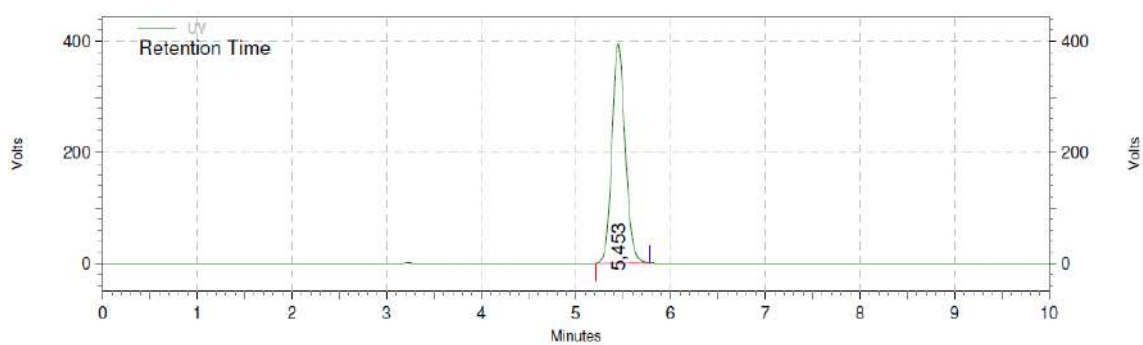
1: Scan ES+
1.07e7



7.7.8. UV graphic

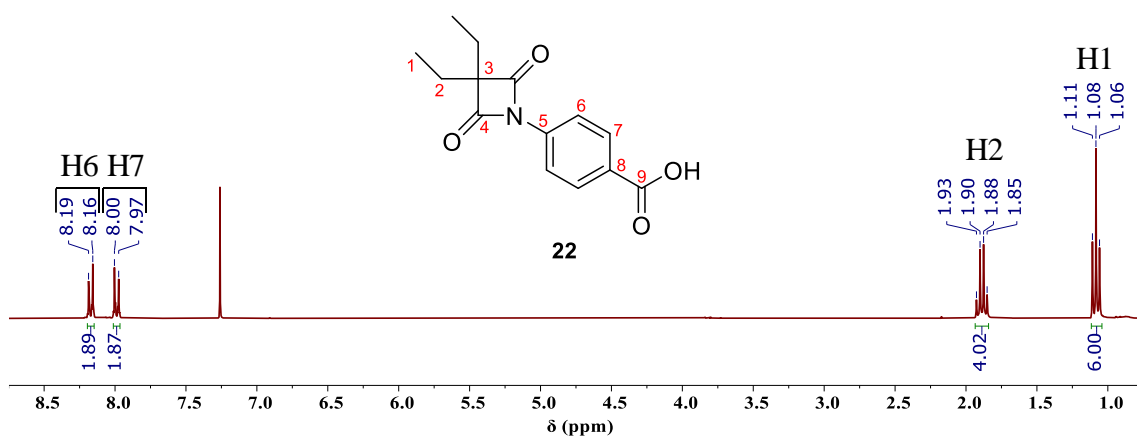


7.7.9.HPLC graphic

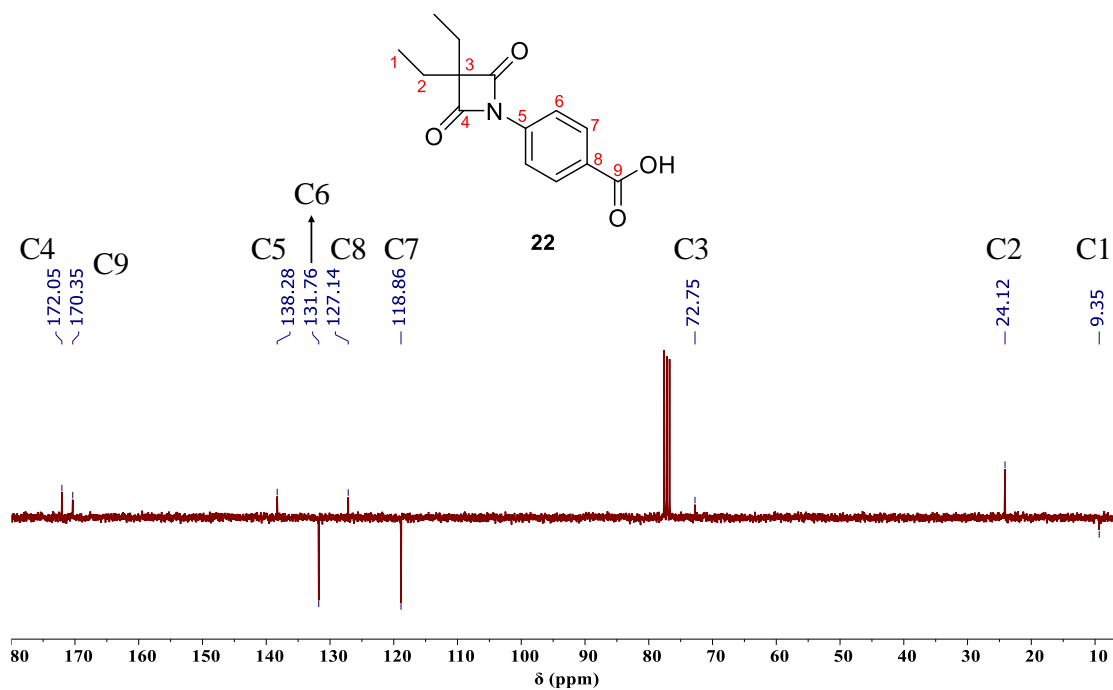


7.8. Characterization of compound (22)

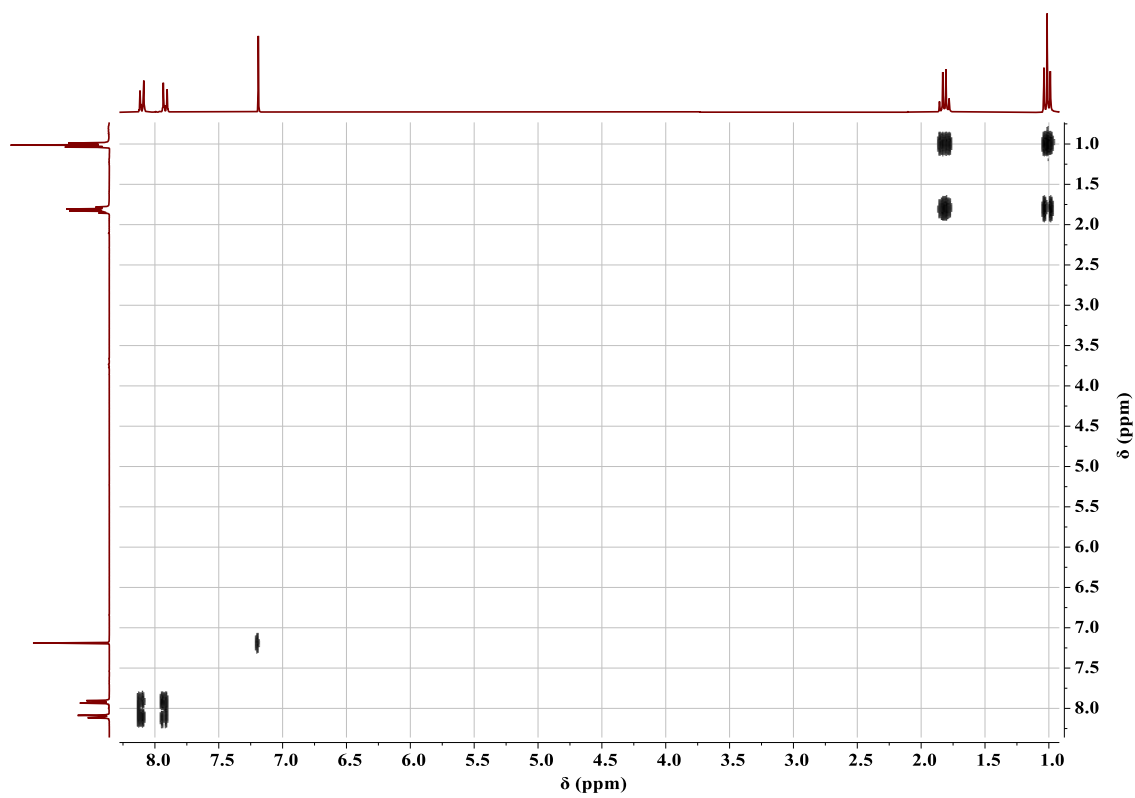
7.8.1. ¹H NMR spectra



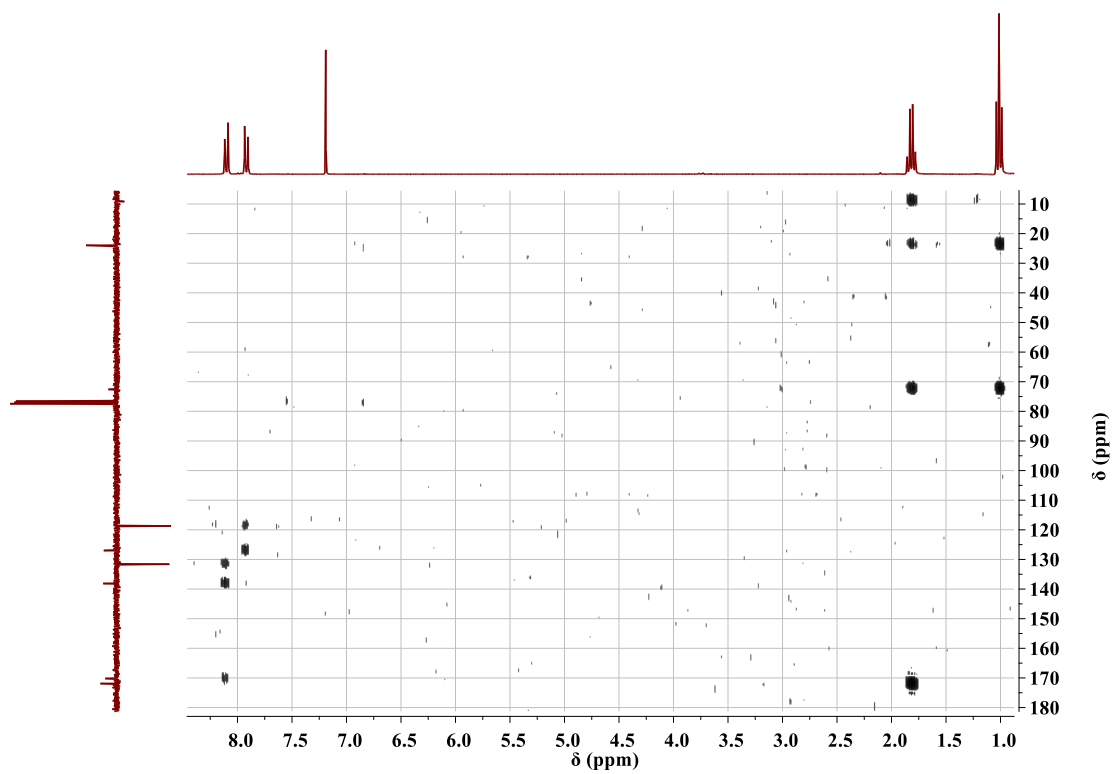
7.8.2. ^{13}C NMR spectra



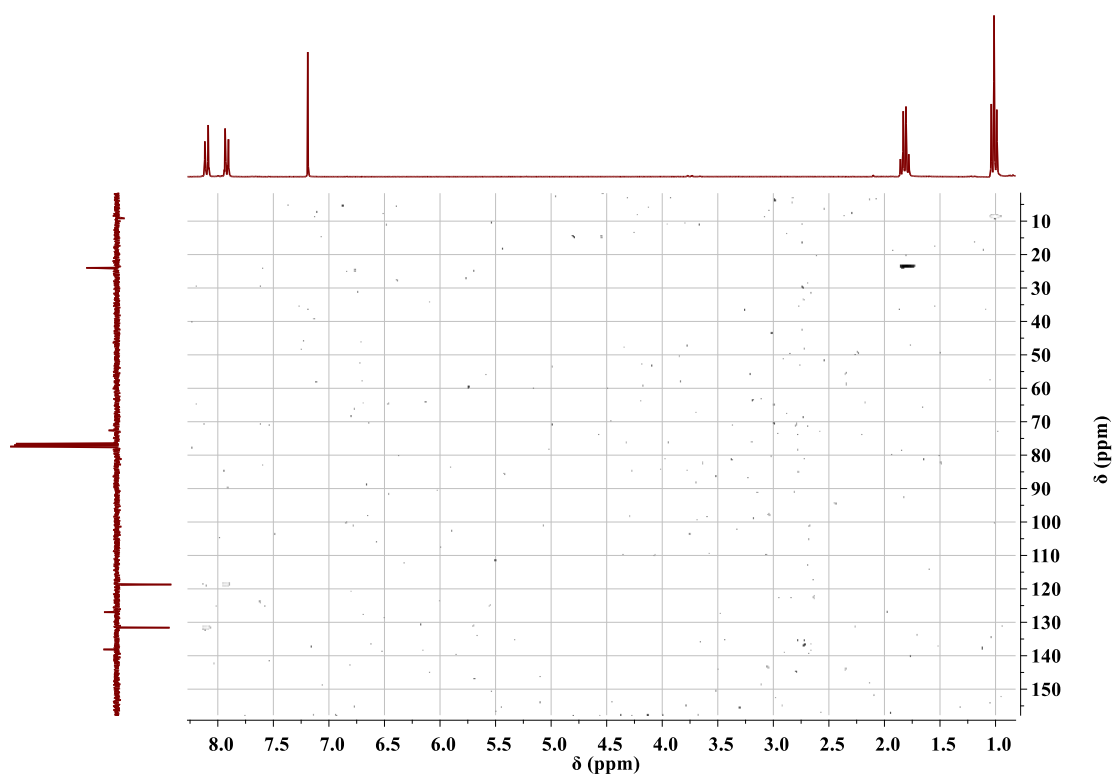
7.8.3. COSY NMR spectra



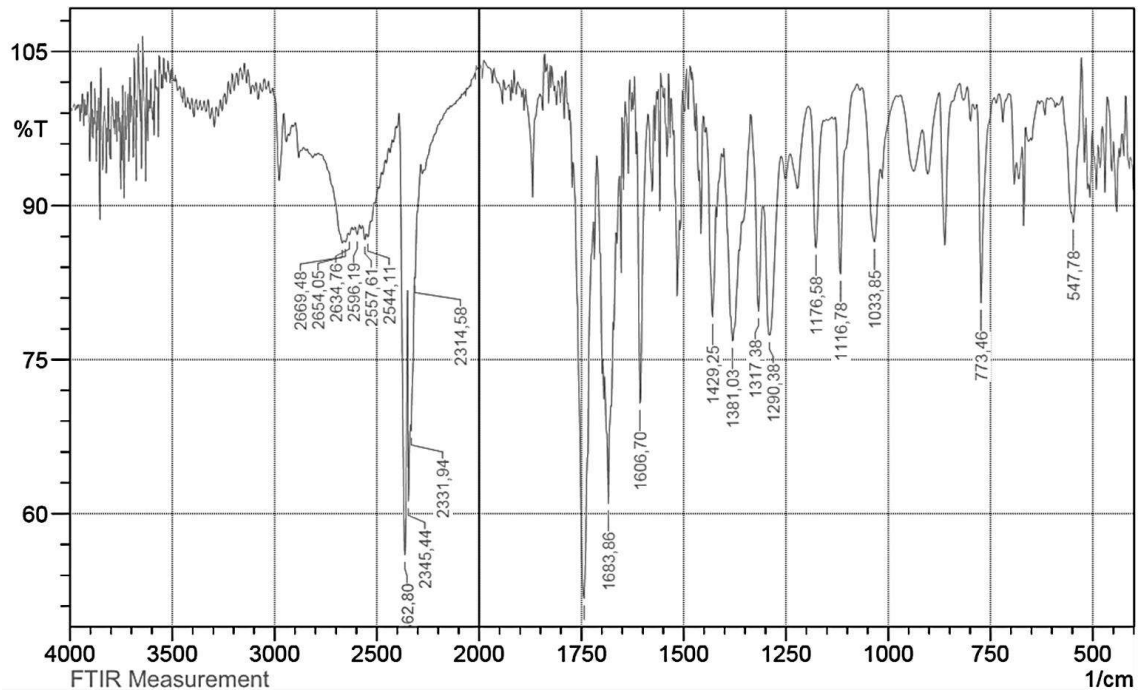
7.8.4. HMBC NMR spectra



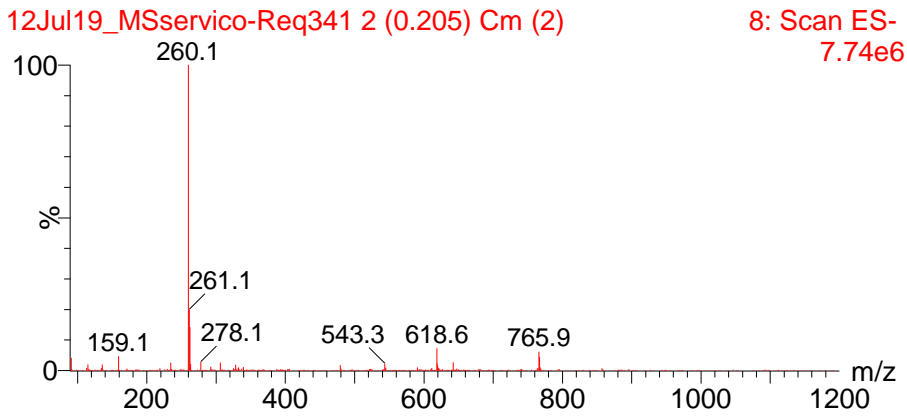
7.8.5. HSQC NMR spectra



7.8.6. FTIR spectra

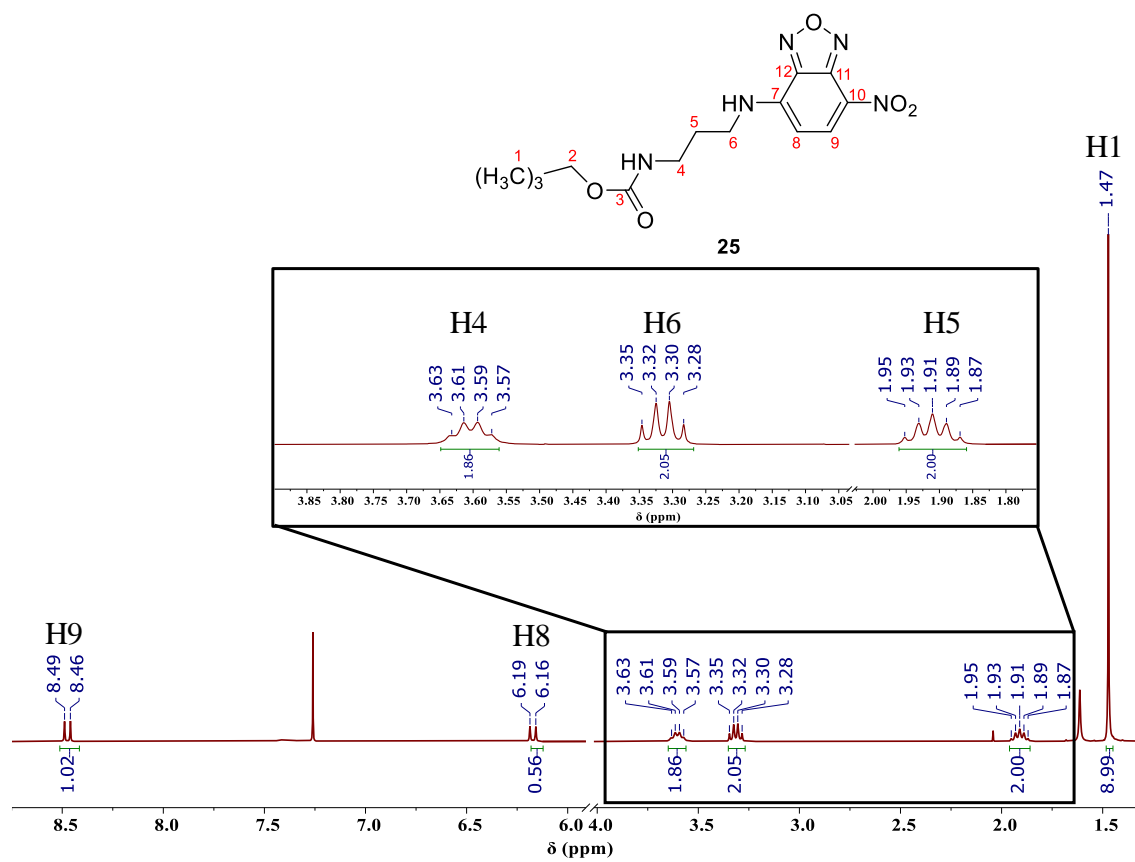


7.8.7. Mass spectra



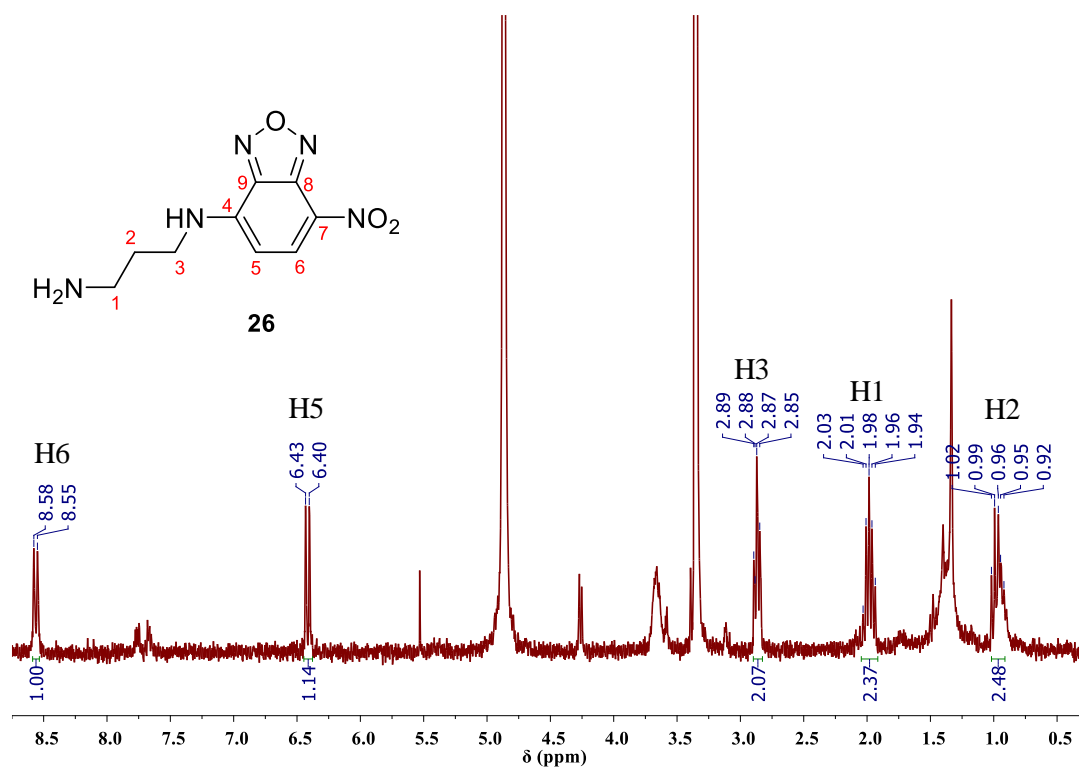
7.9. Characterization of compound (25)

7.9.1. ^1H NMR spectra



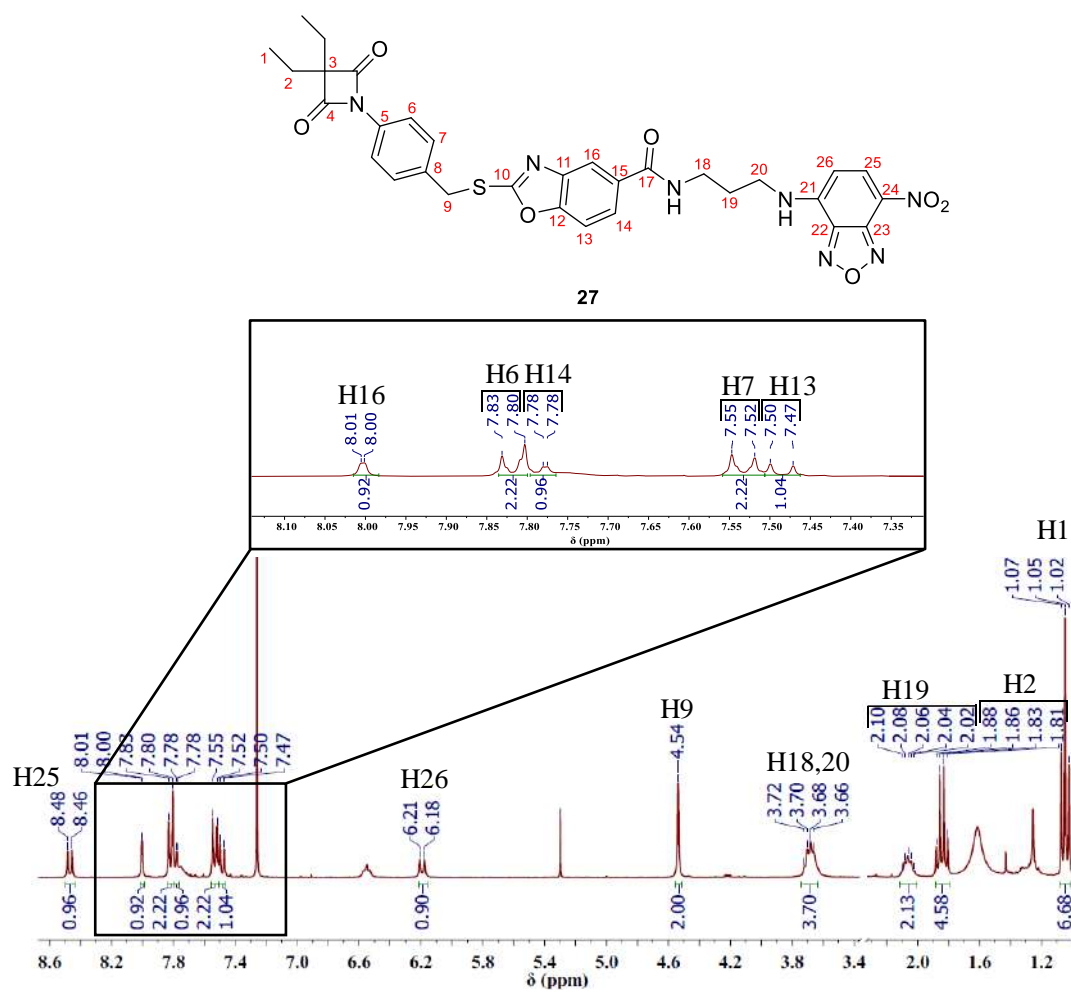
7.10. Characterization of compound (26)

7.10.1. ^1H NMR spectra

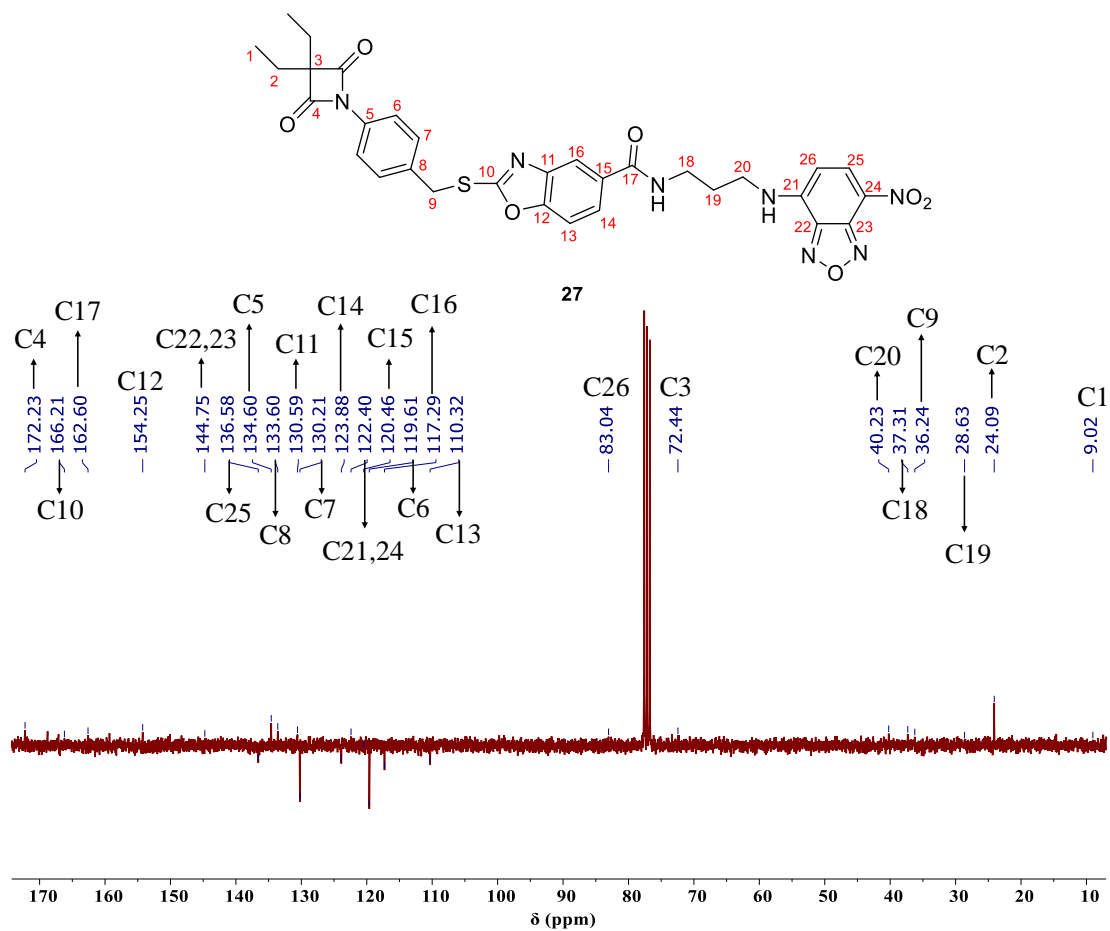


7.11. Characterization of compound (27)

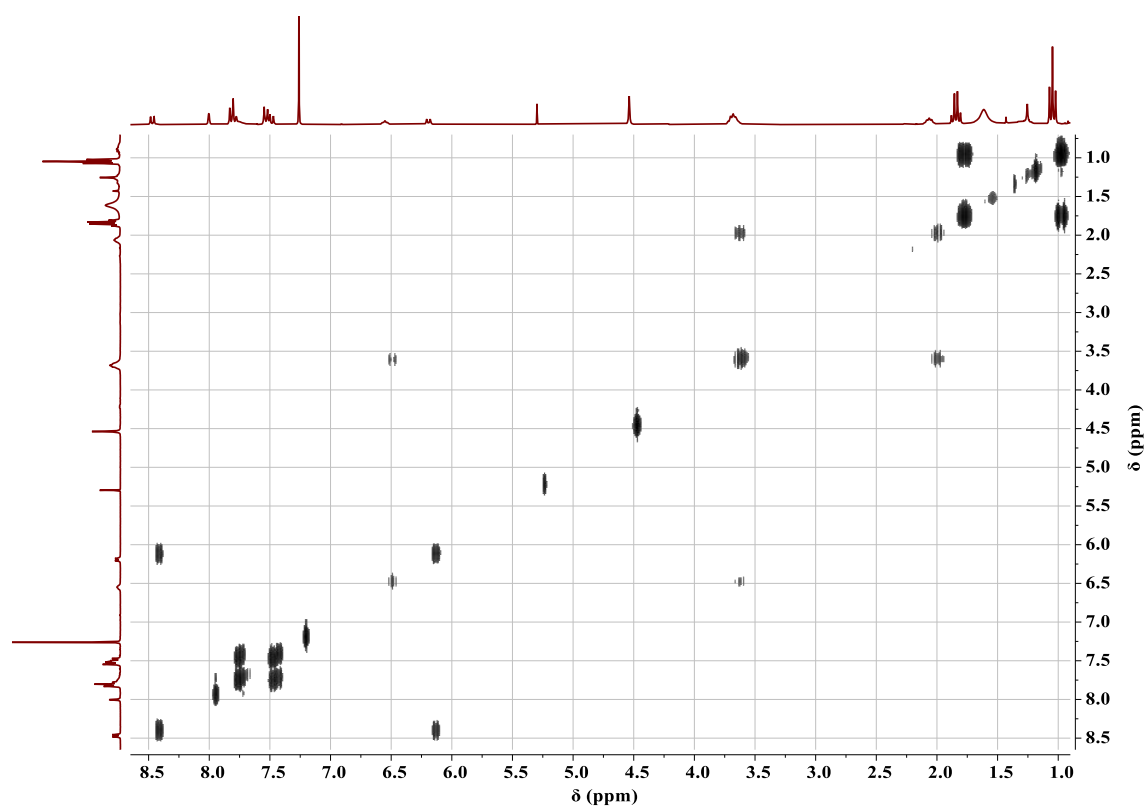
7.11.1. ¹H NMR spectra



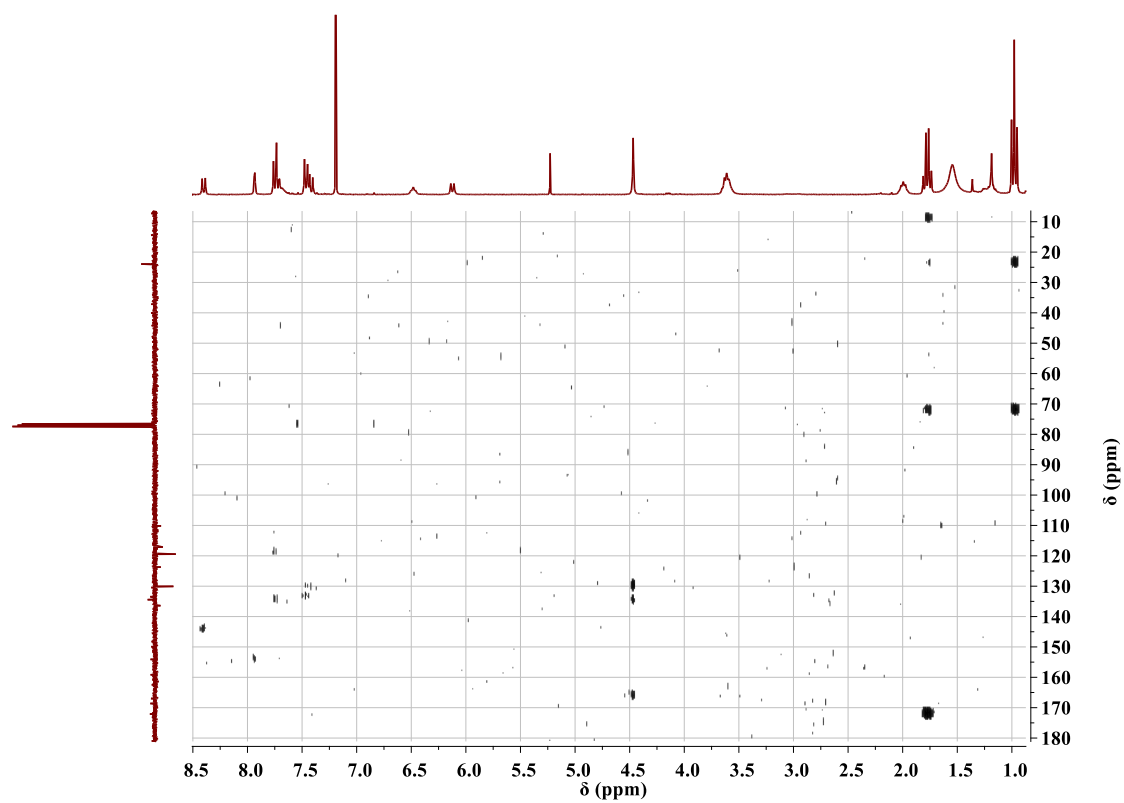
7.11.2. ^{13}C NMR spectra



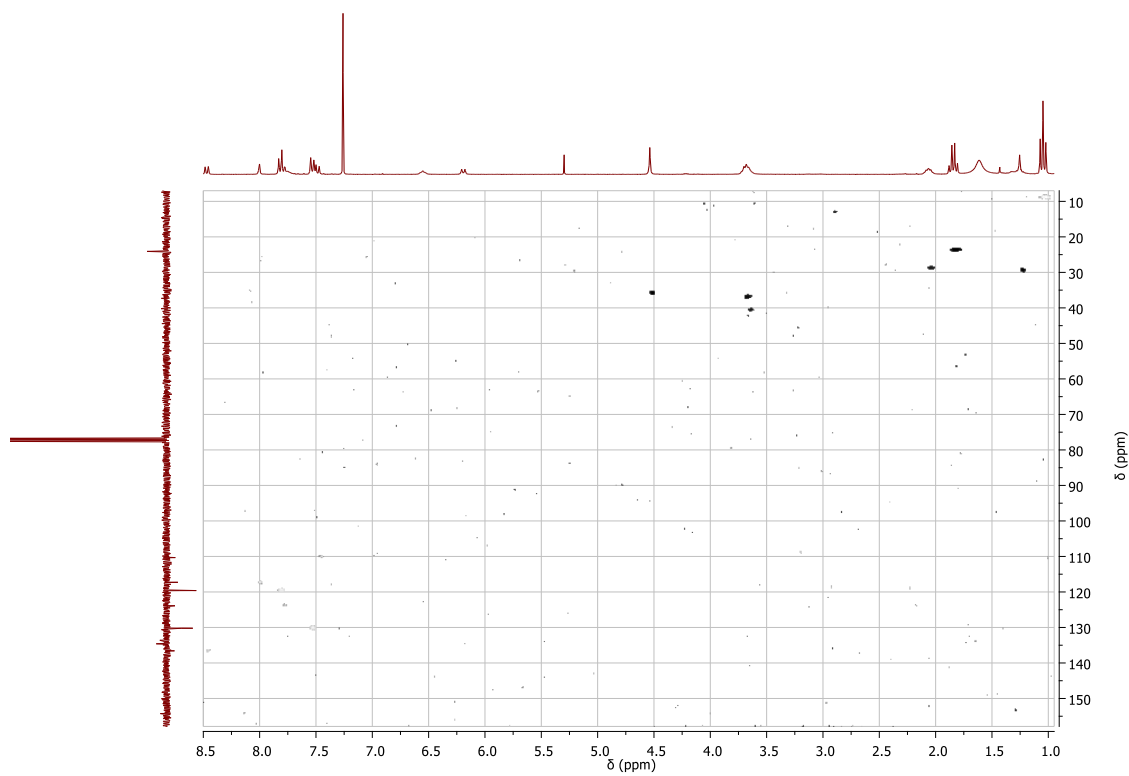
7.11.3. COSY NMR spectra



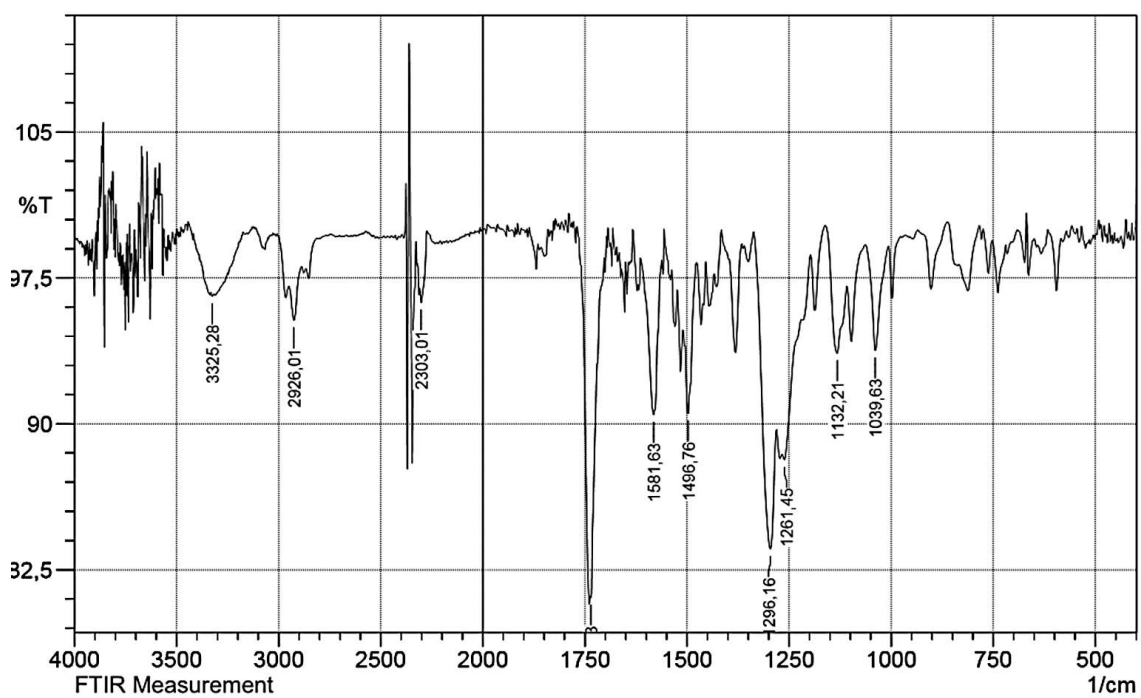
7.11.4. HMBC NMR spectra



7.11.5. HSQC NMR spectra



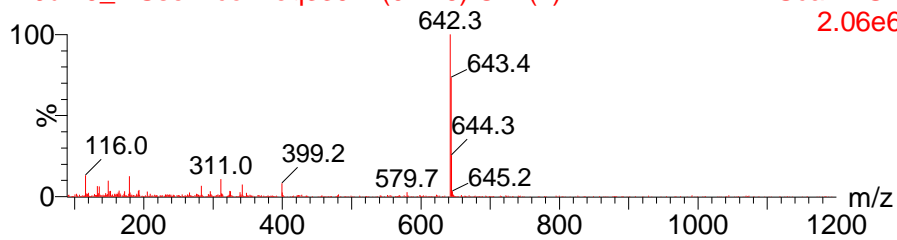
7.11.6. FTIR spectra



7.11.7. Mass spectra

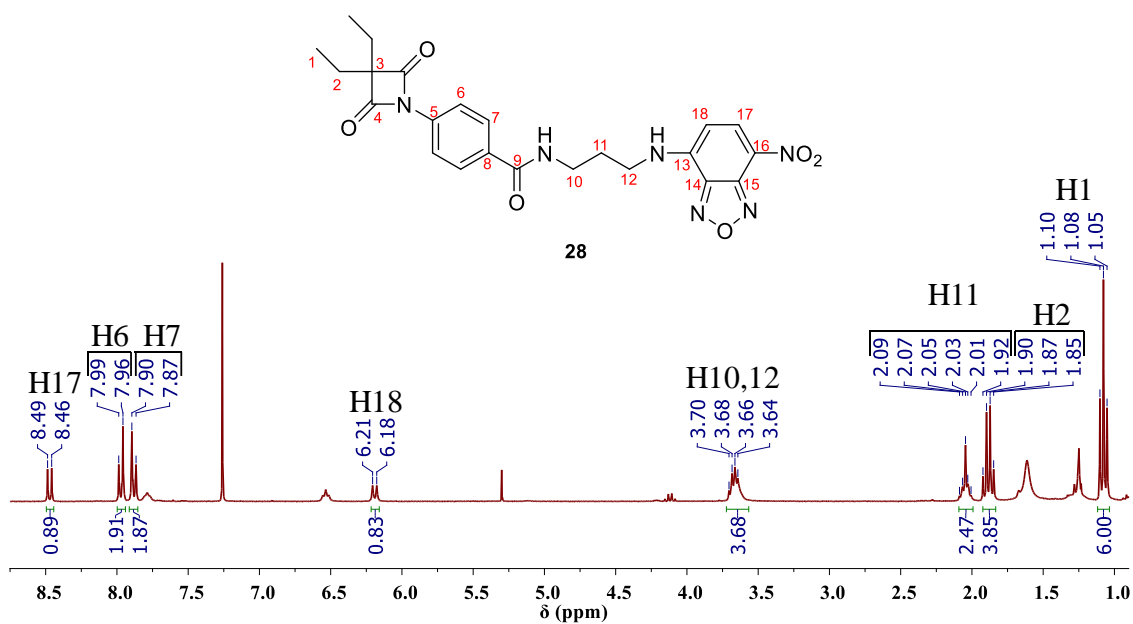
12Jul19_MSservico-Req339 2 (0.246) Cm (2)

12: Scan ES-
2.06e6

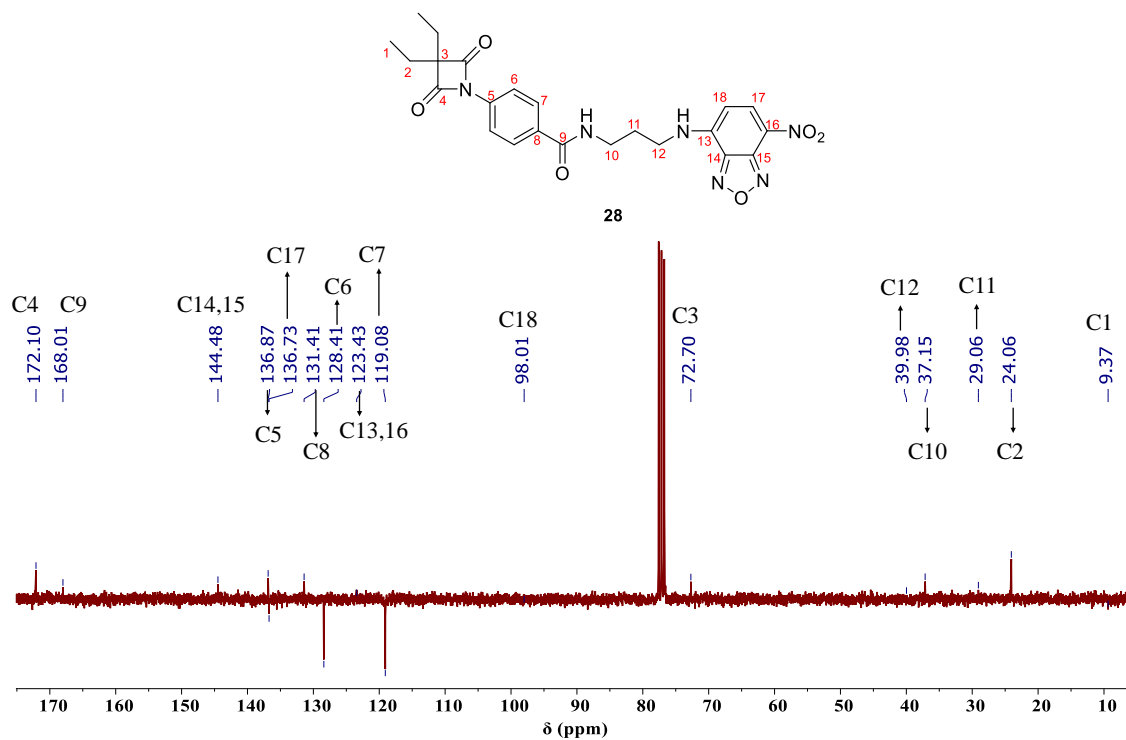


7.12. Characterization of compound (28)

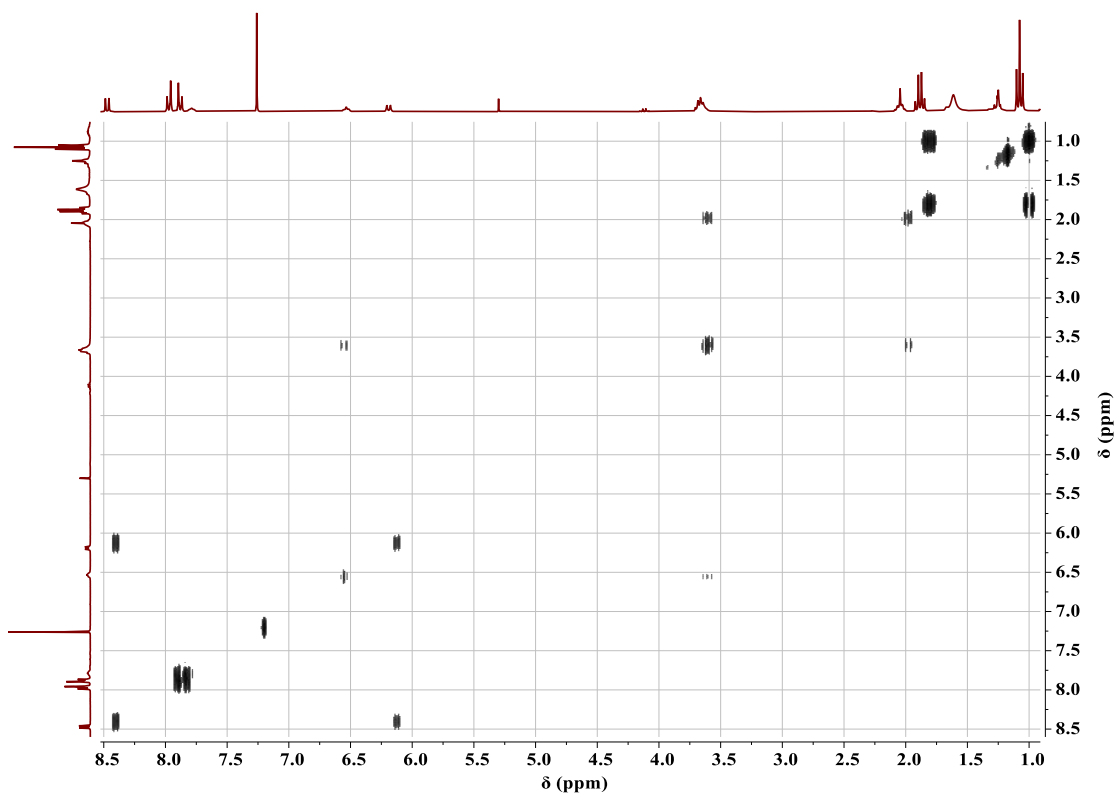
7.12.1. ¹H NMR spectra



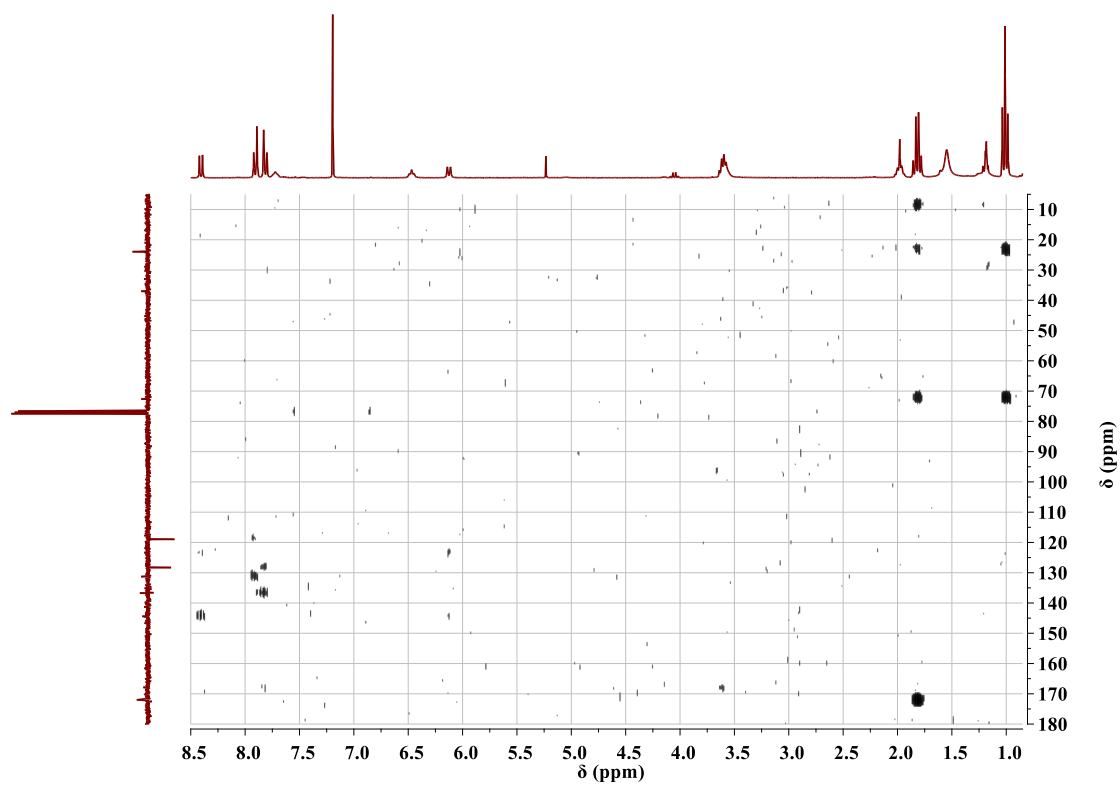
7.12.2. ^{13}C NMR spectra



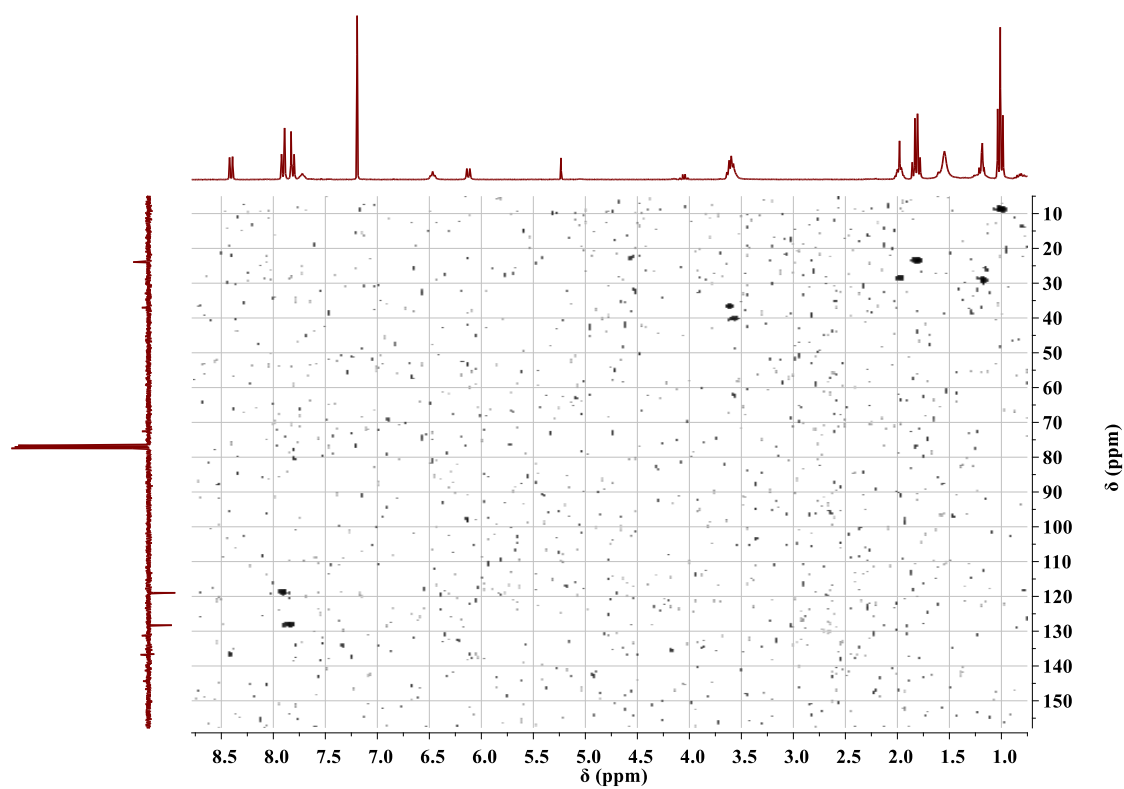
7.12.3. COSY NMR spectra



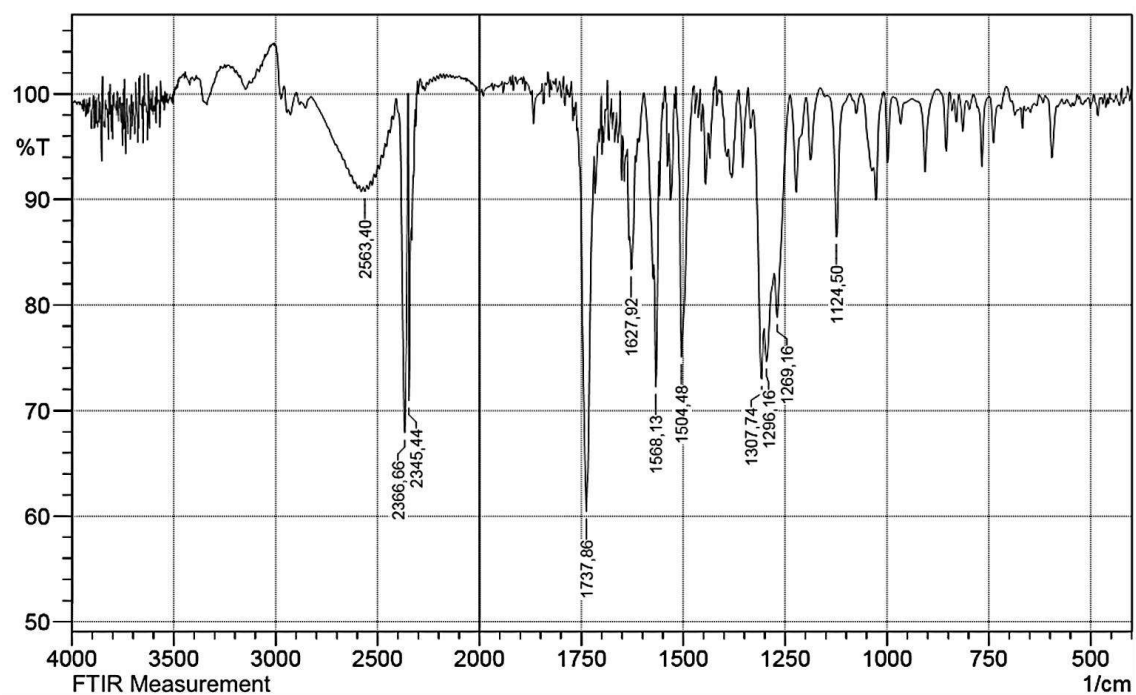
7.12.4. HMBC NMR spectra



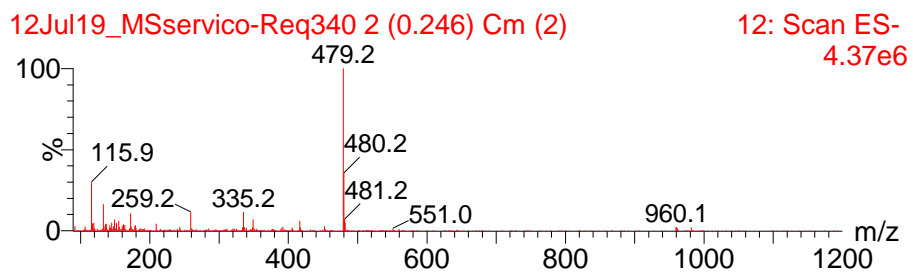
7.12.5. HSQC NMR spectra



7.12.6. FTIR spectra



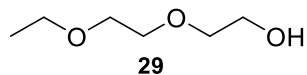
7.12.7. Mass spectra



9.1. Transcutol CG

❖ INCI: Ethoxydiglycol (29)

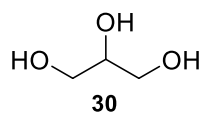
❖ Chemical structure:



9.2. Glycerin

❖ INCI: Glycerin (30)

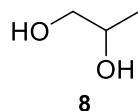
❖ Chemical structure:



9.3. Propylene glycol

❖ INCI: Propylene glycol (8)

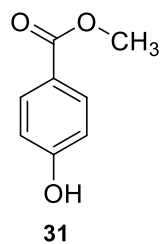
❖ Chemical structure:



9.4. Nipagin™ M Sodium

❖ INCI: Methylparaben (31)

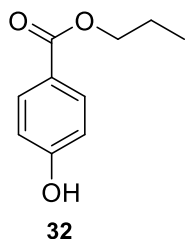
❖ Chemical structure:



9.5. Nipasol M Sodium™

❖ INCI: Propylparaben (32)

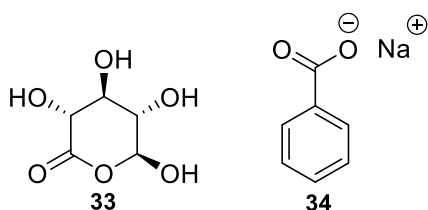
❖ Chemical structure:



9.6. Geogard Ultra™

❖ INCI: Gluconolactone (33) (and) sodium benzoate (34)

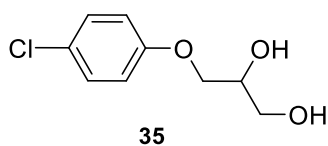
❖ Chemical Structure:



9.7. Saliphenesin

❖ INCI: Chlorphenesin (35)

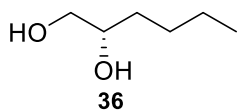
❖ Chemical structure:



9.8. Dermosoft® Hexiol

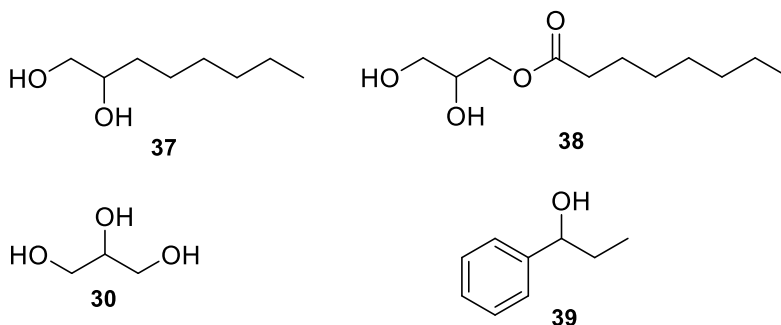
❖ INCI: 1,2-Hexanediol (36)

❖ Chemical Structure:



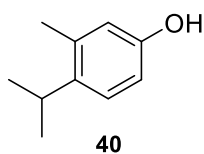
9.9. Dermosoft® LP

- ❖ INCI: Caprylyl glycol (**36**) (and) glyceryl caprylate (**37**) (and) glycerin (**30**) (and) phenylpropanol (**38**) (and) aqua
- ❖ Chemical structure:



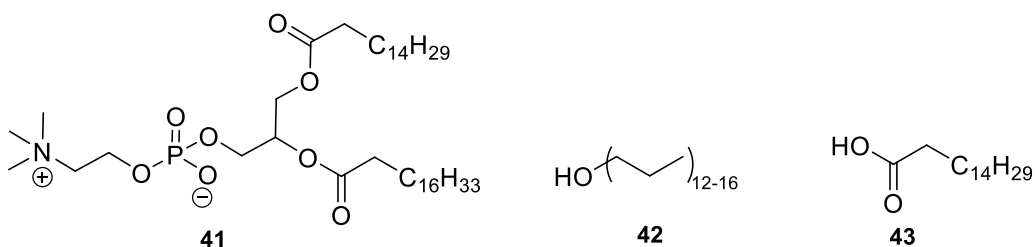
9.10. SymOcide®

- ❖ INCI: *o*-Cymen-5-ol
- ❖ Chemical structure:



9.11. Biophilic™ H MB

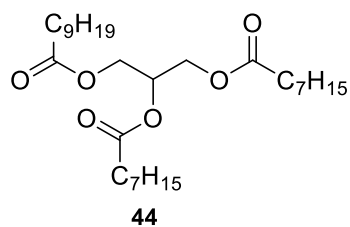
- ❖ INCI: Hydrogenated lecithin (**41**) (and) C12-16 alcohols (**42**) (and) palmitic acid (**43**)
- ❖ Chemical structure:



9.12. TEGOSOFT® CT

❖ INCI: Caprylic/capric triglycerides (44)

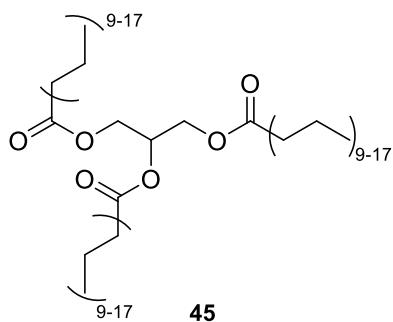
❖ Chemical structure:



9.13. Lipocire™ A SG

❖ INCI: C10-18 Triglycerides (45)

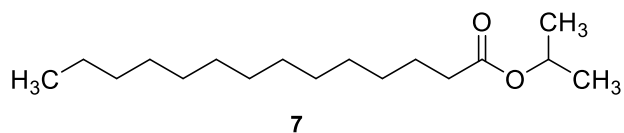
❖ Chemical structure:



9.14. TEGOSOFT® M

❖ INCI: Isopropyl myristate (7)

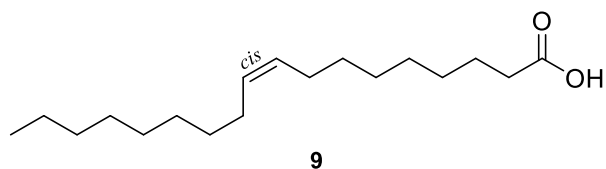
❖ Chemical structure:



9.15. Oleic acid

❖ INCI: Oleic acid (9)

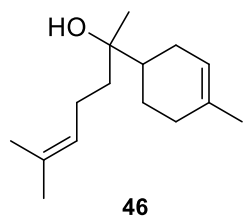
❖ Chemical structure:



9.16. Alpha Bisabolol

❖ INCI: Alpha bisabolol (46)

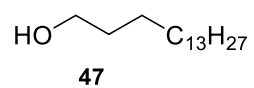
❖ Chemical structure:



9.17. Cetyl alcohol

❖ INCI: Cetyl alcohol (47)

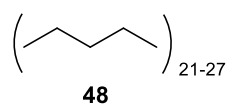
❖ Chemical structure:



9.18. Emosmart™ C28

❖ INCI: C21-C28 Alkane (48)

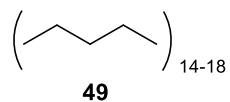
❖ Chemical structure:



9.19. Emogreen™ L15

❖ INCI: C15-19 Alkane (49)

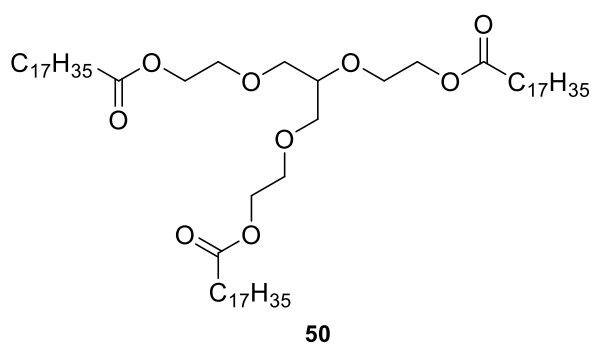
❖ Chemical structure:



9.20. Cithrol™ 10GTIS

❖ INCI: PEG-20 glyceryl triisostearate (50)

❖ Chemical Structure:



❖ Safety data sheet (section 11 - toxicological information): No skin irritation.

